



Indexing and Searching for Similarities of Images with Structural Descriptors via Graph-cuttings Methods

Yi Ren

► To cite this version:

Yi Ren. Indexing and Searching for Similarities of Images with Structural Descriptors via Graph-cuttings Methods. Computer science. Université de Bordeaux, 2014. English. NNT : 2014BORD0215 . tel-01154565

HAL Id: tel-01154565

<https://theses.hal.science/tel-01154565>

Submitted on 22 May 2015

HAL is a multi-disciplinary open access archive for the deposit and dissemination of scientific research documents, whether they are published or not. The documents may come from teaching and research institutions in France or abroad, or from public or private research centers.

L'archive ouverte pluridisciplinaire **HAL**, est destinée au dépôt et à la diffusion de documents scientifiques de niveau recherche, publiés ou non, émanant des établissements d'enseignement et de recherche français ou étrangers, des laboratoires publics ou privés.



Indexing and Searching for Similarities of Images with Structural Descriptors via Graph-cuttings Methods

Yi REN

LaBRI

Université de Bordeaux

A thesis submitted for the degree of

PHD

October 2011 - September 2014

Supervised by

Professeure Jenny Benois-Pineau

Maître de conférences Aurélie Bugeau

Reviewer : Mr Bernard Merialdo and Mr Philippe-Henri Gosselin

Signature from author: Yi REN

Contents

List of Figures	iii
List of Tables	xi
Glossary	xvii
1 Introduction	1
1.1 Problems and Objectives	2
1.2 Contributions	3
1.3 Organization of the Thesis	3
2 Related Work	5
2.1 Image Descriptors	5
2.1.1 Formalization	6
2.1.2 Image Feature Detection	7
2.1.3 Image Feature Extraction and Description	7
2.1.4 Local Image Descriptors	8
2.1.5 Semi-local Image Descriptors	10
2.1.6 Global Image Descriptors	11
2.1.6.1 Color	11
2.1.6.2 Texture	13
2.1.6.3 Gist	15
2.1.7 Similarity Metrics	16
2.2 Image Retrieval in the Real World	17
2.3 Image Representation	18
2.3.1 The Bag-of-Words Model	19

CONTENTS

2.3.2	The State-of-the-art to Improve the Bag-of-Visual-Words Model	21
2.3.2.1	Spatial pyramid image representation	22
2.3.2.2	Superpixels	23
2.3.2.3	Using class-specific codebooks to vote for object position . .	24
2.3.2.4	SpatioGrams versus Histograms	24
2.3.2.5	Spatial orientations of visual word pairs to improve Bag-of- Visual-Words model	25
2.3.2.6	Improve BoW model with respect to feature encoding	25
2.3.3	Region-based Image Representation	25
2.3.4	Graph-based Image Representation and its Applications	26
2.4	Conclusion	27
3	Graph-based Image Representation	29
3.1	An Overview of the Image Graph Model	29
3.2	Weighted Image Graph Representation	30
3.3	Graph Construction	31
3.3.1	Graph Nodes Selection in Image Graph	31
3.3.1.1	Prominent keypoints	31
3.3.1.2	Dense sampling strategy	31
3.3.2	Graph Edges Construction in Image Graph	32
3.3.3	Graph Weights in Image Graph	33
3.3.3.1	Color weight	34
3.3.3.2	Texture weight	36
3.4	Graph Partitioning	37
3.4.1	Graph-based Image Segmentation Problem	38
3.4.2	Image Graph Labeling Problem	38
3.5	Graph Partitioning Approaches	39
3.5.1	Graph Cuts: energy-based method	39
3.5.1.1	Binary labeling	39
3.5.1.2	Extension to multi-label problems	41
3.5.1.3	Graph Cuts from perspective of energy minimization	42
3.5.1.4	Seed selection	45
3.5.1.5	Weakness	45

3.5.1.6	Graph Cuts in applications	47
3.5.2	Normalized Cuts	47
3.5.2.1	Basic concepts and theory	47
3.5.2.2	Computing NCut by eigen-value decomposition	49
3.5.2.3	The grouping algorithm description	50
3.5.2.4	Multiclass cuts of general <i>weighted</i> graph	50
3.5.2.5	Normalized Cuts in applications	51
3.5.3	Kernel Based Multilevel Graph Clustering Algorithms	52
3.5.3.1	The standard k -means clustering algorithm	52
3.5.3.2	Kernel k -means	53
3.5.3.3	Weighted kernel k -means	54
3.5.3.4	Multilevel weighted kernel k -means algorithm	55
3.5.3.5	Kernel k -means in applications	58
3.6	Illustrations of Graph Partitioning	58
3.7	Conclusions	60
4	Bag-of-Bags of Words Model	71
4.1	Overview of the Bag-of-Bags of Words Model	71
4.1.1	Feature Extraction	72
4.1.2	Graph Construction	73
4.1.3	Irregular Subgraphs	74
4.1.4	Bag-of-Bags of Words Description	74
4.2	(Dis-)Similarity Measurement between Histograms	75
4.3	<i>BBoW</i> on Single Level for Image Retrieval	77
4.3.1	Co-occurrence Criteria	78
4.3.2	Weighted Bipartite Graph Matching	79
4.4	Summary of the <i>BBoW</i> model for CBIR	82
4.5	Discussion and Conclusion	83
5	Irregular Pyramid Matching	85
5.1	<i>BBoW</i> on Pyramid Level	85
5.1.1	Graph Partitioning Scheme	85
5.1.2	Irregular Pyramid Matching	86
5.2	<i>BBoW</i> on Pyramid Levels for Image Retrieval	86

CONTENTS

5.2.1	Similarity Measure	87
5.2.2	Global Algorithm for Image Retrieval with BBoW model	87
5.3	Discussion and Conclusion	88
6	Results and Discussion	91
6.1	Image Datasets	91
6.2	Experimental Settings	93
6.2.1	Experimental Settings on <i>SIVAL</i>	94
6.2.2	Experimental Settings on <i>Caltech-101</i>	95
6.2.3	Experimental Settings on <i>PPMI</i>	95
6.3	Evaluation Metrics	95
6.3.1	Performance Measures for Image Retrieval	95
6.3.2	Partition Precision (PP)	97
6.4	Comparison of Co-occurrence Measures for Image Matching in the <i>BBoW</i> Model	98
6.5	Parameters Evaluation	102
6.5.1	Patch Size and Contribution of Color Term	102
6.5.2	Influence of Texture Term	103
6.6	Influence of Neighbourhood Systems	103
6.7	Influence of Distance Metric for Histogram Comparison	105
6.8	Irregular Graph Representation versus SPM for Image Retrieval	106
6.9	Partition Analysis	109
6.9.1	Stability of Graph Partitions	109
6.9.2	Quality of Subgraphs Matching	114
6.10	Conclusion	118
7	Conclusion and Perspectives	119
7.1	Summary of the Work in this Dissertation	119
7.2	Future Work	121
7.2.1	Objective Functions in Edges Weights	121
7.2.2	Improving Segmentation Methods	121
7.2.3	Fusion across Graph Partitions	121
7.2.4	Applications of the <i>BBoW</i> Model	122
Appendix A	Experimental Results in <i>SIVAL</i>	123

Appendix B	Experimental Results in <i>Caltech-101</i>	129
Appendix C	Experimental Results in <i>PPMI</i>	147
Appendix D	Proofs	151
Appendix E	Statistical Test	153
E.1	Paired samples t -interval	153
E.2	Matched Paired t -test	153
E.2.1	Data preparation	154
E.3	Matched Paired t -test and interval	154
E.4	Measurement in theory	155
E.4.1	The limits of data in research	155
E.4.2	Sample size	155
E.4.3	Data preparation	156
E.4.4	The t distribution	157
E.4.5	p -value method	157
E.4.5.1	Basic of Hypothesis Testing	157
E.4.5.2	Level of significance	158
E.4.5.3	A very rough guideline	158
E.4.5.4	Summary	159
	References	161

Abstract

Image representation is a fundamental question for several computer vision tasks. The contributions discussed in this thesis extend the basic bag-of-words representations for the tasks of object recognition and image retrieval.

In the present thesis, we are interested in image description by structural graph descriptors. We propose a model, named *bag-of-bags of words* (BBoW), to address the problems of object recognition (for object search by similarity), and especially Content-Based Image Retrieval (CBIR) from image databases. The proposed BBoW model, is an approach based on *irregular* pyramid partitions over the image. An image is first represented as a connected graph of local features on a regular grid of pixels. Irregular partitions (subgraphs) of the image are further built by using graph partitioning methods. Each subgraph in the partition is then represented by its own signature. The BBoW model with the aid of graphs, extends the classical *bag-of-words* (BoW) model by embedding color homogeneity and limited spatial information through irregular partitions of an image.

Compared to existing methods for image retrieval, such as Spatial Pyramid Matching (SPM), the BBoW model does not assume that similar parts of a scene always appear at the same location in images of the same category. The extension of the proposed model to pyramid gives rise to a method we named *irregular pyramid matching* (IPM).

The experiments demonstrate the strength of our approach for image retrieval when the partitions are stable across an image category. The statistical analysis of subgraphs is fulfilled in the thesis. To validate our contributions, we report results on three related computer vision datasets for object recognition, (localized) content-based image retrieval and image indexing. The experimental results in a database of 13,044 general-purposed images demonstrate the efficiency and effectiveness of the proposed BBoW framework.

Keywords : Computer vision, Pattern recognition, Image analysis, Image segmentation, Graphs, Graph algorithms, Graph Cuts, Graph partitioning, Graph matching, Kernel k-means, Clustering.

Résumé

Dans cette thèse, nous nous intéressons à la recherche d'images similaires avec des descripteurs structurés par découpages d'images sur les graphes.

Nous proposons une nouvelle approche appelée “*bag-of-bags of words*” (BBoW) pour la recherche d'images par le contenu (CBIR). Il s'agit d'une extension du modèle classique dit sac-de-mots (bag of words - BoW). Dans notre approche, une image est représentée par un graphe placé sur une grille régulière de pixels d'image. Les poids sur les arêtes dépendent de caractéristiques locales de couleur et texture. Le graphe est découpé en un nombre fixe de régions qui constituent une partition irrégulière de l'image. Enfin, chaque partition est représentée par sa propre signature suivant le même schéma que le BoW. Une image est donc décrite par un ensemble de signatures qui sont ensuite combinées pour la recherche d'images similaires dans une base de données. Contrairement aux méthodes existantes telles que Spatial Pyramid Matching (SPM), le modèle BBoW proposé ne repose pas sur l'hypothèse que des parties similaires d'une scène apparaissent toujours au même endroit dans des images d'une même catégorie. L'extension de cette méthode à une approche multi-échelle, appelée Irregular Pyramid Matching (IPM), est également décrite. Les résultats montrent la qualité de notre approche lorsque les partitions obtenues sont stables au sein d'une même catégorie d'images. Une analyse statistique est menée pour définir concrètement la notion de partition stable.

Nous donnons nos résultats sur des bases de données pour la reconnaissance d'objets, d'indexation et de recherche d'images par le contenu afin de montrer le caractère général de nos contributions.

Mots-clés : Vision par ordinateur, Reconnaissance de formes, Analyse d'Image, Segmentation d'Images, Graphes, Algorithmes de graphes, Coupe de graphes, Partitionnement de graphe, Appariement de graphes, Noyau k-means, Clustering.

This thesis is dedicated to my parents

Ren XianLiang and Ji XueLan

who have been offering me unconditional love and support from birth ...

Acknowledgements

I would firstly like to thank my two supervisors: Dr. Aurélie BUGEAU and Dr. Jenny BENOIS-PINEAU, for their company over the past three years of Ph.D program as I moved from an idea to a completed study.

I offer my sincere appreciation for the learning opportunities provided by my thesis jury composed of: Dr. Bernard Merialdo, Dr. Philippe-Henri GosseLin, Dr. Alan Hanjalic, Dr. Luc Brun, Dr. Pascal Desbarats. Their pertinent advice helps to polish both this manuscript and presentation of my Ph.D viva voce. In particular, I thank the reviewers, Professor Bernard Merialdo and Professor Philippe-Henri GosseLin for proofreading the thesis; their remarks inspired me to adopt statistical test as more convincing measurement for experiments validation.

I would like to express my deepest gratitude to Dr. Kaninda Musumbu, Dr. Stefka Gueorguieva, Dr. Pascal Desbarats, Dr. Nicolas Hanusse, Dr. Pascal Weil in my laboratory LaBRI: their encouragement when the times got rough are much appreciated and duly noted.

I would also like to thank all my teachers in University of Caen, for generously sharing their time, ideas and dedications during my studies in Master. All valuable knowledge they have taught me built my solid foundation in this domain and contribute what I am today...

This Ph.D research program was supported by CNRS (Centre national de la recherche scientifique) of France & Region of Aquitaine Grant.

List of Figures

2.1	An example of image descriptor components. The similarities or distances between images are based on the similarities or distances between the image feature vectors being extracted. Different types of feature vectors may require different similarity functions. Furthermore, different similarity/distance functions can be applied to the same feature set. The figure is excerpted from Penatti et al.[1].	7
2.2	The major stages for extracting SIFT features. (a) Scale-space extrema detection. (b) Orientation assignment. (c) Keypoint descriptor. The figures are extracted from Lowe's paper [2].	8
2.3	An example of local binary pattern codes. Take value (5) of the center pixel, and threshold the values of its neighbors against it. The obtained value (00010011) is called LBP code.	14
2.4	An overview of the many facets of image retrieval as field of research. The figures are extracted from Dattas paper [3].	18
2.5	The <i>Bag of Words</i> model. The left-most picture illustrates the <i>Bag of Words</i> in <i>document</i> . Other pictures show the <i>Bag of Visual Words</i> in <i>image</i> . These pictures are excerpted from the source of S.Lazebnik. ¹	20
2.6	The Bag-of-Visual Words (BoVW) image representation. The figure is from the source of S.Lazebnik. ²	21

LIST OF FIGURES

2.7	An example of constructing a three-level pyramid. The image has three feature types, indicated by circles, diamonds, and crosses. At the top, the SPM method subdivides the image at three different levels of resolution. Next, for each level of resolution and each grid cell, SPM counts the features that fall in each spatial bin. Finally, SPM weights each spatial histogram according to Equation (2.17). The figure is excerpted from Lazebnik et al. [4].	22
2.8	An example of superpixels. (a) Input image. (b) A “superpixel” map with 200 superpixels via Normalized Cuts algorithm [5]. The figure is excerpted from Mori et al. [6].	23
2.9	A hierarchy of “nested” Graph Words on four layers (on the left) in the same example of image (on the right). Seed is marked as hollow circle in white color, and neighbour nodes are shown as solid circles in black color. The figures are extracted from [7].	28
3.1	An overview of the processing chain for the proposed image graph model. (I) Image is represented by an initial weighted graph. (II) Graph partitioning consists in finding the optimal labeling for each graph nodes. (III) Find the best bipartite matched subgraphs between images pairs (IV) Retrieve images based on signatures that define the similarities between these subgraphs.	30
3.2	Graph construction. (a) Initial SURF keypoints. (b) Filtered keypoints. (c) Seeds selection. (d) Delaunay triangulation over filtered feature points. (e) Graph-cuts result. (f) Labeling result.	32
3.3	Options for the neighbourhood system of image graph.	33
3.4	Block DCT on 8×8 pixel patch.	36
3.5	A block of 8×8 pixel on DCT, the solid dot in black denotes the graph node, the 64 DCT coefficients are scanned in a “zig-zag” fashion.	36
3.6	The DCT (Discrete Cosine Transform) block is scanned in a diagonal zigzag pattern starting at the DC coefficient $d(0,0)$ to produce a list of quantized coefficient values. Here only five AC coefficients $d(1,0)$, $d(0,1)$, $d(0,2)$, $d(1,1)$, $d(2,0)$ in luma (Y') component of YUV system are considered due to their good discriminative properties. . . .	37

3.7	An example of binary labeling on an image graph via Graph Cuts. The graph corresponds to an image that consists of a 3×3 pixels set \mathcal{P} , with observed color intensities I_p in certain color space for each $p \in \mathcal{P}$. Given binary labels $L = \{0, 1\}$, an optimal labeling \mathcal{L} assigns label $l_p \in L$ to each pixel p . One part of this image is excerpted from [8].	40
3.8	Example of α - β swap and α -expansion. (a) initial labeling: α in red, β in green, γ in blue. (b) α - β swap: only number of pixels with label α or β change their labels, pixels with label γ remain unchanged. (c) α -expansion: pixels with different labels can change their labels simultaneously. The figures are excerpted from [9]. This figure is better viewed in <i>color</i>	42
3.9	Seed points are in hollow circle of different colors. The graph nodes are in red solid points.	45
3.10	Examples of seeds selection in prominent keypoints approach. The stability of seeds is hardly reached due to the uncontrolled nature of the images available. All examples of images are from <i>SIVAL</i> dataset [10]. There are three seeds in each image, and these seeds are labelled with their own colors (in red, orange and yellow). This figure is better viewed in <i>color</i>	46
3.11	An overview of the kernel-based multilevel algorithm for graph clustering proposed by Dhillon et al. [11], here $K = 6$. A part of this image is excerpted from [12].	56
3.12	Examples of graph partitioning in 4 irregular subgraphs on five examples in category “ <i>accordion</i> ” from Caltech-101 dataset by three methods: Graph Cuts (GC), Normalized Cut (NC), kernel k -means (KKM). This figure is better viewed in <i>color</i>	59
3.13	Examples of graph partitioning in 4 irregular subgraphs on five examples in category “ <i>faces</i> ” from Caltech-101 dataset by three methods: Graph Cuts (GC), Normalized Cut (NC), kernel k -means (KKM). This figure is better viewed in <i>color</i>	60
3.14	Examples of graph partitioning in 4 irregular subgraphs on five examples in category “ <i>pagoda</i> ” from Caltech-101 dataset by three methods: Graph Cuts (GC), Normalized Cut (NC), kernel k -means (KKM). This figure is better viewed in <i>color</i>	61

LIST OF FIGURES

3.15	Examples of graph partitioning in 4 irregular subgraphs on five examples in category “ <i>trilobite</i> ” from Caltech-101 dataset by three methods: Graph Cuts (GC), Normalized Cut (NC), kernel k -means (KKM). This figure is better viewed in <i>color</i>	62
3.16	Examples of graph partitioning in 4 irregular subgraphs on five examples in category “ <i>cellphone</i> ” from Caltech-101 dataset by three methods: Graph Cuts (GC), Normalized Cut (NC), kernel k -means (KKM). This figure is better viewed in <i>color</i>	63
3.17	Examples of graph partitioning in 4 irregular subgraphs on five examples in category “ <i>motorbikes</i> ” from Caltech-101 dataset by three methods: Graph Cuts (GC), Normalized Cut (NC), kernel k -means (KKM). This figure is better viewed in <i>color</i>	64
3.18	Examples of graph partitioning in 16 irregular subgraphs on five examples in category “ <i>accordion</i> ” from Caltech-101 dataset by three methods: Graph Cuts (GC), Normalized Cut (NC), kernel k -means (KKM). This figure is better viewed in <i>color</i>	65
3.19	Examples of graph partitioning in 16 irregular subgraphs on five examples in category “ <i>faces</i> ” from Caltech-101 dataset by three methods: Graph Cuts (GC), Normalized Cut (NC), kernel k -means (KKM). This figure is better viewed in <i>color</i>	66
3.20	Examples of graph partitioning in 16 irregular subgraphs on five examples in category “ <i>pagoda</i> ” from Caltech-101 dataset by three methods: Graph Cuts (GC), Normalized Cut (NC), kernel k -means (KKM). This figure is better viewed in <i>color</i>	67
3.21	Examples of graph partitioning in 16 irregular subgraphs on five examples in category “ <i>trilobite</i> ” from Caltech-101 dataset by three methods: Graph Cuts (GC), Normalized Cut (NC), kernel k -means (KKM). This figure is better viewed in <i>color</i>	68
3.22	Examples of graph partitioning in 16 irregular subgraphs on five examples in category “ <i>cellphone</i> ” from Caltech-101 dataset by three methods: Graph Cuts (GC), Normalized Cut (NC), kernel k -means (KKM). This figure is better viewed in <i>color</i>	69

3.23	Examples of graph partitioning in 16 irregular subgraphs on five examples in category “motorbikes” from Caltech-101 dataset by three methods: Graph Cuts (GC), Normalized Cut (NC), kernel k -means (KKM). This figure is better viewed in <i>color</i>	70
4.1	The diagram of construction of Bag-of-Bags of Words model.	72
4.2	The dense points sampling approach in <i>BBoW</i> model.	73
4.3	The obtained irregular subgraphs via graph partitioning.	75
4.4	The “Bag-of-Bags of Words” description.	76
4.5	Examples of image graph partitions from category ‘accordion’ in <i>Caltech-101</i> dataset. The partitions of 4 subgraphs are visible in the first row of the figure. The second row of the figure shows 16 subgraphs in the partitioning. The nodes in each subgraph are labelled with the same <i>color</i> . This figure is better viewed in <i>color</i>	80
4.6	Find optimal subgraph matching via <i>Hungarian algorithm</i>	82
4.7	An optimal assignment for a given cost matrix.	82
4.8	The process of CBIR from database in <i>BBoW</i> model.	82
5.1	A schematic illustration of the <i>BBoW</i> representation at each level of the pyramid. At level 0, the decomposition has a single graph, and the representation is equivalent to the classical <i>BoW</i> . At level 1, the image is subdivided into four subgraphs, leading to four features histograms, and so on. Each subgraph is represented by its own color in this figure. This figure is better viewed in <i>color</i>	86
5.2	The comparison of partitioning scheme between SPM and <i>BBoW</i> . At the left side of the figure shows the partitioning scheme of Spatial Pyramid Matching (SPM). At the right side of the figure illustrates the partitioning scheme of the <i>BBoW</i> . Contrary to SPM with nested regular partitions, our partitions are irregular and independent at each level. We keep the same resolution of the image across multilevel. This figure is better viewed in <i>color</i>	89
6.1	Example images from the <i>SIVAL</i> database.	92
6.2	A snapshot of images from <i>Caltech-101</i>	93
6.3	A snapshot of images from <i>PPMI+</i> of the <i>PPMI</i> dataset that contains a person playing the instrument.	93

LIST OF FIGURES

6.4	Comparison of a series of image similarity measures.	99
6.5	Comparison between BoW and <i>BBoW</i> on SIVAL benchmark. (a) The precision-recall curve for a “good” category : “stripednotebook”. (b) The precision-recall curve for a “bad” category : “banana”. (c) Graph descriptors from “stripednotebook”. (d) Graph descriptors from “banana”.	100
6.6	Two examples of graph partitioning via Graph Cuts. The first row shows result of image ‘AjaxOrange079.jpg’, the second row is result of image ‘Ajax-Orange049.jpg’. Both of images are from category “AjaxOrange” in SIVAL dataset. (a)(d) Seeds. (b)(e) Initial image graph with chosen seeds. (c)(f) Labeling result.	101
6.7	An example of image graph partitions on the image <i>minaret0032.jpg</i> from <i>Caltech-101</i> dataset, when joint color-texture is embedded in edge weights. The 1th - 4th columns correspond to graph partitions by setting $\alpha = 0, 0.5, 0.8, 1$ in Equation (E.1) severally. The first row of this figure shows the results of partitions at resolution $r = 1$, where each image is composed of 4 subgraphs. The second row corresponds to 16 partitions at resolution $r = 2$, <i>i.e.</i> 16 subgraphs per image. This figure is better viewed in <i>color</i>	104
6.8	Example of graph partitions of two images as texture factor is considered in edge weights under different neighbourhood systems. This figure is better viewed in <i>color</i>	105
6.9	The margin of mean Average Precision (mAP) for not surpassing categories in <i>Caltech-101</i> dataset. The margin = $\frac{mAP(SPM)-mAP(KKM)}{mAP(KKM)}\%$	108
6.10	Mean Average Precision for surpassing categories in <i>Caltech-101</i> dataset.	108
6.11	The mean Average Precision for 16 typical categories in Caltech101	109
6.12	The first row shows the 4 irregular subgraphs from “good” query images at level 1. The second row shows the 4 irregular subgraphs from “bad” query images at level 1. The nodes of individual subgraphs are labelled with the same color (in red, blue, green, brown). This figure is better viewed in <i>color</i> . . .	113
6.13	A case study of <i>BBoW</i> (via Normalized Cuts). The precision of 8 typical query images: 1st-4th query images are from a “good” category - <i>minaret</i> , 5th-8th query images are from “bad” categories: <i>cellphone</i> and <i>dollar_bill</i>	114

6.14	A case study of <i>BBoW</i> (via Graph Cuts). The precision of 8 typical query images: 1st-4th query images are from a “good” category - <i>minaret</i> , 5th-8th query images are from “bad” categories: <i>cellphone</i> and <i>dollar_bill</i>	115
6.15	A case study of <i>BBoW</i> (via Kernel <i>k</i> -means). The precision of 8 typical query images: 1st-4th query images are from a “good” category - <i>minaret</i> , 5th-8th query images are from “bad” categories: <i>cellphone</i> and <i>dollar_bill</i>	116
6.16	The mean and standard deviation of nodes’ numbers of corresponding subgraphs for intra-category, for 8 typical queries in <i>Caltech-101</i> dataset - at single level 1, <i>i.e.</i> 4 subgraphs.	117
A.1	The overall <i>Precision-Recall</i> curve for a comparison between BBoVW and BoVW in <i>SIVAL</i> dataset [10]. BBoVW: Bag-of-Bags of Visual Word. BoVW: Bag-of-Visual Words. Each image is composed of 4 subgraphs in BBoW. The dictionary of size 1000, as described in Section 6.2.1 of the Chapter 6, is learnt over 30 sample images per class using <i>k</i> -means. The query images are chosen from the rest of the <i>SIVAL</i> dataset for retrieval. In this figure, the red curve corresponds to application of co-occurrence measure defined in Equation (4.4) for image matching in the BBoW Model. The blue/red curve correspond to BoVW with/without points filtration.	124
A.2	A complete comparison of similarity measures by using co-occurrence criteria in BBoW, as defined in Section 4.3.1 of the Chapter 4. Each image is composed of 4 subgraphs. There are six curves in this figure: “Min Histogram Distances” with respect to Equation (4.4) (Curve 1), “Sum-of-mins Histogram Distances” with respect to Equation (4.5) (Curve 2), “Sum-of-maxima Histogram Distances” with respect to Equation (4.9) (Curve 3), “Sums of Histogram Distances” with respect to Equation (4.8) (Curve 4), “Sum-of-means Histogram Distances” with respect to Equation (4.6) (Curve 5), “Sum-of-medians Histogram Distances” with respect to Equation (4.7) (Curve 6). The Curve 4 and 5 are coincident.	125
A.3	The category-based <i>Precision-Recall</i> curve for 25 categories in <i>SIVAL</i> dataset. .	128
B.1	Retrieval results of image “ <i>faces0032</i> ”. This figure is better viewed in <i>color</i> . . .	140
B.2	Retrieval results of image “ <i>faces0036</i> ”. This figure is better viewed in <i>color</i> . . .	141
B.3	Retrieval results of image “ <i>faces0038</i> ”. This figure is better viewed in <i>color</i> . . .	142

LIST OF FIGURES

- B.4 Retrieval results of image “*faces0039*”. This figure is better viewed in *color*. . . 143
- B.5 Retrieval results of image “*faces0049*”. This figure is better viewed in *color*. . . 144
- B.6 The distribution of *average precision* values for query images in 19 surpassing classes + a category “*car_side*” that only contains grayscale images, on the whole *Caltech-101* dataset. The comparison is evaluated between SPM and *BBoW* (KKM) at level 1. Each image is partitioned into 4 subgraphs. 146

List of Tables

3.1	Examples of commonly used kernel functions.	54
6.1	The basic notions for information retrieval systems.	96
6.2	Influence of parameter λ (Equation (3.4)) on image retrieval. For each value, the mean average precision is given. For this experiment, the patch size is set to $n = 5$	102
6.3	Influence of parameter n (section 3.3.3.1) on image retrieval. For each value, the mean average precision is given. For this experiment, $\lambda = 5$	102
6.4	Evaluation of embedding joint color-texture energy in graph weights for image retrieval. Graph weights account for more color features as value of parameter α in Equation (E.1) increases. The mAPs are given for each single level and pyramid. The patch size is set to $n = 5$. $\lambda = 5$. The size of visual codebook is 400. By contrast, the mAP for SPM is 0.409	103
6.5	The influence of distance metrics to compute a cost matrix for graph matching via <i>Hungarian algorithm</i> . Note that the partitions are obtained by KKM. The experiments were run in <i>PPMI</i> dataset, and its settings have been described in Section 6.2.3.	105
6.6	The retrieval performance (mAP \pm standard deviation of APs) on <i>PPMI</i> dataset.	106
6.7	Retrieval performance on subset of <i>Caltech-101</i> dataset composed of 2945 query images and 5975 images from database for retrieval. We set $\alpha = 1$ in Equation (E.1), <i>i.e.</i> only consider color-related term w_{pq}^C in w_{pq} . A postscript: <i>SPM</i> wins <i>BBoW</i> (with <i>KKM</i>) by a small margin with a mAP value of 0.14 , versus 0.1327 for <i>KKM</i> , while <i>SPM</i> has higher <i>std</i> as value of 0.0660	107

LIST OF TABLES

6.8	The comparison of mAPs for <i>BBoW</i> (via GC) vs <i>BBoW</i> (via NCuts) vs <i>BBoW</i> (via KKM) vs SPM on 4 partitions of five examples of images from category “ <i>accordion</i> ”. See Figure 3.12.	111
6.9	The comparison of mAPs for <i>BBoW</i> (via GC) vs <i>BBoW</i> (via NCuts) vs <i>BBoW</i> (via KKM) vs SPM on 4 partitions of five examples of images from category “ <i>faces</i> ”. See Figure 3.13.	111
6.10	The comparison of mAPs for <i>BBoW</i> (via GC) vs <i>BBoW</i> (via NCuts) vs <i>BBoW</i> (via KKM) vs SPM on 4 partitions of five examples of images from category “ <i>pagoda</i> ”. See Figure 3.14.	111
6.11	The comparison of mAPs for <i>BBoW</i> (via GC) vs <i>BBoW</i> (via NCuts) vs <i>BBoW</i> (via KKM) vs SPM on 4 partitions of five examples of images from category “ <i>trilobite</i> ”. See Figure 3.15.	112
6.12	The comparison of mAPs for <i>BBoW</i> (via GC) vs <i>BBoW</i> (via NCuts) vs <i>BBoW</i> (via KKM) vs SPM on 4 partitions of five examples of images from category “ <i>cellphone</i> ”. See Figure 3.16.	112
6.13	The comparison of mAPs for <i>BBoW</i> (via GC) vs <i>BBoW</i> (via NCuts) vs <i>BBoW</i> (via KKM) vs SPM on 4 partitions of five examples of images from category “ <i>motorbikes</i> ”. See Figure 3.17.	112
6.14	The $PP \{Precision(\Gamma_j^k)\}_{k=1,2,3,4} = \{P(g_{j,k})\}_{k=1,2,3,4}$ of corresponding subgraphs for 4 typical “good” queries. Method: <i>BBoW</i> via Normalized Cut.	115
6.15	The $PP \{Precision(\Gamma_j^k)\}_{k=1,2,3,4} = \{P(g_{j,k})\}_{k=1,2,3,4}$ of corresponding subgraphs for 4 typical “bad” queries. Method: <i>BBoW</i> via Normalized Cut.	116
6.16	The mean of node numbers and its standard deviation for corresponding matched subgraphs of intra-category minaret, for 4 typical good queries in <i>Caltech-101</i> dataset, at single level 1, <i>i.e.</i> 4 subgraphs. Method: <i>BBoW</i> via Normalized Cut.	117
6.17	The mean of node numbers and its standard deviation for corresponding matched subgraphs of intra-category cellphone and dollar_bill, for 4 typical bad queries in <i>Caltech-101</i> dataset, at single level 1, <i>i.e.</i> 4 subgraphs. Method: <i>BBoW</i> via Normalized Cut.	117
6.18	The $\{P(g_{j,k})\}_{k=1,\dots,4}$ of corresponding subgraphs for 4 typical “good” queries. Method: <i>BBoW</i> via Normalized Cut.	118
6.19	The $\{P(g_{j,k})\}_{k=1,\dots,4}$ of corresponding subgraphs for 4 typical “bad” queries. Method: <i>BBoW</i> via Normalized Cut.	118

A.1	The <i>precision-recall</i> values of experimental results, as complementary information of Figure A.2. The experiments were run in <i>SIVAL</i> dataset with the aim of comparing a series of similarity measures (co-occurrence criteria) versus the classical bag-of-words model for image retrieval. The first column lists recall values ranging from 0 to 1.0 of 11 intervals. The 2nd-8th columns correspond to the precision values for seven different measures. They are (1) Bag-of-Words (BoW), without filtering points in graph nodes selection; (2) BoW, select graph nodes by points filtration; (3) Bag-of-Bag-of-Visual-Words (BBoVW), using Equation (4.4); (4) BBoVW, using Equation (4.5); (5) BBoVW, using Equation (4.6) or its equivalent by using Equation (4.8); (6) BBoVW, using Equation (4.7); (7) BBoVW, using Equation (4.9) respectively.	126
B.1	KKM versus SPM at single level 1 (4 partitions per image). Performance is measured by calculating the <i>mean Average Precision</i> (mAP) for category-based queries. In addition, the <i>mean</i> of <i>Standard deviation</i> (Std) of <i>Average Precisions</i> (APs) for category-based queries is given. The class names of 20 surpassing categories in which BBoW outperforms SPM are in bold in this table.	130
B.2	Evaluation of BBoW via KKM in <i>Caltech-101</i> dataset. Retrieval performance was evaluated in <i>mean Average Precision</i> (mAP) on subset of <i>Caltech-101</i> dataset composed of 2945 query images and 5975 images from database for retrieval. The size of codebook is 400.	134
B.3	Evaluation of BBoW (via GC) vs BBoW (via NCuts) vs SPM in <i>Caltech-101</i> dataset. Retrieval performance was evaluated in <i>mean Average Precision</i> (mAP) on subset of <i>Caltech-101</i> dataset composed of 2945 query images and 5975 images from database for retrieval. The size of codebook is 400. The highest results for each kind of level are shown in bold.	134
B.4	Retrieval result of image <i>faces0032</i> . There are 5975 images from a subset of <i>Caltech-101</i> dataset for retrieval. Each image is partitioned into 4 subgraphs. The file extension of each image is omitted. The size of codebook is 400. . . .	135
B.5	Retrieval result of image <i>faces0036</i> . There are 5975 images from a subset of <i>Caltech-101</i> dataset for retrieval. Each image is partitioned into 4 subgraphs. The file extension of each image is omitted. The size of codebook is 400. . . .	136

LIST OF TABLES

B.6	Retrieval result of image <i>faces0038</i> . There are 5975 images from a subset of <i>Caltech-101</i> dataset for retrieval. Each image is partitioned into 4 subgraphs. The file extension of each image is omitted. The size of codebook is 400. . . .	137
B.7	Retrieval result of image <i>faces0039</i> . There are 5975 images from a subset of <i>Caltech-101</i> dataset for retrieval. Each image is partitioned into 4 subgraphs. The file extension of each image is omitted. The size of codebook is 400. . . .	138
B.8	Retrieval result of image <i>faces0049</i> . There are 5975 images from a subset of <i>Caltech-101</i> dataset for retrieval. Each image is partitioned into 4 subgraphs. The file extension of each image is omitted. The size of codebook is 400. . . .	139
C.1	The retrieval performance (mAP) on <i>PPMI</i> dataset, using <i>L1</i> distance as cost matrix value for graph matching via <i>Hungarian algorithm</i>	148
C.2	The retrieval performance (mAP) on <i>PPMI</i> dataset, using <i>L2</i> distance as cost matrix value for graph matching <i>Hungarian algorithm</i>	149

List of Algorithms

1	Max-flow/Min-cut Algorithm	41
2	Graph clustering by weighted kernel k-means	55
3	Graph clustering in coarsening phase	57
4	Image comparison via the co-occurrence criteria	79
5	Image comparison via <i>Hungarian algorithm</i> to reorganize histograms	83

GLOSSARY

Glossary

$[X, Y]^T$	A set of the corresponding coordinates for a set of feature points or pixels of an image \mathcal{P}
ν_I	A feature vector or descriptor
$C = \{C_1, \dots, C_B\}$	A codebook or visual dictionary of size B
I	A unit matrix with ones on the main diagonal and zeros elsewhere
L	A set of labels
P	An optimal partition of an image graph
$\delta()$	Kronecker's delta
$\Gamma_j^K = \{\Gamma_j^k\}_{k=1, \dots, K} = \{g_j^1, \dots, g_j^K\}$	K -way partitioning for Image I_j
κ	A kernel function
\mathcal{K}	A kernel matrix
\mathcal{P}_l	A subset of graph nodes assigned label l in an image graph
\mathbb{Z}^*	The set of non-negative integers
Ω	Image database
π_k	The k -th cluster for the clustering $\{\pi_k\}_{k=1}^K$
ρ	Rank
$\{\pi_k\}_{k=1}^K$	A clustering with k clusters
$\{g_{j,k}\}_{k=1, \dots, K}$	The subgraphs in image I_j on single level of graph partitions
$\{g_{j,k}^r\}_{k=1, \dots, K_r}$	The subgraphs in image I_j at resolution r on pyramid level of graph partitions
$\{a_i\}_{i=1}^N$	A set of vectors that the k -means algorithm seeks to cluster
B	The number of bins in codebook
G	Graph

GLOSSARY

G_j	An undirected weighted graph constructed on the image I_j
$I(p)$	The color vector at point p
$I^c(p)$	The intensity of a node or pixel p in color channel c
I_i, I_j	Images
K	The number of clusters
K_r	The fixed number of subgraphs at resolution r of graph partitions
p, q	Nodes in a graph, or pixels in an image
R	The resolution of a pyramidal partition
S	A set of seeds
x_p, y_p	The intrinsic coordinates (x,y) of the node or the pixel p
$\bar{I}_{n \times n}(p)$	mean color vector at point p (over a $n \times n$ patch)
$\mathcal{N}(p)$	The neighbourhood of p
\mathcal{L}	An optimal joint labeling
\mathcal{P}	A set of feature points or pixels of an image
E_j	Graph edges of image I_j
V_j	A set of vertices of image I_j
BoF	Bags of Features
CBIR	Content-Based Image Retrieval, also known as query by image content (QBIC) and content-based visual information retrieval (CBVIR), is the application of computer vision techniques to the image retrieval problem, that is, the problem of searching for digital images in large databases.
Gram matrix	A matrix $G = V^T V$, where V is a matrix whose column are the vectors v_k .
HA	Hard Assignment
ISM	Implicit Shape Model [13]
mAP	mean Average Precision
metric	A metric on a set X is a function $d : X \times X \rightarrow \mathbb{R}$ that is required to satisfy conditions of non-negativity, identity, symmetry and sub additivity.
RGB	Red, Green, Blue color space
ROC	Receiver Operating Characteristic

ROI Region of Interest

SA Soft Assignment

Segmentation In computer vision, segmentation refers to the process of partitioning a digital image into multiple segments (sets of pixels).

Semi-supervised Learning In computer science, semi-supervised learning is a class of machine learning techniques that make use of both labelled and unlabelled data for training - typically a small amount of labelled data with a large amount of unlabelled data.

SIFT Scale-invariant feature transform (SIFT) is an algorithm in computer vision to detect and describe local features in images. The algorithm was published by David Lowe in 1999.

SPM Spatial Pyramid Matching

SURF Speeded Up Robust Features, which is a robust local feature detector, proposed by Herbert Bay et al. in 2006

SVM Support Vector Machine

YUV Color space, which is composed of luma (Y') and two chrominance (U,V) components.

GLOSSARY

Chapter 1

Introduction

Object detection and recognition remain outstanding problems for which there is no off-the-shelf solution, despite a vast amount of literature on the subject. The problem is challenging since characterizing the appearance of an object does not only involve the object itself but also extrinsic factors such as illumination, relative position or even cluttered background in the target image. Currently, object detection and recognition are typically considered as “retrieval” task over a database of images, where content-based image retrieval is one of the core problems.

Content Based Image Retrieval (CBIR), as its name implies, consists in browsing, searching and navigation of images from image databases based on their visual contents. CBIR has been an active area of research for more than a decade. Traditional CBIR systems use low level features like color, texture, shape and spatial location of objects to index and retrieve images from databases. Low level features can be global or local (region based). Global feature based CBIR fails to compare the regions or objects in which a user may be interested. Therefore Region Based Image Retrieval (RBIR) is more effective in reflecting the user requirement. A detailed survey of CBIR techniques can be found in the literature [3, 14, 15].

Recent methods in Content-Based Image Retrieval (CBIR) mostly rely on the bag-of-visual-words (BoW) model [16]. The idea, borrowed from document processing, is to build a visual codebook from all the feature points in a training image dataset. Each image is then represented by a signature, which is a histogram of quantized visual features-words from the codebook. Image features are thus considered as independent and orderless. The traditional BoW model does not embed spatial layout of local features in the image signature. However, this information has shown to be very useful in tasks like image retrieval, image classification, and video indexing. Ren et al. [17] put forward a concept of grouping pixels into “superpixels”.

1. INTRODUCTION

Leibe et al. proposed to adopt codebooks to vote for object position [13]. Birchfield et al. [18] introduced the concept of a spatiogram, which generalizes the histogram to allow higher-order spatial moments to be part of the descriptor. Agarwal et al. [19] proposed “hyperfeatures”, a multilevel local coding. More specifically, hyperfeatures are based on local histogram model encoding co-occurrence statistics within each local neighborhood on multilevel image representations. Lazebnik et al. [4] partitioned an image into increasingly fine grids and computed histograms for each grid cell. The resulting spatial pyramid matching (SPM) method clearly improves the BoW representation. Nevertheless, this method relies on the assumption that a similar part of a scene generally appears at the same position across different images, which does not always hold. Recently, many efforts can be found in the literature, e.g. the Fisher vectors etc. [20, 21] that compete with SPM to give extensions of bag-of-words image representations to encode spatial layout.

Graphs are versatile tools to conveniently represent patterns in computer vision applications and they have been vastly investigated. By representing images with graphs, measuring the similarities between images becomes equivalent to finding similar patterns inside series of attributed (sub)graphs representing them. Duchenne et al. [22] introduced an approximate algorithm based on graph-matching kernel for category-level image classification. Gibert et al. [23] proposed to apply graph embedding in vector spaces by node attribute statistics for classification. Bunke et al. [24] provided an overview of the structural and statistical pattern recognition, and elaborated some of these attempts, such as graph clustering, graph kernels and embedding etc., towards the unification of these two approaches.

1.1 Problems and Objectives

The thesis addresses issues of image representation for object recognition and categorization from images. Compared with the seminal work by Lazebnik et al. [4], we try to address a challenging question: will an irregular segmentation-like partition of images outperform a regular partition (SPM)? Intuitively, it is invariant to the rotation and reasonable shift transformations of image plane. Nevertheless, what can be its resistance to noise and occlusions? How will it compete with SPM when embedded into pyramidal paradigm?

1.2 Contributions

This thesis presents a new approach for Content-Based Image Retrieval (CBIR) that extends the bag-of-words (BoW) model. We aim at embedding joint color-texture homogeneity and limited spatial information through irregular partitioning of an image into a set of predefined number of (sub)graphs. Each partition results from applying graph partitioning methods to an initial connected graph, in which nodes are positioned on a dense regular grid of pixels. The BoW approach is then applied to each of resulting subgraphs independently. An image is finally represented by a set of graph signatures (BoWs), leading to our new representation called *Bag-of-Bags of Words (BBoW)*. As in the spatial pyramid matching approach [4], we also consider a pyramidal representation of images with a different number of (sub)graphs at each level of the pyramid. The comparison of images in a CBIR paradigm is achieved via comparison of the irregular pyramidal partitions. We call this pyramidal approach *Irregular Pyramid Matching (IPM)*.

1.3 Organization of the Thesis

The thesis is structured as follows:

Chapter 1 explains briefly the importance of the topic, the scope and objectives of these studies and our contributions.

Chapter 2 provides a review of the state-of-the-art.

In **Chapter 3**, the application of three typical approaches for semi-regular image graph partitioning is investigated. These methods will pertain to our proposed graph-based image representation in next Chapter.

The proposed *Bag-of-Bags of Words* model is described in **Chapter 4**. The **Chapter 5** extends this model to multi-levels, leading to an approach called *Irregular Pyramid Matching*.

Chapter 6 presents three standard datasets and experimental results on these benchmarks. We compare our results with those of the notable method Spatial Pyramid Matching (SPM), showing the promising performance of our approach.

Finally, we conclude the thesis with a discussion of the perspectives of future work in **Chapter 7**. Complementary results on three image benchmarks can be consulted in appendixes. At the end of the manuscript, a full list of the literature cited in the text is given. Wherever these

1. INTRODUCTION

references have been quoted, they have been cross-referred by their serial number in the list of references.

Chapter 2

Related Work

The primary purpose of this chapter is to provide a snapshot of the current state-of-the-art in image representation and its application to content-based image retrieval (CBIR), as the general context of the thesis. Particularly, as the present work relates closely to pattern recognition by using graphs and image representation, especially with regard to *Bag-of-Words model* and *Spatial Pyramid representation*, we elaborate on them so as to facilitate comparisons with these approaches in Chapter 6.

Firstly, we formulate basic concepts, present the image features, and give a comparative study of different types of image descriptors in terms of local, semi-local and global features. Secondly, a brief introduction of content-based image retrieval is presented. A few illustrative approaches for CBIR are further discussed in detail. Next, we highlight what is known about image features to emphasize these issues that are pertinent to CBIR. Thirdly, in the context of image representation, we introduce the bag-of-features (BoF) framework and its most popular variant the Bag-of-Words (BoW) model. Several typical extensions in pursuit of improving the basic BoW model are enumerated. The chapter concludes with a discussion of graphs as a tool for image representation in the literature. Finally we present the application of graphs to pattern recognition and image indexing, which prompts our proposed *Bag-of-Bags of Words* model in the thesis.

2.1 Image Descriptors

Both the effectiveness and the efficiency of content-based image and video retrieval systems are highly dependent on the image *descriptors* that are being used. The image descriptor is

2. RELATED WORK

responsible for characterizing the image visual content and for computing their similarities, making possible the ranking of images and videos based on their visual properties with regard to a query. In this section, we first formulate the important concepts mathematically. Then we provide a brief overview of the image descriptors. The present chapter only focuses on a few of the robust ones, particularly SIFT [2] and its variants.

2.1.1 Formalization

First of all, we formulate basic concepts before the discussion of image descriptors. We adopt the definitions of Torres et al. [25] in the following formalization.

An **image** I is a pair (\mathcal{P}, \vec{I}) , where

- \mathcal{P} is a finite set of pixels or points in \mathbb{N}^2 , that is, $\mathcal{P} \subset \mathbb{N}^2$,
- $\vec{I}: \mathcal{P} \rightarrow \mathbb{R}^n$ is a function that assigns a vector $\vec{I}(p) \in \mathbb{R}^n$ to each pixel $p \in \mathcal{P}$.

For example, let us denote the coordinates of a pixel p by $p = (x_p, y_p)$, then $\vec{I}(p) = (p_r, p_g, p_b) \in \mathbb{R}^3$ if a color is assigned to the pixel $p \in \mathcal{P}$ in the RGB system.

A **feature vector** ν_I of an image I is defined as a n -dimensional point in \mathbb{R}^n space:

$$\nu_I = (v_1, \dots, v_n)^\top \quad (2.1)$$

An **image descriptor** (or **visual descriptor**) D can be defined as a pair (ϵ_D, δ_D) , where ϵ_D is a feature-extraction algorithm and δ_D is a suitable function for comparing the feature vectors generated from ϵ_D . As illustrated in Figure 2.1,

- ϵ_D encodes image visual properties (e.g. color, texture, shape and spatial relationship of objects) into feature vectors.
- $\delta_D: \mathbb{R}^n \times \mathbb{R}^n \rightarrow \mathbb{R}$ is a *similarity (or distance) function* (e.g. based on a metric) that computes the similarity of the feature vectors between two images (or the distance between their corresponding *feature vectors*, as the opposite).

The examples of possible feature vectors will be discussed in Section 2.1.2.

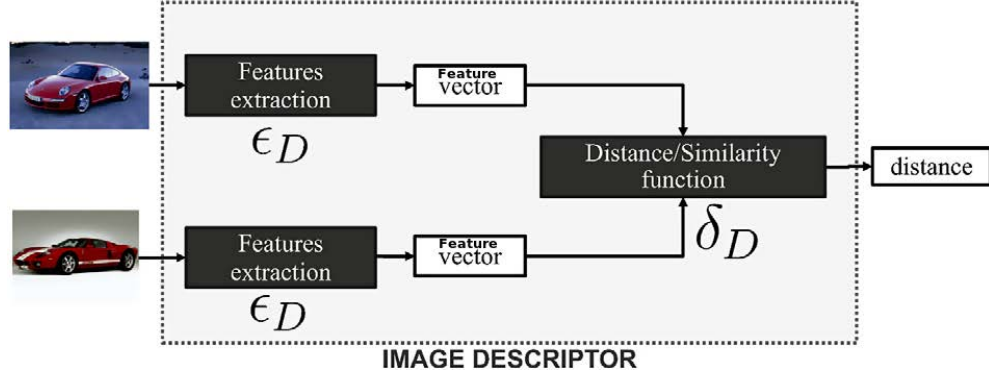


Figure 2.1: An example of image descriptor components. The similarities or distances between images are based on the similarities or distances between the image feature vectors being extracted. Different types of feature vectors may require different similarity functions. Furthermore, different similarity/distance functions can be applied to the same feature set. The figure is excerpted from Penatti et al.[1].

2.1.2 Image Feature Detection

There are many feature detection methods: interest point detection [26], edge detection [27], corner detection [28], blob detection [29, 30] etc. Each method has its own (dis)advantage. The most important image features are the localized features, which are often described by the appearance of *patches* of pixels around the specific point location. A few of examples are *keypoint features* or *interest points* and *corners*.

2.1.3 Image Feature Extraction and Description

Feature-extraction algorithm ϵ_D is used to quantize image feature(s) into feature vector(s). According to different feature extraction algorithms, the generated image descriptor(s) can be either local or semi-local or even global.

An ϵ_D can produce either a single feature vector or a set of feature vectors. In the former case, when a single feature vector must capture the entire information of the visual content, we say that it is a *global descriptor*. In the latter case, a set of feature vectors is associated with different features of the visual content (regions, edges, or small patches around points of interest). We call it *local descriptor*.

The image descriptors can also be divided into several types based on image visual properties such as color, texture, shape, location etc. Three main types are: 1) color descriptors; 2) texture descriptors; 3) shape descriptors.

2. RELATED WORK

In the following sections, we provide a brief overview of these image descriptors.

2.1.4 Local Image Descriptors

Local features have received the most attention in the recent years. The main idea is to focus on the areas containing the most discriminative information. In particular, the descriptors are generally computed around the interest points of the image. Therefore, they are often associated to an interest point detector. A good local descriptor should be invariant to the lightening changes and geometric changes such as rotation, translation, scaling typically. In the following section, we briefly present some typical local image descriptors. For each enumerated descriptor, we give it an acronym in the subsection title.

SIFT *Scale Invariant Feature Transform (SIFT)*, proposed by Lowe [31], has been designed to match different images or objects of a scene. It has unique advantages: largely invariant to changes in scale, illumination, noise, rotation, 3D camera viewpoint (i.e., the same keypoint in different images maps to similar representations) etc., and partially invariant to local affine distortions. Due to its strong stability and these invariance characteristics, SIFT has become the most popular local feature description so far.

As described in [2], there are four major stages for extracting SIFT features: 1) scale-space extrema detection; 2) keypoint localization; 3) orientation assignment; 4) and keypoint descriptor. An illustration is shown in Figure 2.2.

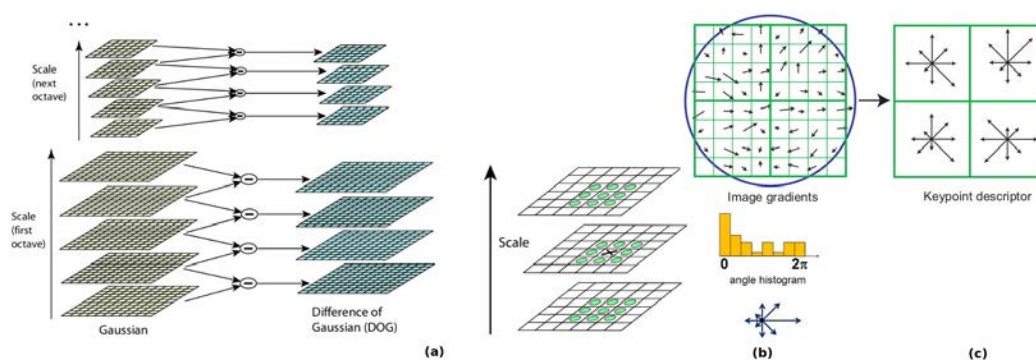


Figure 2.2: The major stages for extracting SIFT features. (a) Scale-space extrema detection. (b) Orientation assignment. (c) Keypoint descriptor. The figures are extracted from Lowe’s paper [2].

First, a DoG (Difference of Gaussian) pyramid is built by convolving the image with a variable-scale Gaussian. Interest points for SIFT features correspond to local extrema of these

DoG images. After that, low contrast and unstable edge points are eliminated from candidate keypoints, interference points are further removed using 2×2 Hessian matrix that is obtained from adjacent difference images. Next, to determine the keypoint orientation, an orientation histogram is computed from the gradient orientations of sample points within $4 \times 4 = 16$ sub-regions (8 orientation bins in each) around the keypoint. The contribution of each neighbouring pixel is weighted by the gradient magnitude. Peaks in the histogram indicate the dominant orientations. Thereby, SIFT, corresponding to a set of orientation histograms, finally gets $4 \times 4 \times 8 = 128$ dimensional feature vector description from 16 sub-regions, according to a certain order. This 128-element vector is then normalized to unit length to enhance invariance to illumination changes.

PCA-SIFT *Principal Component Analysis (PCA)* is a standard technique for dimensionality reduction. Ke et al. [32] proposed to use PCA to decorrelate SIFT components, compressing SIFT dimensions globally from 128 to 20 or even less. PCA-SIFT keeps unchanged the aforementioned first three stages for extracting SIFT features. It mainly contributes to the feature extraction stage. A $2 \times 39 \times 39 = 3042$ dimensional vector is created by concatenating two horizontal and vertical gradient maps from the 41×41 patch centered at the keypoint. Then a projection matrix is used to multiply with this vector, linearly projecting the vector to a low-dimensional feature space. As SIFT, the Euclidean distance is used to compare two feature vectors of PCA-SIFT.

RootSIFT Recently, a new version of SIFT was proposed by R.Arandjelović et A.Zisserman in [33], called RootSIFT. As its name implies, RootSIFT is an element wise square root of the $L1$ normalized SIFT vectors. Therefore, the conversion from SIFT to RootSIFT can be done on-the-fly through $rootsift = \sqrt{sift / \sum(sift)}$, where $sift$ is the $L1$ normalized SIFT vectors. Such an explicit feature mapping makes the smaller bin values more sensitive when comparing the distance between SIFT vectors. It suggests that a model with constant variance can be more accurate for discrimination of data, known as “variance stabilizing transformation” in [34]. The authors claimed that RootSIFT is superior to SIFT in every single setting such as large scale object retrieval, image classification, and repeatability under affine transformations.

SURF *Speeded Up Robust Features (SURF)*, introduced by Bay et al. [35], is a speeded-up version of SIFT. In other words, SURF have lower dimension, higher speed of computation

2. RELATED WORK

and matching, but provide better distinctiveness of features. The SURF rely on determinant of Hessian matrix for both scale and keypoints location. Meanwhile, box filters and integral images are used to replace the procedure of constructing DoG pyramid in SIFT for finding scale-space, which are easily calculated in parallel for different scales. This feature describes a distribution of Haar-wavelet responses of local 4×4 neighborhood sub-regions centred at each extrema point. The response of each sub-region is a four-dimensional vector v representing its underlying intensity structure $v = (\sum d_x, \sum d_y, \sum |d_x|, \sum |d_y|)$, where d_x is the Haar wavelet response in horizontal direction and d_y is the Haar wavelet response in vertical direction. $\sum |d_x|$ and $\sum |d_y|$ are the sum of the absolute values of the responses, $|d_x|$ and $|d_y|$ respectively. Each keypoint is then described with a $4 \times 4 \times 4 = 64$ dimensional feature vector based on the Haar-wavelet responses for all sub-regions.

Sparse and dense features sampling In general, there are two sampling strategies for local image descriptors: 1) sparse features sampling, also known as interest point approach; 2) dense features sampling, as its name indicates, local features are computed on a “dense grid”. We will not detail it here, as a good survey in this respect can be found in the work of Tuytelaars [36].

In this Section, we provide an overview of several notable local image descriptors. They are: SIFT, PCA-SIFT, RootSIFT and SURF. A comparative study of those image descriptors can be found in the literature [37].

2.1.5 Semi-local Image Descriptors

Most shape descriptors fall into this category. Shape description relies on the extraction of accurate contours of shapes within the image or **region of interest (ROI)**. Image segmentation is usually fulfilled as a pre-processing stage. In order for the descriptor to be robust with regard to affine transformations of an object, quasi perfect segmentation of shapes of interest is supposed. The examples of four important shape descriptors are: 1) Fourier descriptors (FD); 2) curvature scale space (CSS) descriptors; 3) angular radial transform (ART) descriptors; 4) image moment descriptors. FD [38] and CSS [39] descriptors are contour-based since they are extracted from the contour, while image moments [40] and ART [41] descriptors are region-based extracted from the whole shape region. A more complete list of shape descriptors can be found in [42].

2.1.6 Global Image Descriptors

Global image features are generally based on color, texture or shape cues. In this Section, we mainly discuss color and texture related features, ignoring shape which is beyond the scope of this work.

2.1.6.1 Color

Color is an important part of the human visual perception. Before going further into the description of color features, it is necessary to define the notion of color spaces. A color space is a mathematical model that enables the representation of colors, usually as a tuple of color components. There exist several color models. Among them we can cite the RGB (Red Green Blue), HSV (Hue Saturation Value) and YUV (luminance-chrominance) models, for instance.

In this Section, we will discuss some examples of color descriptors: the general color histogram and its variants that incorporate color spatial distribution. Most of color features are global, except one special local descriptors called *Color-Structure Descriptor* [43], which is designed for representing local properties.

Color Histogram Probably the most famous global color descriptor is the color histogram [44]. In general, color histogram is divided into: Global Color Histogram (GCH) and Local Color Histogram (LCH). Here, we briefly review GCH only, since LCH is essentially a variant of GCH by computing the GCH in pairs of blocks in an image. A color histogram describes the global color distribution in an image. Each bin of a histogram represents the frequency of a color value within the image or region of interest. It usually relies on a quantization of the color values, which may differ from one color channel to another. Histograms are invariant under geometrical transformations within the region of the histogram computation. However, it does not include any spatial information, and is not robust to large appearance changes in viewing positions, background scene etc.

Color Moments Three order moments are another way of representing the color distribution within the image or a region of the image [45]. *The first order moment* is the *mean* which provides the average value of the pixels of the image. *The standard deviation* is *the second order moment* representing how far color values of the distribution are spread out from each other. *The third order moment*, named *skewness*, can capture the asymmetry degree in the

2. RELATED WORK

distribution. It will be null if the distribution is centred on the mean. Using color moments, a color distribution can be represented in a very compact way. Given an image in a specific color space with *three* channels, the image can be characterized by *nine* moments: three moments for each three color channels. Let us denote the value of the j -th image pixel at the i -th color channel by p_{ij} , and N is the number of the pixels in the image, then three color moments can be defined as:

Moment 1 - Mean:

$$E_i = \sum_{j=1}^N \frac{1}{N} p_{ij} . \quad (2.2)$$

Moment 2 - Standard Deviation:

$$\sigma_i = \sqrt{\left(\frac{1}{N} \sum_{j=1}^N (p_{ij} - E_i)^2 \right)} . \quad (2.3)$$

Moment 3 - Skewness:

$$S_i = \sqrt[3]{\left(\frac{1}{N} \sum_{j=1}^N (p_{ij} - E_i)^3 \right)} . \quad (2.4)$$

Other color descriptors that can be mentioned are the *Dominant Color Descriptor (DCD)* introduced in the MPEG-7 standard.

Color Coherence Vectors Pass et al. [46] proposed to classify each pixel in a given color bucket as either coherent or incoherent, based on whether or not it is part of a large similarly-colored region. For a given color, the number of coherent (α_i) versus incoherent pixels (β_i) with each color are stored as a vector, in form of $\langle (\alpha_1, \beta_1), \dots, (\alpha_n, \beta_n) \rangle$. The authors call it a *Color Coherence Vectors (CCV)*. By the separation of coherent pixels from incoherent pixels, CCV provide finer distinctions than color histograms.

Color Correlogram In spirit of incorporating spatial information in building color histogram, Huang et al. defined a new color feature called the *color correlogram* [47] for image indexing. A *color correlogram* (henceforth *correlogram*) is a statistic describing how pixels with a given color are spatially distributed in the image. Such a statistic is defined as a table (or matrix) indexed by color pairs, where the k -th entry for the component (i, j) specifies the probability of finding a pixel of color j at a distance k from a pixel of color i in an image, where k is a distance chosen from the set of natural numbers \mathbb{N} *a priori*. Let I be an $n_1 \times n_2$ image, whose

colors are quantized into m bins $\mathcal{C} = \{c_1, \dots, c_m\}$. For pixels $p_1 = (x_1, y_1), p_2 = (x_2, y_2)$, we define $|p_1 - p_2| \triangleq \max\{|x_1 - x_2|, |y_1 - y_2|\}$. The correlogram of an image I is thus defined as:

$$\gamma_{c_i, c_j}^{(k)}(I) \triangleq \Pr_{p_1 \in I_{c_i}, p_2 \in I} [p_2 \in I_{c_j} \mid |p_1 - p_2| = k] \quad (2.5)$$

where c_i and c_j are two color bins from \mathcal{C} . By following the same notations as above, we can define a color histogram of I for $i \in \{1, \dots, m\}$ (that counts the number of pixels with a given color bin) as:

$$h_{c_i}(I) \triangleq n_1 \cdot n_2 \cdot \Pr_{p \in I} [p \in I_{c_i}] \quad (2.6)$$

Color correlogram outperforms the traditional color histogram method by including the spatial correlation of colors.

2.1.6.2 Texture

In this subsection, we present several texture cues for global image features. Actually, there is no precise definition of texture. However, one can define texture as the visual pattern having the properties of homogeneity that do not result from the presence of only a single color or intensity. Texture plays an important role in describing innate surface properties of an object and its relationship with the surrounding regions. There are many texture feature extraction techniques that have been proposed until now.

A majority of these techniques are based on the statistical analysis of pixel distributions and others are based on Local Binary Pattern (LBP) [48]. The representative statistical methods are Gray Level Co-occurrence Matrix (GLCM) [49], Markov Random field (MRF) model [50, 51], Simultaneous Auto Regressive (SAR) model [52], Wold decomposition model [53], Edge Histogram Descriptor (EHD) [54, 55] and wavelet moments [56, 57].

Local binary pattern Local binary pattern (LBP) descriptors were proposed by Ojala et al. [48] for texture classification and retrieval. LBP describes the surroundings of a pixel by generating a bit-code from the binary derivatives of a pixel. In its simplest form, the LBP operator only considers the 3-by-3 neighbours around a pixel. The operator generates a binary 1 if the neighbour of the centre pixel has larger value than the centre pixel, otherwise it generates a binary 0 if the neighbour is less than the centre. The eight neighbours of the centre can then be represented with an 8-bit number such as an unsigned 8-bit integer, making it a very compact description. A toy example is shown in Figure 2.3.

2. RELATED WORK

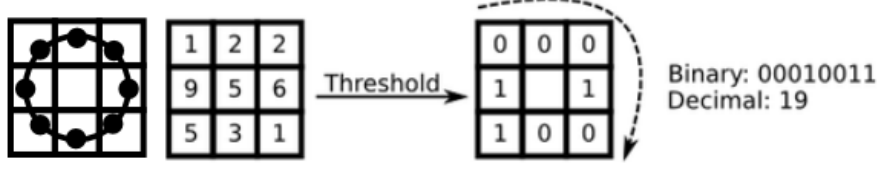


Figure 2.3: An example of local binary pattern codes. Take value (5) of the center pixel, and threshold the values of its neighbors against it. The obtained value (00010011) is called LBP code.

In the general case, given a pixel, the LBP code can be calculated by comparing it with its neighbors as:

$$LBP_{P,R} = \sum_{p=0}^{P-1} s(g_p - g_c) 2^p, \quad s(x) = \begin{cases} 1, & x \geq 0 \\ 0, & x < 0 \end{cases} \quad (2.7)$$

where g_c is the grey-value of the centre pixel and g_0, \dots, g_{P-1} correspond to the grey-values of neighbouring pixels, P is the total number of neighbours and R is the radius of the neighbourhood. After generating the LBP code for each pixel in the image, a histogram of LBP codes is used to represent the texture image.

Over the years, LBP based methods [58, 59] have gained more popularity for their computational simplicity and robust performance in terms of gray scale variations on representative texture databases. More LBP variants can be found in the literature[60].

For instance, to reduce the feature dimension, simple LBPs are further extended to *uniform* LBPs. The uniform patterns are extracted from LBP codes such that they have limited discontinuities (≤ 2) in the circular binary representation, *i.e.* at most two circular 0-1 and 1-0 transitions. In general, a uniform binary pattern has $(P \times (P - 1) + 3)$ distinct output values. To further reduce the feature dimension and achieve rotation invariance, uniform patterns are reduced to *rotation invariant uniform* (riu) LBP codes. It can be defined as:

$$LBP_{P,R}^{riu2} = \begin{cases} \sum_{p=0}^{P-1} s(g_p - g_c) 2^p, & \text{if } U(LBP_{P,R}) \leq 2 \\ P + 1, & \text{otherwise} \end{cases} \quad (2.8)$$

where U is defined as the number of spatial transition (0/1) in that pattern. The mapping from $LBP_{P,R}$ to $LBP_{P,R}^{riu2}$, has $P + 2$ distinct output values, and can be implemented with the help of a lookup table of 2^P elements.

Co-occurrence matrix Gray Level Co-occurrence Matrix (GLCM), as a statistical approach to provide valuable information about the relative position of the neighbouring pixels in an image, was first introduced by Haralick et al. [49] for classifying terrain images.

Give an image I of size $n \times m$, the co-occurrence matrix C , can be defined as:

$$C_{\Delta x, \Delta y}(i, j) = \sum_{x=1}^n \sum_{y=1}^m \begin{cases} 1, & \text{if } I(x, y) = i \text{ and } I(x + \Delta x, y + \Delta y) = j \\ 0, & \text{otherwise} \end{cases} \quad (2.9)$$

where i, j are the image intensity values, (x, y) are the spatial position of the pixel-of-interest; the offset $(x + \Delta x, y + \Delta y)$ specifies the distance d between (x, y) and its neighbour.

The co-occurrence matrix (CM) keeps track of the number of pairs of certain pixels that occur at certain separation distances in the image space. By adjusting the distances over which we check co-occurrences, we can adjust the sensitivity of the CM to geometric changes in the objects appearance caused by viewpoint changes, rotation or object flexing. Note that the *correlogram* defined above in Section 2.1.6.1 can be seen as an extension of GLCM to the color space.

The DCT Coefficient Domain Block discrete cosine transform (DCT) is widely used in image and video compression algorithms. The discrete cosine transform (DCT) is similar to the discrete Fourier transform, i.e. it transforms a signal or image from the spatial domain to the frequency domain. The two-dimensional DCT of an M-by-N matrix A is defined as follows:

$$d_{p,q} = \alpha_p \alpha_q \sum_{m=0}^{M-1} \sum_{n=0}^{N-1} A_{m,n} \cos \left[\frac{\pi}{M} \left(m + \frac{1}{2} \right) p \right] \cos \left[\frac{\pi}{N} \left(n + \frac{1}{2} \right) q \right], \quad \text{with } \begin{matrix} 0 \leq p \leq M-1 \\ 0 \leq q \leq N-1 \end{matrix},$$

$$\text{and } \alpha_p = \begin{cases} 1/\sqrt{M}, & p = 0 \\ \sqrt{2/M}, & 1 \leq p \leq M-1 \end{cases}, \quad \alpha_q = \begin{cases} 1/\sqrt{N}, & q = 0 \\ \sqrt{2/N}, & 1 \leq q \leq N-1 \end{cases}. \quad (2.10)$$

The values $D_{pq} = \{d_{p,q}\}$ are called the DCT coefficients of A.

Bar et al. [61] proposed to use some DCT coefficients to characterize texture features, which have proved to give good results at low computational complexity [62]. In the present work, we adopted DCT coefficients to extract texture patterns. We will discuss it in detail in Section 3.3.3.2 of Chapter 3.

2.1.6.3 Gist

The GIST descriptor was initially proposed in [63]. In cognitive psychology, the gist of the scene [64], refers to a short summary of the scene (the scene category, and a description

2. RELATED WORK

of a few objects that compose the scene). In computer vision, the idea of “gist” is to develop a low dimensional *global* image representation of the scene, which does not require any form of segmentation. It can include from low-level features (e.g., color, spatial frequencies) to intermediate image properties (e.g., surface, volume) and high-level information (e.g., objects, activation of semantic knowledge).

The GIST descriptors have been used for scene recognition [63, 65], depth estimation [66], image retrieval for computer graphics [67], and for providing contextual information as strong prior for the subsequent object detection [68–70]. While GIST descriptors is suitable for retrieving similar objects and scenes which are well aligned, they cannot cope with wide variations in rotation, scaling or viewpoint. An evaluation of GIST descriptors can be found in [71].

2.1.7 Similarity Metrics

In this Section, we introduce different similarity metrics to compare feature vectors. As for similarity measure between histograms, especially the notable one: *Histogram Intersection*, we will discuss them in Section 4.2 of the Chapter 4.

Let us denote by $O = \{o_1, \dots, o_B\}$ and $U = \{u_1, \dots, u_B\}$, are two *normalized* feature vectors with B bins. Particularly, they are normalized to sum to one, *i.e.* $\sum_{b=1}^B o_b = \sum_{b=1}^B u_b = 1$.

Given these two feature vectors, a number of measures for computing their similarity can be used. We can list a few of them: L_1 distance (D_{L_1}), L_2 distance (D_{L_2}), χ^2 distance (D_{χ^2}), Kullback-Leibler divergence (D_{KL}), Jeffrey divergence (D_{Je}) and Battacharyaa distance (D_B) etc. Note that L_1 distance is also known as city block distance or Manhattan distance. Formally, these distances can be formulated as follows:

L_1 distance :

$$D_{L_1}(O, U) = \sum_{b=1}^B |o_b - u_b| . \quad (2.11)$$

L_2 distance :

$$D_{L_2}(O, U) = \left(\sum_{b=1}^B (o_b - u_b)^2 \right)^{1/2} . \quad (2.12)$$

χ^2 distance :

$$D_{\chi^2}(O, U) = \frac{1}{2} \sum_{b=1}^B \frac{(o_b - u_b)^2}{o_b + u_b} . \quad (2.13)$$

Kullback-Leibler divergence :

$$D_{KL}(O, U) = \sum_{b=1}^B o_b \log \frac{o_b}{u_b} . \quad (2.14)$$

Jeffrey divergence :

$$D_{Je}(O, U) = \sum_{b=1}^B \left(o_b \log \frac{o_b}{m_b} + u_b \log \frac{u_b}{m_b} \right) , \quad (2.15)$$

where $m_b = \frac{o_b + u_b}{2}$.

Battacharyaa distance: In statistics, the Bhattacharyya distance, named after mathematician Bhattacharyya [72], measures the similarity of two discrete or continuous probability distributions. Consider two discrete probability distributions p and q over the same domain X , $\sum_{x \in X} p(x) = 1$, $\sum_{x \in X} q(x) = 1$. The Bhattacharyya distance is defined as:

$$D_B(p, q) = -\ln \left(BC(p, q) \right) \quad (2.16)$$

where $BC(p, q) = \sum_{x \in X} \sqrt{p(x)q(x)}$ is the *Bhattacharyya coefficient*. Note that both the chi-square measure and Battacharyaa coefficient can measure the similarity between two distributions. It has been proved in [73] that the Bhattacharyya coefficient is considered as an approximation of the chi-square measure.

In summary, the resemblance between feature vectors can be measured either as a distance (dissimilarity) or a similarity. The distance measures described above are flexible: Most distance measures can be converted into similarities and vice versa.

2.2 Image Retrieval in the Real World

Due to recent advances in image acquisition and data storage, it is necessary to develop appropriate computer systems for browsing, searching and retrieving images from large databases of digital images. In this context, image retrieval has received a lot of attention in the computer vision community in the last twenty years [3, 14, 15, 25, 74–76].

Image retrieval can mainly be divided into two categories: 1) query by text (QBT), often referred to as annotation-based image retrieval (ABIR); 2) query by example (QBE), also known as the Content-Based Image Retrieval (CBIR). The former uses the metadata such as keywords, tags, or descriptions associated with the image to search images. The latter allows to

2. RELATED WORK

retrieve images based on colors, textures, shapes or any other visual information derived from the image itself. In the following manuscript, we refer *image retrieval* to the latter (CBIR) only, unless otherwise noted.

An overview of image retrieval is illustrated in Figure 2.4. Particularly, CBIR is a challenging task, with many problems still unresolved. Given a query image, CBIR is aimed at returning its most similar images in a database. To achieve this goal, we need to choose adapted image features and to define the similarity measures between images in order to compare them. As mentioned in Section 2.1.4, the most popular local image features are SIFT descriptors, SURF etc. Other types of features can also rely on color, texture, shape, spatial location etc. or in a combination of them [77]. In the present work, we focus on *visual signature* and *similarity measures* parts, shown as two core techniques for image retrieval in the diagram of Figure 2.4.

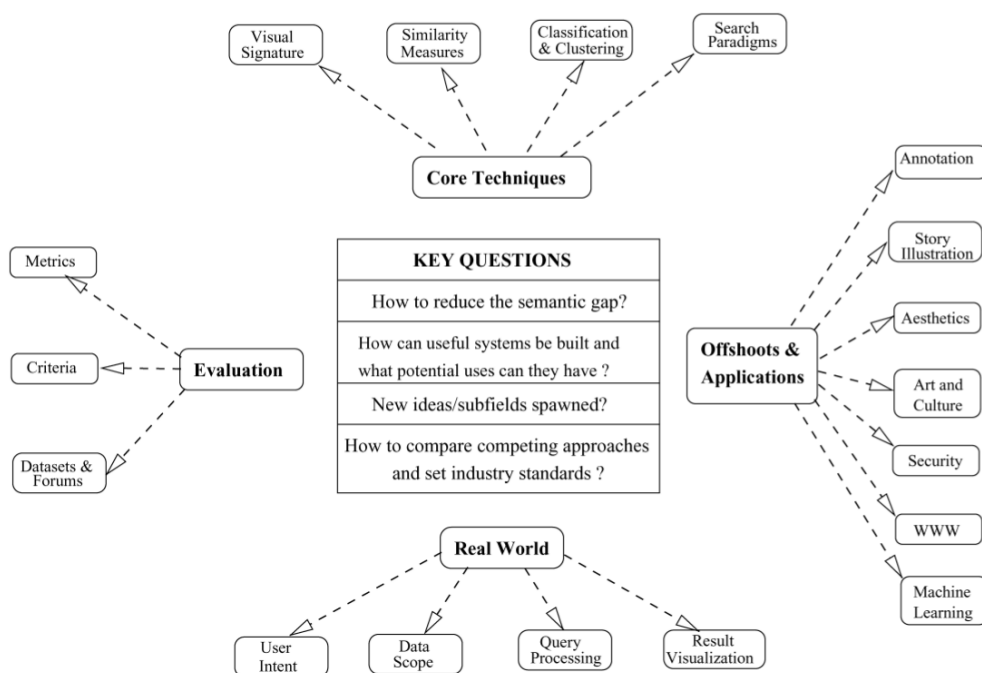


Figure 2.4: An overview of the many facets of image retrieval as field of research. The figures are extracted from Dattas paper [3].

2.3 Image Representation

The image representation is one of key components linked with different tasks, such as object class detection, shape based object recognition [78], image segmentation [79] or image

classification in computer vision. In this Section, we will introduce several of these recent advances in the representation of images.

2.3.1 The Bag-of-Words Model

Local-feature based image representations have been successfully applied to many applications in computer vision, such as object recognition, image matching, image categorization and image retrieval. The famous Bag-of-Features (BoF) framework consists in computing and aggregating statistics derived from the local features such as SIFT [2] etc. to describe the image content. The bag-of-words model is one of the most popular variant of the BoF framework. Many approaches in aforementioned tasks rely on the *bag-of-words model* (BoW) since it was introduced in the seminal papers [16, 80].

The BoW model is originated from texture recognition [81, 82] and document processing [83]. As its name implies, the model was learned from the idea of texture being characterized by the repetition of ‘textons’; as well as from document classification, where a text document is represented as a “bag” of *orderless* words. For a document, a so-called *bag of words* is actually a sparse vector of frequencies of words from a dictionary. The *dictionary* is a vocabulary that consists of *keywords* occurring in text documents. A document is then represented as a histogram over the vocabulary in the dictionary.

Bag of visual words (BoVW) representation is inspired from the aforementioned document representation. An image can be treated as a document on the analogy between words/dictionary in document and *visual words/dictionary* in image. The *visual words*, are also called *codewords*, as an analogy to words in text documents. The *dictionary* in images is also called *codebook*, as an analogy to a word dictionary in text document. In the remainder of the thesis, we therefore use the words “visual words” and “codewords”, “dictionary” and “codebook” interchangeably. An illustration of *Bag of Words* versus *Bag of Visual Words* analogy is shown in Figure 2.5.

To achieve image representation based on this analogy in the BoVW model, we need to define the corresponding “visual words” and “dictionary” in images. More precisely, the bag of visual words model involves the following steps:

1. feature detection;
2. feature extraction/description;

²<http://web.engr.illinois.edu/~slazebni>

2. RELATED WORK



Figure 2.5: The *Bag of Words* model. The left-most picture illustrates the *Bag of Words* in *document*. Other pictures show the *Bag of Visual Words* in *image*. These pictures are excerpted from the source of S.Lazebnik.²

3. codebook generation:

- (a) vocabulary building;
- (b) vocabulary assignment.

We have discussed the first step in Section 2.1.2 and the second step in Section 2.1.3 respectively. Now let us detail the two steps (3(a) and 3(b)) in *codebook generation* for the BoVW model.

The first step is the computation of local feature descriptors such as SIFT [2, 31] or SURF [35] for a set of image patches. These patches can be either at the key-point locations or densely sampled on a regular grid of the image. After that, a clustering technique, typically k -means [84], is applied to quantize these descriptors into a fixed number of clusters. The centres of these generated clusters are the so-called *visual words* or *codewords*. The whole set of cluster centres is the *dictionary* or *codebook*. In this thesis, we denote codebook by $C = \{C_1, \dots, C_B\}$, where B is the codebook size.

During the second step, each image descriptor in a given image will be associated with the nearest visual word or visual words in the *dictionary*. If each descriptor is assigned to a single visual word, we call this assignment measure “Hard Assignment” (HA). Otherwise, we call it “Soft Assignment” (SA) [85–88]. The final image representation is thus made by computing a histogram of codewords occurrences. So an image I_j is represented as an histogram of visual words $h_j = (p(C_1|I_j), \dots, p(C_B|I_j))$. The Figure 2.6 shows an example of the BoVW image representation. There are three examples of images in this figure. Each patch in an image is mapped to certain codeword (hard assignment) through the clustering process. Each image

is thus represented by a sparse histogram of the codewords. This approach is the so-called *bag-of-visual-words* (BoVW) representation [80].

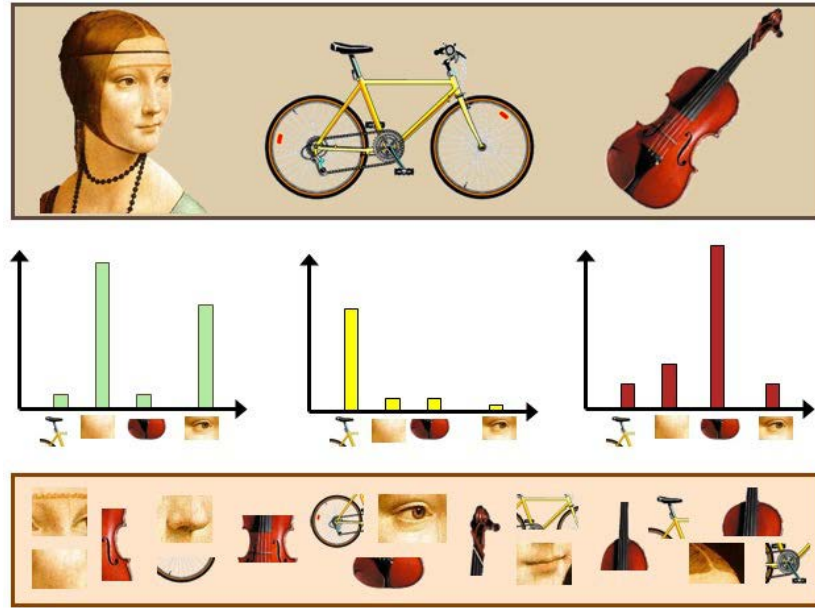


Figure 2.6: The Bag-of-Visual Words (BoVW) image representation. The figure is from the source of S.Lazebnik.³

Several extensions to the traditional bag-of-words image representation have been proposed. We will discuss the most relevant ones in the next section.

2.3.2 The State-of-the-art to Improve the Bag-of-Visual-Words Model

The basic Bag-of-Visual-Words model uses histogram as image signatures. Hence, BoVW method discards all the spatial layout of image features. It also ignores how the image features are distributed across images. However, this information is a key attribute for object recognition and scene classification. Many research efforts have been tackled these constraints. In the following, we will enumerate several approaches that have been proposed in the literature to overcome these limitations.

³<http://web.engr.illinois.edu/~slazebni>

2. RELATED WORK

2.3.2.1 Spatial pyramid image representation

Lazebnik [4] et al. introduced a simple yet effective extension of bag-of-features image representation, named Spatial Pyramid Matching (SPM). The idea is first to recursively subdivide the image into $2^r \times 2^r$ grids at multiple resolutions, then to compute the BoW histograms for each grid sub-block at several spatial granularities, and finally to concatenate histograms of each grid by a formulation of pyramid match kernel:

$$\begin{aligned}\kappa^R(I_i, I_j) &= \mathcal{J}^R + \sum_{r=0}^{R-1} \frac{1}{2^{R-r}} (\mathcal{J}^r - \mathcal{J}^{r+1}) \\ &= \frac{1}{2^R} \mathcal{J}^0 + \sum_{r=1}^R \frac{1}{2^{R-r+1}} \mathcal{J}^r.\end{aligned}\tag{2.17}$$

The weight $\frac{1}{2^{R-r}}$ allows for penalizing low resolutions of a partition, reflecting the fact that higher levels localize the features inside smaller regions more precisely, see Figure 2.7. Using B visual words in a visual dictionary and C grid cells in SPM will result in a histogram of size BC as the final image representation.

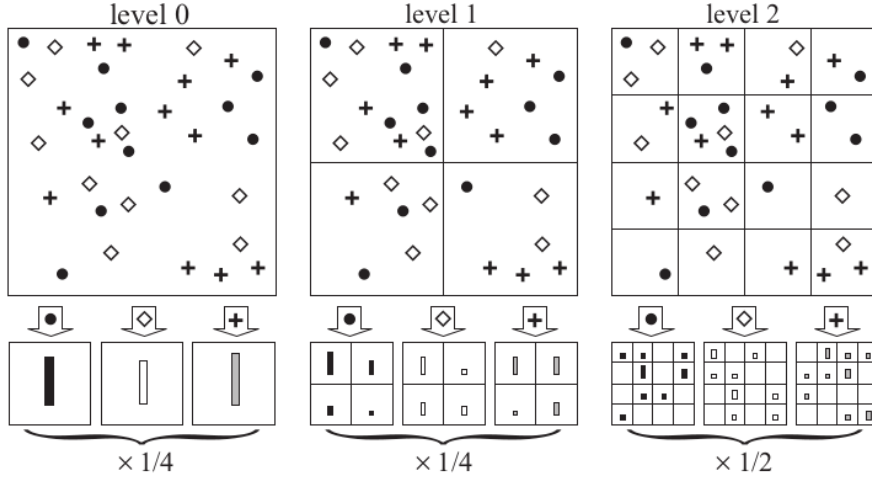


Figure 2.7: An example of constructing a three-level pyramid. The image has three feature types, indicated by circles, diamonds, and crosses. At the top, the SPM method subdivides the image at three different levels of resolution. Next, for each level of resolution and each grid cell, SPM counts the features that fall in each spatial bin. Finally, SPM weights each spatial histogram according to Equation (2.17). The figure is excerpted from Lazebnik et al. [4].

In such a way, the spatial distribution of these visual features is encoded into the final spatial pyramid image representation with level weighted normalizations. Despite on hypothesis of

uniform spatial layout in image, SPM does not only beat the simple BoVW by a large margin but also performs competitively against much elaborate methods.

2.3.2.2 Superpixels

Ren et al. [17] put forward a concept of grouping pixels into “superpixels”. The aim of superpixels is to over-segment image into a large number of coherent, local regions which retain most of the structure necessary for segmentation at the scale of interest. See an example in Figure 2.8. The compact superpixels can capture diverse spatially coherent information and multi-scale visual patterns of a natural image.

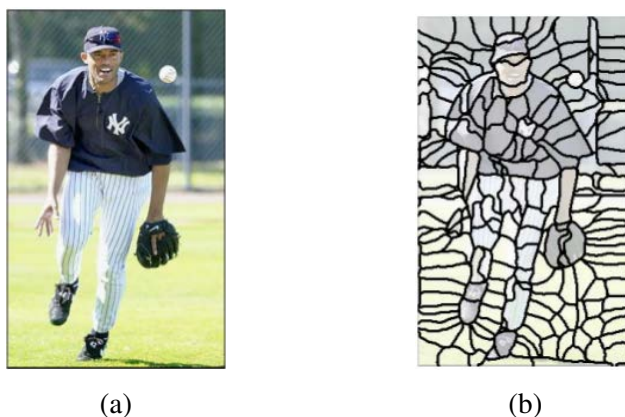


Figure 2.8: An example of superpixels. (a) Input image. (b) A “superpixel” map with 200 superpixels via Normalized Cuts algorithm [5]. The figure is excerpted from Mori et al. [6].

Superpixels are often used as a preprocessing step in computer vision to reduce the complexity of image analysis for later processing stages. The original superpixel algorithm used Normalized Cuts (NCuts) based on contour and texture cues [6, 17]. Later a variety of new superpixel algorithm have been developed, e.g. TurboPixels [89], Simple Linear Iterative Clustering (SLIC) superpixels [90], Superpixels Extracted via Energy-Driven Sampling (SEEDS) [91].

A shortcoming of this approach is: Superpixels are usually expected to align with object boundaries, but this may not hold strictly in practice due to faint object boundaries and cluttered background [92].

2. RELATED WORK

2.3.2.3 Using class-specific codebooks to vote for object position

Leibe et al. [13] proposed to build a class-specific codebook for the target object category. The procedure of codebook generation works as follows. Firstly, image patches from training images are extracted with the Harris interest point detector [28]. Secondly, these patches are treated as individual clusters on which agglomerative clustering is performed initially. The clustering process stops until the similarity between any patches in different clusters is less than a certain threshold. Finally, the codebook is generated from the center of each resulting cluster. The authors called this adapted codebook a *Codebook of Local Appearance*.

Leibe et al. also define an *Implicit Shape Model* (ISM) to model the spatial distribution of each codebook entry under a probabilistic framework. More precisely, $ISM(C) = (I_C, P_{I,C})$, where I_C is the aforementioned *codebook of local appearance* for a given category C , $P_{I,C}$ is a spatial probability distribution for the codebook entry. $P_{I,C}$ estimates where the codebook entry may be found on the object in a non-parametric manner. Hence, the class characteristics are learnt in such a *soft-coded* way. We can vote for object position or even handle *multiple articulated* objects of the same class in testing images.

2.3.2.4 Spatiograms versus Histograms

Histograms, as graphical representation of the data distribution, have been widely used to describe image regions. However, all spatial information is discarded and only features occurrence counts are retained in such a description. Birchfield et al. [18] introduced *spatiograms* as a generalization of the histograms to allow higher-order *spatial moments* to be part of the descriptor. Conaire et al. [93] further proposed an improved spatiogram similarity measure that was derived from the Bhattacharyya coefficient [94] for spatiogram comparison.

Formally, a histogram can be formulated as: Given a discrete function $f : \mathcal{X} \rightarrow \mathcal{Z}$, where $x \in \mathcal{X}$ and $z \in \mathcal{Z}$, a *histogram* of f is $h_f : \mathcal{Z} \rightarrow \mathbb{Z}^*$, where \mathbb{Z}^* is the set of non-negative integers. $h_f(z)$ is the number of elements $x \in \mathcal{X}$ such that $f(x) = z$.

In contrast, for an image I_j , its *spatiograms* can be expressed by rewriting the aforementioned function f as a two-dimensional mapping $I_j : \mathcal{P} \rightarrow \mathcal{Z}$, where $\mathcal{P} = [X, Y]^T$ is a set of pixels of an image, $[X, Y]^T$ is a set of their corresponding coordinates in the image. Hence, the (second-order) *spatiogram* of an image is denoted by:

$$h_{I_j}(b) = \langle n_b, \mu_b, \Sigma_b \rangle, \quad b = 1, \dots, B, \quad (2.18)$$

where n_b is the number of pixels whose values fall into the b th bin, *i.e.* the set $\{n_b\}_{b=1,\dots,B}$ corresponds exactly to the histogram. The μ_b and Σ_b represent the *mean* vector and *covariance* matrices of those pixels' coordinates respectively. B is the number of bins in the spatiogram.

Compared with co-occurrence matrices [49], spatiograms capture the global positions of the pixels rather than their pairwise relationships.

2.3.2.5 Spatial orientations of visual word pairs to improve Bag-of-Visual-Words model

Khan et al. [95] proposed to embed global spatial information of visual words into BoW model through the histograms of orientations for any pairs of visual words of the same type. The authors introduced a notation *Pair of Identical visual Words* (PIW), which is defined as the set of all the pairs of visual words of the same type. A spatial distribution of visual words is represented as a histogram of orientations of the segments formed by PIW.

2.3.2.6 Improve BoW model with respect to feature encoding

Features encoding, *i.e.* transforming local image descriptors into histograms is at the heart of bag-of-visual-words model. A large number of methods have been proposed to improve this encoding process in feature space. Recently, many efforts can be found in the literature regarding this direction. Here we enumerate some notable approaches, such as Fisher vector image representation [20, 21, 96–99], sparse coding [100], locality constrained linear coding (LLC) [101], spatially local coding [102] etc. that compete with SPM to give extensions of bag-of-words image representations to encode spatial layout.

2.3.3 Region-based Image Representation

Many works on region-based image representation (RBIR) can be found in the literature [103, 104]. We introduce several notable ones.

Stricker et al. [45] proposed to divide an image into 5 partially overlapping, fuzzy regions. Next, they compute the first three moments of the color distribution for each region. Finally, an image is represented by a feature vector that is composed of color moments of 5 fuzzy regions for image indexing. That is to say, the index entry consists of 45 (number of regions \times number of color channels \times three moments, *i.e.* $5 \times 3 \times 3$) floating numbers per image for indexing. Based on fuzzy regions, the feature vectors in the index achieve relatively invariance to small translations and small rotations of an image.

2. RELATED WORK

Jing et al. reported their work on RBIR [105–107]. They transformed the local features of regions into a compact and sparse representation. Suppose an image I_j containing N regions $\{R_1, \dots, R_N\}$. The image is described by a vector of the form :

$$\hat{I} = \left\{ (CI_{R_1}, W_{R_1}), \dots, (CI_{R_N}, W_{R_N}) \right\},$$

where CI_{R_i} and W_{R_i} are the codeword index and importance weight of region R_i , the sum of importance weights for an image should be equal to 1, i.e. $\sum_{i=1}^N W_{R_i} = 1$. The codebook is generated by iteratively clustering the features (the first two color moments) of regions from all images in the database. Each region of an image is labelled by a codeword index corresponding to the cluster it belongs to, defined as $I_s = (w_1, \dots, w_N)$, where N is the number of the codewords, $\sum_{i=1}^N w_i = 1$.

Omhover et al. [108, 109] formulated spatial structure of the regions by fuzzy similarity measure. Each region is described by a set of color and shape features. Two regions are compared by measuring their common and distinctive features in the regions.

Gosselin et al. [110] proposed a pairs-of-regions based image representation in specific cases (objects with heterogeneous background). The authors use one color histogram, three texture histograms as the signature of a region. The spatial constraints only apply to pair of adjacency regions, they called this approach “mini-bag”.

Vieux et al. [111] introduced the Bag-Of-Regions (BOR) model inspired from BoVW to tackle the challenging “*semantic gap*” problem - translation between low-level image features and high-level user perceptions. Low level descriptors are first extracted from segmented regions, represented as BoW histograms. Next, co-occurrence criteria such as min, max, median, sum etc. are applied to build the BOR signatures. The authors claimed that BOR signatures are a good counterpart of bag-of-visual-words, and can be more appropriate depending on the specific queries.

2.3.4 Graph-based Image Representation and its Applications

Graphs have been successfully applied in pattern recognition and computer vision. When a graph-based representation is adopted for image description or to represent objects in an image, it frequently entails some form of *Graph Matching*. Graph matching is a mapping in aim to find a correspondence between the nodes/edges of one (possibly larger) graph to the other that model the patterns of interest. Depending on how the matching problem is formulated, graph matching can be categorized into four classes: 1) Exact graph matching; 2) Inexact graph

matching; 3) Graph embeddings and graph kernels; 4) Other graph matching techniques. The first category and the second one are respectively restricted to strict and more or less difference in the structure of the graphs being matched. The third one are the techniques actually gaining a growing interest in recent literature [22–24, 112, 113]. In this manuscript, we only cite one instance: *Graph Words*, which has highly motivated our present work.

Graph Words Karaman proposed a graph-based image representation via “Graph Words” [7]. The idea of the method consists in building a set of “small” graphs on multiple nested layers, and then in fitting these graph features to bag-of-visual-words approach, as demonstrated in Figure 2.9. The author defined a maximum of four layers of Graphs Words due to high computational cost of the approach. From bottom to top, the first layer contains only a fixed number of seeds points which are positioned at salient SURF points with higher response [35]. The second to fourth layer correspond respectively to graphs with 3, 6 and 9 nearest neighbours of the seeds. Graph edges are generated by Delaunay triangulation on each layer separately. Under such definition, the number of graphs at each layer is the same. Graph comparison can be achieved by Context Dependent Kernel (CDK) [114]. In contrast to traditional visual dictionary, each codeword is defined as the median graph that minimizes the distance to all the graphs of the corresponding cluster. The spatial layout is therefore embedded at feature level in such multi-resolution of graph structure.

2.4 Conclusion

In this Chapter, we have presented image descriptors, image representation and image retrieval in real world, particularly Content-Based Image Retrieval (CBIR). With respect to image representation, we mainly focus on the *bag-of-visual-words* model and its variants. One of severe limitations of the *bag-of-visual-words* model is that it ignores the spatial layouts among the image patches, which are very important information in image representation. Several effective methods have been proposed to incorporate the spatial information into BoVW. We enumerated a few of notable ones. In the present work, we are especially interested in using graphs as a tool to model spatial relationships among image features. This idea has motivated our direction in the next Chapter.

2. RELATED WORK

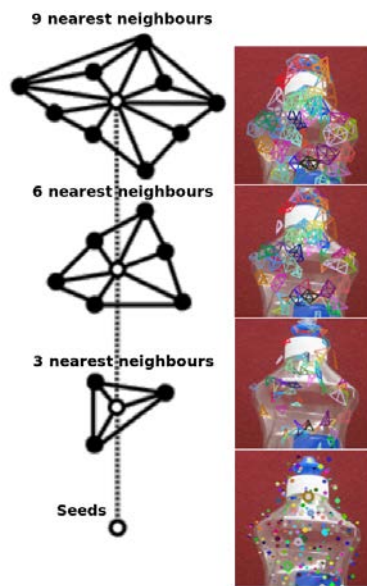


Figure 2.9: A hierarchy of “nested” Graph Words on four layers (on the left) in the same example of image (on the right). Seed is marked as hollow circle in white color, and neighbour nodes are shown as solid circles in black color. The figures are extracted from [7].

Chapter 3

Graph-based Image Representation

As discussed in Chapter 2, graphs are powerful tools to model spatial information in image representation. Graph-based representations are of pivotal importance in computer vision and pattern recognition [115]. Describing the image patterns with such representations is quite natural and find applications in both low level image processing and high level vision tasks. The patterns and objects in images are identified by decomposing the image into parts and analysing the relationships/structure between them.

In this Chapter, we first introduce the image graph model. Next, we explain how this proposed model is described by a weighted image graph. The weighted image graph is composed of graph nodes, edges and the corresponding edge weights. An edge weight measures the similarity between two nodes of the edge. Then we discuss the weighted graph construction process step by step. Different objective functions for edge weights are designed. Finally, three graph partitioning methods are presented for dividing the image graph into a series of subgraphs. These subgraphs is then used as image descriptors embedding the color/texture homogeneity and limited spatial information of the image.

3.1 An Overview of the Image Graph Model

Let us first introduce the key components and concepts of the image graph model for image retrieval. The processing chain for image graph model includes the following steps: 1) graph construction; 2) graph partitioning; 3) (sub)graph matching; 4) image retrieval. See Figure 3.1.

3. GRAPH-BASED IMAGE REPRESENTATION

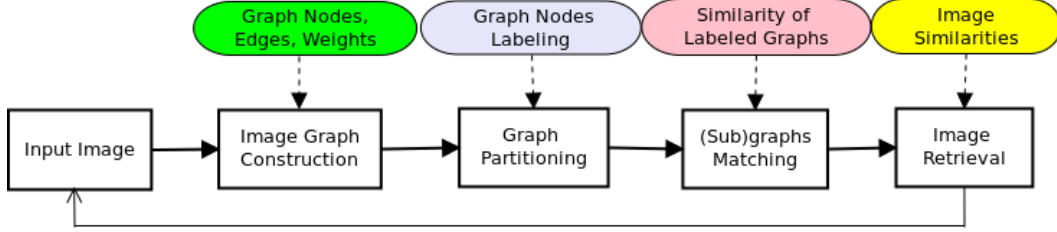


Figure 3.1: An overview of the processing chain for the proposed image graph model. (I) Image is represented by an initial weighted graph. (II) Graph partitioning consists in finding the optimal labeling for each graph nodes. (III) Find the best bipartite matched subgraphs between images pairs (IV) Retrieve images based on signatures that define the similarities between these subgraphs.

3.2 Weighted Image Graph Representation

Intuitively, a graph represents a set of elements and a set of pairwise relationships between these elements. The elements are called **nodes** or **vertices**, and the pairwise relationships between the nodes are called **edges**.

A graph $G = (V, E)$ is represented by a set of vertices V and a collection of edges $E \subseteq V \times V$. Each edge connects a pair of vertices. If all edges in a graph have no orientation, *i.e.*, the edge (a, b) is identical to the edge (b, a) , then this graph is called *undirected graph*. An *edge-weighted graph* (or for short, *weighted graph*), is defined as a pair (G, w) in which $w(e) : e \rightarrow \mathbb{R}$ is a weight function mapping each edge $e \in E$ to its weight. Weighted graphs, as a model, are used in numerous problems, such as networks where graph nodes are linked with different weights (distance, cost, etc.). Note that a graph can be viewed as an edge-weighted graph where all edges have a weight equalling to 1.

An input image database Ω , is composed of N RGB images $\Omega = \{I_1, \dots, I_N\}$. We define $G_j = (V_j, E_j, W_j)$ as the *undirected weighted image graph* constructed on the image I_j . The set of vertices V_j contains a subset of pixels \mathcal{P} of the image I_j and at the limit can contain all of them. The graph edges E_j connect these vertices with a specified neighbourhood system. W_j is an affinity matrix of size $|V_j| \times |V_j|$, whose entry at row p , and column q is W_{pq} , defined as:

$$W_{pq} = \begin{cases} w_{pq} & \text{if } p, q \in E_j \\ 0 & \text{if } p, q \notin E_j, \end{cases} \quad (3.1)$$

where w_{pq} represents the edge-based similarity between two vertices p and q .

3.3 Graph Construction

With the above notation, we can now define the graph nodes (vertices), graph edges and graph weights in image graph.

3.3.1 Graph Nodes Selection in Image Graph

We experimented two methods for nodes selection. We describe them in the following.

3.3.1.1 Prominent keypoints

Feature extraction First, a feature-extraction algorithm is used to extract the feature points either on the whole image or on the mask of the object being retrieved. An example can be seen in Figure 3.2(a), where the SURF points [35] are chosen in our experiments. A threshold (Thr_h) on the Hessian of the SURF descriptors is set. The larger the threshold value, the less keypoints are selected. A good value for Thr_h could be from 300 to 500, depending from the image contrast. By default, the value of Thr_h is set to 400.

Key points filtering Next, all the extracted feature points are further sorted by their feature strengths. In such a way, the most strong/prominent key points with the most representative features remain. In some cases, the extracted points may be very close to each other, which leads to unbalanced graph edges. To avoid that, we filter the feature points by preserving only the most prominent key point over any 10-pixels diametrical region. After filtration, we obtain a set of reduced keypoints $\mathcal{P} = \{p_1, \dots, p_n\}$, see Figure 3.2(b). However, graph nodes obtained in such a way are very sparse and irregular in either the number of nodes or the distances in between, losing interesting information potentially.

3.3.1.2 Dense sampling strategy

First image pixels are chosen by dense sampling the points at a fixed spacing on a regular grid. Next, the local SIFT features [2] of these points are extracted from their image patches. We call this approach Bag-of-Features Grid SIFT (BF-GSIFT) [36].

This sampling approach gives a constant amount of features per image area since all patches with strong or less contrast contribute equally to the overall image representation. In contrast to the previous strategy, *i.e.* prominent keypoints selection, that has more arbitrary spatial relations between features, dense sampling keeps simple spatial relations between features in

3. GRAPH-BASED IMAGE REPRESENTATION

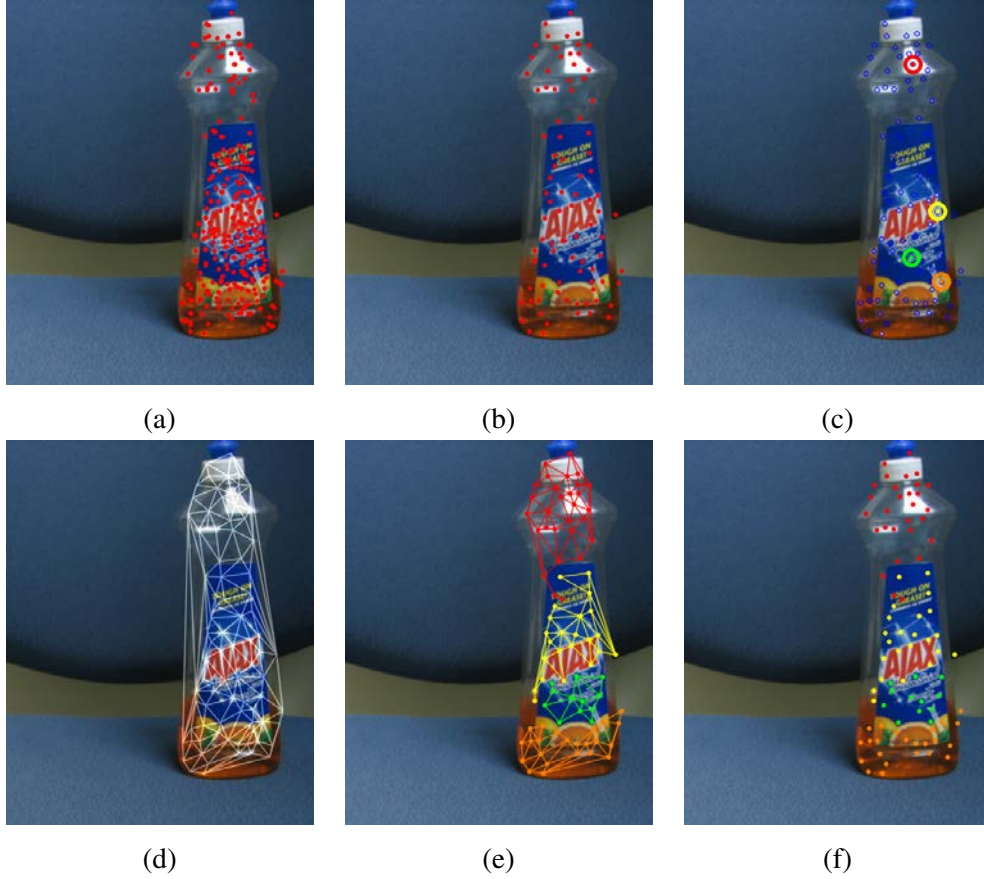


Figure 3.2: Graph construction. (a) Initial SURF keypoints. (b) Filtered keypoints. (c) Seeds selection. (d) Delaunay triangulation over filtered feature points. (e) Graph-cuts result. (f) Labeling result.

reserve by following a regular pattern. On the downside, dense sampling cannot reach the same level of repeatability as obtained with interest points unless sampling is performed extremely densely but then the number of features quickly grows unacceptably large. In practice, researchers often use an overlap between patches of 50% or less. As in SPM [4], we adopt 8-pixels spacing, 16-pixels patch size, to reach a compromise between repeatability of interest points and reasonable size of features.

3.3.2 Graph Edges Construction in Image Graph

Once vertices are fixed, we adopt a suitable neighbourhood system to generate graph edges based on the strategy of nodes selection. The purpose is to keep the spatial structure between local features so that it is invariant to image translation, scaling, and rotation.

In general, there are three options for graph edges construction: 1) Delaunay Triangulation, 2) 4-neighbourhood, 3) 8-neighbourhood.

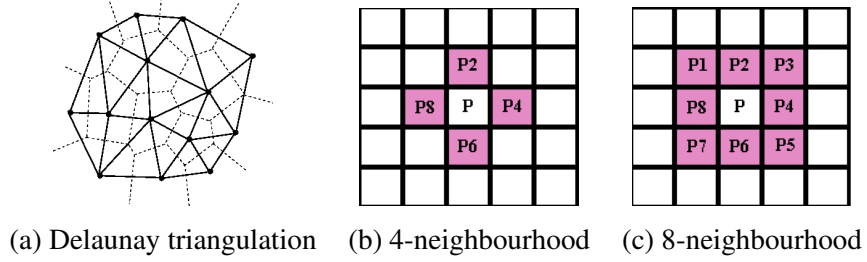


Figure 3.3: Options for the neighbourhood system of image graph.

In the context of prominent keypoints, a Delaunay triangulation (DT) [116] is performed over all filtered points set \mathcal{P} to generate the edges of image graph. The DT process aims to maximize the minimum angle of all triangles' angles. Therefore, it avoids skinny triangles between edges. More precisely, the Delaunay triangulation of a point set is a collection of edges satisfying an “empty circle” property: For each edge we can find a circle containing the edge's endpoints but not containing any other points. This kind of triangulation is equivalent to the nerve of the cells in a Voronoi diagram. An example of Delaunay triangulation on top of the Voronoi diagram (in dotted lines) can be seen in Figure 3.3(a). Another example of DT over the vertices of an image graph is shown in Figure 3.2(d). This technique is used for the prominent keypoints approach.

For the dense sampling approach, a regular d -neighbourhood ($d = 4$ or $d = 8$) system is used. The 4-neighbourhood of vertex p are the four pixels to the north (p_2), south (p_6), east (p_4), and west (p_8), see Figure 3.3(b). The 8-neighbourhood of node p also includes the diagonals, namely pixels p_1, \dots, p_8 , see Figure 3.3(c).

3.3.3 Graph Weights in Image Graph

Following the aforementioned definitions, let us suppose that the graph edges E connect the vertices with a predefined neighbourhood system. The edge affinity matrix W of size $|V| \times |V|$, is assumed to be non-negative and symmetric.

As discussed in Section 2.1.6, color and texture are two predominant factors to characterize the image features. Therefore, in the present work, we design an edge-weight function that combines joint color-texture features. For an edge between two nodes p and q , its weight is

3. GRAPH-BASED IMAGE REPRESENTATION

defined as follows:

$$\begin{aligned} w_{pq} &= e^{-\lambda \cdot \alpha \cdot C_{pq} \Sigma_C^{-1} C_{pq}^T} \cdot e^{-\lambda \cdot (1-\alpha) \cdot T_{pq} \Sigma_T^{-1} T_{pq}^T} \\ &= \left(w_{pq}^C\right)^\alpha \cdot \left(w_{pq}^T\right)^{1-\alpha}. \end{aligned} \quad (3.2)$$

where w_{pq}^C is a *color-related* weight term, and w_{pq}^T is a *texture-related* weight term. The parameter α controls the relative impact of local color and texture patterns on the edge weights of the graph and can be adjusted in the optimization process. Edge weights *1*) only take color information into account if $\alpha = 1$; 2) factor color out, considering texture only if $\alpha = 0$; 3) combine color and texture features if $0 < \alpha < 1$.

We adopt the positive definite Gaussian function in Equation (E.1), due to its good property that has been proved in the literature [5, 117–119]. In the next two Subsections, we elaborate the color term and texture term respectively.

3.3.3.1 Color weight

Color Space Selection A color space is used to specify a three-dimensional color coordinate system and a subspace of the system in which colors are represented as three points [75]. In the present work, we finally decide to adopt YUV color space instead of RGB color space [120], for the following reasons:

YUV color space has independent color channels, in terms of one luma (Y') and two chrominance (UV) components. Moreover, there are couples of main disadvantages [121] with the RGB color space: *1*) It is not independent, has redundant information in color channels; *2*) The RGB color space is not perceptually uniform; *3*) All components (R, G, B) have equal importance and, therefore, these values have to be quantized with the same precision.

Given an input color image, we first decorrelate the RGB fields into the YUV color space by Equation (3.3). The Y stands for the luma component (the brightness) and U and V are the chrominance (color) components. We use the YUV color space, since it has independent color channels and allows to better deal with illumination changes.

$$Y = 0.299R + 0.587G + 0.114B \quad (3.3a)$$

$$U = (B - Y) * 0.565 \quad (3.3b)$$

$$V = (R - Y) * 0.713 \quad (3.3c)$$

The color weights on the edges are defined as:

$$w_{pq}^C = e^{-\lambda \cdot C_{pq} \Sigma_C^{-1} C_{pq}^T} = e^{-\lambda \cdot (\bar{C}_p - \bar{C}_q) \Sigma_C^{-1} (\bar{C}_p - \bar{C}_q)^T}, \quad (3.4)$$

where $C_{pq} = \bar{C}_p - \bar{C}_q$, $\bar{C}_p = (\bar{Y}_p, \bar{U}_p, \bar{V}_p)$ and $\bar{C}_q = (\bar{Y}_q, \bar{U}_q, \bar{V}_q)$ account for the *mean color vector* over a $n \times n$ patch centred on points p and q respectively in YUV color space. In our experiments, these two vectors are each computed over a 5×5 region in 4-neighbourhood system centred on p and q . As the aforementioned discussion, we use the YUV color space in order to have independent color channels.

We denote $Y_p = Y(x, y)$, respectively $U_p = U(x, y)$ and $V_p = V(x, y)$, as the color channel values at point $p = (x, y)$ in the coordinate system of the whole image. The mean color vector reads $\bar{C}_p = (\bar{Y}_p, \bar{U}_p, \bar{V}_p)$ where:

$$\bar{Y}_p = \frac{1}{n^2} \sum_{u=-n}^n \sum_{v=-n}^n Y(x+u, y+v),$$

$$\bar{U}_p = \frac{1}{n^2} \sum_{u=-n}^n \sum_{v=-n}^n U(x+u, y+v),$$

and

$$\bar{V}_p = \frac{1}{n^2} \sum_{u=-n}^n \sum_{v=-n}^n V(x+u, y+v).$$

The covariance matrix

$$\Sigma_C = \begin{bmatrix} \sigma_Y^2 & 0 & 0 \\ 0 & \sigma_U^2 & 0 \\ 0 & 0 & \sigma_V^2 \end{bmatrix}$$

is computed from, for all three channels, the mean of the mean color vector of all nodes. Moreover, the covariance matrix Σ_C is considered diagonal because of channels' independence. As in [122], the covariance is defined for each channel as:

$$\sigma_Y^2 = \langle (\bar{Y}_p - \bar{Y}_q)^2 \rangle$$

$$\sigma_U^2 = \langle (\bar{U}_p - \bar{U}_q)^2 \rangle$$

$$\sigma_V^2 = \langle (\bar{V}_p - \bar{V}_q)^2 \rangle$$

where $\langle . \rangle$ denotes the expectation over all the edges $(p, q) \in E$ of the image graph G .

3. GRAPH-BASED IMAGE REPRESENTATION

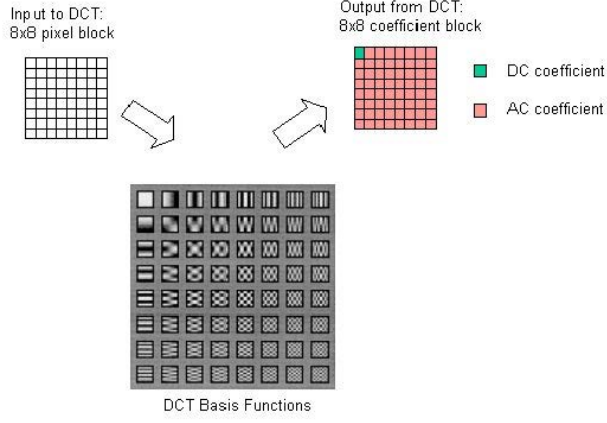


Figure 3.4: Block DCT on 8×8 pixel patch.

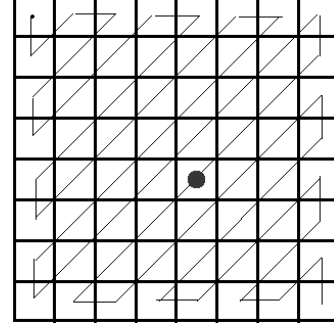


Figure 3.5: A block of 8×8 pixel on DCT, the solid dot in black denotes the graph node, the 64 DCT coefficients are scanned in a “zig-zag” fashion.

3.3.3.2 Texture weight

Texture based on DCT Given an image graph, the 2D block DCT-based transform is processed on 8×8 blocks of pixels around each graph node with level shift. As shown in Figure 3.4, each block contains one DC coefficient (in green) and 63 other AC coefficients (in red). The DC coefficient represents the average intensity value of the patch, and carries most of the energy and the perceptual information. The AC coefficients contain frequency information. The position of graph node within the block is shown in Figure 3.5.

The texture-related weight term w_{pq}^T based on DCT is defined as:

$$w_{pq}^T = e^{-\lambda \cdot \mathbf{T}_{pq} \Sigma_T^{-1} \mathbf{T}_{pq}^T} = e^{-\lambda \cdot (\mathbf{T}_p - \mathbf{T}_q) \Sigma_T^{-1} (\mathbf{T}_p - \mathbf{T}_q)^T} \quad (3.5)$$

where $\mathbf{T}_{pq} = \mathbf{T}_p - \mathbf{T}_q$, \mathbf{T}_p is a row vector composed of k low frequency AC coefficients in 8×8 DCT block centred on point p . \mathbf{T}_q is defined similarly. The covariance Σ_T is computed over DCT blocks for each coefficient independently over each node in G .

The vector \mathbf{T}_p has the following variants depending on the number of coefficients and the channel(s) in the YUV color system from which these coefficients are extract: 1) five low frequency coefficients in luma (Y) component (Equation (3.6)), its corresponding covariance is defined in Equation (3.7), see Figure 3.6; 2) ten low frequency coefficients in luma (Y) component (Equation (3.8)); 3) five low frequency coefficients in luma (Y) component, plus two low frequency coefficients in chrominance components (U and V) respectively (Equation (3.9)).

$$T_p = (d_Y(1, 0), d_Y(0, 1), d_Y(0, 2), d_Y(1, 1), d_Y(2, 0)) \quad (3.6)$$

$$\Sigma_T = \text{diag}[\sigma_{d(1,0)}^2, \sigma_{d(0,1)}^2, \sigma_{d(0,2)}^2, \sigma_{d(1,1)}^2, \sigma_{d(2,0)}^2] \quad (3.7)$$

$$T_p = (d_Y(1, 0), d_Y(0, 1), d_Y(0, 2), d_Y(1, 1), d_Y(2, 0), d_Y(3, 0), d_Y(2, 1), d_Y(1, 2), d_Y(0, 3)) \quad (3.8)$$

$$T_p = (d_Y(1, 0), d_Y(0, 1), d_Y(0, 2), d_Y(1, 1), d_Y(2, 0), d_U(1, 0), d_U(0, 1), d_V(1, 0), d_V(0, 1)) \quad (3.9)$$

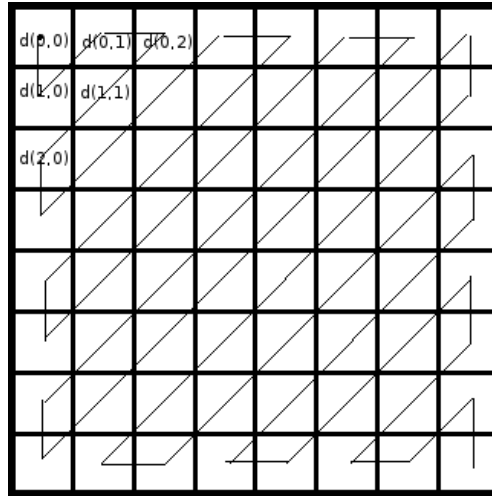


Figure 3.6: The DCT (Discrete Cosine Transform) block is scanned in a diagonal zigzag pattern starting at the DC coefficient $d(0,0)$ to produce a list of quantized coefficient values. Here only five AC coefficients $d(1,0)$, $d(0,1)$, $d(0,2)$, $d(1,1)$, $d(2,0)$ in luma (Y') component of YUV system are considered due to their good discriminative properties.

3.4 Graph Partitioning

After that the weighted image graph has been built, we can now shift our focus to the problem of graph partitioning. *Graph partitioning* is also called *graph clustering*. In this model of clustering, we are given an image graph G_j for each image I_j in the database. We seek to partition the graph G_j into fixed K disjoint unconnected subgraphs $\{g_{j,1}, \dots, g_{j,K}\}$, such that $\forall k \neq l, g_{j,k} \cap g_{j,l} = \emptyset$ and $G_j = \{\bigcup_{k=1}^K g_{j,k}\} \cup \mathcal{E}_j$, where $\mathcal{E}_j \subset E_j$ are the removed edges to divide G_j by graph cuttings. The partitioning divides vertices V_j into a set of the vertices $\{v_{j,1}, \dots, v_{j,K}\}$ in the corresponding subgraphs, such that $v_{j,m} \cap v_{j,n} = \emptyset$ for $m \neq n$. We denote this K -way partitioning [123] by $\Gamma_j^K = \{\Gamma_j^k\}_{k=1, \dots, K} = \{g_{j,1}, \dots, g_{j,K}\}$.

3. GRAPH-BASED IMAGE REPRESENTATION

3.4.1 Graph-based Image Segmentation Problem

Graph partitioning can be considered as a graph-based image segmentation problem as well [124]. The idea of graph-based image segmentation is that the set of points are represented as a weighted undirected graph $G = (V, E, W)$, where a set of vertices (nodes) V represents the points in the image. E is a set of edges connecting the nodes. W is an affinity matrix of size $|V| \times |V|$, whose entries are the weights of the edges. An entry of W is zero if there is no edge between the corresponding vertices. The weight on each edge $W(i, j)$ is a function of the similarity between the nodes i and j . The graph G is segmented into K disjoint sets by cutting the edges connecting these K parts. The degree of similarity between any two parts is the total weights of the edges that separate them.

3.4.2 Image Graph Labeling Problem

Graph partitioning can also be considered as a labeling problem. Given a set of vertices V and a finite set of labels $L = \{1, 2, \dots, K\}$, for any node $p \in V$, we are looking for the optimal label $l_p \in L$, such that the joint labeling $\mathcal{L} = \{l_1, \dots, l_{|V|}\} \in L^{|V|}$ satisfies a specified objective function. Reciprocally, an optimal labeling \mathcal{L} on the image graph can be represented by an optimal partition \mathbf{P} of graph nodes, where $\mathbf{P} = \{\mathcal{P}_l \mid l \in L\}$, and $\mathcal{P}_l = \{p \in \mathcal{P} \mid l_p = l\}$ is a subset of graph nodes assigned label l . Obviously, there is a bijective function (mapping) between partition \mathbf{P} and labeling \mathcal{L} .

Energy minimization Many computer vision problems, including labeling problem can be formulated in terms of energy minimization. For the image graph $G = (V, E)$, the energy function contains two terms:

$$J(L) = \sum_{p \in V} f_p(l_p) + \sum_{(p,q) \in E} f_{pq}(l_p, l_q). \quad (3.10)$$

l_p denotes the label of graph node $p \in V$ that must belong to a finite label set L . The unary terms $f_p(\cdot)$ encode the data penalty functions, and the pairwise terms $f_{pq}(\cdot, \cdot)$ are interaction potentials.

This energy (Equation (3.10)) is often derived in the context of Markov Random Fields (MRF) [50, 51]: a minimum of energy $J(L)$ corresponds to a maximum a-posteriori (MAP) labeling \mathcal{L} .

3.5 Graph Partitioning Approaches

In this Section, we review three graph partitioning methods, namely, Graph Cuts, Normalized Cuts and kernel k -means. As you will see in the next Chapters, we use and compare these three approaches within our system for image retrieval.

3.5.1 Graph Cuts: energy-based method

The Graph Cut [8, 9, 125, 126] is a semi-supervised method based on *min-cut/max-flow* algorithms from combinatorial optimization. This technique can be used to find the *global* minimum of some multi-dimensional energy functions. The formulation of Graph Cuts can be either perceived from graph partition point of view (Section 3.5.1.1), or regarded as an energy minimization on a graph from energy point of view (Section 3.5.1.3).

3.5.1.1 Binary labeling

In the context of Graph Cuts, the weighted graph $G = (V, E)$ has two distinguished vertices called the *terminals*. One of the terminals $s \in V$ is called the *source* and the other one $t \in V$ is called the *sink*. A cut $C \subset E$ is a set of edges such that the terminals are separated in the *induced* graph $G(C) = (V, E - C)$. In addition, no proper subset of C separates the terminals in $G(C)$. The cost of the cut C , denoted $|C|$, equals the sum of its edge weights. The *minimum* cut problem on a graph is to find a cut with the smallest cost among all cuts. There are a large number of fast algorithms for this problem in the binary labeling case. For example, in combinatorial optimization domain, the minimum s/t cut problem can be solved in polynomial time by finding a maximum flow from the source s to the sink t . This is the so-called *max-flow/min-cut algorithm*. In practice, the algorithm is based on the *Ford-Fulkerson* algorithm [127]. An example is shown in Figure 3.7.

Main idea for Min-cut/Max-flow methods Before introducing the min-cut/max-flow problem, let us give the following definition.

Definition 1. Flow network A *flow network* is defined as a directed graph where an edge has a non-negative capacity. For an edge $(p, q) \in E$, its capacity is denoted by $c(p, q)$.

3. GRAPH-BASED IMAGE REPRESENTATION

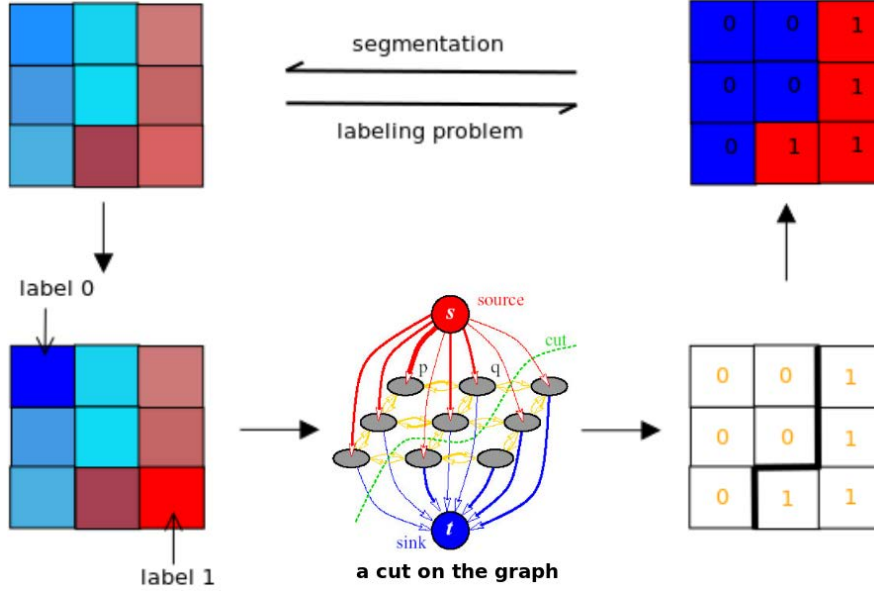


Figure 3.7: An example of binary labeling on an image graph via Graph Cuts. The graph corresponds to an image that consists of a 3×3 pixels set \mathcal{P} , with observed color intensities I_p in certain color space for each $p \in \mathcal{P}$. Given binary labels $L = \{0, 1\}$, an optimal labeling \mathcal{L} assigns label $l_p \in L$ to each pixel p . One part of this image is excerpted from [8].

Definition 2. Flow A flow in G is a real-valued (often integer) function that satisfies the following three properties:

- (a) Capacity constraint: for all $p, q \in V$, $f(p, q) \leq c(p, q)$.
- (b) Skew symmetry: for all $p, q \in V$, $f(p, q) = -f(q, p)$.
- (c) Flow conservation: for all $p \in \{V \setminus \{s, t\}\}$, $\sum_{q \in V} f(p, q) = 0$.

Definition 3. Capacity The capacity of a flow is the sum of the weights of the edges from two partitions A and B with $s \in A$ and $t \in B$.

In theory, the minimum cut problem can be solved by computing the maximum flow between the terminals, according to the following theorem from Ford and Fulkerson [128].

Theorem 1. Min-cut/max-flow theorem In a flow network, the maximum amount of flow passing from the source to the sink is equal to the minimum capacity that, when removed in a specific way from the network, causes the situation that no flow can pass from the source to the sink. In short, for any directed graph with arc capacity function C and distinct vertices s and t , the maximum value of an s - t flow is equal to the minimum capacity over all s - t cuts. Moreover, a maximum flow on G will saturate a set of edges that gives us the minimum cut.

From this theorem, an algorithm has been proposed. It requires two following definitions to understand it.

Definition 4. Augmenting path A path from the source s to the sink t that can deliver an increased flow is called a flow augmenting path.

Definition 5. Residual Graph of a flow network is a graph which indicates additional possible flow. If there is a path from the source to the sink in a residual graph, then it is possible to add flow. Every edge of a residual graph has a value called residual capacity which is equal to original capacity of the edge minus current flow. Residual capacity is basically the current capacity of the edge.

The min-cut/max-flow algorithm can now be given: The minimum cut edges can be ob-

Algorithm 1 Max-flow/Min-cut Algorithm

Require: Graph $G = (V, E)$, source s , terminal t , capacity C

Ensure: Return f as the Max-flow, and $(X, V - X)$ as the Min-cut

```

1: set  $P \leftarrow 0$  (flow 0 on all edges), set  $opt \leftarrow false$ 
2: while not  $opt$  do
3:   Construct the residual graph  $G_f$ 
4:   Find a directed path  $P$  from  $s$  to  $t$  in  $G_f$  (an augmenting path)
5:   if such an augmenting path  $P$  exists then
6:     Update flow  $f$  along  $P$ 
7:   else
8:     set  $opt \leftarrow true$ 
9:     set  $X$  the set of vertices in  $G_f$  reachable from  $s$ 
10:  end if
11: end while

```

tained by the following steps: 1) Run Ford-Fulkerson Algorithm 1 and consider the final residual graph. 2) Find the set of vertices that are reachable from the source in the residual graph. 3) All edges which are from a reachable vertex to a non-reachable vertex are minimum cut edges.

3.5.1.2 Extension to multi-label problems

The weighted graph $G = (V, E)$ may involve more than two *terminals*. The multi-labeling problem can be considered as the generalization of the minimum s/t cut problem. An exam-

3. GRAPH-BASED IMAGE REPRESENTATION

ple is the multi-way cut. The problem becomes NP-hard even in the simplest discontinuity-preserving case. Therefore, some approximate methods such as α - β swap and α -expansion [8, 9] are often used.

Definition 6. α - β swap Given a pair of labels α, β , a move from a partition P (labeling \mathcal{L}) to a new partition P' (labeling \mathcal{L}') is called an α - β swap if $\mathcal{P}_l = \mathcal{P}'_l$ for any label $l \neq \alpha, \beta$.

Definition 7. α -expansion Given a label α , a move from a partition P (labeling \mathcal{L}) to a new partition P' (labeling \mathcal{L}') is called an α -expansion if $\mathcal{P}_\alpha \subset \mathcal{P}'_\alpha$ and $\mathcal{P}'_l \subset \mathcal{P}_l$ for any label $l \neq \alpha$.

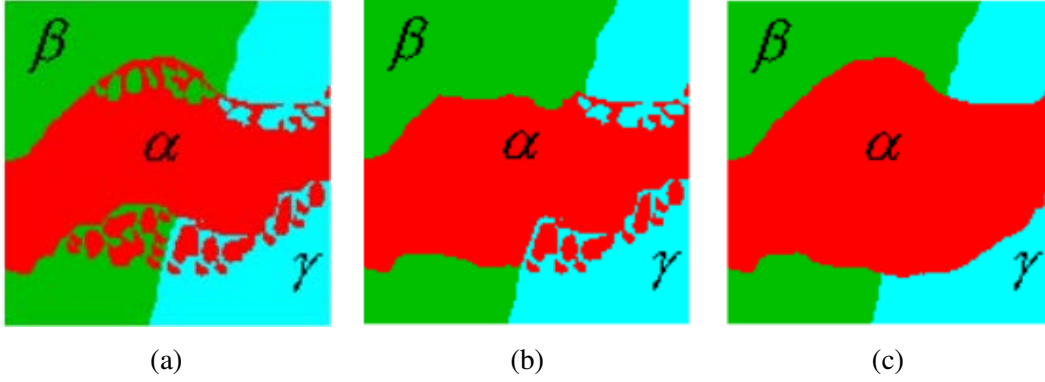


Figure 3.8: Example of α - β swap and α -expansion. (a) initial labeling: α in red, β in green, γ in blue. (b) α - β swap: only number of pixels with label α or β change their labels, pixels with label γ remain unchanged. (c) α -expansion: pixels with different labels can change their labels simultaneously. The figures are excerpted from [9]. This figure is better viewed in *color*.

3.5.1.3 Graph Cuts from perspective of energy minimization

In the present work, the Graph Cut is used to minimize energy functions of two terms:

$$\begin{aligned}
 J(\mathcal{L}) &= J_{data}(\mathcal{L}) + J_{smooth}(\mathcal{L}) \\
 &= \sum_{p \in V} J_d(p, l_p) + \sum_{(p,q) \in E} J_s(p, q) \\
 &= \sum_{p \in S} J_d(l_p) + \sum_{(p,q) \in E} J_s(p, q) .
 \end{aligned} \tag{3.11}$$

$J_{data}(\mathcal{L})$ is the *data term*. In our case, it is only applied to user-defined hard constraints (seeds here) imposed on the initialization of Graph Cuts. We denote a set of seed points by $S = \{s_1, \dots, s_K\}$, where K is the *predefined* number of subgraphs obtained after graph partitioning. The seeds are placed on the image before running the Graph Cuts algorithm.

The goal of the data term is to fix the label of the seed points. For instance, the seed point s_i must end up with label i after the energy minimization process. This idea can be formulated as in [9]:

$$J_d(l_p) = \begin{cases} 0 & \text{if } p = s_i \text{ \& } l_p = i \\ \infty & \text{otherwise.} \end{cases} \quad (3.12)$$

As for the *smoothness term* $J_{smooth}(\mathcal{L})$, this term measures the discontinuity between node p and its neighboring pixels. The use of α -expansion imposes three constraints on the smoothing term J_{smooth} , see Equation (3.11):

1. $J_{smooth}(\alpha, \beta) = 0 \Leftrightarrow \alpha = \beta$ or $J_{smooth}(\alpha, \beta) \neq 0 \Leftrightarrow \alpha \neq \beta$
2. $J_{smooth}(\alpha, \beta) = J_{smooth}(\beta, \alpha) \geq 0$
3. $J_{smooth}(\alpha, \beta) \leq J_{smooth}(\alpha, \gamma) + J_{smooth}(\gamma, \beta)$

The first two terms tell that an energy between two different labels α and β should be non-zero. If it is zero, then two labels are the same. The last term defines the triangle rule. A short cut is always cheaper or similar than taking the whole path. If the smoothness term only satisfies the first two terms, it is called a *semi-metric term*. If the last term is also satisfied, it is said a *metric term*. The α -expansion algorithm can only be used with metric terms. Otherwise, the alpha-beta swap can be used with semi-metric or metric terms. Note that in Equation (3.11), $J_{smooth}(\mathcal{L})$ satisfies the *metric term*.

To follow the pre-stated requirements, we will encourage that any two neighbouring nodes $(p, q) \in \mathcal{E}$ are 1) spatially close to each other; 2) if node p and q have similar colors, they tend to have the same label.

$J_{smooth}(\mathcal{L})$ is directly linked to w_{pq} , the edge weights of the image graph. The w_{pq} is defined as in Equation (E.1). In the present work, we propose the following variant definitions for $J_{smooth}(\mathcal{L})$:

$$J_s(p, q) = w_{pq}(1 - \delta(l_p, l_q)) , \quad (3.13)$$

or

$$J_s(p, q) = \frac{w_{pq}}{\|p - q\|^2}(1 - \delta(l_p, l_q)) , \quad (3.14)$$

or

$$J_s(p, q) = w_{pq}f_d(p, q)(1 - \delta(\ell_p, \ell_q)) , \quad (3.15)$$

3. GRAPH-BASED IMAGE REPRESENTATION

where $\delta(\ell_p, \ell_q)$ is the Kronecker's delta:

$$\delta(\ell_p, \ell_q) = \begin{cases} 0, & \text{if } \ell_p \neq \ell_q \\ 1, & \text{if } \ell_p = \ell_q. \end{cases} \quad (3.16)$$

In Equation (3.15), the distance between nodes is introduced via $f_d(p, q)$. This distance term $f_d(p, q)$ is defined as:

$$f_d(p, q) = \exp\left(-\lambda_2(p - q)\Sigma_d^{-1}(p - q)^T\right). \quad (3.17)$$

The matrix Σ_d is also considered diagonal. Let us denote $d(p, q)$ as the L_2 distance between the node p and q . The $d(p, q) = \sqrt{(x_p - x_q)^2 + (y_p - y_q)^2}$. We propose several definitions for Σ_d as follows:

1)

$$\Sigma_d = \begin{bmatrix} \bar{d}_E(p, q) & 0 \\ 0 & \bar{d}_E(p, q) \end{bmatrix}, \quad (3.18)$$

where $\bar{d}_E(p, q)$ is the mean distance of all neighbouring points in the graph G , *i.e.*

$$\begin{aligned} \forall (p, q) \in E, \bar{d}_E(p, q) &= \frac{\sum_{(p, q) \in E} d(p, q)}{|E|} \\ &= \frac{\sum_{(p, q) \in E} \sqrt{(x_p - x_q)^2 + (y_p - y_q)^2}}{|E|}. \end{aligned} \quad (3.19)$$

2)

$$\Sigma_d = \frac{\sum_{(p, q) \in E} \left(d(p, q) - \bar{d}_E(p, q)\right)}{|E|}. \quad (3.20)$$

3)

$$\Sigma_d = \frac{\sum_{(p, q) \in E} \left((d(p, q) - \bar{d}_E(p, q)) \cdot Pr(E)\right)}{|E|}, \quad (3.21)$$

where $Pr(E)$ is the probability of the distance of an edge falls into the bin that $d(p, q)$ belongs to. In our experiments, we set the number of bin size to 10.

Among the above three options for the distance term, the Equation (3.18) is easier to compute and has been proven to achieve better graph cuts result. However, we have also observed that embedding distance factor $f_d(p, q)$ in the smoothness term does not give any improvement to partition results; in the case of sparse sampling, it is even worse. Therefore, we decide that $f_d(p, q)$ can be factored out of the equations. In our case, we use Equation (3.13), *i.e.*, we only consider color and (or) texture factor(s) in the smoothness term in the following discussion.

3.5.1.4 Seed selection

1) In the case of prominent keypoints approach: to ensure that seeds with different labels will fall into heterogeneous regions in the image, we select seeds in such a way:

a) The fixed number of seed points $\mathcal{S} \subset \mathcal{P}$ are chosen among the most prominent keypoints in \mathcal{P} ; *b)* Different seeds should not be too close to each other and they should fall into heterogeneous region of their own in the image. To achieve this purpose, we set empirically both color and distance threshold to differentiate one seed from the other chosen ones.

For the i^{th} seed point $p_i \in \mathcal{S}$, the data term is defined as:

$$D(p_i, \ell) = \begin{cases} 0 & \text{if } \ell = \ell_i \\ \infty & \text{otherwise.} \end{cases} \quad (3.22)$$

An example is shown in Figure 3.2(c).

2) In the context of dense sampling: The seed points are chosen from nodes that are the closest to the barycentre of each regular cell, see Figure 3.9.

More complex seeds selection measures (such as, choosing interest points that have the most strong response; separating different seeds with enough distance based on image size or resolution) have been investigated, without improving the performance.

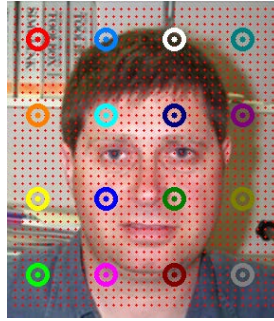


Figure 3.9: Seed points are in hollow circle of different colors. The graph nodes are in red solid points.

3.5.1.5 Weakness

Due to the uncontrolled nature of the images available, automatically and precisely selecting seeds from image is still beyond the reach of the state-of-the-art in computer vision.

3. GRAPH-BASED IMAGE REPRESENTATION

More precisely, if the seed points are manually selected, then the high level of user interaction makes the Graph Cuts method useless; if the seeds are automatically selected, then the k seed points will be highly dependent on the relationship between the background and the interest object. Hence, in prominent keypoints approach, we applied a mask on the image *before* running Graph Cuts to generate graph features. Unfortunately, the obtained seeds were still not stable. As shown in Figure 3.10, three seeds between two images “fluor5Banana095” and “fluor5Banana097” are relatively stable. In contrast, all three seeds in image “fluor5Banana098” have fallen into background. Moreover, two of these seeds are not matched with these ones in other two images.



Figure 3.10: Examples of seeds selection in prominent keypoints approach. The stability of seeds is hardly reached due to the uncontrolled nature of the images available. All examples of images are from *SIVAL* dataset [10]. There are three seeds in each image, and these seeds are labelled with their own colors (in red, orange and yellow). This figure is better viewed in *color*.

3.5.1.6 Graph Cuts in applications

The Graph Cuts based methods have wide applications in computer vision community, such as clustering (image segmentation) [129], image labeling [130, 131], image restoration [9, 132], multicamera scene reconstruction [8], registration [133, 134], object tracking [135], interactive seeded segmentation [122, 125], reducing metrication errors, filtering, stereo matching [8], recovering the deformation map etc.

3.5.2 Normalized Cuts

As a spectral clustering technique, *Normalized Cuts (NCuts)* [5], is an unsupervised method based on two *graph-theoretic criteria*: maximize the total dissimilarity between different subgraphs as well as the similarity within each subgraph. Its principle is to find a minimal cut which is a combination of edges having minimal sum of edge values (*i.e.* find the least alike pairs of nodes). Removing these edges divides the graph G_j into unconnected subgraphs, such that the similarity between nodes within a subgraph is greater than the similarity between nodes in separated subgraphs. The advantage of the normalized cut method is that it considers two aspects of graph segmentation: minimal cut (*i.e.* better separation) and preferring segments of large size.

3.5.2.1 Basic concepts and theory

The set of points in an arbitrary feature space can be represented as a weighted undirected graph $G = (V, E)$, where the nodes of the graph are the points in the feature space and an edge is formed between every pair of nodes. The weight on each edge, w_{ij} , represents the similarity between nodes i and j .

A graph can be partitioned into two *disjoint* sets \mathcal{A} and \mathcal{B} , with $\mathcal{A} \cap \mathcal{B} = \emptyset$ and $\mathcal{A} \cup \mathcal{B} = V$, by removing edges connecting the two parts.

Definition 8. Link Let us denote $links(\mathcal{A}, \mathcal{B})$ to be the sum of the edge weights between nodes in two *disjoint* sets \mathcal{A} and \mathcal{B} .

$$links(\mathcal{A}, \mathcal{B}) = \sum_{p \in \mathcal{A}, q \in \mathcal{B}} w_{pq} . \quad (3.23)$$

Definition 9. Degree We furthermore define the *degree* of \mathcal{A} as the links of nodes in \mathcal{A} to all the vertices in the graph G , that is, $degree(\mathcal{A}) = links(\mathcal{A}, V)$.

3. GRAPH-BASED IMAGE REPRESENTATION

Definition 10. Association The *association* (sum of all the weights) within the cluster \mathcal{A} is denoted by

$$assoc(\mathcal{A}, \mathcal{A}) = \sum_{p \in \mathcal{A}, q \in \mathcal{A}} w_{pq} . \quad (3.24)$$

Definition 11. Cut The degree of *dissimilarity* between \mathcal{A} and \mathcal{B} can be measured by $cut(\mathcal{A}, \mathcal{B})$, which is defined as the sum of all the weights being cut,

$$cut(\mathcal{A}, \mathcal{B}) = \sum_{p \in \mathcal{A}, q \in \mathcal{B}} w_{pq} . \quad (3.25)$$

Using a minimum cut as a segmentation criterion does not result in reasonable clusters, since the smallest cuts usually involve isolating a single pixel. Instead of using the value of total edge weight connecting the two partitions, Shi et al. [5] proposed a disassociation measure to compute the cut cost as a fraction of the total edge connections to all the nodes in the graph. It is called the Normalized Cut (NCut). The Normalized Cut examines the affinities (similarities) between nearby pixels and tries to separate groups that are connected by weak affinities.

Definition 12. Normalized Cut (NCut) The *disassociation* criterion for normalized cut of \mathcal{A} and \mathcal{B} is given by

$$NCut(\mathcal{A}, \mathcal{B}) = \frac{cut(\mathcal{A}, \mathcal{B})}{assoc(\mathcal{A}, V)} + \frac{cut(\mathcal{A}, \mathcal{B})}{assoc(\mathcal{B}, V)} , \quad (3.26)$$

where $assoc(\mathcal{A}, V) = assoc(\mathcal{A}, \mathcal{A}) + cut(\mathcal{A}, \mathcal{B}) = \sum_{p \in \mathcal{A}, q \in V} w(p, q)$ is the total connection from nodes in \mathcal{A} to all nodes in the graph and $assoc(\mathcal{B}, V)$ is similarly defined.

Definition 13. Normalized association (Nassoc) The normalized *association* can be defined as

$$Nassoc(\mathcal{A}, \mathcal{B}) = \frac{assoc(\mathcal{A}, \mathcal{A})}{assoc(\mathcal{A}, V)} + \frac{assoc(\mathcal{B}, \mathcal{B})}{assoc(\mathcal{B}, V)} , \quad (3.27)$$

where $assoc(\mathcal{A}, \mathcal{A})$ and $assoc(\mathcal{B}, \mathcal{B})$ are total weights of edges connecting nodes within \mathcal{A} and \mathcal{B} respectively.

Shi et al. [5] have proven that minimizing the disassociation (Equation (3.26)) is equivalent to maximizing the association (Equation (3.27)) within the groups according to Equation (3.28).

$$NCut(\mathcal{A}, \mathcal{B}) = 2 - Nassoc(\mathcal{A}, \mathcal{B}) . \quad (3.28)$$

The two equivalent objective functions above can also be interpreted as seeking to minimize the cut relative to the degree of a cluster instead of its size. Hence, the objectives in Equation (3.26)

and Equation (3.27) can be expressed as Equation (3.29) and Equation (3.30) respectively, as follows:

$$\min_{\mathcal{A}, \mathcal{B}} \left(\frac{\text{links}(\mathcal{A}, \mathcal{B})}{\text{degree}(\mathcal{A})} + \frac{\text{links}(\mathcal{B}, \mathcal{A})}{\text{degree}(\mathcal{B})} \right) \quad (3.29)$$

$$\max_{\mathcal{A}, \mathcal{B}} \left(\frac{\text{links}(\mathcal{A}, \mathcal{A})}{\text{degree}(\mathcal{A})} + \frac{\text{links}(\mathcal{B}, \mathcal{B})}{\text{degree}(\mathcal{B})} \right) \quad (3.30)$$

3.5.2.2 Computing NCut by eigen-value decomposition

Unfortunately, computing the optimal NCut is NP-complete. Instead, Shi et al. suggested solving NCuts as a regular eigenvalue problem by computing a real-valued assignment of nodes to groups. Let \mathbf{x} be an *indicator vector* of $|V|$ dimension, where $x_p = 1$ if node p is in \mathcal{A} and $x_p = -1$ otherwise. W is an $|V| \times |V|$ symmetrical matrix with $W(p, q) = w_{pq}$. $\mathbf{l} = \{1, \dots, 1\}^\top$ is an $|V| \times 1$ vector of all ones. Let $\mathbf{d} = W\mathbf{l}$ be the row sums of the symmetrical matrix W , $d(p) = \sum_q w_{pq}$, be the total connection from node p to all other nodes, and $D = \text{diag}(\mathbf{d})$ is the corresponding $|V| \times |V|$ diagonal matrix with \mathbf{d} on its diagonal, $D_{pp} = \sum_{q=1}^{|V|} w_{pq}$.

With the above notations, Shi et al. [5] have proved that minimizing the Normalized Cut over all possible indicator vectors \mathbf{x} is equivalent to minimizing the Rayleigh quotient [136] in the following Equation (3.31).

$$\arg \min \text{NCut}(\mathbf{x}) = \arg \min_{\mathbf{y}(p) \in \{1, -1\}, \mathbf{y}^T D \mathbf{l} = 0} \frac{\mathbf{y}^T (D - W) \mathbf{y}}{\mathbf{y}^T D \mathbf{y}} = \mathbf{y}_1. \quad (3.31)$$

where $\mathbf{y} = ((1 + \mathbf{x}) - b(1 - \mathbf{x}))/2$, $b = \frac{k}{1-k}$, $k = \frac{\sum_{x_i > 0} d_i}{\sum_i d_i}$. Obviously, \mathbf{y} is a vector consisting of 1s and -bs such that $\mathbf{y} \cdot \mathbf{d} = 0$. Here in Equation (3.31), \mathbf{y}_1 is the second smallest eigenvector corresponding to the 2nd smallest eigenvalue of Equation (3.32).

$$(D - W)\mathbf{y} = \lambda D\mathbf{y}. \quad (3.32)$$

The Equation (3.32) can be turned into a regular eigenvalue problem:

$$(\mathbf{I} - N)\mathbf{z} = \lambda \mathbf{z}, \quad (3.33)$$

where \mathbf{I} is unit matrix and $N = D^{-\frac{1}{2}} W D^{\frac{1}{2}}$ is the *normalized* affinity matrix and $\mathbf{z} = D^{\frac{1}{2}} \mathbf{y}$. The matrix $(D - W)$ is called the *Laplacian matrix*, which is known to be positive semi-definite [137]¹.

¹The real matrix A is called positive semi-definite if $\mathbf{z}^T A \mathbf{z} \geq 0$, where \mathbf{z}^T denotes the transpose of the vector \mathbf{z} . A is a Hermitian matrix all of whose eigenvalues are non-negative.

3. GRAPH-BASED IMAGE REPRESENTATION

3.5.2.3 The grouping algorithm description

Assume that an image is to be segmented via Normalized Cut, the algorithm of Normalized Cut is summarized as follows:

- (1) Define the feature description matrix for a given image and a weighting function.
- (2) Set up a weighted graph $G = (V, E)$, compute the edge weights and summarize information into W and D , as described in Section 3.5.2.2. The entries of matrix W is $W(p, q) = w_{pq}$. Its definition can be referred to Equation (E.1).
- (3) Define the matrix D , a $N \times N$ diagonal matrix with $d(p) = \sum_q W(p, q)$ on its diagonal.
- (4) Solve $(D - W)x = \lambda Dx$ for eigenvectors with the smallest eigenvalues.
- (5) Use the eigenvector with second smallest eigenvalue to bipartition the graph by finding the splitting points so that NCut is minimized.
- (6) Decide whether the current partition is stable and check the value of the resulting NCut. If the current partition should be subdivided, recursively repartition the segmented parts (go to step 2), otherwise exit.

The stability criterion is defined to measure the degree of smoothness in the eigenvector values. The simplest definition is based on first computing the histogram of the eigenvector values and then computing the ratio between the minimum and maximum values in the bins. In our experiments, we set a threshold on the ratio described above. The eigenvector which is smaller than the threshold is unstable. The value is set to be 0.05 in all our experiments.

3.5.2.4 Multiclass cuts of general *weighted* graph

Concerning multiclass K -way partitioning $\Gamma_{V_j}^K$ on a given I_j , the K -way normalized cut problem [123] is to minimize the links that escape a cluster relative to the total “weight” of the cluster. The $NCuts$ objective function, as a generalization of Equation (3.29), is expressed as:

$$WNCuts(G_j) = \min_{v_{j,1}, \dots, v_{j,K}} \sum_{k=1}^K \frac{links(v_{j,k}, V_j \setminus v_{j,k})}{w(v_{j,k})} \quad (3.34)$$

Then Equation (3.30) can be rewritten as:

$$WNassoc(G_j) = \max_{v_{j,1}, \dots, v_{j,K}} \sum_{k=1}^K \frac{links(v_{j,k}, v_{j,k})}{w(v_{j,k})} \quad (3.35)$$

Again, minimizing the disassociation factor in Equation (3.34) is equivalent to maximizing the association criterion in Equation (3.35).

Beside Normalized Cut objective function, we enumerate three prominent partitioning objectives for reference as follows:

Kernighan-Lin Objective The partitions in Kernighan-Lin (K-L) [138] are required to be of equal size. Suppose $G = (V, E, W)$ is divided into K partitions, then its objective can be written as

$$KL(G) = \min_{v_{j,1}, \dots, v_{j,K}} \sum_{k=1}^K \frac{\text{links}(v_{j,k}, V_j \setminus v_{j,k})}{|v_{j,k}|}, \quad (3.36)$$

subject to $|v_{j,k}| = |V_j|/K, \forall k = 1, \dots, K$.

Ratio Cut The Ratio cut [139] is a generalization of the Kernighan-Lin Objective. It does *not* require the partitions to be equal (sans cluster size restrictions). Its objective aims to minimize the cut between clusters and the remaining vertices. It is expressed as

$$RCut(G_j) = \min_{v_{j,1}, \dots, v_{j,K}} \sum_{k=1}^K \frac{\text{links}(v_{j,k}, V_j \setminus v_{j,k})}{|v_{j,k}|}. \quad (3.37)$$

Ratio Association The ration association [5], also known as average association, seeks to maximize within-cluster association relative to the size of the cluster. The objective reads as

$$RAssoc(G_j) = \max_{v_{j,1}, \dots, v_{j,K}} \sum_{k=1}^K \frac{\text{links}(v_{j,k}, v_{j,k})}{|v_{j,k}|}. \quad (3.38)$$

3.5.2.5 Normalized Cuts in applications

The Normalized Cut was initially proposed by J.Shi and J.Malik [5] for image segmentation. On the one hand, NCuts treat image segmentation as a graph partitioning problem, many researchers have applied it to (spectral) graph clustering [118, 119, 123, 140]. On the other hand, since NCuts can extract the global impression of an image, it is frequently used as a pre-processing step in image precessing, for example, superpixels [17].

3. GRAPH-BASED IMAGE REPRESENTATION

3.5.3 Kernel Based Multilevel Graph Clustering Algorithms

The Normalized Cut can be quite slow because it requires the solution of large sparse eigenvalue problems. Dhillon et al. [119] have developed a fast multilevel algorithm that directly optimizes various weighted graph clustering objectives by *kernel k-means* (KKM). The authors proved that different objective functions such as those from Ratio cut [139] and *NCuts* can be unified mathematically as a *matrix trace maximization problem* [141]. Therefore, given a general graph weight matrix W , the graph clustering processes can be refined depending on an updated adjacency matrix for the current level, following three phases: coarsening, based-clustering and refinement. In this thesis, we get the best results when adopting this algorithm for graph partitioning. More detail about this approach and its three phases are described below.

3.5.3.1 The standard k -means clustering algorithm

K -means [84] is an unsupervised learning algorithm that solves the well known clustering problem. The standard k -means procedure classifies a given data set through k clusters fixed *a priori*.

Given a set of vectors $\{\mathbf{a}_i\}_{i=1}^N = \{\mathbf{a}_1, \dots, \mathbf{a}_N\}$ ¹, the k -means algorithm seeks to find K clusters π_1, \dots, π_K that minimize the objective function:

$$\mathcal{D}(\{\pi_k\}_{k=1}^K) = \sum_{k=1}^K \sum_{\mathbf{a}_i \in \pi_k} d(\mathbf{a}_i, \mathbf{m}_k) = \sum_{k=1}^K \sum_{\mathbf{a}_i \in \pi_k} \|\mathbf{a}_i - \mathbf{m}_k\|^2, \quad (3.39)$$

where

$$\mathbf{m}_k = \frac{\sum_{\mathbf{a}_i \in \pi_k} \mathbf{a}_i}{|\pi_k|}$$

is the *centroid* (or *mean*) of the k -th cluster π_k for the clustering (or partitioning) $\{\pi_k\}_{k=1}^K$, $d(\mathbf{a}_i, \mathbf{m}_k)$ is the distance between the vector \mathbf{a}_i and the centroid \mathbf{m}_k . The term $\|\mathbf{a}_i - \mathbf{m}_k\|^2$ is a chosen distortion measure (squared Euclidean distance here) between data vector \mathbf{a}_i and the cluster centre \mathbf{m}_k .

A disadvantage of k -means is that clusters are only separable by *linear* hyperplane. A kernel version of k -means is used to counter this weakness, allowing data to be separated in non-linear space.

¹ \mathbf{a}_i is a point in \mathbb{R}^m

3.5.3.2 Kernel k -means

The *kernel k -means* algorithm [142], as its name implied, is a kernel version of k -means. The difference between standard k -means and kernel k -means objective function is that we replace \mathbf{a}_i in Equation (3.39) with a mapping function $\phi(\mathbf{a}_i)$, as following:

$$\begin{aligned} \mathcal{D}(\{\pi_k\}_{k=1}^K) &= \sum_{k=1}^K \sum_{\mathbf{a}_i \in \pi_k} d(\phi(\mathbf{a}_i), \widetilde{\mathbf{m}}_k) \\ &= \sum_{k=1}^K \sum_{\mathbf{a}_i \in \pi_k} \|\phi(\mathbf{a}_i) - \widetilde{\mathbf{m}}_k\|^2 \\ &= \sum_{k=1}^K \sum_{\mathbf{a}_i \in \pi_k} \left(\phi(\mathbf{a}_i) \cdot \phi(\mathbf{a}_i) - \frac{2 \sum_{\mathbf{a}_j \in \pi_k} \phi(\mathbf{a}_i) \cdot \phi(\mathbf{a}_j)}{|\pi_k|} + \frac{\sum_{\mathbf{a}_j, \mathbf{a}_l \in \pi_k} \phi(\mathbf{a}_j) \cdot \phi(\mathbf{a}_l)}{|\pi_k|^2} \right), \end{aligned} \quad (3.40)$$

where

$$\widetilde{\mathbf{m}}_k = \frac{\sum_{\mathbf{a}_i \in \pi_k} \phi(\mathbf{a}_i)}{|\pi_k|}$$

is the *centroid* of the k -th cluster π_k for the clustering $\{\pi_k\}_{k=1}^K$, $\phi(\mathbf{a}_i)$ denotes the data point \mathbf{a}_i in transformed space. The function ϕ is essential for mapping data points to a higher dimensional feature space. This mapping results in linear separators in that higher feature space, which correspond to non-linear separators in the original input space.

As explained in [143], a positive semi-definite matrix can be interpreted as a Gram matrix¹. Hence, any positive semi-definite matrix \mathcal{K} can be considered as a kernel matrix. Let us define a *kernel* matrix \mathcal{K} , whose entry $\mathcal{K}_{ij} = \phi(\mathbf{a}_i) \cdot \phi(\mathbf{a}_j) = \kappa(\mathbf{a}_i, \mathbf{a}_j)$, and $\kappa(\cdot, \cdot)$ is a kernel function to map the original points to inner products. Then, the squared Euclidean distances between points and centroids (both are in \mathbb{R}^m) can be computed only by *inner products*, i.e. the elements of kernel matrix. As shown in Equation (3.40), only inner products are used in this computation. We do not even need to know explicit representations of $\phi(\mathbf{a}_i)$ and $\phi(\mathbf{a}_j)$ in order to compute the distances between points and centroids. A few of popular kernel functions are listed in Table 3.1.

¹Given a set of vectors $\{\mathbf{a}_i\}_{i=1}^N = \{\mathbf{a}_1, \dots, \mathbf{a}_N\}$ (points in \mathbb{R}^m), the Gram matrix G is the matrix of all possible inner products of $\{\mathbf{a}_i\}_{i=1}^N$, i.e., $g_{ij} = \mathbf{a}_i^T \mathbf{a}_j$, where $(\cdot)^T$ denotes the transpose.

3. GRAPH-BASED IMAGE REPRESENTATION

Table 3.1: Examples of commonly used kernel functions.

Polynomial Kernel	$\kappa(\mathbf{a}_i, \mathbf{a}_j) = (\mathbf{a}_i \cdot \mathbf{a}_j + c)^d$
Gaussian Kernel	$\kappa(\mathbf{a}_i, \mathbf{a}_j) = \exp(-\ \mathbf{a}_i - \mathbf{a}_j\ ^2 / 2\sigma^2)$
Sigmoid Kernel	$\kappa(\mathbf{a}_i, \mathbf{a}_j) = \tanh(c(\mathbf{a}_i \cdot \mathbf{a}_j) + \theta)$

3.5.3.3 Weighted kernel k -means

In the weighted graph, the edge weights play an important role. For that reason, a weighted version of the kernel k -means is used for graph partitioning in our applications.

The weighted kernel k -means was first introduced in [123], its objective function can be written as the minimization of:

$$\mathcal{D}(\{\pi_k\}_{k=1}^K) = \sum_{k=1}^K \sum_{\mathbf{a}_i \in \pi_k} w_i d(\phi(\mathbf{a}_i), \widetilde{\mathbf{m}}_k) = \sum_{k=1}^K \sum_{\mathbf{a}_i \in \pi_k} w_i \|\phi(\mathbf{a}_i) - \widetilde{\mathbf{m}}_k\|^2, \quad (3.41)$$

where

$$\widetilde{\mathbf{m}}_k = \frac{\sum_{\mathbf{a}_i \in \pi_k} w_i \phi(\mathbf{a}_i)}{\sum_{\mathbf{a}_i \in \pi_k} w_i} = \underset{\mathbf{z}}{\operatorname{argmin}} \sum_{\mathbf{a}_i \in \pi_k} w_i \|\phi(\mathbf{a}_i) - \mathbf{z}\|^2$$

represents the “best” cluster representative, and the weights are non-negative ($w_i \geq 0$). Similarly in Equation (3.40), the clusters can be computed by using the entries of kernel matrix since the term

$$\begin{aligned} w_i \|\phi(\mathbf{a}_i) - \widetilde{\mathbf{m}}_k\|^2 &= \phi(\mathbf{a}_i) \cdot \phi(\mathbf{a}_i) - \frac{2 \sum_{\mathbf{a}_j \in \pi_k} w_j \phi(\mathbf{a}_i) \cdot \phi(\mathbf{a}_j)}{\sum_{\mathbf{a}_j \in \pi_k} w_j} + \frac{\sum_{\mathbf{a}_j, \mathbf{a}_l \in \pi_k} w_j w_l \phi(\mathbf{a}_j) \cdot \phi(\mathbf{a}_l)}{(\sum_{\mathbf{a}_j \in \pi_k} w_j)^2} \\ &= \mathcal{K}_{ii} - \frac{2 \sum_{\mathbf{a}_j \in \pi_k} w_j \mathcal{K}_{ij}}{\sum_{\mathbf{a}_j \in \pi_k} w_j} + \frac{\sum_{\mathbf{a}_j, \mathbf{a}_l \in \pi_k} w_j w_l \mathcal{K}_{jl}}{(\sum_{\mathbf{a}_j \in \pi_k} w_j)^2}, \end{aligned} \quad (3.42)$$

only requires computing inner products.

The basic graph partitioning procedure by weighted kernel k -means is illustrated in Algorithm 2. If the number of data points is n , the data dimension is m , the total number of iterations is τ , then the time complexity of the algorithm is $\mathcal{O}(n^2(\tau + m))$. The complexity can be further reduced to $\mathcal{O}(nz \cdot \tau)$, if kernel matrix \mathcal{K} is a sparse matrix, with nz as the number of nonzero entries in the matrix ($nz = n^2$ for a dense kernel matrix).

Algorithm 2 Graph clustering by weighted kernel k-means

Require: Weighted graph $G = (V, E, W)$, kernel matrix \mathcal{K} , fixed clusters number K , optional initial clusters $\{\pi_c^{(0)}\}_{c=1}^K$, iteration counter t , optional maximum number of iterations t_{max} .

Ensure: Output final clusters $\{\pi_k\}_{k=1}^K$.

- 1: set $t \leftarrow 0$, initialize the K clusters π_1^0, \dots, π_K^0 if not given.
 - 2: **while** $t < t_{max}$ or not converged **do**
 - 3: **for each** graph node $a_i \in V$ **do**
 - 4: **for every** cluster k **do**
 - 5: compute $w_i d(\phi(a_i), \widetilde{m}_k)$ in Equation (3.42)
 - 6: **end for**
 - 7: $c^*(a_i) = \operatorname{argmin}_k (w_i d(\phi(a_i)))$
 - 8: **end for**
 - 9: Update the clusters as $\pi_c^{(t+1)} = \{a : c^*(a_i) = c\}$.
 - 10: set $t \leftarrow t + 1$
 - 11: **end while**
 - 12: output final clusters $\{\pi_k^{(t)}\}_{k=1}^K$.
-

3.5.3.4 Multilevel weighted kernel k -means algorithm

The multilevel scheme Dhillon et al. developed a general graph clustering algorithm based on multilevel methods [11]. This algorithm works for a wide class of graph clustering objectives. It includes three phases: coarsening, based-clustering and refinement. We describe each of these phases in more detail below. An illustration of this multilevel K -way partitioning scheme for irregular graphs is shown in Figure 3.11.

Coarsening phase Let us denote the edge weight between vertices x and y by $e(x, y)$, weights of vertices x and y are $w(x)$ and $w(y)$ respectively. We define the weight of a vertex as its degree (see Definition 9), in case of Normalized Cuts.

Starting with the initial graph $G_0 = (V_0, E_0, W_0)$, the coarsening phase repeatedly transforms the graph into smaller graphs G_1, G_2, \dots, G_m such that $|V_0| > |V_1| > \dots > |V_m|$. During coarsening phase, a set of nodes of the graph G_l is combined into a single *super vertex* in a coarser graph G_{l+1} . The super vertex is formed in such a way: Given an unmarked vertex x in graph $G_l = (V_l, E_l, W_l)$, we seek to combine the vertex x with another vertex $y \in V_l$ that assures

3. GRAPH-BASED IMAGE REPRESENTATION

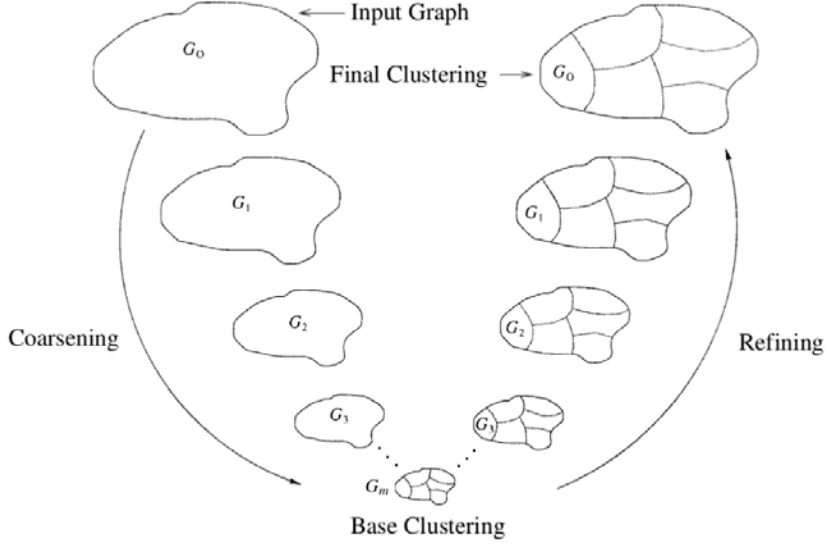


Figure 3.11: An overview of the kernel-based multilevel algorithm for graph clustering proposed by Dhillon et al. [11], here $K = 6$. A part of this image is excerpted from [12].

the following criterion:

$$\max \left(\frac{e(x, y)}{w(x)} + \frac{e(x, y)}{w(y)} \right). \quad (3.43)$$

The weights of the super vertices of the coarser graph reflect the weights of the vertices of the finer graph. This procedure is described as in Algorithm 3.

Base clustering phase After the coarsening phase, we get the coarsest graph G_m that contains much smaller number of vertices than the initial graph G_0 . We can specify how smaller G_m to be by using a pre-defined parameter. In the experiments, we keep coarsening the graph as long as the number of graph nodes is sufficiently larger than $\max(\frac{|V|}{5K}, 20)$, where K is a fixed number of desired clusters. Once the coarsening phase is finished, we can apply different graph clustering objectives (see Section 3.5.2.4) on the coarsest graph until K clusters are obtained. We call this phase as “base clustering”. In the present work, we use the *NCuts* objective function, as defined in Equation (3.34). This initial clustering is efficient in terms of speed, since the coarsest graph G_m is significantly smaller than the input graph G_0 .

Refinement phase In the final refining phase, given a graph G_l , we build the finer graph G_{l-1} (G_{l-1} is the same graph used in level $l - 1$ in the coarsening phase). An initial clustering for the graph G_{l-1} is defined in the following way: If a super vertex is in the cluster k in G_l , then

all nodes in G_{l-1} that formed this super vertex are in cluster k . At all levels except the coarsest level of G_m , the initial clustering of the graph is extended from the previous coarser level.

As justified in [141], both a general weighted kernel k -means objective and a weighted graph partitioning objective can be mathematically expressed as matrix trace maximizations problem. This equivalence has important significations: we can directly apply the weighted kernel k -means algorithm, as described in Algorithm 2, to optimize the graph partitioning objectives such as Ratio cut, Normalized cut and ratio association etc, and vice versa. Hence, after the initialization step, we run the weighted kernel k -means algorithm recursively to refine the clustering from the coarsest graph G_m to the original graph G_0 . The algorithm can converge very quickly at each level, due to good initial clustering.

Algorithm 3 Graph clustering in coarsening phase

Require: Initial graph $G_0 = (V_0, E_0, W_0)$.

Ensure: Output a series of smaller graphs G_1, G_2, \dots, G_m on coarse level $l = 1, 2, \dots, m$.

```

1: set  $t \leftarrow 0, \forall x \in V_0, \text{unmark}(x)$ .
2: while  $l < m$  do
3:   for current level  $l$  with its corresponding graph  $G_l = (V_l, E_l, W_l)$  do
4:      $\text{unmark}(x), x \in V_l$ 
5:     repeat
6:       for each unmarked  $x \in V_l$  do
7:         if  $\nexists y \in V_l$  that is unmarked then
8:            $\text{mark}(x)$ 
9:         else
10:          find  $y$  that satisfies the Equation (3.43)
11:          super vertex  $z \leftarrow$  merge  $x$  and  $y$ 
12:           $w(z) = w(x) + w(y)$ 
13:        end if
14:      end for
15:    until  $\text{marked}(x)$  is true,  $\forall x \in V_l$ 
16:  end for
17: end while

```

3. GRAPH-BASED IMAGE REPRESENTATION

3.5.3.5 Kernel k -means in applications

In real life data set, the structures are often hard to be separated in linear space. Kernel k -means (KKM) has been suitable to identify clusters that are non-linearly separable in input space. For instance, Dhillon et al. [123] applied KKM to diametrical clustering of gene expression and handwriting recognition, and achieved good results. One of disadvantages for KKM is that the number of cluster centres need to be predefined.

3.6 Illustrations of Graph Partitioning

In this Section, several examples are enumerated on the graph partitioning results obtained by using the aforementioned three different partitioning methods. The images are selected from six categories: “*accordion*” (Figure 3.12 and Figure 3.18), “*faces*” (Figure 3.13 and Figure 3.19), “*pagoda*” (Figure 3.14 and Figure 3.20), “*trilobite*” (Figure 3.14 and Figure 3.20), “*cellphone*” (Figure 3.16 and Figure 3.22), and “*motorbikes*” (Figure 3.17 and Figure 3.23) in *Caltech-101* dataset [144]. Here we only list five examples per category. More details will be discussed in Section 6.9.1 of the Chapter 6.

Figure 3.12, Figure 3.13, Figure 3.14, Figure 3.15, Figure 3.16 and Figure 3.17 present images that are divided into 4 subgraphs with three different methods: either Graph Cuts (GC) or Normalized Cuts (NC) or kernel k -means (KKM). The name of each image is marked on the left side of the figure.

In like manner, Figure 3.18, Figure 3.19, Figure 3.20, Figure 3.21, Figure 3.22 and Figure 3.23 illustrate the partitioning results in which each image is composed of 16 irregular subgraphs. The 1-3 columns in each figure correspond to the partitioning results obtained via Graph Cuts (GC), Normalized Cut (NC), kernel k -means (KKM) respectively.

Some observations on these (eight) figures: 1) There exist very small subgraphs that contain only a few of isolated points in partitions, e.g. an isolated green point on image *accordion0031* (GC) in the Figure 3.12; two scattered red points in *pagoda0035* (GC) and *pagoda0047* (GC) in Figure 3.14; two isolated points in blue and garnet red color respectively in *faces0039* (GC) in Figure 3.19 etc. 2) In case of 4 partitions per image, object of interest can be represented by only one or two subgraphs. 3) Despite the weights (objective function) defined on the graph edges are the same, the partitioning results (obtained subgraphs) vary from individual to individual in the same image.

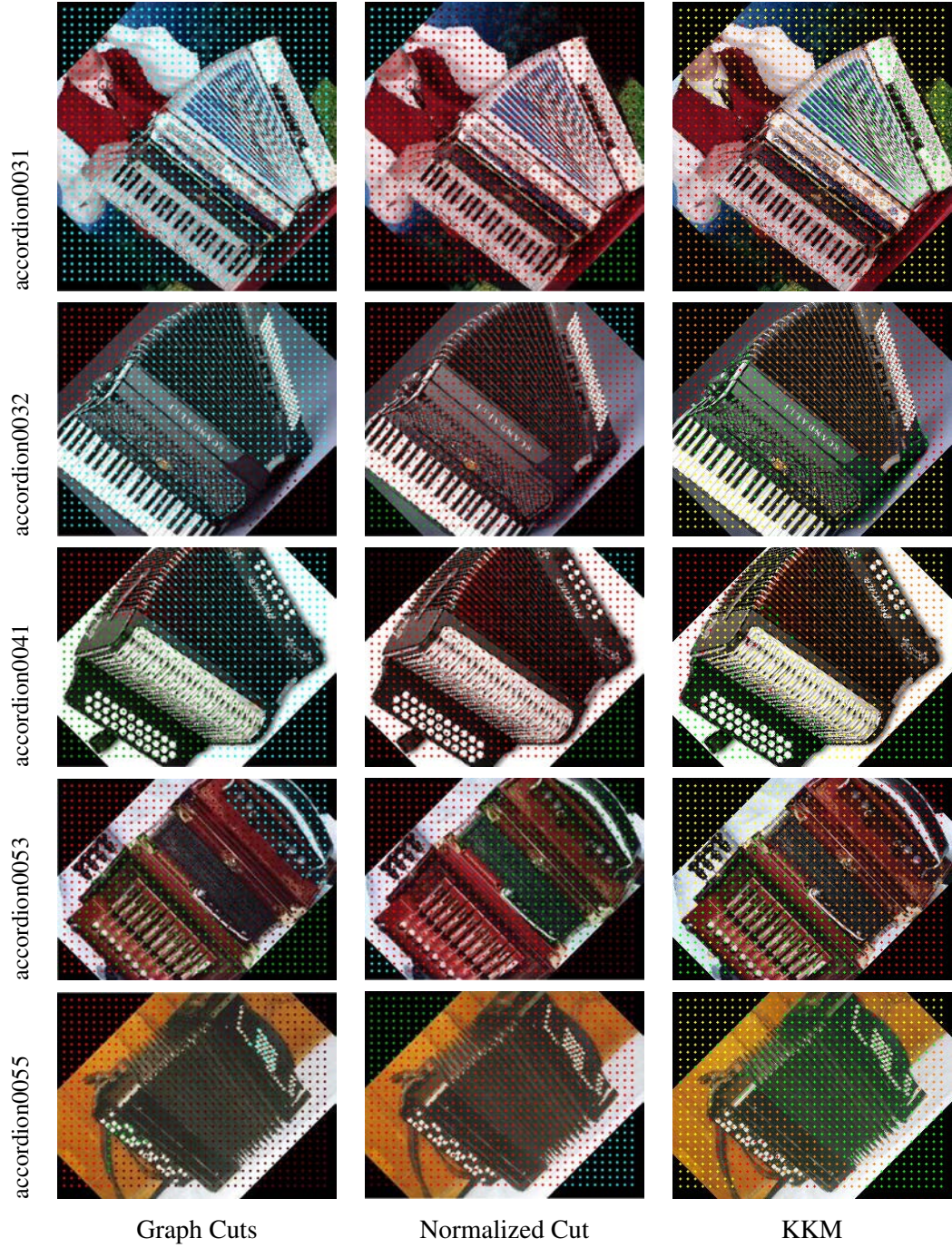


Figure 3.12: Examples of graph partitioning in 4 irregular subgraphs on five examples in category “*accordion*” from Caltech-101 dataset by three methods: Graph Cuts (GC), Normalized Cut (NC), kernel k -means (KKM). This figure is better viewed in *color*.

3. GRAPH-BASED IMAGE REPRESENTATION



Figure 3.13: Examples of graph partitioning in 4 irregular subgraphs on five examples in category “faces” from Caltech-101 dataset by three methods: Graph Cuts (GC), Normalized Cut (NC), kernel k -means (KKM). This figure is better viewed in *color*.

3.7 Conclusions

In this Chapter, we have presented three typical graph partitioning approaches: Graph Cuts, Normalized Cuts, and kernel based multilevel graph clustering algorithm. These three methods will be used in our proposed model in the next Chapter 4 and be compared in Chapter 6.

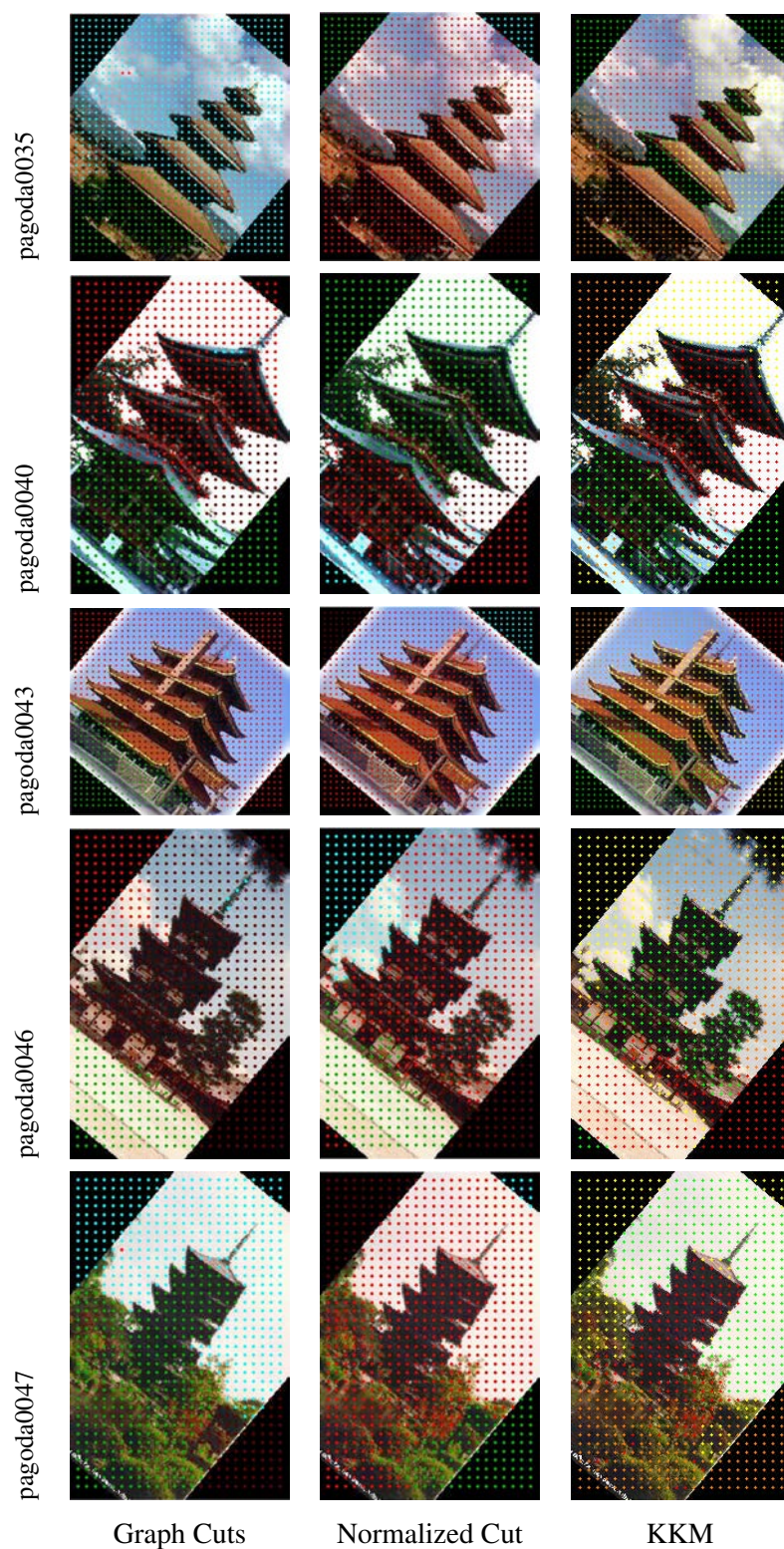


Figure 3.14: Examples of graph partitioning in 4 irregular subgraphs on five examples in category “pagoda” from Caltech-101 dataset by three methods: Graph Cuts (GC), Normalized Cut (NC), kernel k -means (KKM). This figure is better viewed in *color*.

3. GRAPH-BASED IMAGE REPRESENTATION

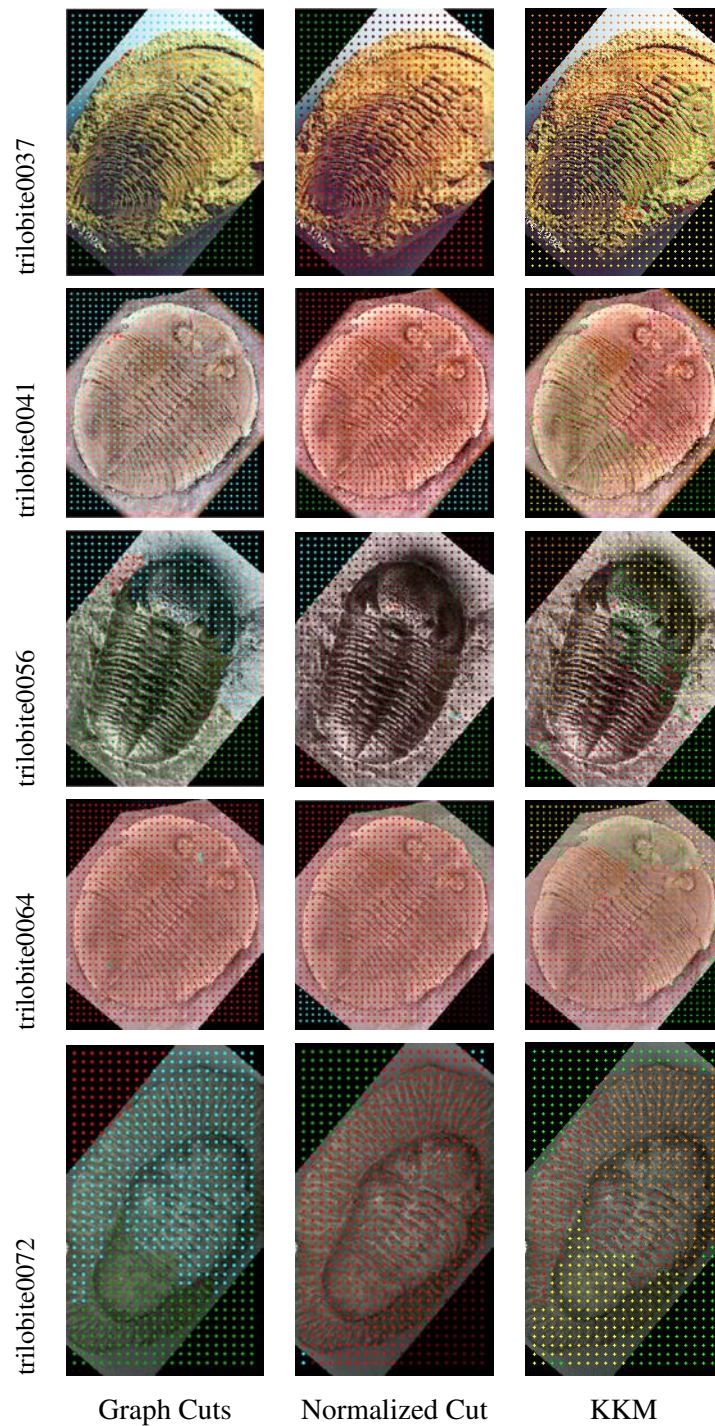


Figure 3.15: Examples of graph partitioning in 4 irregular subgraphs on five examples in category “trilobite” from Caltech-101 dataset by three methods: Graph Cuts (GC), Normalized Cut (NC), kernel k -means (KKM). This figure is better viewed in *color*.

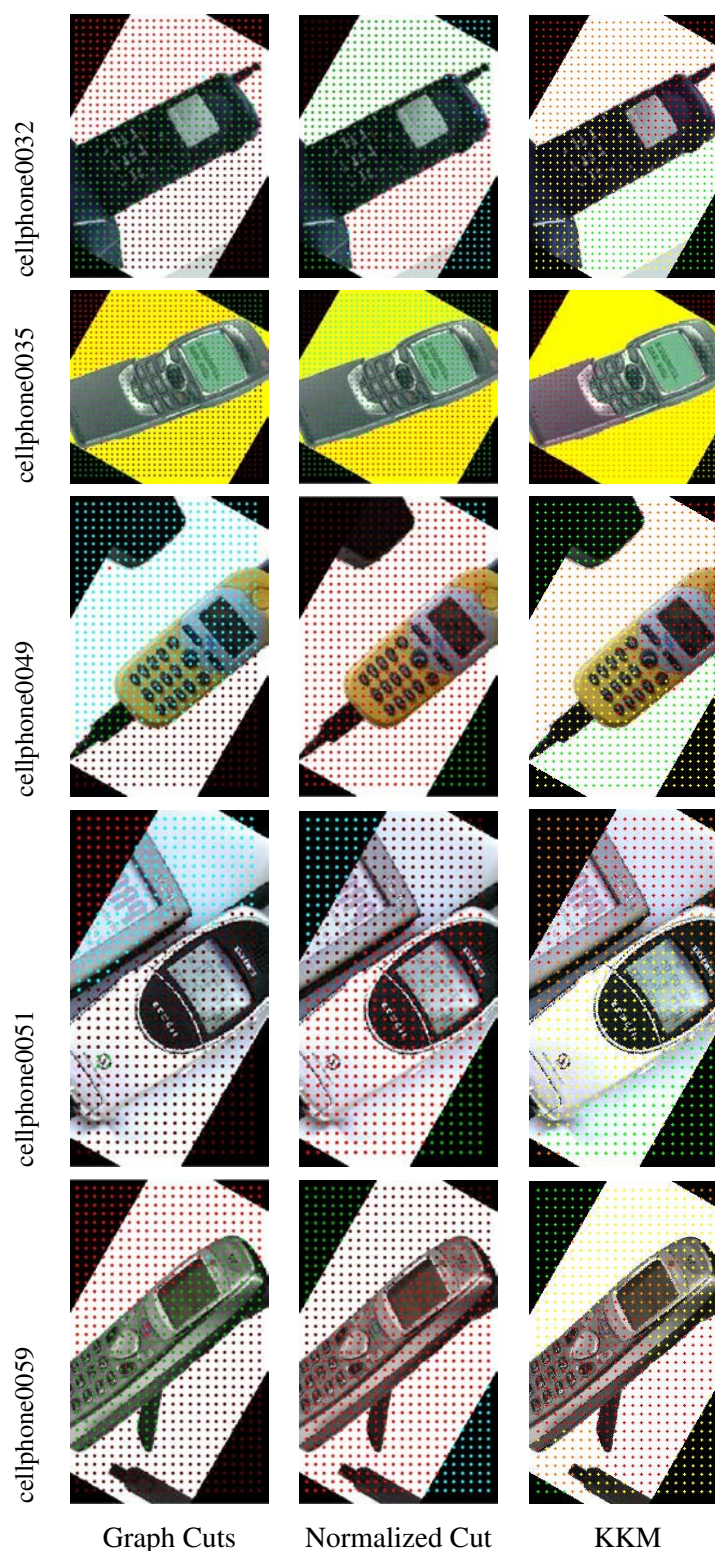


Figure 3.16: Examples of graph partitioning in 4 irregular subgraphs on five examples in category “cellphone” from Caltech-101 dataset by three methods: Graph Cuts (GC), Normalized Cut (NC), kernel k -means (KKM). This figure is better viewed in *color*.

3. GRAPH-BASED IMAGE REPRESENTATION

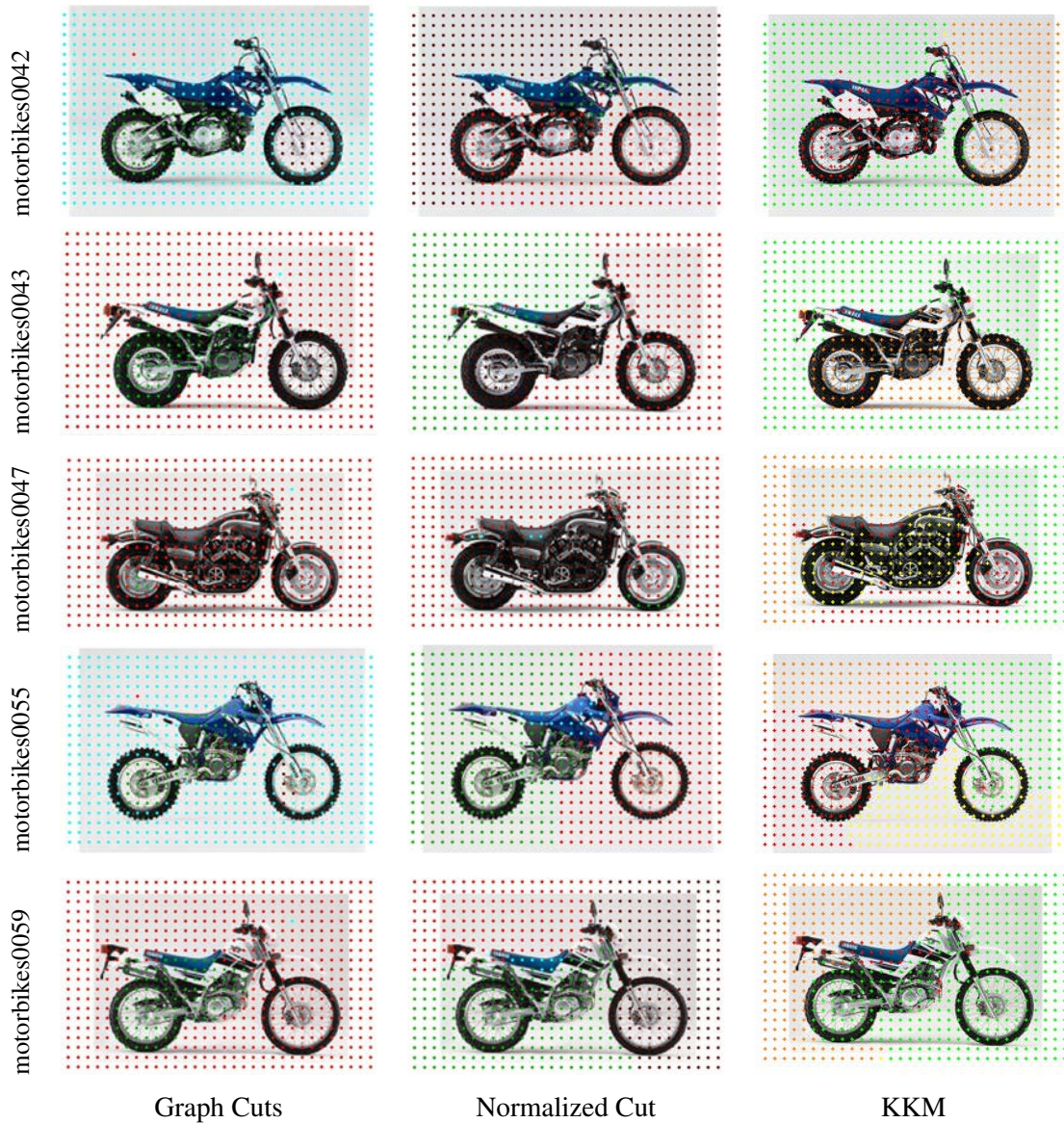


Figure 3.17: Examples of graph partitioning in 4 irregular subgraphs on five examples in category “motorbikes” from Caltech-101 dataset by three methods: Graph Cuts (GC), Normalized Cut (NC), kernel k -means (KKM). This figure is better viewed in *color*.

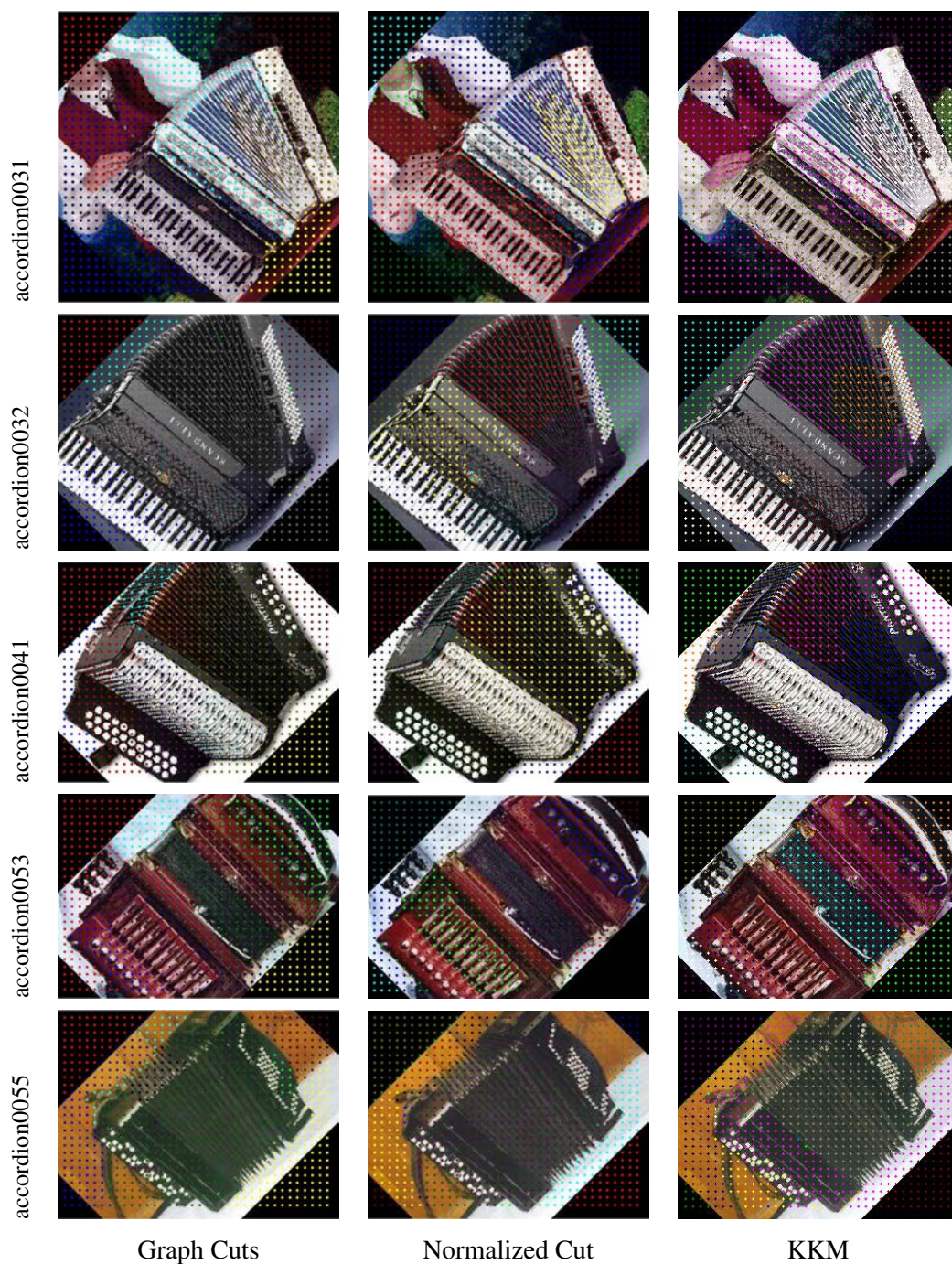


Figure 3.18: Examples of graph partitioning in 16 irregular subgraphs on five examples in category “*accordion*” from Caltech-101 dataset by three methods: Graph Cuts (GC), Normalized Cut (NC), kernel k -means (KKM). This figure is better viewed in *color*.

3. GRAPH-BASED IMAGE REPRESENTATION



Figure 3.19: Examples of graph partitioning in 16 irregular subgraphs on five examples in category “faces” from Caltech-101 dataset by three methods: Graph Cuts (GC), Normalized Cut (NC), kernel k -means (KKM). This figure is better viewed in *color*.

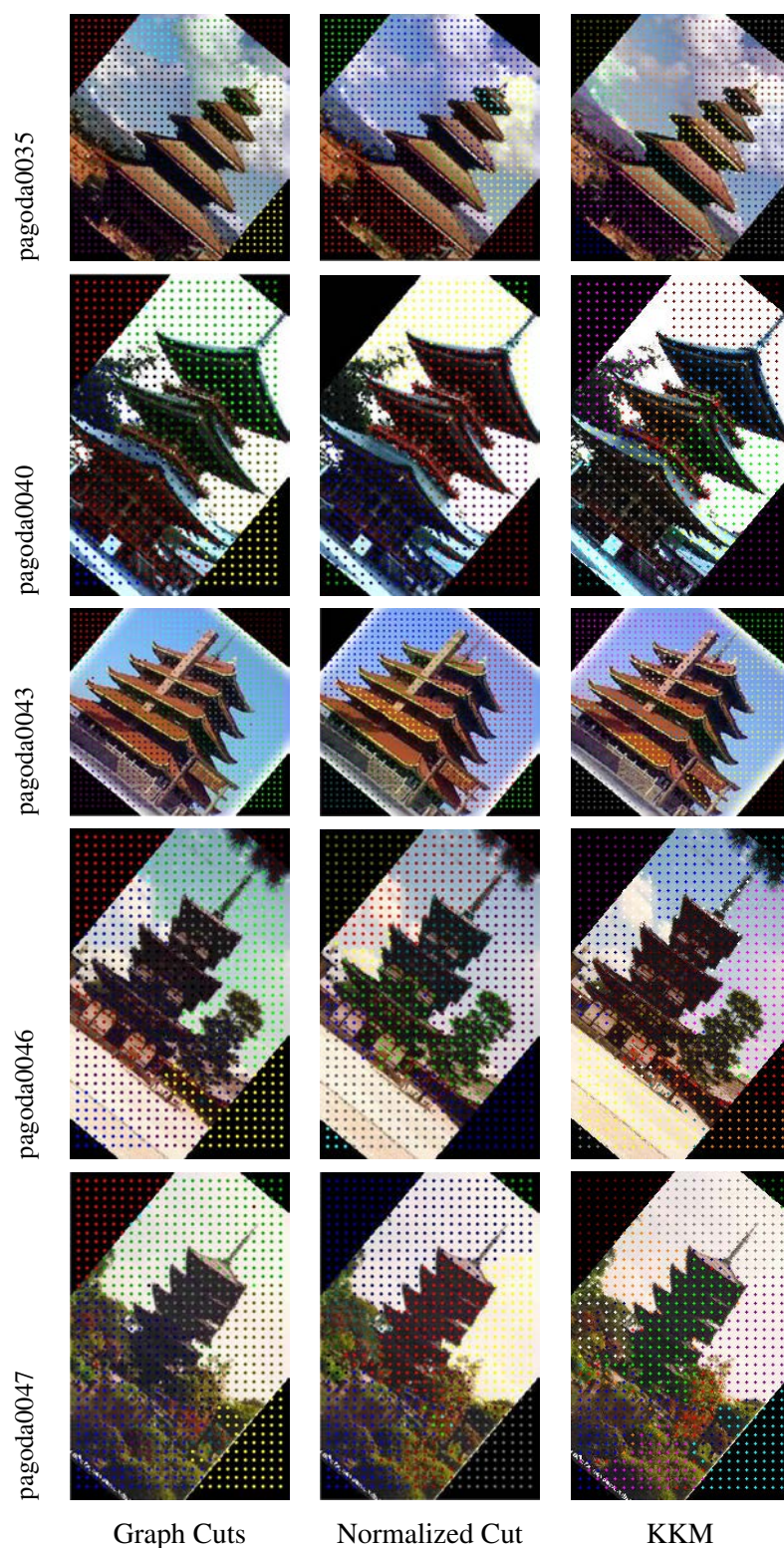


Figure 3.20: Examples of graph partitioning in 16 irregular subgraphs on five examples in category “pagoda” from Caltech-101 dataset by three methods: Graph Cuts (GC), Normalized Cut (NC), kernel k -means (KKM). This figure is better viewed in *color*.

3. GRAPH-BASED IMAGE REPRESENTATION

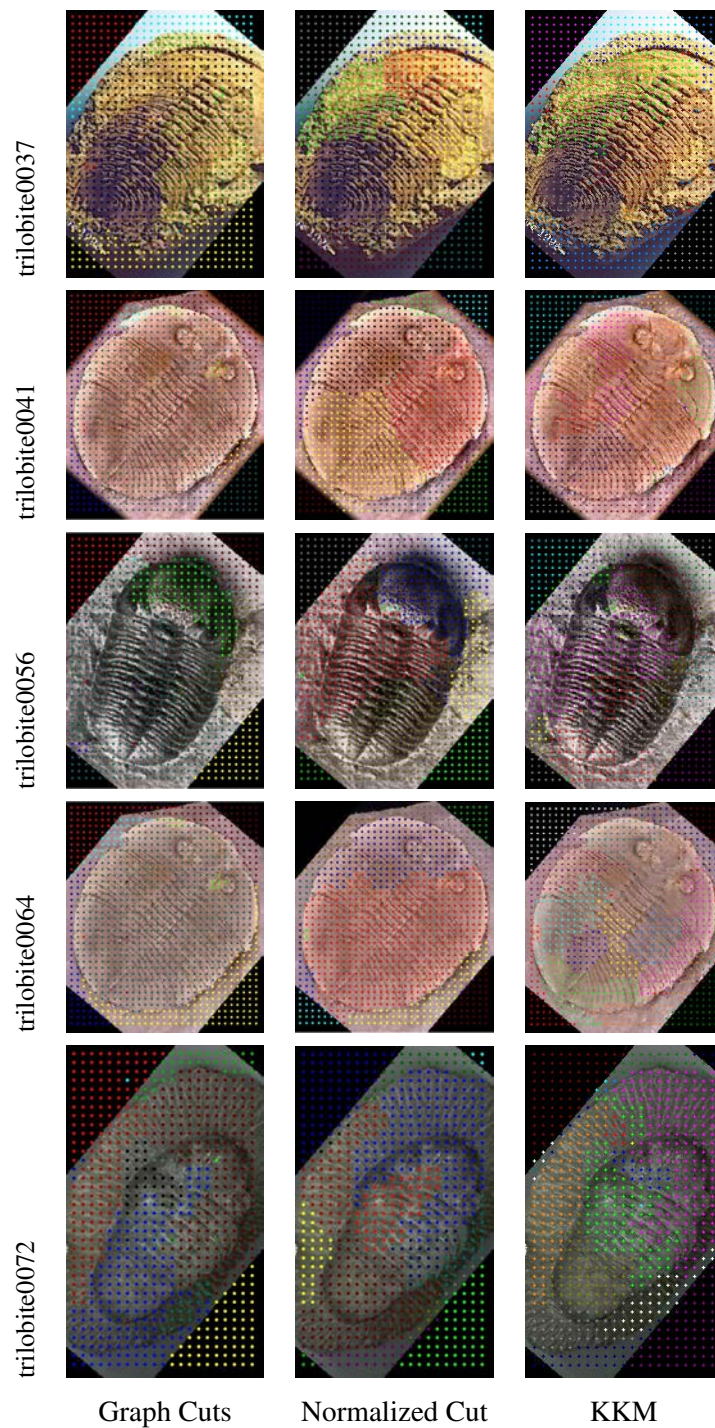


Figure 3.21: Examples of graph partitioning in 16 irregular subgraphs on five examples in category “trilobite” from Caltech-101 dataset by three methods: Graph Cuts (GC), Normalized Cut (NC), kernel k -means (KKM). This figure is better viewed in *color*.

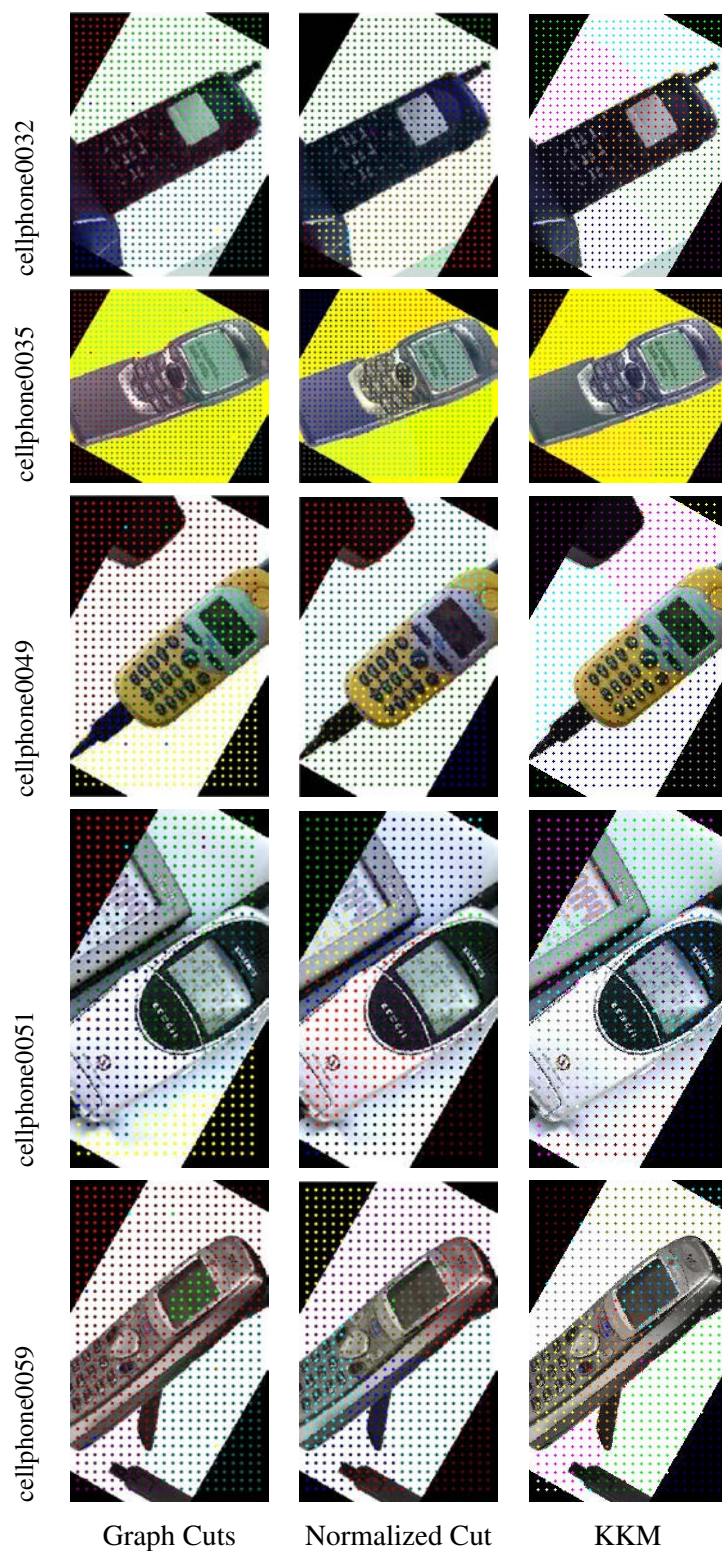


Figure 3.22: Examples of graph partitioning in 16 irregular subgraphs on five examples in category “cellphone” from Caltech-101 dataset by three methods: Graph Cuts (GC), Normalized Cut (NC), kernel k -means (KKM). This figure is better viewed in *color*.

3. GRAPH-BASED IMAGE REPRESENTATION



Figure 3.23: Examples of graph partitioning in 16 irregular subgraphs on five examples in category “motorbikes” from Caltech-101 dataset by three methods: Graph Cuts (GC), Normalized Cut (NC), kernel k -means (KKM). This figure is better viewed in *color*.

Chapter 4

Bag-of-Bags of Words Model

In this chapter, we introduce the proposed ‘Bag-of-Bags of Words’ model. We aim to model an image by graphs. An image is first represented as an *undirected weighted* graph. This initial image graph is partitioned into a *fixed* number of subgraphs that describe similar components in the image. Each subgraph is further described by bag-of-words features. Finally, a novel graph-based image representation model derives from those subgraphs descriptors.

4.1 Overview of the Bag-of-Bags of Words Model

Before introducing our model formally, here we explain its general principle and construction. Bag-of-Bags of Words for a given image, is a set of Bag-of-Words (BoWs). Each of BoWs is computed on vertices of image subgraph obtained by irregular partition of image graph. Next, the rationale for our “Bag-of-Bags” is in the correlation with two notable concepts: 1) Bag of Features (BoF) [31], *i.e.*, the unordered set of local descriptors extracted from an image. These local features are extracted from either fixed grid points or detected points of interest in the image. 2) “Bag-of-Words” (BoW) model, as proposed by Sivic et al. [16] and Csurka et al. [80]. Indeed, our description is a set of unordered features (BoF), each feature being a BoW built upon an image subgraph.

We will now describe a methodology for the construction of *BBoW* model. Then in Section 4.1.4, we will formalize the model more thoroughly. In Section 4.3, we present our contribution regarding the use of our *BBoW* model for image retrieval.

The *BBoW* model of an image is built as follows: 1) Select a reduced number of pixels V ; 2) Build an initial image graph G ; 3) Partition the graph G into K subgraphs; 4) Compute a

4. BAG-OF-BAGS OF WORDS MODEL

signature for each subgraph.

The signature of a subgraph is a histogram of codeword occurrences, obtained by assigning the feature vector of each graph node in this subgraph to the closest visual word in the codebook. Hence, an image composed of K subgraphs is characterized by a set of K histograms. An overview of the proposed framework is shown in Figure 4.1. In the following, we will detail how to construct the *BBoW* model step by step.

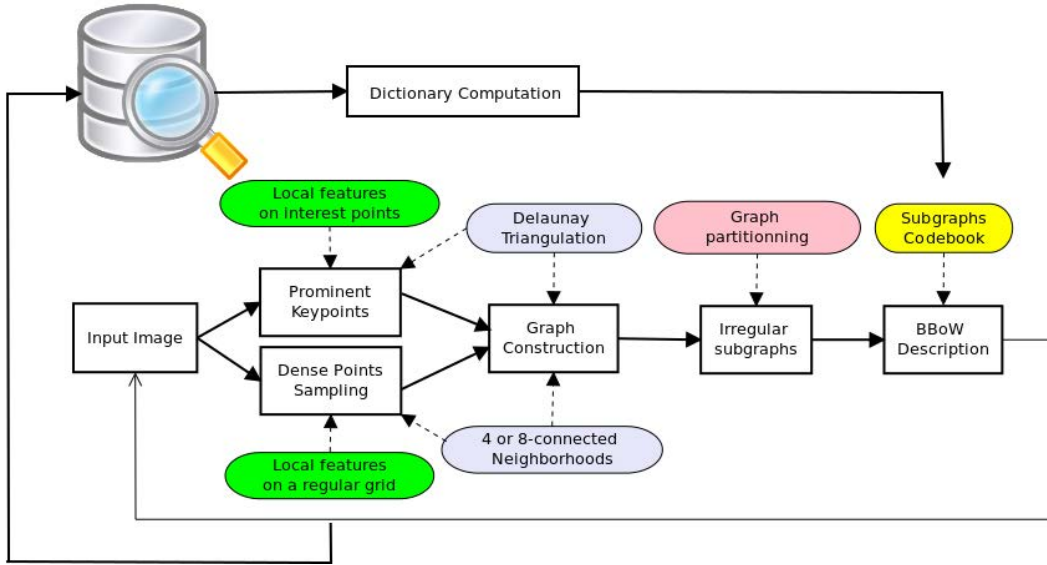


Figure 4.1: The diagram of construction of Bag-of-Bags of Words model.

4.1.1 Feature Extraction

Firstly, given an input image I_j , we extract local image features from image patch. Different types of popular descriptors such as SIFT [2] or SURF [35] etc., can be used to describe local features as vectors from the patches. The local features are extracted from either prominent keypoints or dense sampling points on regular grid.

In case of prominent keypoints approach, any interest points detection algorithms can be used to extract keypoints. In the present work, we use SURF [35] as image descriptors to extract feature points under the mask of the image for the interest object. In order to avoid these points are too close to each other in positions, we filter those points by keeping only the most prominent keypoint over any 10-pixels diametrical region. The obtained filtered keypoints $\mathcal{P} = \{p_1, \dots, p_n\}$ are selected as vertices of the initial image graph.

4.1 Overview of the Bag-of-Bags of Words Model

In case of dense sampling strategy, the image features are computed using only the SIFT [2] feature vectors of *all* dense sampling points. We use an overlap between patches of 50% to reach a compromise between repeatability of interest points and reasonable size of features. Its corresponding pipeline is illustrated in Figure 4.2.

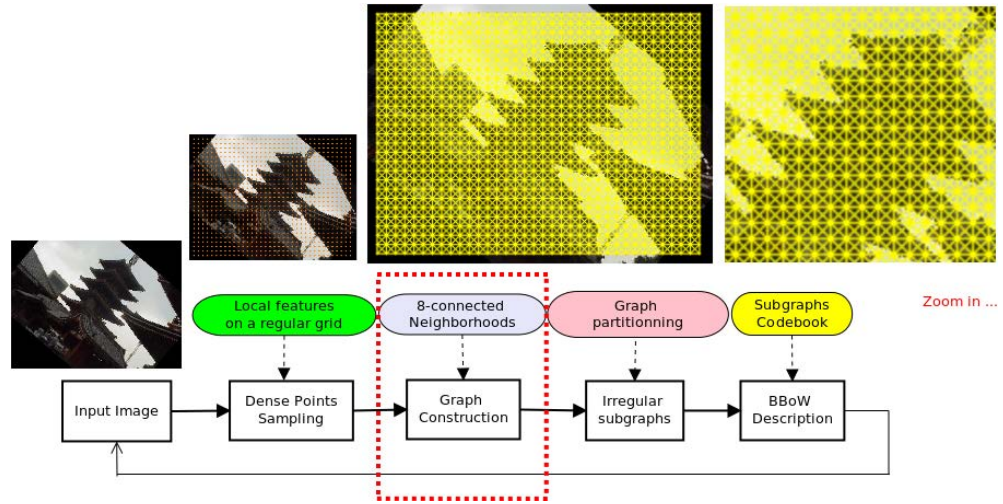


Figure 4.2: The dense points sampling approach in *BBoW* model.

4.1.2 Graph Construction

Secondly, we build an *undirected weighted* graph $G_j = (V_j, E_j, W_j)$ on the image I_j . We call it the *initial image graph*.

As defined in Section 3.3.1 and Section 4.1.1, the *graph nodes* are positioned on either *filtered* prominent keypoints or on the dense sampling points at a regular grid. Once these graph nodes are localized, we head to generate edges and define the corresponding weights of these edges. The *graph edges* represent relationship between graph nodes. They are generated by linking these vertices in specified neighbourhood system (see Figure 3.3), as we have discussed in Section 3.3.2. In such a way, one connected image graph is generated for each image. The *edge weight* reflects the similarity between the two nodes of that edge. Such a similarity measurement depends on a specified objective function. Let us denote by W , a symmetric matrix of edge weights between all nodes. Then the edge weights are represented by non-zero entries of this affinity matrix W , see Equation (3.1).

4. BAG-OF-BAGS OF WORDS MODEL

4.1.3 Irregular Subgraphs

Thirdly, the initial image graph is separated into a fixed number of K partitions (sub-graphs) [12] via graph partitioning.

Case study: prominent keypoints approach in *BBoW* model Let us denote $G = (V, E)$ a graph generated by the Delaunay triangulation. The vertices set V contains all the feature points, *i.e.* $V = \mathcal{P}$. The edges set E contains all unordered pairs of points $\{p, q\}$ that are neighbours in the Delaunay graph. We want to separate graph G into K smaller graphs via Graph Cuts. This can be formulated as a labeling problem: given a points set \mathcal{P} in image I_j , and a label set $L = \{l_1, \dots, l_K\}$, for each $p \in \mathcal{P}$, we are looking for its label $l(p) = l_p \in L$.

In order to be consistent with the image content, we construct a set of sub-graphs $\{g_{j,1}, \dots, g_{j,K}\}$, according to the following requirements: each sub-graph, l) should be as compact as possible; 2) should have, as much as possible, a uniform color. To solve this labeling problem, we minimize the energy function defined in Equation (3.11) of Chapter 3, via α -expansion [8] algorithm in Graph Cuts. An illustration will be given in Section 6.4 of the Chapter 6.

Case study: dense sampling approach in *BBoW* model Since prominent keypoints approach in *BBoW* model does not exhibit promising result, we hence go for dense sampling approach in the following discussion. An example of irregular subgraphs obtained by dense sampling approach in *BBoW* model, is illustrated in Figure 4.3.

As discussed in Section 3.4, we assess three standard approaches for irregular graph partitions in the *BBoW* model. These methods are: Graph Cuts, Normalized Cuts and kernel-based multilevel weighted graph cuts. Here we stress that the idea of applying graph partitioning methods to image graph is not novel, *e.g.*, [124, 145, 146]. Our contribution lies in rigorously demonstrating that irregular (sub)graph-based representation is well-suited to pre-clustering interest points accounting for color and texture similarity, and that this representation extends BoWs model with spatial layouts, combines the advantages of SPM as well.

4.1.4 Bag-of-Bags of Words Description

Fourthly, we compute image signatures by designing a measure for describing these sub-graphs. As in the standard *BoW* approach, we first build a codebook from all image features in a training image dataset. The codebook is computed by using k-means clustering method

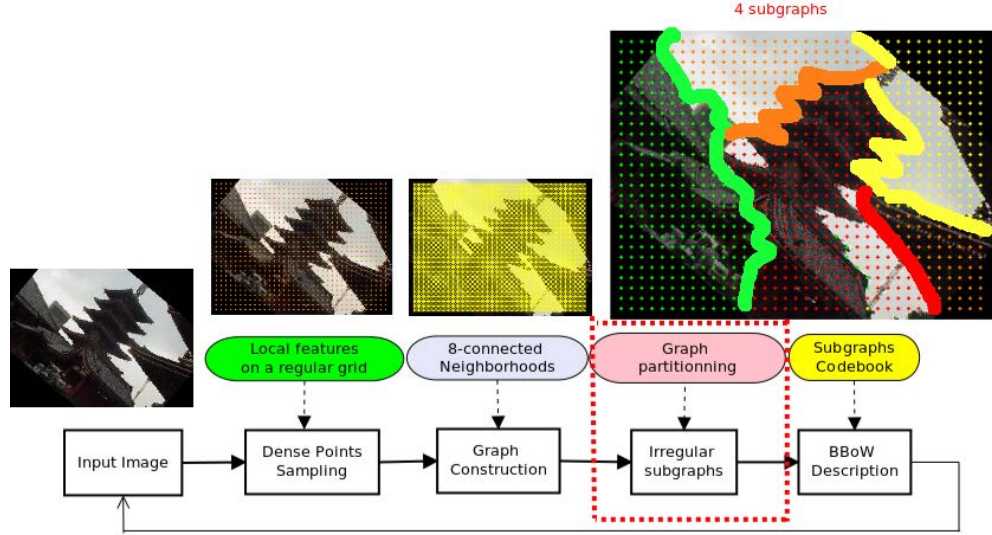


Figure 4.3: The obtained irregular subgraphs via graph partitioning.

over these features vectors, therefore, it is independent from any partitioning scheme. The codewords C then correspond to the centres of the learned clusters. A bag of visual word representation, *i.e.* a histogram of word frequencies, is then assigned to each subgraph.

Let us denote by $H_{j,k}$ a signature of the subgraph $g_{j,k}$ ($k = 1, \dots, K$) in image I_j . $H_{j,k}$ is a Bag-of-Words histogram, obtained by assigning the SIFT (or SURF) features within the subgraph $g_{j,k}$ to the nearest codeword (hard assignment), as in the standard *BoW* approach. Hence, the *BBow* representation of image I_j for this partitioning is a histogram vector $H_j = \{H_{j,1}, \dots, H_{j,K}\}$ of length K , normalized by the number of nodes in the initial image graph G_j . With such a normalization, the larger subgraphs are privileged. We call H_j the “*Bag-of-Bags of Words*” (*BBow*) description. See Figure 4.4.

4.2 (Dis-)Similarity Measurement between Histograms

A histogram is a collection of bins that count a frequency distribution of data. This important statistical characteristic is useful to represent the distribution of pixel intensity, color and texture of images. The histogram representation has several advantages. It is easy to compute, intuitive and invariant to translation and rotation about view plane etc. When images are characterized by histograms, comparing images is equivalent to computing the distances or (dis-)similarities between their model histograms.

4. BAG-OF-BAGS OF WORDS MODEL

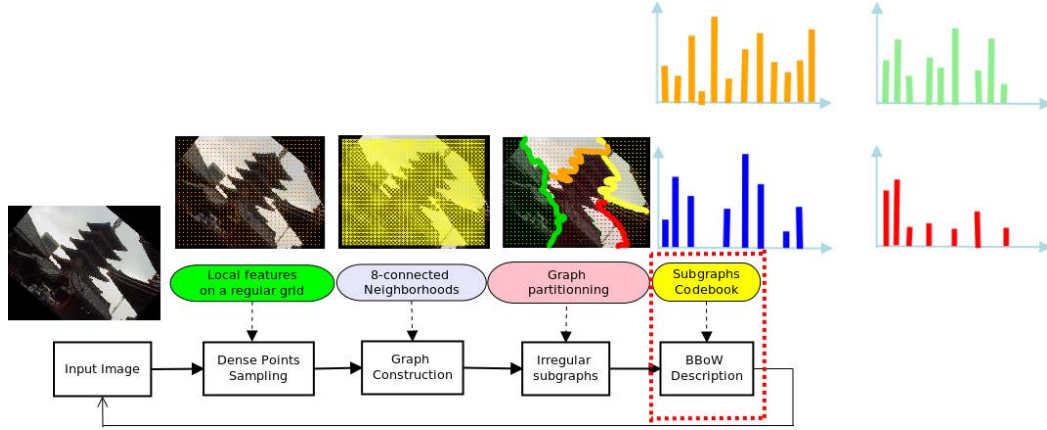


Figure 4.4: The “Bag-of-Bags of Words” description.

A number of measures for computing the histogram distance have been proposed. There exist two main categories of distances between histograms: the bin-by-bin distances and the cross-bin distances.

The bin-by-bin type of distances require histograms with the same number of bins. We can list a few of them: L_1 distance (Equation (2.11)), L_2 distance (Equation (2.12)), χ^2 statistics (Equation (2.13)), histogram intersection (Equation (4.2)), Kullback-Leibler divergence (Equation (2.14)), Jeffrey divergence (Equation (2.15)) etc. They are labeled as D_{L_1} , D_{L_2} , D_{χ^2} , K_{\cap} , D_{KL} and D_{Je} , respectively in this thesis. The performance of bin-by-bin distance depends on the number of bins in the histogram. When the number of bins is high, the distance is discriminative, but not robust. Contrarily, if the number of bins is low, the distance is robust, but not discriminative.

As for the cross-bins distances, two typical cross-bin metrics are Mahalanobis distance [147] and Earth Mover’s Distance (EMD) [148]. Mahalanobis distance measures the separation of two distributions. Formally speaking, Mahalanobis distance belongs to the family of Quadratic-Form distance [149, 150]. When two compared distributions are vectors, for example, two histograms, Mahalanobis distance is defined as:

$$QF^A(G, H) = \sqrt{(G - H)^T A (G - H)}, \quad (4.1)$$

where G and H are two histograms with the same bin size and A is the bin-similarity matrix that is the inverse of covariance matrix. Equation (4.1) is a metric (semi-metric) if A is positive-definitive (positive-semidefinite). The EMD measures the minimal cost that must be paid to

transform one distribution into the other. This distance can operate on variable-length representations of the distribution. It is widely used in content-based image retrieval to compute distances between the color histograms of two images [151].

For couples of the aforementioned distances, they have been formulated in Section 2.1.7 of the Chapter 2. In the following, we will give emphasis to an important similarity measure - *histogram intersection*, which is adopted in the present work.

Histogram intersection: Let us denote by $G = \{g_1, \dots, g_B\}$ and $H = \{h_1, \dots, h_B\}$, are two *normalized* histograms with B bins. Particularly, these two histograms are normalized to one, i.e. $\sum_{b=1}^B g_b = \sum_{b=1}^B h_b = 1$. Histogram intersection (*HI*) is defined as:

$$K_{\cap}(G, H) = \sum_{b=1}^B \min(g_b, h_b) . \quad (4.2)$$

Histogram intersection was first introduced by Swain et al. [44] as a technique of comparing image and model histograms for color indexing. It is a useful similarity measure for images and is even proved to be an effective *kernel* for machine learning [152]. The similarity measures in the *BBoW* model are based on histogram intersection.

There is an alternative way to compute *HI*:

$$K_{\cap}(G, H) = \frac{1}{2} \sum_{b=1}^B (g_b + h_b - |g_b - h_b|) , \quad (4.3)$$

which improves computation efficiency, e.g. programming for a GPU, since we do not need to explicitly compare the values of each bin. We verify the equivalence of Equation (4.2) and Equation (4.3) in the Appendix D.

4.3 *BBoW* on Single Level for Image Retrieval

We now review how to apply the *bag-of-bags of words* model for image retrieval on a single level of a partition.

In the framework of content-based image retrieval (CBIR), the most common method for comparing two images is using either a *similarity* metric or an image *distance* measure. Both of them can be in various dimensions. And they can consider the similarity of color, texture, shape etc. or in a combination of them in images. The distance measure is negatively correlated

4. BAG-OF-BAGS OF WORDS MODEL

with the corresponding similarity metric. That is to say, the more two images are similar, the lower the distance value will be. For example, the distance is zero if two images are exactly matched, *i.e.*, they are identical.

In the *BBoW* model, after image graph partitioning, each image contains a fixed number of K subgraphs. The image is thus represented by K BoVW histograms (subgraph signatures). Using histograms to describe subgraphs, a comparison between two images I_i and I_j becomes equivalent to similarity search when comparing histogram signatures of their subgraphs. We have adopted two strategies to define the similarity between images. We will explain the two strategies in the following Section.

4.3.1 Co-occurrence Criteria

The first strategy to compare the two sets of subgraphs from two images consists in using co-occurrence criteria such as those defined in [111].

We adopt the idea of RootSIFT [33] by first L1 normalizing the histograms and then computing the histogram intersection of them. Since any image I_i is represented by a set of histograms of its subgraphs $H_i = \{H_{i,1}, \dots, H_{i,K}\}$; a (dis)similarity measure between two (sub)graphs can be easily computed as we just need to compare their histogram signatures. In such a way, we relate the similarity between two images with the similarity between BoW histograms of the subgraphs in two images.

We have experimented different strategies to combine the $K \times K$ distances between a pair of query image I_i , and database image I_j from their corresponding histogram sets H_i and H_j : *minimum*, resp. *sum of min*, resp. *mean*, resp. *median*, resp. *sum*, resp. *maximum*, etc. of all distances.

To compare two images I_i and I_j that are composed of K subgraphs for each, we define a series of similarity measures. We detail them as follows:

$$S_{\min}(I_i, I_j) = \min_{k=\{1,\dots,K\}} \min_{k'=\{1,\dots,K\}} \left\{ \sum_{b=1}^B \min(H_{i,k}(b), H_{j,k'}(b)) \right\}, \quad (4.4)$$

$$S_{\text{sum-of-mins}}(I_i, I_j) = \sum_{k=1}^K \min_{k'=\{1,\dots,K\}} \left\{ \sum_{b=1}^B \min(H_{i,k}(b), H_{j,k'}(b)) \right\}, \quad (4.5)$$

$$S_{\text{sum-of-means}}(I_i, I_j) = \sum_{k=1}^K \text{mean}_{k'=\{1,\dots,K\}} \left\{ \sum_{b=1}^B \min(H_{i,k}(b), H_{j,k'}(b)) \right\}, \quad (4.6)$$

$$S_{\text{sum-of-medians}}(I_i, I_j) = \sum_{k=1}^K \text{median}_{k'=\{1,\dots,K\}} \left\{ \sum_{b=1}^B \min(H_{i,k}(b), H_{j,k'}(b)) \right\}, \quad (4.7)$$

$$S_{\text{sum}}(I_i, I_j) = \sum_{k=1}^K \sum_{k'=1}^K \left\{ \sum_{b=1}^B \min(H_{i,k}(b), H_{j,k'}(b)) \right\}, \quad (4.8)$$

$$S_{\text{sum-of-maxima}}(I_i, I_j) = \sum_{k=1}^K \max_{k'=\{1,\dots,K\}} \left\{ \sum_{b=1}^B \min(H_{i,k}(b), H_{j,k'}(b)) \right\}. \quad (4.9)$$

Our experiments have shown a better behaviour with Equation (4.4). We will discuss the experimental results later in Section 6.4 of Chapter 6. This promising results based on Equation (4.4) promoted our second strategy in the Section 4.3.2.

In summary, image comparison via the co-occurrence criteria can be described in Algorithm 4.

Algorithm 4 Image comparison via the co-occurrence criteria

Require: Given Image I_i with its K subgraphs $\{g_{i,k}\}_{k=1}^K$ and I_j with its K subgraphs $\{g_{j,k'}\}_{k'=1}^K$

Ensure: Return a similarity score between image I_i and I_j

- 1: **for** each subgraph $g_{i,k}$ in image I_i **do**
 - 2: compute the BoVW histogram $h_{i,k}$ of the corresponding subgraph
 - 3: **end for**
 - 4: **for** each subgraph $g_{j,k'}$ in image I_j **do**
 - 5: compute the BoVW histogram $h_{j,k'}$ of the corresponding subgraph
 - 6: **end for**
 - 7: Similarity(I_i, I_j) = $S_{(*)}(I_i, I_j)$, where $(*)$ is one of the co-occurrence criteria defined in Section 4.3.1.
-

4.3.2 Weighted Bipartite Graph Matching

As discuss in previous Section, we compare images through comparing histogram signatures of their subgraphs. Indeed, the subgraph attributed to label k can be at any position in the image, see Figure 4.5. The spatial arrangement is lost if an image in a database undergoes rotation, for instance. Hence, in order to overcome this issue, we cannot match histograms of the subgraphs directly after the graph partitioning steps in *BBoW* model. We therefore need to find optimal subgraphs matching between pairs of images so as to reorganize the histograms in the *BBoW* description.

4. BAG-OF-BAGS OF WORDS MODEL

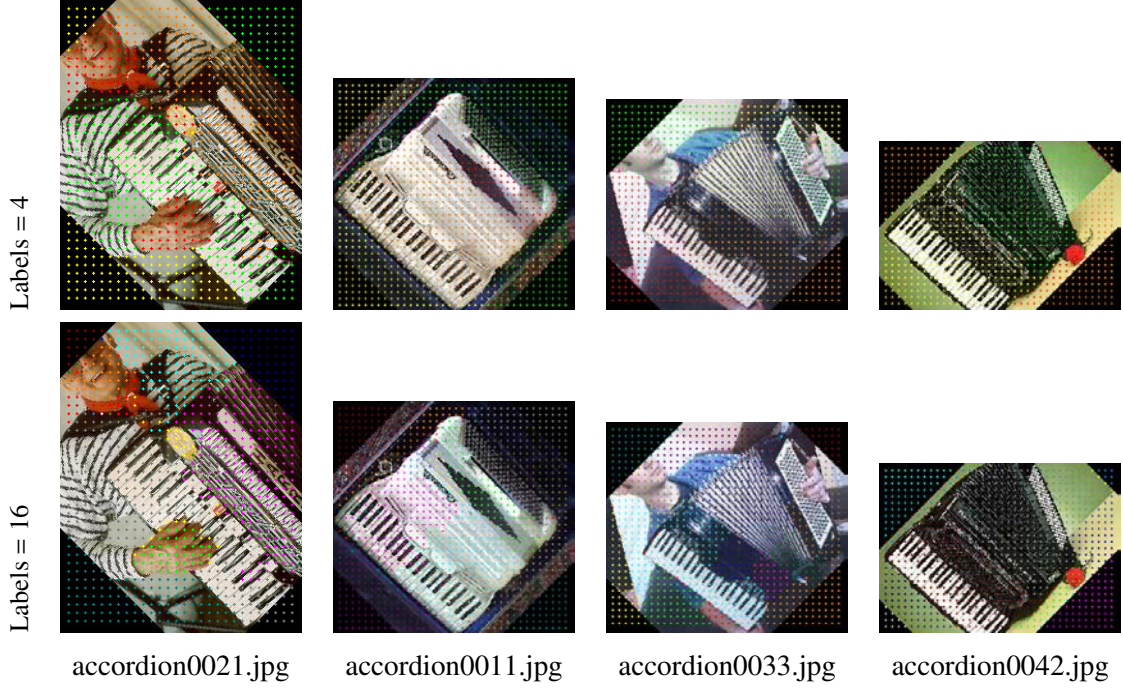


Figure 4.5: Examples of image graph partitions from category ‘accordion’ in *Caltech-101* dataset. The partitions of 4 subgraphs are visible in the first row of the figure. The second row of the figure shows 16 subgraphs in the partitioning. The nodes in each subgraph are labelled with the same color. This figure is better viewed in *color*.

Given two images I_i and I_j , and their corresponding subgraphs $\{g_{i,k}\}_{k=1}^K$ and $\{g_{j,k'}\}_{k'=1}^K$, we are facing an assignment problem: given two sets of (sub)graphs (for two images), we need to find the *perfect matching* or *complete matching* which maximizes the similarity between all matched (sub)graphs. This problem may also be phrased as a minimization problem by considering images I_i and I_j as two partitions of a bipartite graph, the distance between the signatures of subgraphs as a set of edge weights. The classical solution to this assignment problem requires the use of a combinatorial optimization algorithm. For this purpose, we rely on the *Hungarian algorithm* [153] to solve the problem in polynomial time $\mathcal{O}(K^3)$, where K is the number of subgraphs in the image.

The *Hungarian algorithm* minimizes the discrete transport cost (edge cost of the bipartite graph) between two sets of objects (histograms of subgraphs in our case). The cost matrix $D_{i,j}$

between the pair of images I_i and I_j reads:

$$D_{i,j} = \begin{bmatrix} d_{i,j}^{11} & \dots & d_{i,j}^{1K_r} \\ \vdots & & \vdots \\ d_{i,j}^{K_r 1} & \dots & d_{i,j}^{K_r K_r} \end{bmatrix}, \quad (4.10)$$

where

$$d_{i,j}^{k,l} = \sum_{b=1}^B |H_{i,k}(b) - H_{j,l}(b)|$$

is the L_1 distance between $H_{i,k}$ and $H_{j,l}$, which corresponds to the use of *histogram intersection*. The proof can be found in the Claim B of the Appendix D.

Figure 4.6 shows a toy example illustrating the subgraph matching process. Given two image I_i and I_j and their BBoW description $H_i = \{H_{i,a}, H_{i,b}, H_{i,c}, H_{i,d}\}$, $H_j = \{H_{j,1}, H_{j,2}, H_{j,3}, H_{j,4}\}$, the histogram distance of any pair of subgraphs between two images are computed. An example of these distance values are shown as entries of a matrix in Figure 4.7. In this example, the histogram distance between the subgraph $g_{i,a}$ of image I_i and the subgraph $g_{j,1}$ of image I_j is 11. The *Hungarian algorithm* finds the minimum cost assignment for the cost matrix. The subgraph $g_{i,a}$ in image I_i is optimal matched with the subgraph $g_{j,1}$ in image I_j , since the transport cost (11) is the minimum value (underlined in red color) among these values of the first row.

For computational efficiency, this matching step can be pre-computed once and stored. A distance table and a label table can be constructed optionally, which records the distance between all subgraphs being compared, and their corresponding labels. The distance values are the entries in the aforementioned cost matrix $D_{i,j}$. With this distance table, the procedure of bipartite graph matching can be simplified to search in the look up tables. The storage space being taken by the lookup tables is offset by the saved time, especially as the size of the subgraphs increases.

After the processing step via the *Hungarian algorithm*, each label k of subgraph $g_{i,k}$ in image I_i is associated to one label $k' = f_i(k)$ of subgraph $g_{j,k'}$ in image I_j . We thus reorganize the labels between the two sets of histograms $\{H_{i,k}\}_{k=1, \dots, K}$ and $\{H_{j,k'}\}_{k'=1, \dots, K}$ in BBoW. Therefore, the pairs of histograms to compare are identified. We call this step *bipartite subgraphs matching*.

4. BAG-OF-BAGS OF WORDS MODEL

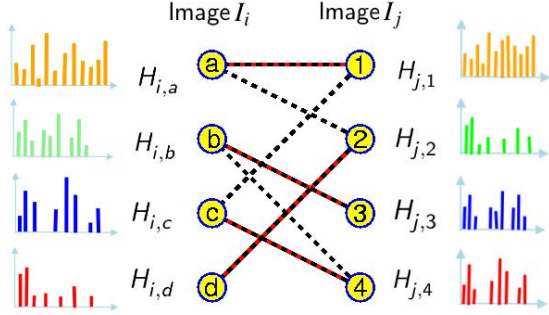


Figure 4.6: Find optimal subgraph matching via *Hungarian algorithm*.

	1	2	3	4
a	<u>11</u>	12	18	40
b	14	15	<u>13</u>	22
c	11	17	19	<u>23</u>
d	17	<u>14</u>	20	28

Figure 4.7: An optimal assignment for a given cost matrix.

Finally, the similarity score of two images I_i and I_j can be expressed by *histogram intersection kernel*, formally introduced in Equation (4.2):

$$K_{\cap}(H_{i,k}, H_{j,k}) = \sum_{b=1}^B \min(H_{i,k}(b), H_{j,k}(b)) . \quad (4.11)$$

Here k corresponds the k -th subgraph, B is the number of bins.

Essentially, for the first strategy of using co-occurrence criteria, e.g. Equation (4.4) etc., it can be seen as the application of the Histogram Intersection kernel [44, 152] (Equation (4.11)) directly to the histograms of *any orderless* subgraphs between two compared images.

To sum up, the second strategy can be interpreted in Algorithm 5.

4.4 Summary of the *BBoW* model for CBIR

Figure 4.8 demonstrates the procedure of image comparison in Bag-of-Bags of Words model from an image database. Note that both Algorithm 4 and Algorithm 5 require computing the *bag-of-visual-words* histogram for each subgraph.

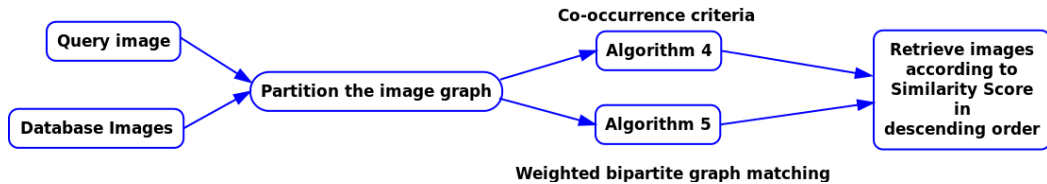


Figure 4.8: The process of CBIR from database in *BBoW* model.

Algorithm 5 Image comparison via *Hungarian algorithm* to reorganize histograms

Require: Given Image I_i with its K subgraphs $\{g_{i,k}\}_{k=1}^K$ and I_j with its K subgraphs $\{g_{j,k}\}_{k=1}^K$

Ensure: Return a similarity score between image I_i and I_j

- 1: **for** each subgraph $g_{i,k}$ in image I_i **do**
 - 2: compute the BoVW histogram $h_{i,k}$ of the corresponding subgraph
 - 3: **end for**
 - 4: **for** each subgraph $g_{j,k}$ in image I_j **do**
 - 5: compute the BoVW histogram $h_{j,k}$ of the corresponding subgraph
 - 6: **end for**
 - 7: Build $D_{i,j}$ in Equation (4.10)
 - 8: Run the *Hungarian algorithm* to reorganize histograms of subgraphs $\{i.e., \text{ each label } k \text{ of subgraph } g_{i,k} \text{ in image } I_i \text{ is associated to one label } k' = f_i(k) \text{ of subgraph } g_{j,k'} \text{ in image } I_j\}$
 - 9: Set $H_i \leftarrow \{H_{i,k}\}_{k=1,\dots,K}$
 - 10: Set $H_j \leftarrow \{H_{i,k'}\}_{k'=1,\dots,K}$
 - 11: $\text{Similarity}(I_i, I_j) = K_{\cap}(H_i, H_j)$
-

4.5 Discussion and Conclusion

In the present Chapter, we have presented a novel model for image representation. The proposed *BBoW* model with the aid of graphs, extends the classical bag-of-words (BoW) model, by embedding color homogeneity and limited spatial information through irregular partitions of an image. The model well addresses fundamental limitations of the classical *Bag-of-Words* model [16] and the *regular* structure of spatial pyramid representation [4]. We have also proposed to embed spatial layout into our *BBoW* representation by bipartite subgraphs matching via *Hungarian algorithm*. To the best of our knowledge, we are the first to apply *Hungarian algorithm* to subgraphs matching on the task of spatial layout analysis in image representation.

We have observed that the generated subgraphs are often too small after graph partitioning process. In such cases, subgraphs contain only a few of nodes. This makes the *BBoW* description less representative. In order to be more effective, we may consider removing these small or inconsistent subgraphs. However, this technique will produce another problem: how to deal with a set of histograms of different size in the final *BBoW* description. Again, if we choose a different number of resolutions for different type of images, it also involves the same problem: compare set of histograms of different size.

In the next Chapter, we propose to extend our model to multiple levels inspired by previous

4. BAG-OF-BAGS OF WORDS MODEL

works, such as Montanvert et al. [154].

Chapter 5

Irregular Pyramid Matching

In Chapter 4, we have introduced the proposed *bag-of-bags of words* (*BBoW*) model. The *BBoW* model, is an approach based on irregular partitions over the image. An image is first represented as a connected graph of local features on a regular grid of pixels. Next, irregular partitions (subgraphs) of the image are further built by using graph partitioning methods. Each subgraph in the partition is then represented by its own signature. The *BBoW* model with the aid of graphs, extends the classical *bag-of-words* (BoW) model in *image* space instead of *feature* space, by embedding color homogeneity and limited spatial information through irregular partitions of an image. In this chapter, we extend this proposed model to pyramid levels, leading to an approach that we call *irregular pyramid matching*.

5.1 *BBoW* on Pyramid Level

In this Section, we first introduce the graph partitioning scheme on multi-levels in the bag-of-bags of words model. Then we describe the procedure of irregular pyramid matching.

5.1.1 Graph Partitioning Scheme

As in Spatial Pyramid Matching [4], we aim to build a pyramid of partitions at several “resolutions” ($r = 0 \dots R$). At resolution r of image partitions, the image graph G_j is split into a set of $K_r = 2^{2r}$ subgraphs $\{g_{j,1}^r, \dots, g_{j,K}^r\}$. We name it *pyramidal image graph partitioning scheme*. An example is shown in Figure 5.1, where the initial image graph is divided into a fixed number of subgraphs at different resolutions.

5. IRREGULAR PYRAMID MATCHING

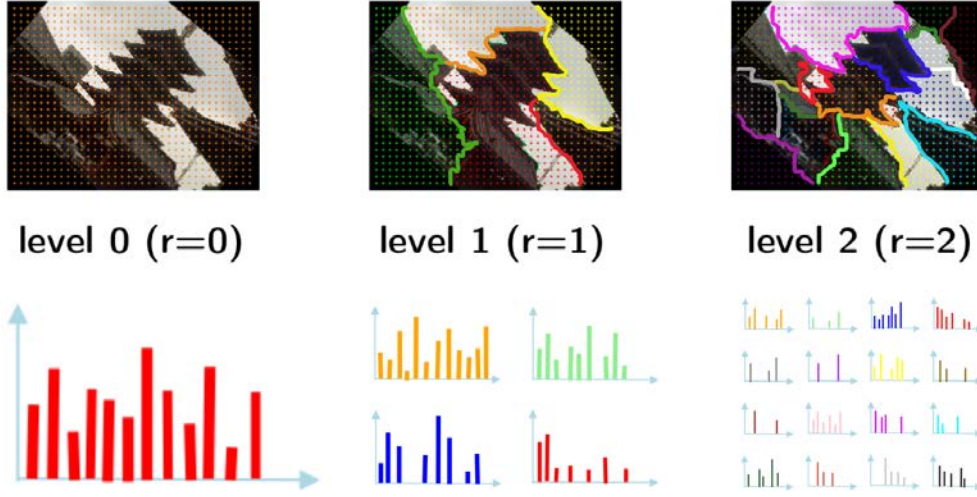


Figure 5.1: A schematic illustration of the *BBoW* representation at each level of the pyramid. At level 0, the decomposition has a single graph, and the representation is equivalent to the classical *BoW*. At level 1, the image is subdivided into four subgraphs, leading to four features histograms, and so on. Each subgraph is represented by its own color in this figure. This figure is better viewed in *color*.

5.1.2 Irregular Pyramid Matching

In Section 4.1.4, the *BBoW* description is based on a fixed number of partitions at a single level on the whole image. After the pyramidal image graph partitioning step, *BoW* histograms are computed within each subgraph, then the histograms from all subgraphs are concatenated together to generate the final representation of the image. Such an extension of *BBoW* model to pyramid gives rise to a method we name *irregular pyramid matching (IPM)*. In case where only the level $l = 0$ is used to compute image signature, *BBoW* reduces to *BoW* representation.

5.2 BBoW on Pyramid Levels for Image Retrieval

After generating visual signature of the image on pyramid levels in *BBoW* model, we need to define the corresponding similarity measures to compare images.

5.2.1 Similarity Measure

Once bipartite subgraphs matching is fulfilled, we can directly apply the *level weighted intersection* as described in [4] to compare images:

$$\begin{aligned}\kappa(I_i, I_j) &= \mathcal{J}(H_{i,k}^R, H_{j,k'}^R) + \sum_{r=0}^{R-1} \frac{1}{2^{R-r}} (\mathcal{J}^r - \mathcal{J}^{r+1}) \\ &= \frac{1}{2^R} \mathcal{J}(H_{i,1}^0, H_{j,1}^0) + \sum_{r=1}^R \frac{1}{2^{R-r+1}} \mathcal{J}(H_{i,k}^r, H_{j,k'}^r),\end{aligned}\quad (5.1)$$

where

$$\mathcal{J}(H_{i,k}^r, H_{j,k'}^r) = \sum_{b=1}^B \min(H_{i,k}^r(b), H_{j,k'}^r(b))$$

is the histogram intersection function in [152], B is the *bag of words* codebook size, which is related to the $L1$ norm [44]. k and k' here are the indices of the corresponding subgraphs being matched after rearrangement of histograms via *Hungarian algorithm*. The weight $\frac{1}{2^{R-r}}$ allows for penalizing low resolutions of a partition, reflecting the fact that higher levels localize the features inside smaller graphs more precisely. Hence, in our approach, we propose to apply directly the level weighted intersection to irregular partitions obtained by graph cuts methods, following the idea of SPM [4].

5.2.2 Global Algorithm for Image Retrieval with BBoW model

After discussion, we summarize the global algorithm in *BBoW* model for its application for image retrieval.

1. Local features extraction at interest point locations, or nodes in a dense grid.
 - (a) Prominent keypoints
 - (b) Dense points sampling
2. Codebook generation (dictionary is level independent, built off line).
3. Graph Construction (define graph nodes, weighted edges) for each image.
4. Partition the initial image graph into a fixed number of irregular subgraphs on multiple resolution for each image.
5. Build BoW histograms of the subgraphs.
6. Compare images based on specific similarities measure.

5.3 Discussion and Conclusion

In this Chapter, we have embedded our *BBoW* model into a pyramid approach. Hence, the final signature of the image has been built as a concatenation of BoW histograms from each level of the pyramid, where each BoW histogram is *normalized* by the number of nodes in the initial image graph. With such a normalization, the *larger* subgraphs are privileged. We call it Bag-of-Bags of Words (*BBoW*) description in pyramid. With such descriptors, we match graph pyramid *level by level*. Hence, we always match the partitions of the same *granularity*. The number of pyramid level is chosen to be the same in the database. Therefore, we do not have any problem in matching images with different number of subgraph histograms.

Note that the Spatial Pyramid Matching [4] scheme partitions an image recursively into a coarse-to-fine (sub)regions, *i.e.*, their partitions are *nested*, as introduced in Section 2.3.2.1 of Chapter 2. In contrast, our partitions are independent at each level in the *BBoW* model, see Figure 5.2. Moreover, we keep the same resolution of images during partitioning. That means we do *not* use a Gaussian pyramid [155–157] as main concept of *pyramid* does. The *main reason* that we have adopted this strategy is attributed to avoid obtaining isolated (too small) subgraphs, leading to the *BBoW* description less representative.

In the next Chapter, we will evaluate our model in different respects, especially, its application for image retrieval.

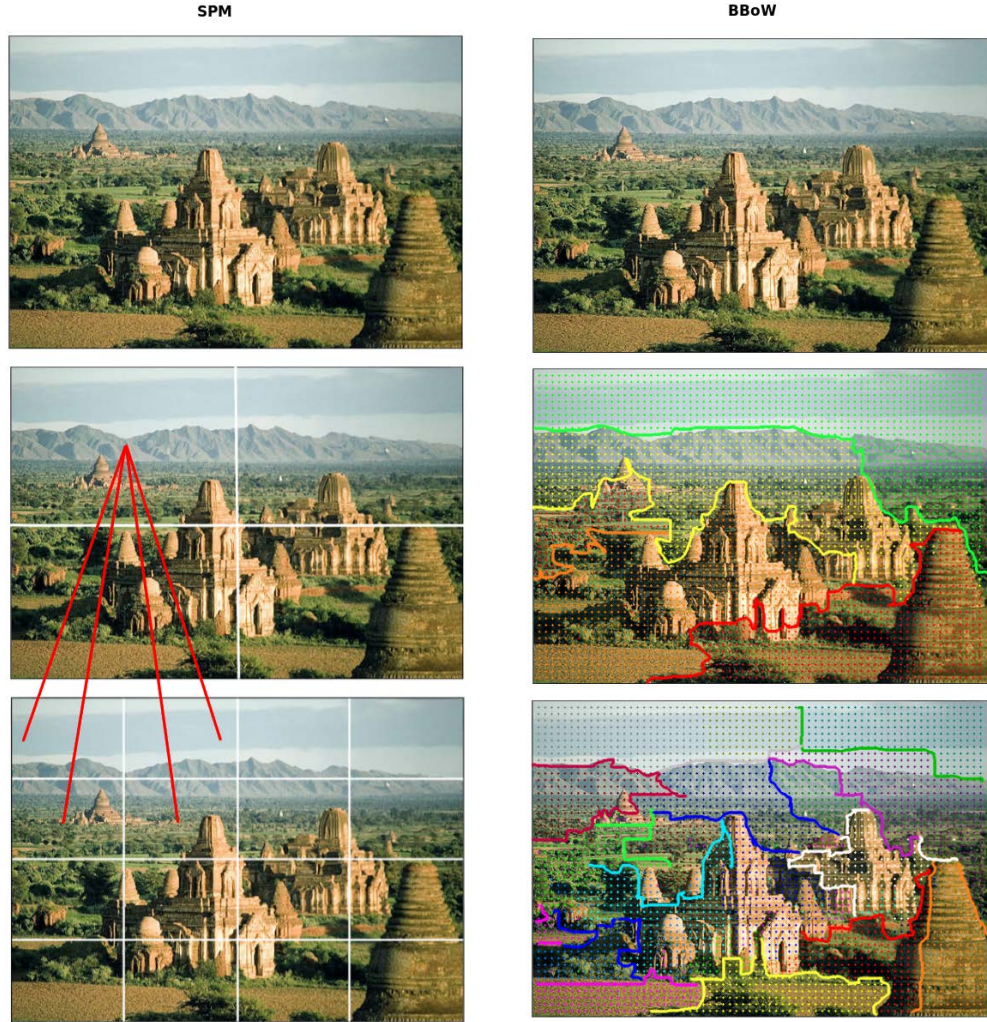


Figure 5.2: The comparison of partitioning scheme between SPM and *BBoW*. At the left side of the figure shows the partitioning scheme of Spatial Pyramid Matching (SPM). At the right side of the figure illustrates the partitioning scheme of the *BBoW*. Contrary to SPM with nested regular partitions, our partitions are irregular and independent at each level. We keep the same resolution of the image across multilevel. This figure is better viewed in *color*.

5. IRREGULAR PYRAMID MATCHING

Chapter 6

Results and Discussion

In this chapter, we present an evaluation of different aspects of our model with respect to graph partitioning and the application to image retrieval, *i.e.*, to retrieve all images that are similar to a given image from a database.

First of all, we introduce three datasets and their experimental settings for dictionary computation, image queries will be explained. Next, we introduce metrics for evaluation of image retrieval efficiency with our *BBoW* model. Then some experiments are reported on the comparison of similarity metrics used in image matching. For selected graph-cut algorithms, we will report on optimal parameters selection for graph construction. Our irregular partition model will then be compared to the famous SPM approach which deploys regular embedding of quantized features and we will discuss the perspectives of the proposed model at the end.

6.1 Image Datasets

In this Section, we present the datasets used for this work. The proposed Bag-of-Bags of Words model was evaluated on three benchmarks: *SIVAL*¹ dataset [10], *Caltech-101*² dataset [144] and the *People Playing Musical Instrument (PPMI)*³ dataset [158, 159].

The *SIVAL* (*Spatially Independent, Variable Area, and Lighting*) benchmark contains 1500 images among 25 different categories, 60 images per category. Each image is 1024 pixels in width and 768 pixels in height, has a total of $1024 \times 768 = 786,432$ pixels. Each category consists of images of single objects photographed against highly diverse backgrounds. The

¹<http://www.cs.wustl.edu/~sg/multi-inst-data/>

²http://www.vision.caltech.edu/Image_Datasets/Caltech101/Caltech101.html

³<http://ai.stanford.edu/~bangpeng/ppmi.html>

6. RESULTS AND DISCUSSION

objects may occur anywhere spatially in the image and also may be photographed at a wide-angle or close up. This benchmark emphasizes the task of *localized* Content-Based Image Retrieval [160], where the user is only interested in a portion of the image (object), and the rest of the image (background) is irrelevant. Therefore, it allows to clearly identify the content of images for which the method has good performance, and for which it does not. An excerpt of SIVAL dataset is presented in Figure 6.1.



Figure 6.1: Example images from the *SIVAL* database.

The *Caltech-101* dataset includes 101 distinct objects categories with high intra-class appearance and shape variability, plus a background class for a total of 102 categories. The number of images in each category varies from 31 to 800. The whole database contains 9,144 images overall. The average size of the images is around 300×300 pixels. This dataset is one of the most diverse and thoroughly studied databases for object recognition. A wide range of studies have chosen this popular database for experimental validation. Therefore, this benchmark acts as a common standard for comparison of different state-of-the-art algorithms without bias due to different datasets. An excerpt of *Caltech-101* dataset is presented in Figure 6.2.

The *PPMI* dataset contains images of humans interacting with twelve different musical instruments. They are: bassoon, cello, clarinet, erhu, flute, French horn, guitar, harp, recorder, saxophone, trumpet, and violin. For each instrument, it contains images of people either playing (*PPMI+*) or just holding (*PPMI-*) the instrument. The *PPMI* dataset emphasizes on understanding subtle interactions between humans and objects. The twelve binary classes (*PPMI+* images) are used in our experiments. *PPMI+* is composed of twelve categories. Each category contains 200 images, *i.e.* for a total of $12 \times 200 = 2400$ images. All images in *PPMI+* are

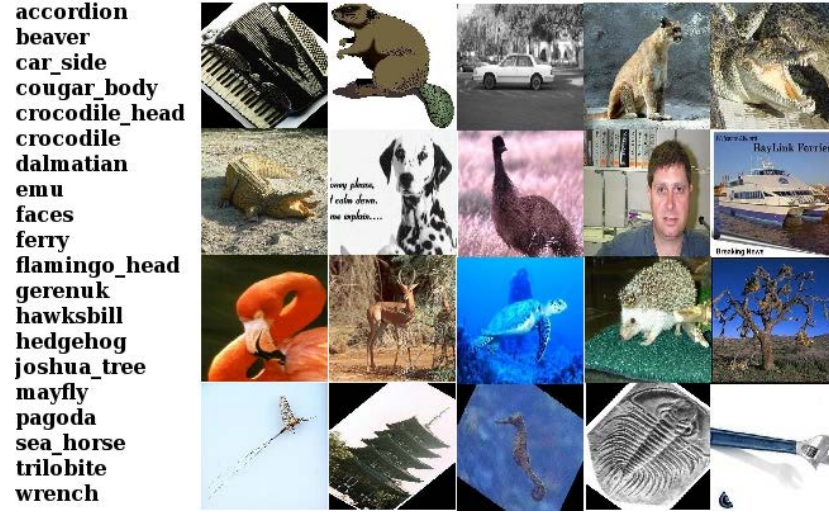


Figure 6.2: A snapshot of images from *Caltech-101*.

normalized, in resolution of 258×258 pixels. A snapshot of the *PPMI+* dataset is shown in Figure 6.3.



Figure 6.3: A snapshot of images from *PPMI+* of the *PPMI* dataset that contains a person playing the instrument.

6.2 Experimental Settings

We now detail experimental settings defined on these three datasets respectively.

All the experiments are performed on a computer with Intel i7 CPU, 2.8GHz processor, 8 GB RAM, Linux Ubuntu 12.04.3 LTS as operating system.

Many kinds of image features may be used in the *BBoW* model. However, since our objective is to test the *BBoW* model and to study the influence of the stability of image partitions on image retrieval rather than to evaluate features, we decide to choose popular yet not sophisti-

6. RESULTS AND DISCUSSION

cated local image descriptors. In the current implementation, we use SIFT [2] and SURF [35], which have been proven to be robust and effective [37]. Furthermore, for *each* database, we have experimentally selected an appropriate dictionary size (visual words obtained via hard assignment) and use it in *all* experiments. Note that we do not report on this selection, as it is already a well-studied problem [85–88]. A better setting could be used for performance tuning as in [161].

6.2.1 Experimental Settings on SIVAL

In the context of Graph Cuts, the motivation of running experiments on SIVAL is threefold. Firstly, we need to verify if an image graph composed of prominent keypoints is representative enough to describe an object in an image, compared with the bag-of-words model. Secondly, we aim to check if interest points can be well clustered based on their color similarity. Thirdly, we hope to examine the influence of different parameters on graph partitions. In practice, we use a library¹ from Boykov and Kolmogorov [8, 9, 126] as the implementation of α -expansion for Graph Cuts.

For each category, we use 30 images for training, the rest 30 images for image retrieval. We use an *extended* 128 *dimension* version of SURF-128 feature descriptor, as described in Bay et al. [35]. The sums of d_x and $|d_x|$ are computed separately for $d_y < 0$ and $d_y \geq 0$. Similarly, the sums of d_y and $|d_y|$ are split up according to the sign of d_x , thereby doubling the number of features. We randomly sample SURF vectors from training images and learn a quantization codebook using k -means with 500 and 1000 clusters respectively. More precisely, the codebook is first computed using k -means clustering method over all SURF descriptors of the filtered keypoints from the *masked* images² in a learning database. The codewords C then correspond to the centres of the learned clusters.

In order to compare prominent keypoints approach in *BBoW* model with the traditional bag-of-words (BoW) model, we computed BoW histograms on exactly the same feature points set to build the initial image graphs. A *bag-of-visual-words* representation, *i.e.*, a histogram of word frequencies, is thus assigned to each subgraph obtained by graph partitioning via Graph Cuts.

¹<http://vision.csd.uwo.ca/code/>

²The image mask falls on the object of interest in the image.

6.2.2 Experimental Settings on *Caltech-101*

In *Caltech-101* database, we randomly sample 30 images per category for training and up to 50 images per category for testing. We could use SURF [35], as the settings in SIVAL. But we finally adopt SIFT features [2] instead, in order to follow the approach in SPM [4]. To be more precise, we use the dense sampling grid points from the whole image to build initial connected graphs. The local SIFT features [2] are then extracted from these grid points based on 8-pixels spacing and 16-pixels patch size. A dictionary of size 400 is learnt over 30 sample images per class using k -means. The query images are chosen from the rest of the dataset for retrieval evaluation. For all experiments in *Caltech-101* dataset, we use the same codebook built as above.

Performance is measured by calculating the *mean Average Precision* (mAP) for all queries, as described in TREC-style evaluation¹. In addition, the *mean of Standard deviation* (Std) of *Average Precisions* (APs) for *category-based* queries is given.

6.2.3 Experimental Settings on *PPMI*

For each class, 100 *normalized PPMI*+ images are randomly selected for training and the remaining 100 images are considered to be the testing set. We fix the dictionary size as 1024. As *Caltech-101*, we use the dense SIFT as image features for *BBoW* descriptions.

6.3 Evaluation Metrics

Performance Evaluation (PE) is of crucial importance in producing robust techniques. To assess the performance of our model for image retrieval, we use classical evaluation metrics for information retrieval. We also introduce a new metric that is specifically designed for evaluating the stability of partitions and subgraphs matching, with the aim of evaluating three different methods in the *BBoW* model for graph partitioning. These metrics are introduced as follows.

6.3.1 Performance Measures for Image Retrieval

Evaluation of retrieval performance is a crucial problem in Content-based image retrieval (CBIR). Since CBIR and information retrieval (IR) have close relationship, many standard IR

¹<http://trec.nist.gov/>

6. RESULTS AND DISCUSSION

evaluation protocols are used directly in CBIR.

We review some basic notions for an IR system. The query can be considered as a binary decision problem. The decision can be represented in a structure known as a confusion matrix or contingency table. The confusion matrix has four categories: true positives (TP), false positives (FP), true negatives (TN), false negatives (FN). A confusion matrix is shown in Table 6.1.

Table 6.1: The basic notions for information retrieval systems.

	Relevant	Not relevant
Retrieved	true positives (TP)	false positives (FP)
Not retrieved	false negative (FN)	true negatives (TN)

In the context of evaluation of *unranked* retrieval sets, the two most frequent measures for IR effectiveness are *precision* and *recall*. *Precision* and *recall* are single-value metrics based on the whole list of documents returned by an IR system. They are defined for the case where an IR system returns a set of documents for a given query.

Precision (P) is the fraction of retrieved documents that are relevant, defined in Equation (6.1). *Recall* (R) is the fraction of relevant documents that are retrieved, as in Equation (6.2).

$$Precision = \frac{\#(\text{relevant items retrieved})}{\#(\text{retrieved items})} = P(\text{relevant} \mid \text{retrieved}). \quad (6.1)$$

$$Recall = \frac{\#(\text{relevant items retrieved})}{\#(\text{relevant items})} = P(\text{retrieved} \mid \text{relevant}). \quad (6.2)$$

Mathematically, it is possible to interpret precision and recall not as ratios (fractions), but as probabilities: *precision* is the probability that a (randomly selected) retrieved document is relevant; *recall* is the probability that a (randomly selected) relevant document is retrieved in a search.

Given the confusion matrix defined in Table 6.1, we are able to rewrite the *precision* and *recall* metrics as:

$$Precision = \frac{TP}{TP + FP}, \quad (6.3)$$

$$Recall = \frac{TP}{TP + FN}, \quad (6.4)$$

in Equation 6.3 and 6.4 respectively.

Average precision The *Average Precision (AP)* is the average of the precision value obtained for the set of top k documents existing after each relevant document is retrieved, and this value is then averaged over information needs.

$$AP = \frac{\sum_{i=1}^k (Precision(i) \times rel(i))}{\#(\text{relevant items})} \quad (6.5)$$

where $rel(k)$ is an indicator function equalling to one if the item at rank k is a relevant document, zero otherwise. $Precision(k)$ means the precision at cut-off k in the item list.

Mean average precision The *mean Average Precision (mAP)* for a set of queries is the mean of the average precision scores for each query. It is defined as:

$$mAP = \frac{\sum_{q=1}^Q AP(q)}{Q} \quad (6.6)$$

where Q is the number of queries.

To assess the stability of the proposed *BBoW* model, given particular similarity metrics used in image matching, we also compute the *standard deviation (std)* of APs in image retrieval.

6.3.2 Partition Precision (PP)

In order to qualify the performance of our approach, we introduce a new measure. We call it *Partition Precision (PP)* at n first retrieved images. For a particular query image I_j , we denote N_{rel} as the number of relevant images rel for this query. The set of ranked retrieved images is denoted by η , $\eta(d)$ is the retrieved image at rank d . I_j is excluded from η . $\eta(d) \in rel$ if I_j and $\eta(d)$ are from the same category. We say that $g_{j,k}$ and $g_{\eta(d),k'}$ are matched, if they are bipartite matching subgraphs after rearrangement of histograms via *Hungarian algorithm*; moreover they fall into same region types (background, object, etc.) of the image I_j and $\eta(d)$ respectively. In general, only “object” and “heterogeneous background” are considered. The criterion of *heterogeneous* background is defined case by case, since in many cases, the background is cluttered in the target image being compared. It is hard to tell if subgraph $g_{j,k}$ in image I_j is matched exactly with subgraph $g_{\eta(d),k'}$ in image $I_{\eta(d)}$. For example, 1) If $g_{j,k}$ falls into one part of the object, subgraph $g_{\eta(d),k'}$ almost covers all the object, these two subgraphs are considered as ‘matched’. 2) If a generated subgraph is not stable (it either stretches across object/background or contains isolated points), this subgraph will not match any subgraph of the other image.

6. RESULTS AND DISCUSSION

We define a $\eta \times K$ matrix M , its entry is:

$$M_{d,k} = \begin{cases} 1 & \text{if } \eta(d) \in \text{rel} \text{ and } g_{j,k}, g_{\eta(d),k'} \text{ match,} \\ 0 & \text{otherwise} \end{cases} \quad (6.7)$$

to describe the stability of partitioning G_j into $\Gamma_j^K = \{\Gamma_j^k\}_{k=1,\dots,K} = \{g_{j,1}, \dots, g_{j,K}\}$, i.e. K -way partitioning.

The *Partition Precision (PP)* at $n = |\eta|$ is thus given by a vector of length K :

$$\{Precision(\Gamma_j^k)\}_{k=1,\dots,K} = \frac{1}{|\eta|} \sum_{d=1 \dots |\eta|} M_{d,k} \quad (6.8)$$

where $M_{d,k}$ is an element of matrix M .

The partition precision of *intra-class* (see Table 6.18 and Table 6.19) is defined as:

$$\{P(\Gamma_j^k)\}_{k=1,\dots,K} = \frac{1}{|N_{rel}|} \sum_{d=1 \dots |\Omega|} M_{d,k} \quad (6.9)$$

where $M_{d,k}$ is an element of matrix M .

In essence, $\{Precision(\Gamma_j^k)\}_{k=1,\dots,K} = \underbrace{[1, \dots, 1]}_K$ if all n images are relevant, and all the corresponding subgraphs are matched across image category that I_j belongs in. Each vector element (corresponding to each subgraph $g_{j,k}$) of this measure lies in the range of 0 to 1.

6.4 Comparison of Co-occurrence Measures for Image Matching in the *BBoW* Model

In this section we present the results of experiments we conducted on the SIVAL dataset with the approach of sparse sampling via keypoints detection. The whole experiment was performed with the approach of Delaunay triangulation of graph nodes. The Graph Cuts algorithm was therefore used for graph partitioning, as explained in Section 3.3 of Chapter 3 (Graph Construction) for specific definition of our energy potentials on Delaunay triangulated graph.

A (dis)similarity measure between two (sub)graphs can be easily computed as we just need to compare two histograms. We here adopt the idea of RootSIFT [33] by first L1 normalizing the histograms and then compute the *histogram intersection* (HI) of them. Nevertheless, we still need to compute the similarity between two images, knowing that they both contain K subgraphs, i.e. K histograms for K subgraphs.

We have experimented different strategies to combine the $K \times K$ distances between a pair of query image I_i and database image I_j from their corresponding histogram sets H_i and H_j :

6.4 Comparison of Co-occurrence Measures for Image Matching in the BBoW Model

maximum, resp. *minimum*, resp. *mean*, resp. *median*, resp. *sum*, etc. of all distances in operation, as explained in Section 4.3.1 of Chapter 4.

As shown in Figure 6.4, the *similarity measure* in Equation (4.4) corresponds to the best discriminative *distance measure* between two images. We recall this measure:

$$d(I_i, I_j) = 1 - \left\{ \min_{u=\{1, \dots, K\}} \min_{v=\{1, \dots, K\}} \left(\sum_{b=1}^B \min(H_{i,u}(b), H_{j,v}(b)) \right) \right\}. \quad (6.10)$$

A complete comparison of different measures including that of classical Bag-of-Words model can be found in more detail in Table A.1, Figure A.1 and Figure A.2 of the Appendix A respectively.

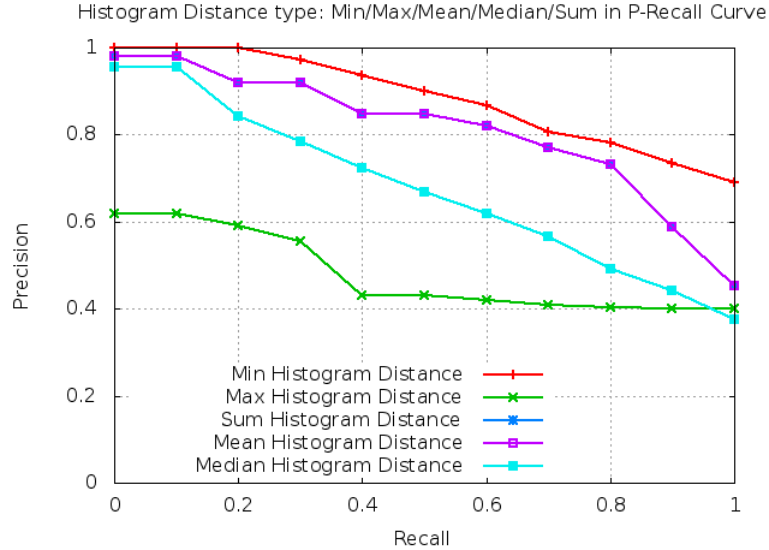


Figure 6.4: Comparison of a series of image similarity measures.

Performance of image retrieval is measured by calculating precision, recall, and the mAP over each category, since that mixing of all categories has no sense for disparity of the object appearance across categories.

For three categories : “*stripednotebook*”, “*goldmedal*”, “*woodrollingpin*” among 25 categories, the proposed BBoVW method performs better than BoVW. Two examples are presented in Figure 6.5, demonstrating the results for a “good” category and a “bad” category. In Figure 6.5 (c) and Figure 6.5 (d), the four subgraphs are generated via Graph Cuts. They are displayed in red, green, yellow, and orange colors respectively. The mean improvement of mAP on these three relevant categories is of 8%. As for “bad” categories, the discrepancy of

6. RESULTS AND DISCUSSION

results is too high to make a meaningful statistics. The complete results for all 25 categories of SIVAL dataset are presented in Figure A.3 of the Appendix A.

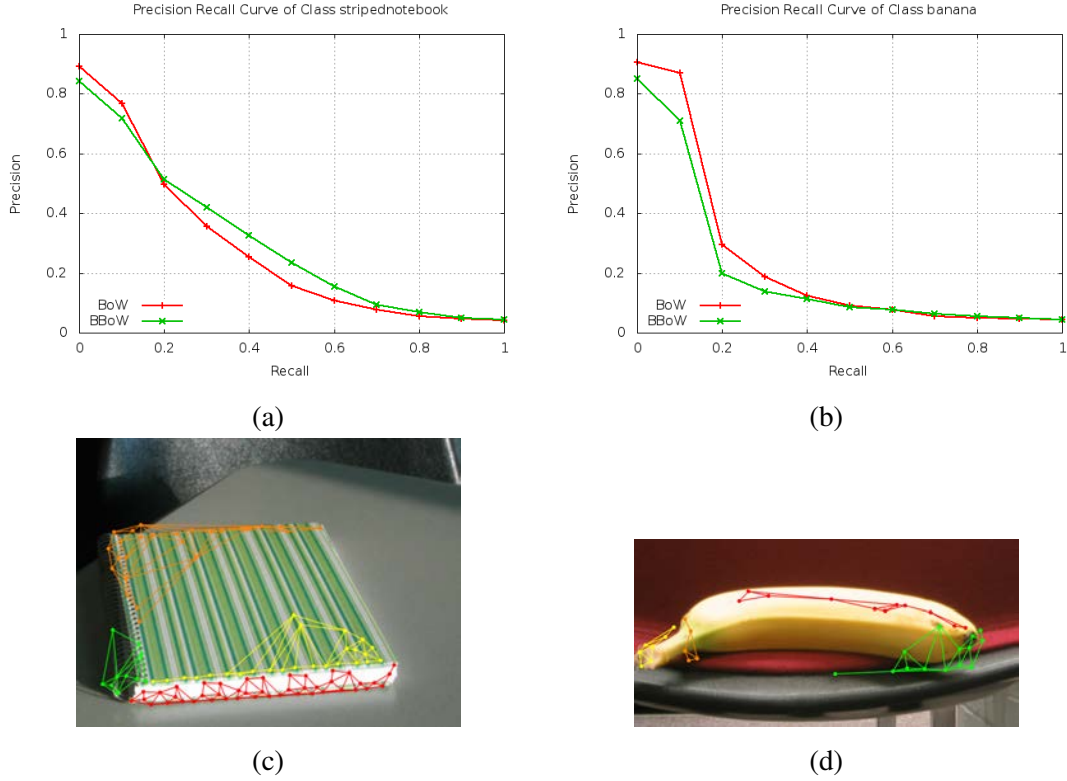


Figure 6.5: Comparison between BoW and *BBoW* on SIVAL benchmark. (a) The precision-recall curve for a “good” category : “stripednotebook”. (b) The precision-recall curve for a “bad” category : “banana”. (c) Graph descriptors from “stripednotebook”. (d) Graph descriptors from “banana”.

The results via Graph Cuts hold the clue to the causes of the unfavourable result. As can be observed in Figure 6.6, the number of graph nodes in each label set is unbalanced; the points in the same label are not clustered into one image region; there exist isolated points that are far from their corresponding similar component; one subgraph (these points with the same label) can cross object and background.

The experiments demonstrate that the approach of using prominent keypoints as graph nodes is sensitive to the stability of feature points. However, this stability is not ensured since interest points often appear on the border between object and background or the regions of high contrast. Moreover, the distance factor in energy term, *i.e.* $f_d(p, q)$ in Equation (3.15), does not

6.4 Comparison of Co-occurrence Measures for Image Matching in the *BBoW* Model

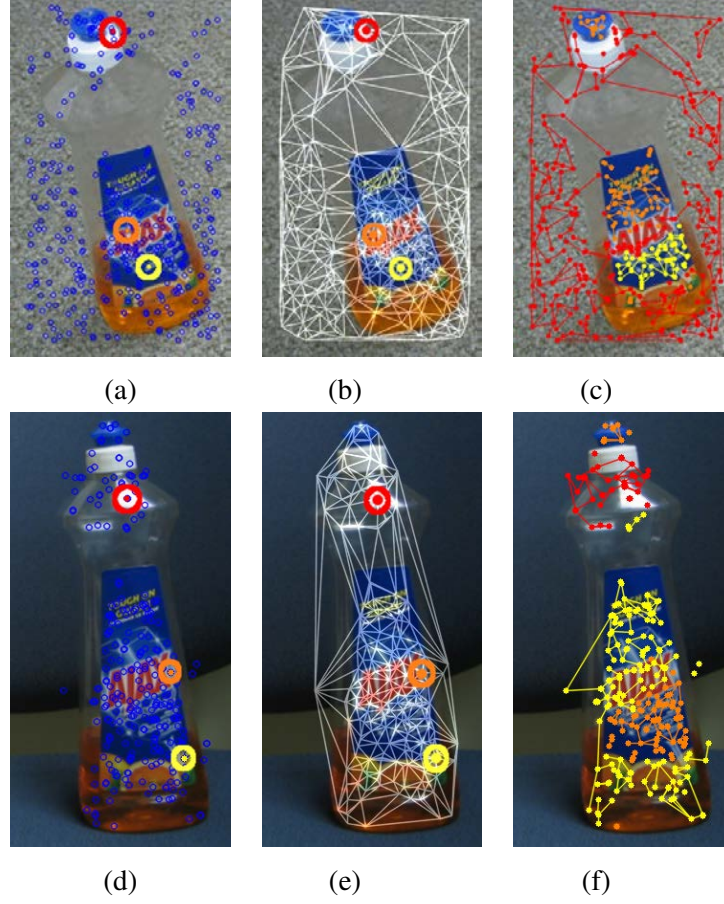


Figure 6.6: Two examples of graph partitioning via Graph Cuts. The first row shows result of image ‘AjaxOrange079.jpg’, the second row is result of image ‘AjaxOrange049.jpg’. Both of images are from category “AjaxOrange” in SIVAL dataset. (a)(d) Seeds. (b)(e) Initial image graph with chosen seeds. (c)(f) Labeling result.

give any improvement, in most cases, is even worse.

Based on the above reasons, we drop the prominent keypoints approach, adopt dense sampling pixels as graph nodes for further experiments. Furthermore, the *SIVAL* database is limited in complexity of scenes; it is not sufficiently large and thus is not used widely as a common benchmark. Hence in the follow-up of this Chapter, we will present results on *Caltech-101* and *PPMI* databases.

6. RESULTS AND DISCUSSION

6.5 Parameters Evaluation

In this Section, we study the impact of the different parameters in the *BBoW* model on image retrieval performance.

6.5.1 Patch Size and Contribution of Color Term

We start by testing the parameters' influence of our method for image retrieval. Two parameters have been evaluated: the patch size n defined in section 3.3.3.1 and the parameter λ from the edges weight (in Equation (3.4)). For efficiency, the experiments were conducted on a subset of *Caltech-101* database that contains 4 images per category, for a total of 404 images. The parameter α is set to one in Equation (E.1). Here we present the results for Graph Cuts and Normalized Cuts methods.

The performance is evaluated by mean Average Precision (mAP) values, and is shown in tables 6.2 and 6.3.

Table 6.2: Influence of parameter λ (Equation (3.4)) on image retrieval. For each value, the mean average precision is given. For this experiment, the patch size is set to $n = 5$.

	Mean Average Precision for the IMPK approach with 3 levels			
	$\lambda = 0$	5	20	100
NC	0.386079	0.389737	0.386185	0.380554
GC	0.373073	0.382115	0.377872	0.375660

Table 6.3: Influence of parameter n (section 3.3.3.1) on image retrieval. For each value, the mean average precision is given. For this experiment, $\lambda = 5$.

	Mean Average Precision for the IMPK approach with 3 levels			
	$n = 3$	5	7	9
NC	0.380546	0.388987	0.389456	0.388229
GC	0.379723	0.382115	0.377215	0.375741

These results highlight that these parameters do not have much influence on the quality of results using either Graph Cuts (GC) or Normalized Cuts (NC). For the following experiments, we therefore decided to use $n = 5$ and $\lambda = 5$.

6.5.2 Influence of Texture Term

In order to improve the stability of the graph partitions, we try incorporating texture features w_{pq}^T into graph weights w_{pq} , by assigning $\alpha \neq 1$ in Equation (E.1). For this purpose, we conducted an experiment in a reduced dataset of *Caltech-101*, including 201 images for query, 403 images for retrieval. By setting $\alpha = 0, 0.5, 0.6, 0.7, 0.8, 0.9, 1$, respectively in Equation (E.1), we are able to investigate the evolution of retrieval performance as less texture features were jointly embedded into graph weights with local color in *BBoW* model.

As explained in Table 6.4, the best performance in retrieval reaches as $\alpha = 0.8$ in Equation (E.1). However, the best mAP value just gives slightly improvement from considering only color features in edges weights. Furthermore, take a close examination of the partitioned image (sub)graphs, for example, a case study in Figure 6.7, the obtained subgraphs are more reasonable in separating image regions.

Indeed, the performance of image retrieval in mAP demonstrates that the use of complementary texture features in DCT domain generally did not improve the retrieval accuracy in our experiments. We can explain this by the different nature of these features and insufficiency of a direct application of them in a joint probability manner in the graph-cut objective function.

Table 6.4: Evaluation of embedding joint color-texture energy in graph weights for image retrieval. Graph weights account for more color features as value of parameter α in **Equation** (E.1) increases. The mAPs are given for each single level and pyramid. The patch size is set to $n = 5$. $\lambda = 5$. The size of visual codebook is 400. By contrast, the mAP for SPM is **0.409**.

Level	$\alpha = 0$ (only texture)		$\alpha = 0.5$		$\alpha = 0.6$		$\alpha = 1$ (only color)	
	Single level	Pyramid	Single level	Pyramid	Single level	Pyramid	Single level	Pyramid
L=0	0.3779		0.3779		0.3779		0.3779	
L=1	0.3739	0.3761	0.3603	0.3761	0.3636	0.3778	0.3731	0.3800
L=2	0.3731	0.3787	0.3820	0.3826	0.3744	0.3831	0.3837	0.3857

6.6 Influence of Neighbourhood Systems

We studied the influence of different neighbourhood systems on the graph partitions.

As can be seen in Figure 6.8, the first row shows graph partitions on a synthetic image, the second row displays the partitioning results on nature image “accordion0001.jpg” from

6. RESULTS AND DISCUSSION

Level	$\alpha = 0.7$		$\alpha = 0.8$		$\alpha = 0.9$		$\alpha = 1$ (only color)	
	Single level	Pyramid	Single level	Pyramid	Single level	Pyramid	Single level	Pyramid
L=0	0.3779		0.3779		0.3779		0.3779	
L=1	0.3666	0.3791	0.3630	0.3738	0.3622	0.3725	0.3731	0.3800
L=2	0.3775	0.3838	0.3804	0.3860	0.3831	0.3843	0.3837	0.3857

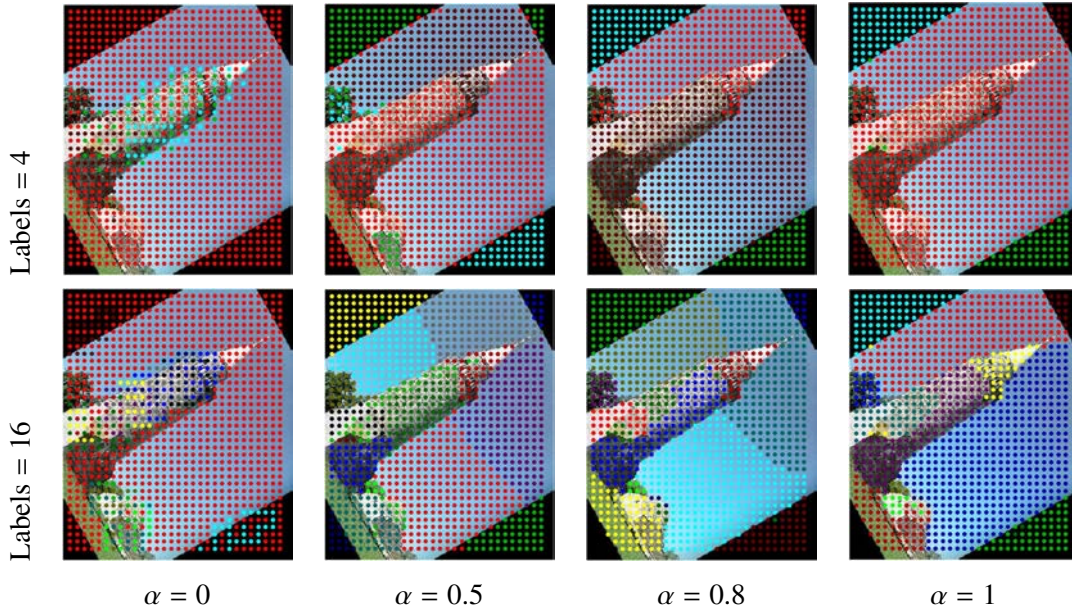


Figure 6.7: An example of image graph partitions on the image *minaret0032.jpg* from *Caltech-101* dataset, when joint color-texture is embedded in edge weights. The 1^{th} - 4^{th} columns correspond to graph partitions by setting $\alpha = 0, 0.5, 0.8, 1$ in **Equation (E.1)** severally. The first row of this figure shows the results of partitions at resolution $r = 1$, where each image is composed of 4 subgraphs. The second row corresponds to 16 partitions at resolution $r = 2$, *i.e.* 16 subgraphs per image. This figure is better viewed in *color*.

Caltech-101 dataset. We can observe that labels propagate in more reasonable ways along edges or around the border of areas of contrast under 4-connected neighbourhood system.

We have testified that such favourable behaviours happen only when texture factor is considered in **Equation (E.1)**, *i.e.* $\alpha \neq 0$. The neighbourhood system has no obvious effect on graph partitions if only color factor is embedded in edge weights.

6.7 Influence of Distance Metric for Histogram Comparison

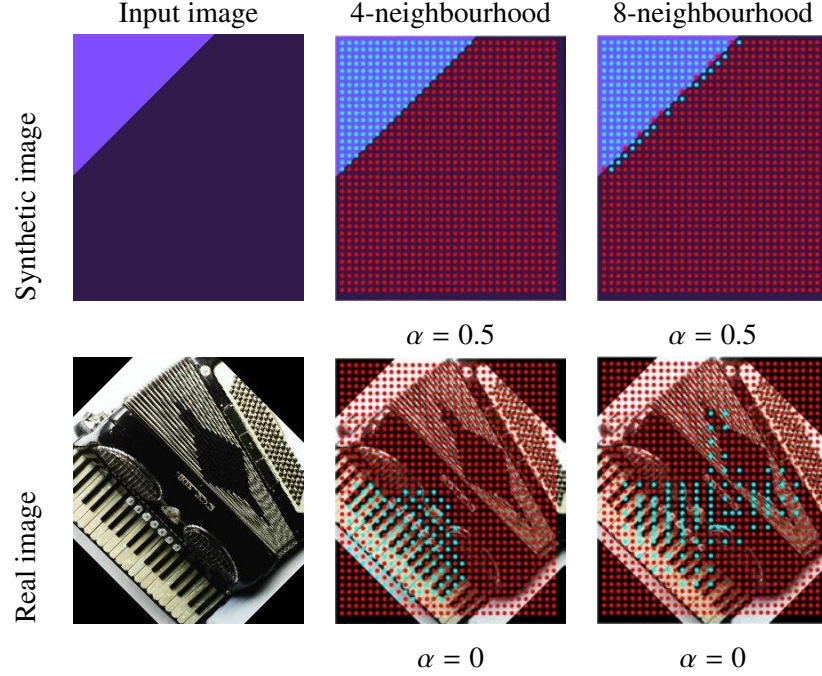


Figure 6.8: Example of graph partitions of two images as texture factor is considered in edge weights under different neighbourhood systems. This figure is better viewed in *color*.

6.7 Influence of Distance Metric for Histogram Comparison

In this Section, we study the influence of distance metrics on *BBoW* model. As shown in Table 6.5, applying *L1* distance achieves in overall better performance than *L2* distance. Furthermore, the former can be beneficial to computational complexity than the latter. We therefore decide to use *L1* metric for the following experiments. Out of consistence, we adopt *L1* distance in *Hungarian algorithm* as well, as mentioned in Section 4.3.2 of Chapter 4.

Table 6.5: The influence of distance metrics to compute a cost matrix for graph matching via *Hungarian algorithm*. Note that the partitions are obtained by KKM. The experiments were run in *PPMI* dataset, and its settings have been described in Section 6.2.3.

Level	KKM (<i>L1</i> metric)		KKM (<i>L2</i> metric)	
	Single level	Pyramid	Single level	Pyramid
L=1	0.1126 ± 0.0185	0.1134 ± 0.0193	0.1146 ± 0.0202	0.1146 ± 0.0204
L=2	0.1117 ± 0.0178	0.1122 ± 0.0185	0.1140 ± 0.0198	0.1140 ± 0.0200

6.8 Irregular Graph Representation versus SPM for Image Retrieval

As discussed in the Section 3.5 of Chapter 3, we apply three methods to build irregular pyramid partitions in the *BBoW* model. These three approaches are: Graph Cuts, Normalized Cuts and kernel k -means to optimize multilevel weighted graph cuts, respectively. In this section, we will evaluate the impact of these three graph partitioning methods in *BBoW* model on the performance of image retrieval. Moreover, we compare the proposed *Bag-of-Bags of Words* model to notable image representation in *Spatial Pyramid Matching* (SPM).

Firstly, we run experiment on the PPMI dataset. As shown in Table 6.6, the performance of *BBoW* (via KKM) is very close to SPM, yet our model is globally more stable, as smaller *std* values attest.

Table 6.6: The retrieval performance (mAP \pm standard deviation of APs) on *PPMI* dataset.

	Level 0 (BoW)	Level 1	Level 2	Pyramid
NC	0.109 \pm 0.031	0.104 \pm 0.022	0.106 \pm 0.025	0.108 \pm 0.027
GC	0.109 \pm 0.031	0.104 \pm 0.022	0.106 \pm 0.024	0.108 \pm 0.027
KKM	0.109 \pm 0.031	0.113 \pm 0.019	0.113 \pm 0.019	0.115 \pm 0.020
SPM	0.109 \pm 0.031	0.115 \pm 0.036	0.121 \pm 0.043	0.118 \pm 0.041

Secondly, we compare the *BBoW* model with SPM on popular *Caltech-101* benchmark. We also give a comparative study of three graph partitioning methods in an attempt to reach a better stability during the graph partitioning process. The experimental validation of our model will be discussed below as well.

As can be seen in Table 6.7, comparative analysis of this experimental results proves that the multilevel *KKM* algorithm is more effective than the other two methods in *BBoW* model. Its success justifies important contribution by kernel k -means in refinement phase of graph clustering. It also suggests that better graph partitioning strategy can improve image retrieval performance for the proposed *BBoW* model. The relative poor performance of Graph Cuts in *BBoW* indicates the need of improving seed selection strategy.

6.8 Irregular Graph Representation versus SPM for Image Retrieval

Table 6.7: Retrieval performance on subset of *Caltech-101* dataset composed of 2945 query images and 5975 images from database for retrieval. We set $\alpha = 1$ in Equation (E.1), *i.e.* **only consider color-related term** w_{pq}^C in w_{pq} . A postscript: *SPM* wins *BBoW* (with *KKM*) by a small margin with a mAP value of **0.14**, versus **0.1327** for *KKM*, while *SPM* has higher *std* as value of **0.0660**.

Methods	Kernel k -means	Graph cuts	Normalized Cuts
mAP \pm mean Std	0.1327 \pm 0.0445	0.0989 \pm 0.0467	0.1074 \pm 0.0484

Based on the results shown in Table 6.7, we decide to adopt multilevel *KKM* algorithm for graph partitioning in *BBoW*. We aim at answering a challenging question: will an irregular, segmentation-like partition (*BBoW*) of images outperform a regular partition (*SPM*) [4] of images for image retrieval? In order to answer this question, we run a comparative experiment on the *whole Caltech-101* dataset ($\alpha = 1$ in Equation (E.1), *i.e.* **only consider color-related term** w_{pq}^C in w_{pq}).

The experimental results show that *BBoW* achieves less performance than *SPM* with a margin of **18.5%** in overall retrieval mAP. The distribution of mAP margin for not surpassing categories can be found in Figure 6.9. However, if we take a further look at the corresponding APs($\pm std$) values per category, we find that in 19 categories (in red color) out of 101 classes, *BBoW* performs better than *SPM* (in blue color), as can be seen in Figure 6.10. Note that category “*car_side*” is composed of all gray-level images, therefore we do *not* count it as a contribution of surpassing category.

A comparison between *BBoW* (via GC or NC) and *SPM* is presented on figure 6.11, illustrated by the mAPs values on sixteen categories excerpted from *Caltech-101* dataset. The result highlights the fact that for the most of the categories, *SPM* has a much higher retrieval performance than *BBoW* (via GC) or *BBoW* (via NC). These categories explain the importance difference in the global performance on all the database (as described previously). However, for *certain* categories, *BBoW* (via either Graph Cuts or Normalized Cuts) is as good as or better than *SPM*.

In summary, despite that *BBoW* model under performs *SPM* in overall performance, our proposed model (via Graph Cuts or NCuts or *KKM*) can still achieve better results in 25 categories than *SPM*. We found that kernel-based multilevel weighted graph cuts algorithm outperforms Graph Cuts and Normalized Cuts in both computation time and partitioning results. Graph Cuts, derived from its energy minimization nature, is unavoidable to get unbalanced

6. RESULTS AND DISCUSSION

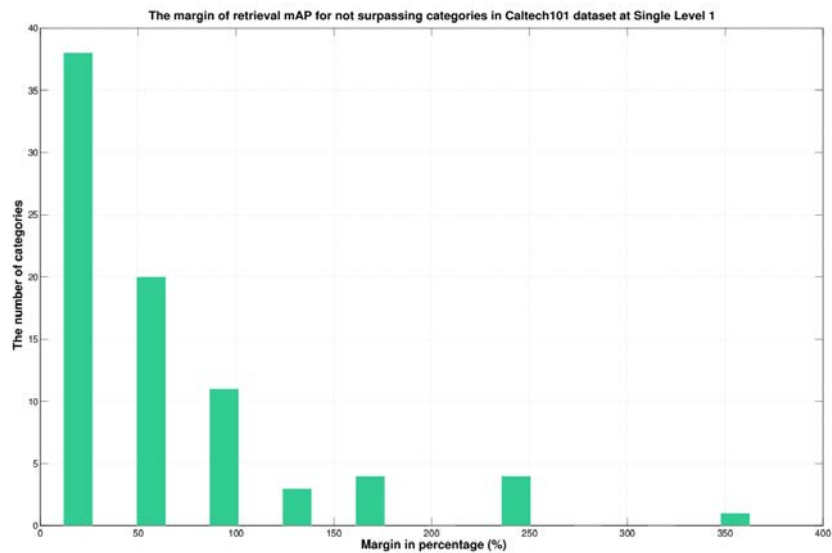


Figure 6.9: The margin of mean Average Precision (mAP) for not surpassing categories in *Caltech-101* dataset. The margin = $\frac{mAP(SPM) - mAP(KKM)}{mAP(KKM)} \%$.

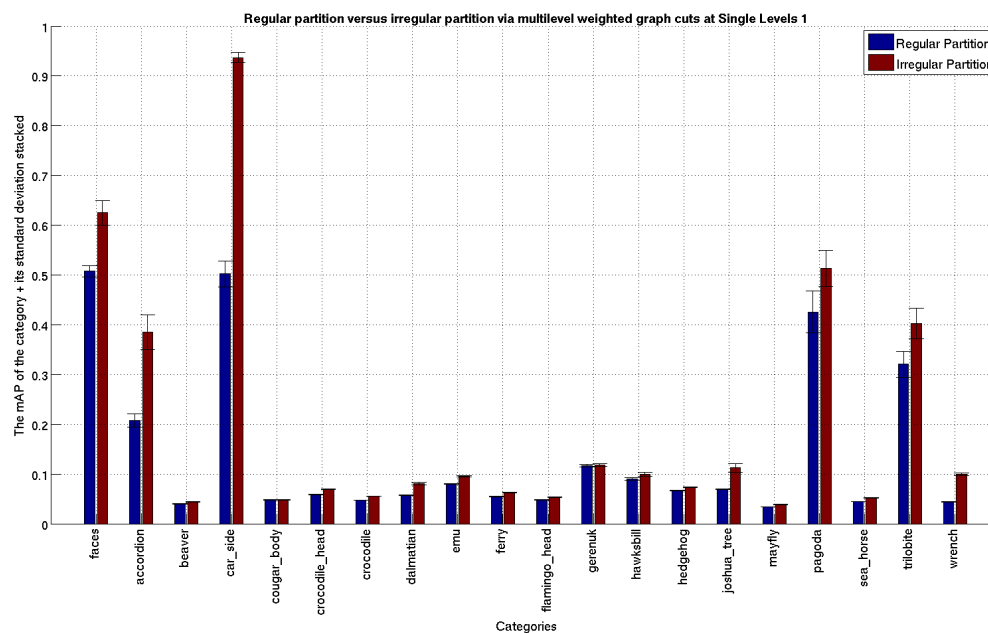


Figure 6.10: Mean Average Precision for surpassing categories in *Caltech-101* dataset.

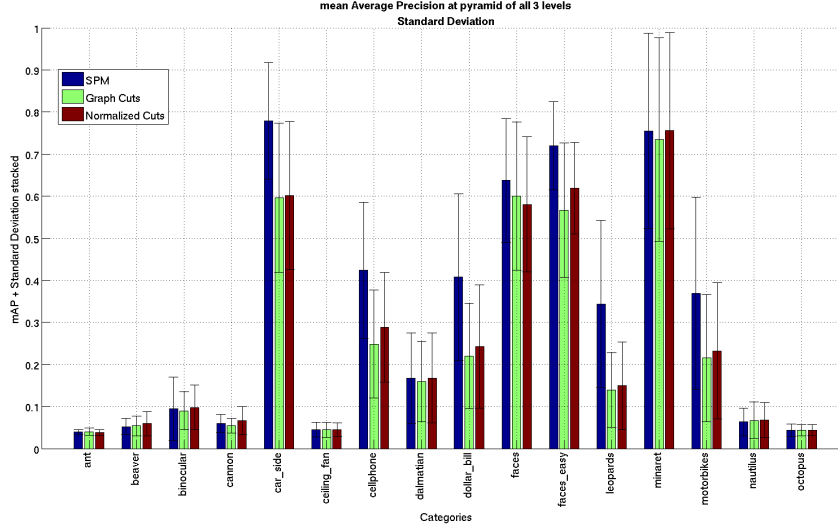


Figure 6.11: The mean Average Precision for 16 typical categories in Caltech101 subgraphs. Normalized Cut, however, can produce relatively balanced sub-graph size. But it requires eigenvalue computation which is time-consuming and overloads memory easily as size of image graph increases. By using multilevel kernel based graph clustering method, we are able to avoid disadvantages of the two other methods.

6.9 Partition Analysis

Now we present a detailed analysis of the stability of graph partitions, and how does this stability influence the performance of image retrieval.

6.9.1 Stability of Graph Partitions

In order to understand results in previous Section 6.8 more clearly, let us further look at the obtained graph partitions in *BBoW* model.

The explanatory case studies of graph partitions First of all, we review the six typical categories (“*accordion*”, “*faces*”, “*pagoda*”, “*trilobite*”, “*cellphone*”, “*motorbikes*”) that have been enumerated in Section 3.6 of the Chapter 3. We now do further analysis of these images with the aim of discovering the relationship between the graph partitions and the performance of image retrieval.

6. RESULTS AND DISCUSSION

Taking each image as a query, retrieval performance was evaluated in mAP on subset of *Caltech-101* dataset composed of 5975 images from database for retrieval. The patch size is set to $n = 5$. $\lambda = 5$. We here only give a concise evaluation on the case of 4 partitions. The corresponding mAPs are listed in Table 6.8 resp. Figure 3.12, Table 6.9 resp. Figure 3.13, Table 6.10 resp. Figure 3.14, Table 6.11 resp. Figure 3.15, Table 6.12 resp. Figure 3.16, Table 6.13 resp. Figure 3.17¹.

It is shown that our *BBoW* model clearly outperforms SPM for all examples of images listed in Figure 3.12, Figure 3.13, Figure 3.14 and Figure 3.15, from four different categories: “*accordion*”, “*faces*”, “*pagoda*”, “*trilobite*”. Particularly for the “*faces*” category, *BBoW* via KKM gives the best results. As can be seen on the third column of Figure 3.13, our method is able to represent the “*faces*” with only one or two subgraphs. The other subgraphs in the background are also stable in the sense that almost the same subgraphs can be found in each high-ranking retrieved image within “*faces*” category. More details can be referred to the Table B.4 resp. Figure B.1, Table B.5 resp. Figure B.2, Table B.6 resp. Figure B.3, Table B.7 resp. Figure B.4, Table B.8 resp. Figure B.5 in Appendix B. The same case holds in category “*trilobite*”, where *BBoW* via Normalized Cut surpasses SPM. The second column of Figure 3.15 presents the partitioning results on five images from the “*trilobite*” category. Once again, it can be observed that the partitions are stable.

Figure 3.16 and Figure 3.17 on the other hand represents two categories (“*cellphone*” and “*motorbikes*”) for which our method fails. The partitions obtained almost do not exhibit any consistency across the images from the same category. The resulting histograms are therefore each time very different. Obviously, we cannot expect any good retrieval.

The statistical analysis of subgraphs In order to give a deeper understanding on why our method suits for certain categories and not for the others, let us go through again the other three case studies: a “good” category (“*minaret*”), and two “bad” ones (“*cellphone*”, “*dollar_bill*”).

Figure 6.12 presents the partitioning results at level 1, *i.e.* 4 subgraphs. The first row of the Figure 6.12 illustrates good queries from “*minaret*” class in which *BBoW* outperforms SPM. Once again, our method is able to represent the “*minaret*” (object) with only one or two subgraph(s). The other subgraphs in the background are also stable.

¹The file extension of each image is omitted in these Tables and Figures. The highest value of mAPs is shown in bold for each query image.

Table 6.8: The comparison of mAPs for *BBoW* (via GC) vs *BBoW* (via NCuts) vs *BBoW* (via KKM) vs SPM on 4 partitions of five examples of images from category “*accordion*”. See Figure 3.12.

Image	GC	NCuts	KKM	SPM
accordion0031	0.3439	0.6328	0.5835	0.0718
accordion0032	0.6238	0.6047	0.5994	0.3693
accordion0041	0.7535	0.6080	0.6401	0.4414
accordion0053	0.4886	0.6382	0.5673	0.2957
accordion0055	0.7175	0.6119	0.6211	0.1909

Table 6.9: The comparison of mAPs for *BBoW* (via GC) vs *BBoW* (via NCuts) vs *BBoW* (via KKM) vs SPM on 4 partitions of five examples of images from category “*faces*”. See Figure 3.13.

Image	GC	NCuts	KKM	SPM
faces0032	0.6979	0.6729	0.9086	0.5949
faces0036	0.6431	0.5716	0.9146	0.5139
faces0038	0.6240	0.4250	0.9314	0.4991
faces0039	0.5938	0.6098	0.9042	0.6094
faces0049	0.5453	0.4881	0.9091	0.5404

Table 6.10: The comparison of mAPs for *BBoW* (via GC) vs *BBoW* (via NCuts) vs *BBoW* (via KKM) vs SPM on 4 partitions of five examples of images from category “*pagoda*”. See Figure 3.14.

Image	GC	NCuts	KKM	SPM
pagoda0035	0.2647	0.3246	0.6960	0.5297
pagoda0040	0.5955	0.5449	0.6894	0.6722
pagoda0043	0.8271	0.3784	0.7534	0.6794
pagoda0046	0.4102	0.5622	0.7596	0.7169
pagoda0047	0.6674	0.4556	0.7185	0.5542

The second row of the Figure 6.12 shows four bad queries from *cellphone* and *dollar_bill* categories in which SPM achieves better performance than our method. We have the same

6. RESULTS AND DISCUSSION

Table 6.11: The comparison of mAPs for *BBoW* (via GC) vs *BBoW* (via NCuts) vs *BBoW* (via KKM) vs SPM on 4 partitions of five examples of images from category “*trilobite*”. See Figure 3.15.

Image	GC	NCuts	KKM	SPM
trilobite0037	0.5975	0.7040	0.6342	0.4386
trilobite0041	0.3561	0.6575	0.6612	0.5174
trilobite0056	0.6229	0.8055	0.6550	0.5787
trilobite0064	0.3551	0.6805	0.6645	0.5087
trilobite0072	0.6823	0.8540	0.6186	0.2240

Table 6.12: The comparison of mAPs for *BBoW* (via GC) vs *BBoW* (via NCuts) vs *BBoW* (via KKM) vs SPM on 4 partitions of five examples of images from category “*cellphone*”. See Figure 3.16.

Image	GC	NCuts	KKM	SPM
cellphone0032	0.2372	0.2439	0.1448	0.3429
cellphone0035	0.1742	0.0567	0.1018	0.3215
cellphone0049	0.1153	0.1832	0.1197	0.3117
cellphone0051	0.2644	0.5100	0.3845	0.7288
cellphone0059	0.2768	0.3254	0.2098	0.3637

Table 6.13: The comparison of mAPs for *BBoW* (via GC) vs *BBoW* (via NCuts) vs *BBoW* (via KKM) vs SPM on 4 partitions of five examples of images from category “*motorbikes*”. See Figure 3.17.

Image	GC	NCuts	KKM	SPM
motorbikes0042	0.3622	0.2407	0.2347	0.4885
motorbikes0043	0.4249	0.2950	0.2308	0.5262
motorbikes0047	0.3024	0.2630	0.1998	0.5967
motorbikes0055	0.3668	0.2704	0.1691	0.4293
motorbikes0059	0.3943	0.1734	0.3839	0.5856

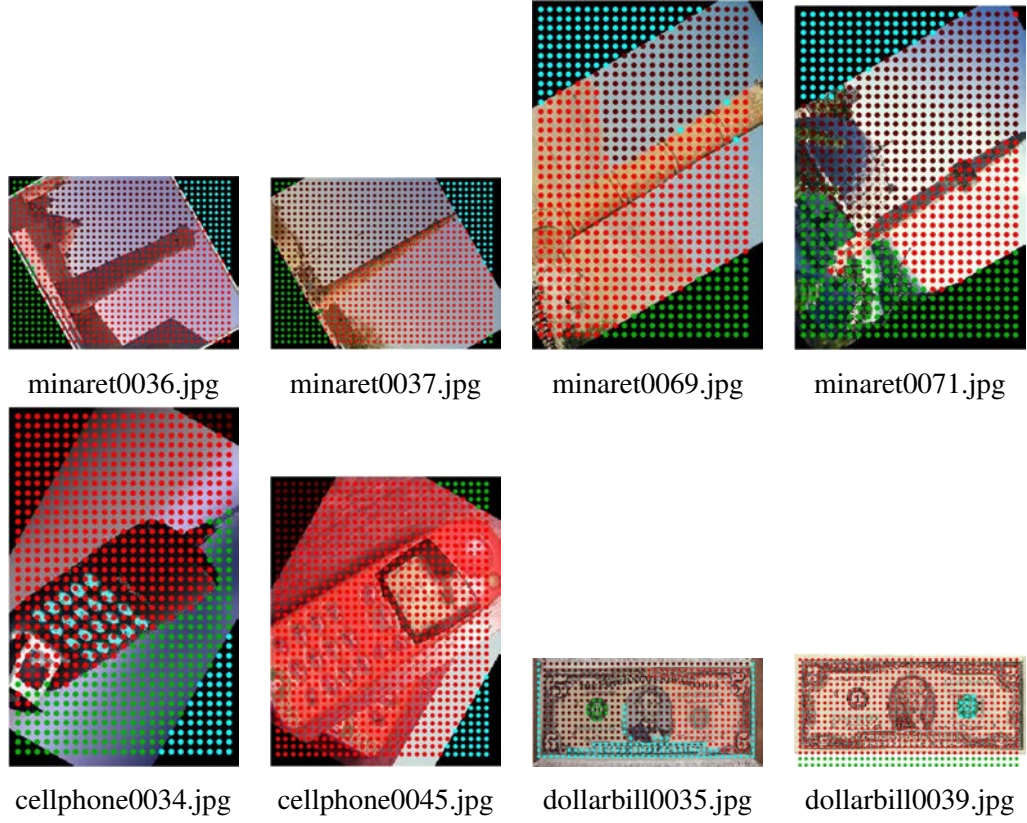


Figure 6.12: The first row shows the 4 irregular subgraphs from “good” query images at level 1. The second row shows the 4 irregular subgraphs from “bad” query images at level 1. The nodes of individual subgraphs are labelled with the same color (in red, blue, green, brown). This figure is better viewed in *color*.

observation on the obtained partitions, *i.e.*, the partitions are not consistent across the images from the same category. Obviously, we cannot expect any good retrieval as well.

We now detail the retrieval performance and the statistics of the (sub)graphs for these eight query images. One can see in Figure 6.13 (Graph Cuts), Figure 6.14 (NCuts) and Figure 6.15(KKM) that our method outperforms SPM [4] in “good” categories. In this case, the partitions from either NCuts or Graph Cuts are stable across the images of the same category. The mean number of nodes in “correctly” matched subgraphs together with the standard deviation are presented in Figure 6.16. The standard deviation is high for “bad” categories, whereas it is more uniform for “good” category.

6. RESULTS AND DISCUSSION

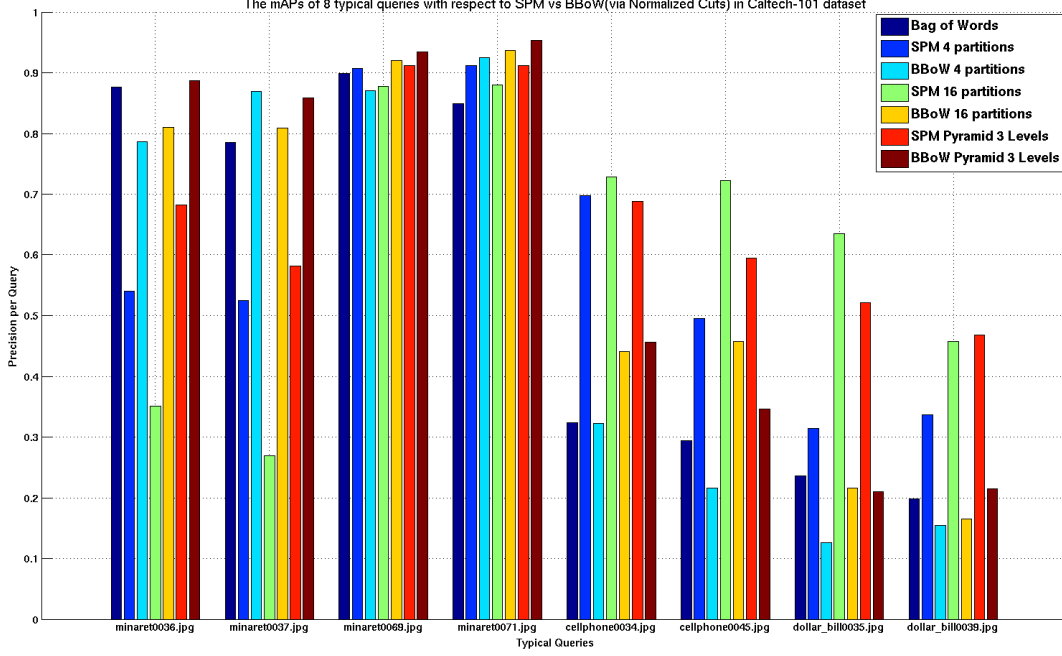


Figure 6.13: A case study of *BBoW* (via Normalized Cuts). The precision of 8 typical query images: 1st-4th query images are from a “good” category - *minaret*, 5th-8th query images are from “bad” categories: *cellphone* and *dollar_bill*.

6.9.2 Quality of Subgraphs Matching

To access subgraphs matching, we use the *partition precision* introduced in Section 6.3.2. The *partition precision* (PP) of 4 subgraphs for 8 typical queries ($|\eta| = 30$) are shown in table 6.14 and table 6.15. We find that in “good” categories, the $Precision(\Gamma_j^k)$ for each subgraph $g_{j,k}$ is close to 1, signifies that the subgraphs are matched correctly more often. That illustrates the discriminative power of graph descriptors among inter-class. While $\{P(\Gamma_j^k)\}_{k=1,\dots,4}$ are high, it means the image graph partitions tend to be more stable. In “bad” categories, this happens less often.

In the context of intra-category, the *Partition Precision* (PP) for query image I_j is thus given by a row vector of length K :

$$\{P(g_{j,k})\}_{k=1, \dots, K} = \frac{1}{|N_{rel}|} \sum_{d=1 \dots |N_{rel}|} M_{d,k} \quad (6.11)$$

where $M_{d,k}$ is an element of matrix M . The above vector thus characterizes the goodness of match of each subgraph in a query image to the subgraphs of images of the same category in

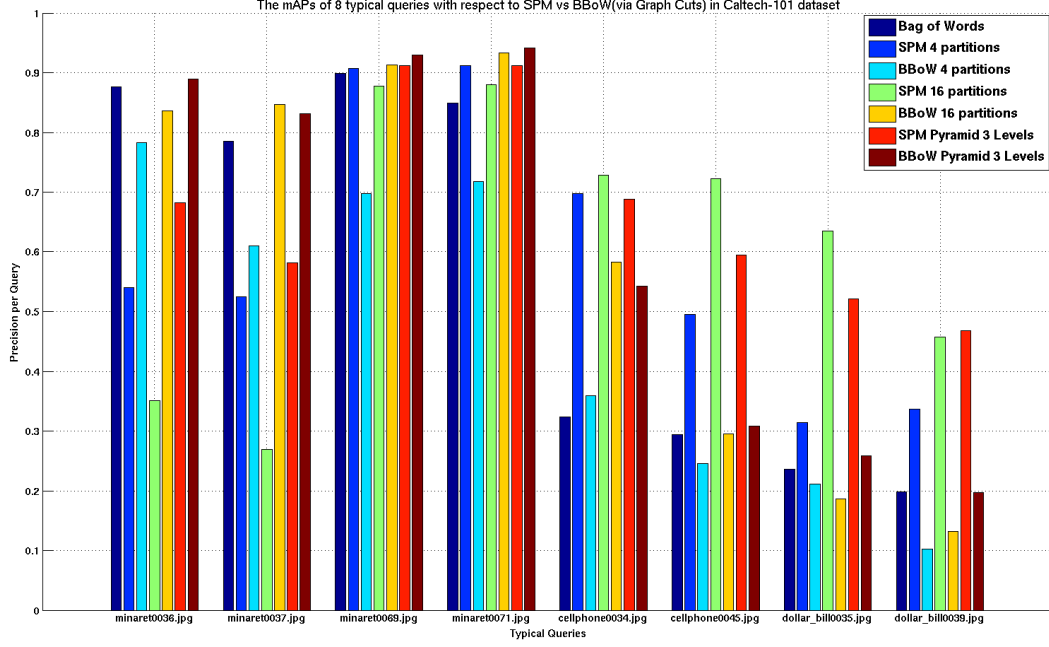


Figure 6.14: A case study of *BBoW* (via Graph Cuts). The precision of 8 typical query images: 1st-4th query images are from a “good” category - *minaret*, 5th-8th query images are from “bad” categories: *cellphone* and *dollar_bill*.

Table 6.14: The $PP \{Precision(\Gamma_j^k)\}_{k=1,2,3,4} = \{P(g_{j,k})\}_{k=1,2,3,4}$ of corresponding subgraphs for 4 typical “good” queries. Method: *BBoW* via Normalized Cut.

Query image I_j	$g_{j,1}$	$g_{j,2}$	$g_{j,3}$	$g_{j,4}$
minaret0036	0.933	0.867	0.833	0.867
minaret0037	1.0	0.9	0.833	0.933
minaret0069	1.0	0.967	0.9	1.0
minaret0071	0.967	0.9	0.833	0.8

the database Ω . Table 6.18 and 6.19 show figures for the partition precision of 4 typical queries of a “good” category and of two “bad” categories. The corresponding number of nodes for each subgraph, as illustrated in Figure 6.16, is also listed in Table 6.16 and Table 6.17 respectively in detail. Note that in Table 6.17, the standard deviation on a number of nodes is generally larger than that one in Table 6.16.

In Table 6.18, one can see that in the “good” categories, the worst matching percentage (the numbers in bold) is better than that in “bad” queries. Hence, this correlates with better

6. RESULTS AND DISCUSSION

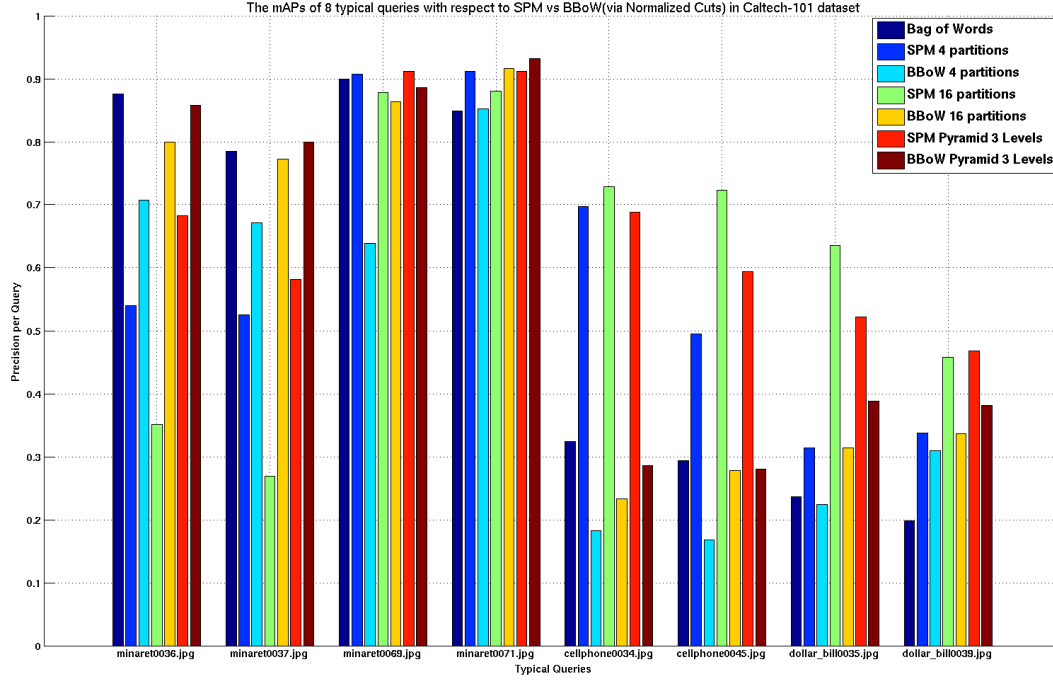


Figure 6.15: A case study of *BBoW* (via Kernel k -means). The precision of 8 typical query images: 1st-4th query images are from a “good” category - *minaret*, 5th-8th query images are from “bad” categories: *cellphone* and *dollar_bill*.

Table 6.15: The $PP \{Precision(\Gamma_j^k)\}_{k=1,2,3,4} = \{P(g_{j,k})\}_{k=1,2,3,4}$ of corresponding subgraphs for 4 typical “bad” queries. Method: *BBoW* via Normalized Cut.

Query image I_j	$g_{j,1}$	$g_{j,2}$	$g_{j,3}$	$g_{j,4}$
cellphone0034	0.433	0.467	0.3	0.433
cellphone0045	0.3	0.3	0.267	0.267
dollar_bill0035	0.133	0.2	0.167	0.133
dollar_bill0039	0.133	0.233	0.133	0.2

stability of nodes’ numbers, as in Figure 6.16, where the number of nodes within the matched subgraphs is quite imbalance in the “bad” categories.

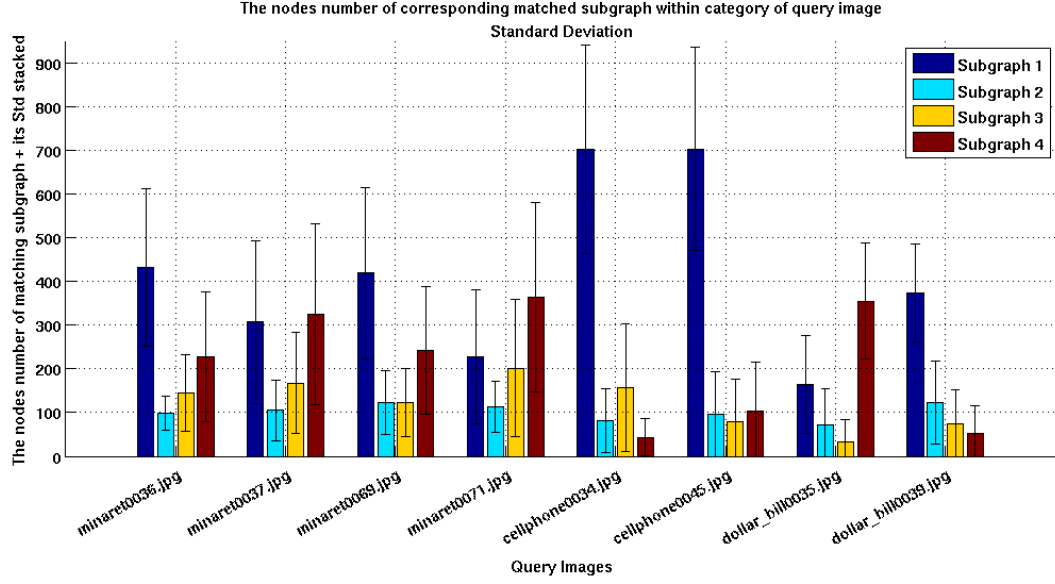


Figure 6.16: The mean and standard deviation of nodes' numbers of corresponding subgraphs for intra-category, for 8 typical queries in *Caltech-101* dataset - at single level 1, *i.e.* 4 subgraphs.

Table 6.16: The mean of node numbers and its standard deviation for corresponding matched subgraphs of intra-category minaret, for 4 typical good queries in *Caltech-101* dataset, at single level 1, *i.e.* 4 subgraphs. Method: *BBoW* via Normalized Cut.

I_j	Precision	$g_{j,1}$	$g_{j,2}$	$g_{j,3}$	$g_{j,4}$
minaret0036	0.7864	433 \pm 180	99 \pm 38	145 \pm 88	228 \pm 148
minaret0037	0.8694	307 \pm 185	105 \pm 70	168 \pm 116	326 \pm 207
minaret0069	0.8699	419 \pm 196	123 \pm 73	123 \pm 79	243 \pm 147
minaret0071	0.9252	228 \pm 153	113 \pm 58	202 \pm 157	365 \pm 217

Table 6.17: The mean of node numbers and its standard deviation for corresponding matched subgraphs of intra-category cellphone and dollar_bill, for 4 typical bad queries in *Caltech-101* dataset, at single level 1, *i.e.* 4 subgraphs. Method: *BBoW* via Normalized Cut.

I_j	Precision	$g_{j,1}$	$g_{j,2}$	$g_{j,3}$	$g_{j,4}$
cellphone0034	0.4412	703 \pm 239	82 \pm 73	157 \pm 147	43 \pm 43
cellphone0045	0.4576	703 \pm 233	96 \pm 97	80 \pm 97	104 \pm 111
dollar_bill0035	0.1263	164 \pm 111	72 \pm 83	34 \pm 50	355 \pm 132
dollar_bill0039	0.1540	374 \pm 111	123 \pm 94	74 \pm 78	53 \pm 63

6. RESULTS AND DISCUSSION

Table 6.18: The $\{P(g_{j,k})\}_{k=1,\dots,4}$ of corresponding subgraphs for 4 typical “good” queries. Method: *BBoW* via Normalized Cut.

Query image I_j	$g_{j,1}$	$g_{j,2}$	$g_{j,3}$	$g_{j,4}$
minaret0036	0.773	0.746	0.626	0.6
minaret0037	0.786	0.72	0.626	0.6
minaret0069	0.773	0.44	0.6	0.613
minaret0071	0.8	0.506	0.6	0.413

Table 6.19: The $\{P(g_{j,k})\}_{k=1,\dots,4}$ of corresponding subgraphs for 4 typical “bad” queries. Method: *BBoW* via Normalized Cut.

Query image I_j	$g_{j,1}$	$g_{j,2}$	$g_{j,3}$	$g_{j,4}$
cellphone0034	0.724	0.638	0.569	0.241
cellphone0045	0.724	0.362	0.569	0.552
dollar_bill0035	0.431	0.686	0.392	0.176
dollar_bill0039	0.275	0.824	0.06	0.418

6.10 Conclusion

In this Chapter, we provided our experimental results on three image benchmarks, to validate the proposed *BBoW* model. We also compared *BBoW* with a notable approach *spatial pyramid matching*. As compared with Spatial Pyramid Matching (SPM), the *BBoW* model overcomes the practical limitations of assuming similar parts of scenes very often appear in similar regular grid cells. Particularly, we emphasize that the partitions in *BBoW* are *not* nested across multiple levels.

We also gave an analysis of the images sampled from four “good” categories and two “bad” categories in *Caltech-101* dataset, as case studies to reveal the relationship between the stability of graph partitions and the performance of image retrieval. We have found: despite that the *BBoW* model does not perform as good as SPM overall, the strength of our method is promising for image retrieval when the partitions are stable across an image category, e.g. “*accordion*”, “*faces*”, “*pagoda*”, “*trilobite*” categories in *Caltech-101* dataset, see Section 6.9.1 and Appendix B for reference. The experiments demonstrate that our proposed method is globally more stable and performs better than SPM in 19 objects categories.

Chapter 7

Conclusion and Perspectives

In this chapter, we will summarize the contributions made in the present work and then enumerate possible directions for the future research.

7.1 Summary of the Work in this Dissertation

In this thesis, we have proposed a novel model as a way of graph-based image representation, namely *Bag-of-Bags of Words (BBoW)*, to incorporate both the appearance and spatial information under its description. Basically, *BBoW* is a bag of signatures, each of which is built on a subgraph in image. The construction of *BBoW* model is composed of four steps: 1) Local features extraction; 2) Image graph construction; 3) Irregular subgraphs generation; and 4) *BBoW* description. The *BBoW* description is a combination of a bag of signatures. Each signature is built on a subgraph in the image.

In the process of graph construction, we mainly adopted two approaches: 1) prominent keypoints; 2) dense sampling for graph nodes selection. We have also designed several objective functions to define the weights of edges in the image graph. These objective functions are related to either color information or texture features of graph nodes, and they may combine both of them as well, *i.e.* like joint color-texture descriptors. Furthermore, we formulated different types of edge-weight terms, then analysed their influences on the stability of image graph partitioning in the following step.

We then evaluated three graph partitioning methods: *Graph Cuts*, *Normalized Cuts* and kernel *k*-means to optimize multilevel weighted graph cuts (*KKM*), for irregular image partition in the third step. A criterion for measuring the stability of subgraphs has been defined. It has

7. CONCLUSION AND PERSPECTIVES

been shown that *KKM* approach achieved better result than the other two partitioning methods. This finding suggests that better graph partitioning strategy can improve the performance for the *BBoW* model.

In *BBoW* model, each subgraph is described by a *bag-of-visual-words* histogram as its signature. An image is thus represented by concatenating those signatures together with level weighted normalizations. For matching *BBoWs*, a crucial technique, called *bipartite subgraphs matching* was used. With this technique, the *BBoW* achieves spatial invariance in image representation.

In contrast to the state-of-the-art technique such as Fisher vector image representation [20, 21, 99] and spatially local coding [102] etc. that compete with SPM to give extensions of bag-of-words image representations to encode spatial layout, our model takes into account spatial constraints in the *image* space instead of *feature* space. Our approach incorporates color and limited spatial information into image representation for image retrieval.

Finally, we validated the *BBoW* model for a given task of image retrieval in three datasets (*SIVAL*, *PPMI*, *Caltech-101*) with a total of 13,044 images. The obtained results are encouraging, especially when the obtained partitions are stable across the images from the same category. The experiments on one of the most well-known benchmark *Caltech-101* demonstrate that applying kernel *k*-means to graph clustering process produces better image retrieval results, as compared with other graph partitioning methods such as Graph Cuts and Normalized Cuts for *BBoW* model. Moreover, this proposed method achieves comparable results and outperforms *SPM* in 19 object categories on the whole *Caltech-101* dataset.

To formally evaluate the performance of the model, we have introduced a new vector features: *partition precision*. It characterizes the quality of matching of each subgraph in the image graph. Scalar metrics could be induced from *partition precision*, but require a thorough study of their properties. We formalized the model, proposed the methodological chain for its construction in images, developed a comparison methodology for matching images by *BBoW* in a CBIR framework.

We have further extended the model to its pyramidal extension, where a *non-nested* multi-levels scheme of image partitions was proposed. The *irregular* partitions at each level are *independent* of those at other level(s). An image represented by a pyramid of fixed number of partitions is described by a *bottom-up reordered* collection of *BBoW* for all levels. The matching of these descriptions has been called *irregular pyramid matching* (IPM).

7.2 Future Work

As future work, we consider defining an information fusion scheme based on the “vertical” property across multiple resolutions of image graph partitions, and applying a multi-class classifier to the proposed *BBoW* model for image classification. Adding more discriminative texture features in *BBoW*, in addition to studying effective ways to embed texture information is another interesting direction. A comparison to state-of-the-art algorithms like *deep learning* [162, 163] would obviously be important to carry on in the future.

In summary, we plan to improve and extend our *BBoW* model mainly in the following four directions:

7.2.1 Objective Functions in Edges Weights

As discussed in Section 6.9 of Chapter 6, the stability of graph partitions is nevertheless not always ensured with the predefined functions for edge weights. To improve this stability, we plan to use other objective functions for edge weights in graph partitioning methods. We also aim to test other discriminative texture features, such as Local binary patterns (LBP) [48] and Multi-factal spectrum (MFS) [164, 165], then study different ways to combine color and texture features in edge weights.

7.2.2 Improving Segmentation Methods

The *BBoW* model can potentially adopt *any* automatic image segmentation methods combined with the *bag-of-words* model. With such extensions, many interesting options remain to be explored.

For example, in the context of Graph Cuts, we can adaptively change the regularization parameter λ , as justified in Candemir et al. [166]: using adaptive regularization parameters for the different parts of the image improves the segmentation result than using a single regularization parameter. The proposed method adjusts the effect of the regularization parameter using the probabilities of pixels being part of the boundary. Intuitively, it can produce better segmentation results than the original graph cut approach for the best λ .

7.2.3 Fusion across Graph Partitions

Agarwal et al. [19] proposed a multilevel local coding method called “hyperfeatures”, which are “features of (local sets of) features (from lower level)”. This approach is based

7. CONCLUSION AND PERSPECTIVES

on local histogram model encoding co-occurrence statistics within each local neighbourhood at multilevel. The level 0 (base level) contains bag of features (BoF) histograms, *i.e.* global histograms over quantized image descriptors. The higher level consists of local histograms generated by repeatedly aggregating local BoF histograms from previous lower level features. The codebook of hyperfeatures is learned from all features at the corresponding level during training.

In contrast, current implementation of *BBoW* model does *not* feed lower level features into the computational process of higher levels. At each resolution of the image partitions, subgraphs are built independently on single level basis. The BoW approach is next applied to individual resulting subgraphs independently as well. That is to say, the signatures (histograms) of (sub)graphs are *independent* of the resolutions of image partitions. Moreover, the codebook in *BBoW* is *independent* from any partitioning scheme. Inspired by “hyperfeatures”, we may as well build our “hyperfeatures” in *BBoW* by the fusion of features across graph partitions.

7.2.4 Applications of the *BBoW* Model

From a more fundamental point of view, there are some other aspects of the proposed model that we are interested in tackling in the future. First of all, we are interested to see how robust our model is against noisy data. Secondly, we intend to further develop statistical analysis of subgraphs in order to interpret these graph descriptors (subgraphs) and to study further their stability with respect to graph partitioning. Thirdly, many distance metrics and similarity functions can be applied to define similarity measures for comparing the images.

From an applicative point of view, we aim to validate the generality of this model on wide range of data sets for tasks of object image classification and scene classification. Another applicative foreseen work is to apply *BBoW* to images with large resolutions, as the graph descriptors can be more representative in terms of larger image space.

Appendix A

Experimental Results in *SIVAL*

Bag-of-Bags of Visual Word (BBoVW) versus Bag-of-Visual Words (BoVW) in *SIVAL* dataset

In this Appendix, we enumerate experimental results in *SIVAL* dataset. In Figure A.1, BoVW and BBoW are compared. Figure A.2 demonstrates the impact of different co-occurrence criteria (see Section 4.3.1) on the performance of image retrieval. More details can also be referred in Table A.1. At the end of the appendix, we list the category-based *Precision-Recall* curve for 25 categories in *SIVAL* dataset.

A. EXPERIMENTAL RESULTS IN *SIVAL*

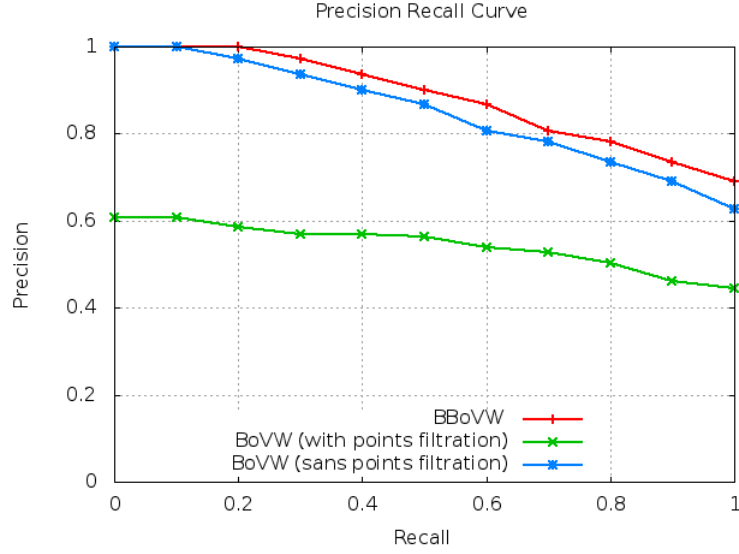


Figure A.1: The overall *Precision-Recall* curve for a comparison between BBoVW and BoVW in *SIVAL* dataset [10]. BBoVW: Bag-of-Bags of Visual Word. BoVW: Bag-of-Visual Words. Each image is composed of 4 subgraphs in BBoW. The dictionary of size 1000, as described in Section 6.2.1 of the Chapter 6, is learnt over 30 sample images per class using *k*-means. The query images are chosen from the rest of the *SIVAL* dataset for retrieval. In this figure, the red curve corresponds to application of co-occurrence measure defined in Equation (4.4) for image matching in the BBoW Model. The blue/red curve correspond to BoVW with/without points filtration.

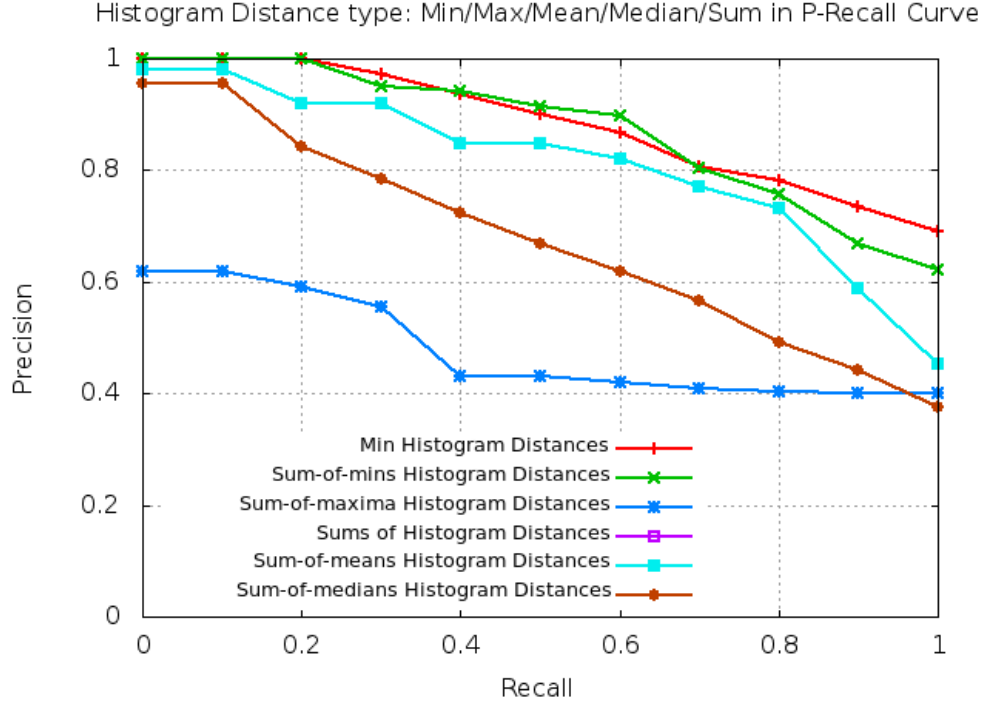
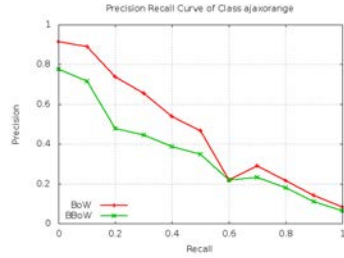


Figure A.2: A complete comparison of similarity measures by using co-occurrence criteria in BBoW, as defined in Section 4.3.1 of the Chapter 4. Each image is composed of 4 subgraphs. There are six curves in this figure: “Min Histogram Distances” with respect to Equation (4.4) (Curve 1), “Sum-of-mins Histogram Distances” with respect to Equation (4.5) (Curve 2), “Sum-of-maxima Histogram Distances” with respect to Equation (4.9) (Curve 3), “Sums of Histogram Distances” with respect to Equation (4.8) (Curve 4), “Sum-of-means Histogram Distances” with respect to Equation (4.6) (Curve 5), “Sum-of-medians Histogram Distances” with respect to Equation (4.7) (Curve 6). The Curve 4 and 5 are coincident.

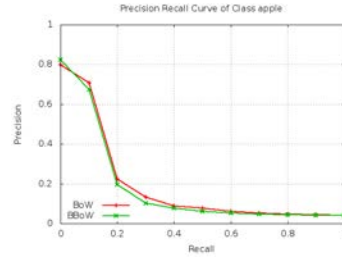
A. EXPERIMENTAL RESULTS IN SIVAL

Table A.1: The *precision-recall* values of experimental results, as complementary information of Figure A.2. The experiments were run in *SIVAL* dataset with the aim of comparing a series of similarity measures (co-occurrence criteria) versus the classical bag-of-words model for image retrieval. The first column lists **recall** values ranging from 0 to 1.0 of 11 intervals. The 2nd-8th columns correspond to the **precision** values for seven different measures. They are (1) Bag-of-Words (BoW), without filtering points in graph nodes selection; (2) BoW, select graph nodes by points filtration; (3) Bag-of-Bag-of-Visual-Words (BBoVW), using Equation (4.4); (4) BBoVW, using Equation (4.5); (5) BBoVW, using Equation (4.6) or its equivalent by using Equation (4.8); (6) BBoVW, using Equation (4.7); (7) BBoVW, using Equation (4.9) respectively.

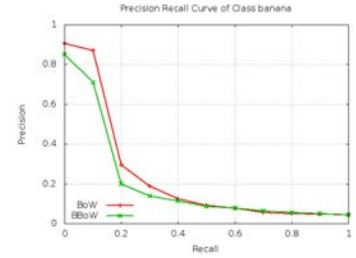
Recall	BoW (with points filtra- tion)	BoW (sans points filtra- tion)	BBoVW (min)	BBoVW (sum-of- min)	BBoVW (mean) (sum)	BBoVW (median)	BBoVW (max)
0	0.6077	1.0000	1.0000	1.0000	0.9794	0.9571	0.6180
0.1	0.6077	1.0000	1.0000	1.0000	0.9794	0.9571	0.6180
0.2	0.5854	0.9722	1.0000	1.0000	0.9198	0.8430	0.5914
0.3	0.5699	0.9356	0.9722	0.9500	0.9198	0.7832	0.5545
0.4	0.5699	0.9007	0.9356	0.9426	0.8489	0.7246	0.4319
0.5	0.5625	0.8667	0.9007	0.9136	0.8489	0.6687	0.4299
0.6	0.5393	0.8077	0.8667	0.8966	0.8217	0.6201	0.4193
0.7	0.5289	0.7815	0.8077	0.8039	0.7695	0.5659	0.4079
0.8	0.5039	0.7345	0.7815	0.7562	0.7330	0.4910	0.4026
0.9	0.4606	0.6910	0.7345	0.6690	0.5875	0.4421	0.4008
1.0	0.4441	0.6270	0.6910	0.6203	0.4543	0.3765	0.4008



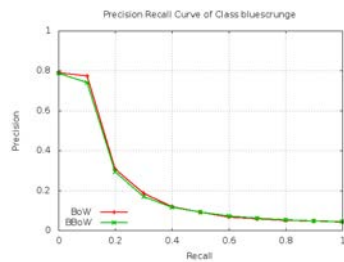
(1) “ajaxorange”



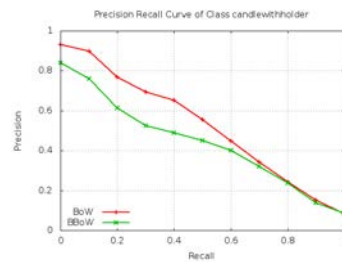
(2) “apple”



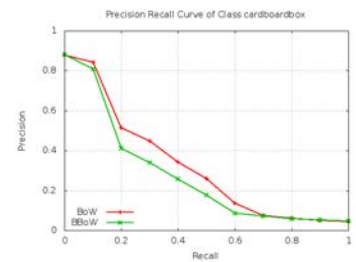
(3) “banana”



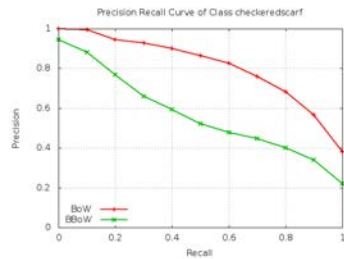
(4) “bluescrunge”



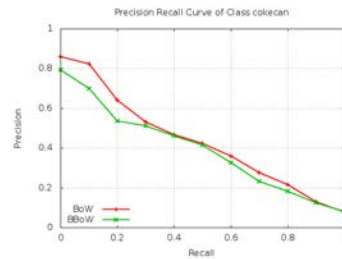
(5) “candlewithholder”



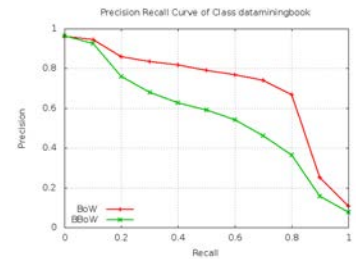
(6) “cardboardbox”



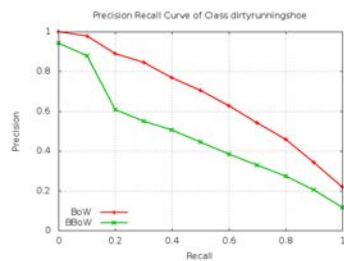
(7) “checkeredscarf”



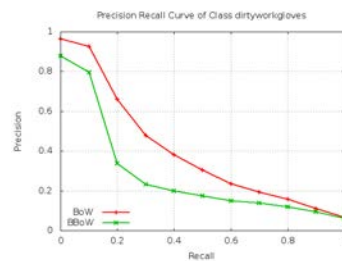
(8) “cokecan”



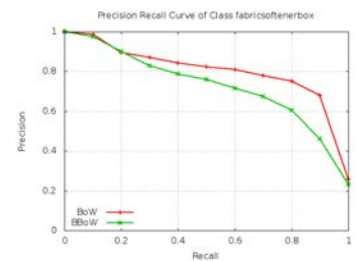
(9) “dataminingbook”



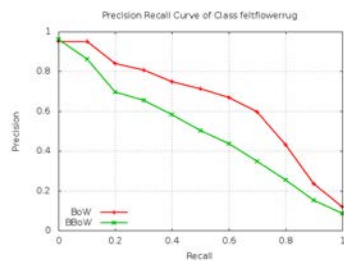
(10) “dirtyrunningshoe”



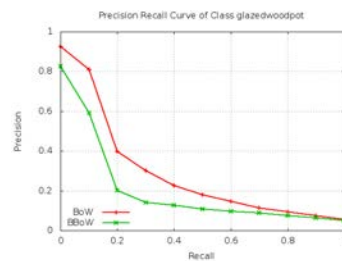
(11) “dirtyworkgloves”



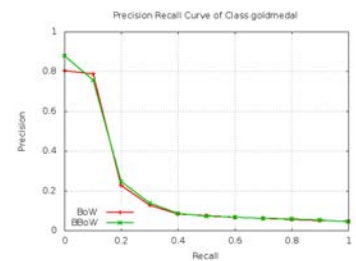
(12) “fabricsoftenerbox”



(13) “feltflowerrug”



(14) “glazedwoodpot”



(15) “goldmedal”

Figure is continued on next page

A. EXPERIMENTAL RESULTS IN SIVAL

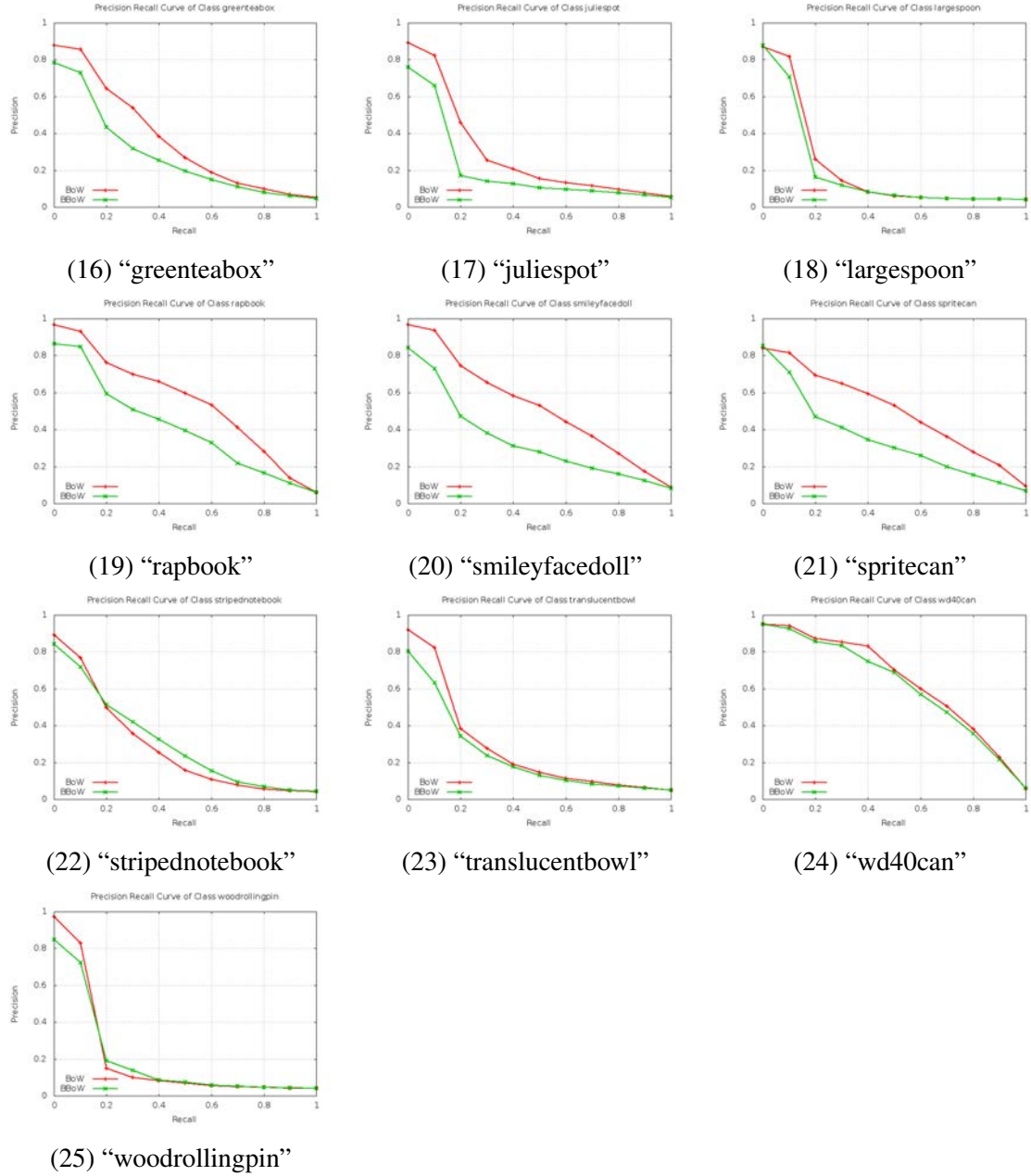


Figure A.3: The category-based *Precision-Recall* curve for 25 categories in SIVAL dataset.

Appendix B

Experimental Results in *Caltech-101*

Irregular partition versus regular partition (4 partitions) in *Caltech-101* dataset

In this Appendix, we enumerate experimental results in *Caltech-101* dataset [144]. Firstly, we provide a thorough comparison between BBoW via KKM and SPM at single level 1, *i.e.*, 4 partitions per image. The category-based *average precisions* (APs) and their corresponding *standard deviation* (Std) are given in Table B.1. Secondly, we list global retrieval performance of BBoW via KKM (see Table B.2), BBoW via Graph Cuts, BBoW via Normalized Cut, vs SPM (see Table B.3) in *Caltech-101* dataset. Thirdly, we give a case study in “*faces*” category, on five image samples: *face0032.jpg*, *face0036.jpg*, *face0038.jpg*, *face0039.jpg*, *face0049.jpg*. The retrieval result of these images can be referred in Table B.8, Table B.8, Table B.8, Table B.8 and Table B.8. The twenty high-ranking retrieved images are shown in Figure B.1, Figure B.2, Figure B.3, Figure B.4 and Figure B.5 respectively. The Figure B.6 at the end of the Appendix demonstrates the distribution of *average precision* values of image retrieval from 20 surpassing classes on the whole *Caltech-101* dataset, which corresponds to the comparison between SPM and BBoW (via KKM) in Figure 6.10 of Chapter 6.

B. EXPERIMENTAL RESULTS IN *CALTECH-101*

Table B.1: KKM versus SPM at single level 1 (4 partitions per image). Performance is measured by calculating the *mean Average Precision* (mAP) for category-based queries. In addition, the *mean of Standard deviation* (Std) of *Average Precisions* (APs) for category-based queries is given. The class names of 20 surpassing categories in which BBoW outperforms SPM are in bold in this table.

Category	KKM	SPM
accordion	0.385293 \pm 0.034851	0.207360 \pm 0.013254
airplanes	0.413404 \pm 0.022305	0.497083 \pm 0.017586
anchor	0.031988 \pm 0.000033	0.038990 \pm 0.017586
ant	0.032702 \pm 0.000024	0.038593 \pm 0.000160
barrel	0.038911 \pm 0.000252	0.048919 \pm 0.000331
bass	0.035115 \pm 0.000130	0.035672 \pm 0.000153
beaver	0.044052 \pm 0.000208	0.040120 \pm 0.000176
binocular	0.082245 \pm 0.003426	0.088818 \pm 0.002682
bonsai	0.056256 \pm 0.000536	0.081623 \pm 0.002495
brain	0.097014 \pm 0.002912	0.209377 \pm 0.010595
brontosaurus	0.038470 \pm 0.000132	0.043102 \pm 0.000624
buddha	0.038242 \pm 0.000293	0.062125 \pm 0.001258
butterfly	0.032844 \pm 0.000075	0.051467 \pm 0.001036
camera	0.079828 \pm 0.002130	0.083248 \pm 0.002157
cannon	0.040772 \pm 0.000158	0.043540 \pm 0.000154
car_side	0.936784 \pm 0.009839	0.502484 \pm 0.026168
ceiling_fan	0.033498 \pm 0.000116	0.046372 \pm 0.000839
cellphone	0.123537 \pm 0.005341	0.585297 \pm 0.047094
chair	0.028742 \pm 0.000030	0.038689 \pm 0.000184
chandelier	0.046490 \pm 0.000700	0.079150 \pm 0.002979
cougar_body	0.048053 \pm 0.000572	0.047543 \pm 0.000537
cougar_face	0.108225 \pm 0.004573	0.145203 \pm 0.007586
crab	0.045433 \pm 0.000216	0.050637 \pm 0.000217
crayfish	0.030563 \pm 0.000054	0.036594 \pm 0.000183
crocodile_head	0.069741 \pm 0.000469	0.058625 \pm 0.000183
crocodile	0.055612 \pm 0.000281	0.047820 \pm 0.000137
cup	0.031344 \pm 0.000090	0.043547 \pm 0.000423
dalmatian	0.080749 \pm 0.002716	0.057390 \pm 0.000782

Category	KKM	SPM
dollar_bill	0.155946 \pm 0.015800	0.257488 \pm 0.021435
dolphin	0.043022 \pm 0.000691	0.048055 \pm 0.000533
dragonfly	0.033162 \pm 0.000130	0.067029 \pm 0.002376
electric_guitar	0.027219 \pm 0.000052	0.034073 \pm 0.000333
elephant	0.046102 \pm 0.000169	0.068008 \pm 0.001012
emu	0.095289 \pm 0.001826	0.080677 \pm 0.000648
euphonium	0.077108 \pm 0.005508	0.143292 \pm 0.013213
ewer	0.028828 \pm 0.000059	0.050840 \pm 0.000547
faces_easy	0.466651 \pm 0.013404	0.792831 \pm 0.014526
faces	0.625172 \pm 0.024970	0.507579 \pm 0.011634
ferry	0.062891 \pm 0.000586	0.054964 \pm 0.000384
flamingo_head	0.053898 \pm 0.000817	0.048436 \pm 0.000405
flamingo	0.041907 \pm 0.000323	0.042201 \pm 0.000357
garfield	0.150050 \pm 0.014269	0.249209 \pm 0.032951
gerenuk	0.118079 \pm 0.002724	0.117126 \pm 0.002524
gramophone	0.036627 \pm 0.000292	0.057139 \pm 0.001890
grand_piano	0.101731 \pm 0.005926	0.256620 \pm 0.046962
hawksbill	0.099645 \pm 0.004240	0.089760 \pm 0.002817
headphone	0.070314 \pm 0.001214	0.071579 \pm 0.001249
hedgehog	0.073309 \pm 0.001101	0.066357 \pm 0.000632
helicopter	0.054875 \pm 0.000964	0.059860 \pm 0.000730
ibis	0.046930 \pm 0.000297	0.067726 \pm 0.000855
inline_skate	0.218006 \pm 0.022726	0.255739 \pm 0.039931
joshua_tree	0.112597 \pm 0.008576	0.069606 \pm 0.001067
kangaroo	0.076910 \pm 0.000999	0.084116 \pm 0.001101
ketch	0.074639 \pm 0.002689	0.125492 \pm 0.006056
lamp	0.025754 \pm 0.000025	0.036246 \pm 0.000239
laptop	0.050636 \pm 0.001054	0.094036 \pm 0.004868
leopards	0.193289 \pm 0.008734	0.505134 \pm 0.037995
llama	0.062376 \pm 0.000347	0.067072 \pm 0.000470

B. EXPERIMENTAL RESULTS IN *CALTECH-101*

Category	KKM	SPM
lobster	0.038376 \pm 0.000053	0.046944 \pm 0.000315
lotus	0.057295 \pm 0.001080	0.084398 \pm 0.003726
mandolin	0.034653 \pm 0.000181	0.051805 \pm 0.001065
mayfly	0.038675 \pm 0.000191	0.033540 \pm 0.000060
menorah	0.042762 \pm 0.000631	0.111245 \pm 0.011053
metronome	0.146016 \pm 0.017831	0.248172 \pm 0.035696
minaret	0.563488 \pm 0.065599	0.761386 \pm 0.036978
motorbikes	0.346897 \pm 0.029450	0.484363 \pm 0.024733
nautilus	0.044776 \pm 0.000464	0.058587 \pm 0.000915
octopus	0.061111 \pm 0.002890	0.065611 \pm 0.002946
okapi	0.067656 \pm 0.000787	0.072923 \pm 0.000662
pagoda	0.513619 \pm 0.036199	0.425830 \pm 0.041670
panda	0.053463 \pm 0.000800	0.090087 \pm 0.004122
pigeon	0.039460 \pm 0.000170	0.073331 \pm 0.004327
pizza	0.060974 \pm 0.000669	0.119683 \pm 0.003788
platypus	0.049821 \pm 0.000454	0.058274 \pm 0.001475
pyramid	0.037786 \pm 0.000275	0.047032 \pm 0.000553
revolver	0.041841 \pm 0.000527	0.139438 \pm 0.014844
rhino	0.053988 \pm 0.000427	0.070488 \pm 0.000643
rooster	0.038159 \pm 0.000067	0.070629 \pm 0.002187
saxophone	0.051035 \pm 0.000975	0.056405 \pm 0.002127
schooner	0.051375 \pm 0.000954	0.108890 \pm 0.004279
scissors	0.067095 \pm 0.001286	0.072949 \pm 0.002014
scorpion	0.048849 \pm 0.000461	0.054160 \pm 0.000542
sea_horse	0.052618 \pm 0.000627	0.045046 \pm 0.000303
snoopy	0.105323 \pm 0.003779	0.153791 \pm 0.007804
soccer_ball	0.066348 \pm 0.001613	0.167095 \pm 0.014295
stapler	0.071884 \pm 0.002658	0.176760 \pm 0.017047
starfish	0.057088 \pm 0.000645	0.078110 \pm 0.001997
stegosaurus	0.049275 \pm 0.000891	0.059037 \pm 0.001392
stop_sign	0.094728 \pm 0.007429	0.181281 \pm 0.028480
strawberry	0.054906 \pm 0.000795	0.075049 \pm 0.002515
sunflower	0.057008 \pm 0.000710	0.118955 \pm 0.007903

Category	KKM	SPM
tick	0.054855 \pm 0.000598	0.127073 \pm 0.010927
trilobite	0.402440 \pm 0.030194	0.320938 \pm 0.025972
umbrella	0.056691 \pm 0.001422	0.067263 \pm 0.003963
watch	0.063100 \pm 0.001088	0.208610 \pm 0.019351
water_lilly	0.052405 \pm 0.000660	0.067605 \pm 0.002194
wheelchair	0.050173 \pm 0.000360	0.090569 \pm 0.005537
wild_cat	0.042200 \pm 0.000045	0.046515 \pm 0.000066
windsor_chair	0.134152 \pm 0.013343	0.484939 \pm 0.050621
wrench	0.099297 \pm 0.003050	0.044359 \pm 0.000353
yin_yang	0.112368 \pm 0.007473	0.387628 \pm 0.070575

B. EXPERIMENTAL RESULTS IN *CALTECH-101*

Table B.2: Evaluation of BBoW via KKM in *Caltech-101* dataset. Retrieval performance was evaluated in *mean Average Precision* (mAP) on subset of *Caltech-101* dataset composed of 2945 query images and 5975 images from database for retrieval. The size of codebook is 400.

Level	BBoW via KKM	
	Single-level	Pyramid
0 (BoW)	0.1177	
1 (4 subgraphs)	0.1327	0.1468
2 (16 subgraphs)	0.1346	0.1487

Table B.3: Evaluation of BBoW (via GC) vs BBoW (via NCuts) vs SPM in *Caltech-101* dataset. Retrieval performance was evaluated in *mean Average Precision* (mAP) on subset of *Caltech-101* dataset composed of 2945 query images and 5975 images from database for retrieval. The size of codebook is 400. The highest results for each kind of level are shown in bold.

Level	GC	NCuts	SPM
0 (BoW)	0.1177	0.1177	0.1177
1 (4 subgraphs)	0.0988	0.1074	0.1440
2 (16 subgraphs)	0.1138	0.1252	0.1623
Pyramid (3 levels)	0.1220	0.1290	0.1571

Table B.4: Retrieval result of image *faces0032*. There are 5975 images from a subset of *Caltech-101* dataset for retrieval. Each image is partitioned into 4 subgraphs. The file extension of each image is omitted. The size of codebook is 400.

Rank	Query Image: <i>faces0032</i>	
	Retrieved Image	Similarity Score
0	<i>faces0032</i>	1.000000
1	<i>faces0036</i>	0.433973
2	<i>faces0041</i>	0.417084
3	<i>faces0030</i>	0.416204
4	<i>faces0019</i>	0.414498
5	<i>faces0049</i>	0.411848
6	<i>faces0037</i>	0.410790
7	<i>faces0031</i>	0.408819
8	<i>faces0024</i>	0.406523
9	<i>faces0052</i>	0.406178
10	<i>faces0039</i>	0.405109
11	<i>faces0022</i>	0.403870
12	<i>faces_easy0032</i>	0.402360
13	<i>faces0028</i>	0.401460
14	<i>faces0056</i>	0.401203
15	<i>faces0025</i>	0.397665
16	<i>faces0007</i>	0.393696
17	<i>faces0077</i>	0.391315
18	<i>faces0013</i>	0.391071
19	<i>faces0068</i>	0.390517
20	<i>faces0034</i>	0.389672

B. EXPERIMENTAL RESULTS IN *CALTECH-101*

Table B.5: Retrieval result of image *faces0036*. There are 5975 images from a subset of *Caltech-101* dataset for retrieval. Each image is partitioned into 4 subgraphs. The file extension of each image is omitted. The size of codebook is 400.

Rank	Query Image: <i>faces0036</i>	
	Retrieved Image	Similarity Score
0	<i>faces0036</i>	1.000000
1	<i>faces0028</i>	0.452821
2	<i>faces0037</i>	0.451399
3	<i>faces0019</i>	0.439082
4	<i>faces0030</i>	0.436981
5	<i>faces0024</i>	0.435277
6	<i>faces0032</i>	0.433973
7	<i>faces0039</i>	0.433855
8	<i>faces0035</i>	0.427126
9	<i>faces0041</i>	0.424875
10	<i>faces_easy0027</i>	0.415037
11	<i>faces_easy0036</i>	0.414607
12	<i>faces0013</i>	0.413940
13	<i>faces0060</i>	0.413052
14	<i>faces0001</i>	0.411890
15	<i>faces0052</i>	0.411418
16	<i>faces0025</i>	0.410744
17	<i>faces0007</i>	0.406628
18	<i>faces0005</i>	0.405569
19	<i>faces0049</i>	0.404169
20	<i>faces0038</i>	0.403834

Table B.6: Retrieval result of image *faces0038*. There are 5975 images from a subset of *Caltech-101* dataset for retrieval. Each image is partitioned into 4 subgraphs. The file extension of each image is omitted. The size of codebook is 400.

Rank	Query Image: <i>faces0038</i>	
	Retrieved Image	Similarity Score
0	<i>faces0038</i>	1.000000
1	<i>faces_easy0038</i>	0.431964
2	<i>faces0024</i>	0.409894
3	<i>faces_easy0039</i>	0.409855
4	<i>faces0001</i>	0.408111
5	<i>faces0035</i>	0.406003
6	<i>faces0036</i>	0.403834
7	<i>faces0072</i>	0.399052
8	<i>faces0037</i>	0.398655
9	<i>faces0028</i>	0.397389
10	<i>faces0060</i>	0.397364
11	<i>faces0019</i>	0.393373
12	<i>faces0058</i>	0.392206
13	<i>faces0041</i>	0.391568
14	<i>faces0031</i>	0.387039
15	<i>faces0076</i>	0.384997
16	<i>faces0039</i>	0.384812
17	<i>faces0073</i>	0.383936
18	<i>faces0023</i>	0.382831
19	<i>faces0029</i>	0.382656
20	<i>faces0069</i>	0.380980

B. EXPERIMENTAL RESULTS IN *CALTECH-101*

Table B.7: Retrieval result of image *faces0039*. There are 5975 images from a subset of *Caltech-101* dataset for retrieval. Each image is partitioned into 4 subgraphs. The file extension of each image is omitted. The size of codebook is 400.

Rank	Query Image: <i>faces0039</i>	
	Retrieved Image	Similarity Score
0	<i>faces0039</i>	1.000000
1	<i>faces_easy0039</i>	0.492047
2	<i>faces0037</i>	0.453770
3	<i>faces0036</i>	0.433855
4	<i>faces0024</i>	0.431958
5	<i>faces0031</i>	0.420975
6	<i>faces0041</i>	0.418923
7	<i>faces0025</i>	0.418823
8	<i>faces0035</i>	0.415585
9	<i>faces0001</i>	0.409270
10	<i>faces0030</i>	0.406591
11	<i>faces0032</i>	0.405109
12	<i>faces0052</i>	0.402744
13	<i>faces0028</i>	0.402086
14	<i>faces0022</i>	0.402020
15	<i>faces0044</i>	0.396445
16	<i>faces0040</i>	0.394949
17	<i>faces0012</i>	0.394629
18	<i>faces0019</i>	0.393024
19	<i>faces0006</i>	0.390893
20	<i>faces0013</i>	0.389758

Table B.8: Retrieval result of image *faces0049*. There are 5975 images from a subset of *Caltech-101* dataset for retrieval. Each image is partitioned into 4 subgraphs. The file extension of each image is omitted. The size of codebook is 400.

Rank	Query Image: <i>faces0049</i>	
	Retrieved Image	Similarity Score
0	<i>faces0049</i>	1.000000
1	<i>faces_easy0049</i>	0.491986
2	<i>faces0052</i>	0.485214
3	<i>faces0037</i>	0.464228
4	<i>faces0068</i>	0.447968
5	<i>faces0058</i>	0.441230
6	<i>faces0024</i>	0.438325
7	<i>faces0048</i>	0.437363
8	<i>faces0019</i>	0.436970
9	<i>faces0006</i>	0.436073
10	<i>faces0034</i>	0.432234
11	<i>faces0030</i>	0.423637
12	<i>faces0031</i>	0.420341
13	<i>faces0005</i>	0.416484
14	<i>faces0080</i>	0.415709
15	<i>faces0032</i>	0.411848
16	<i>faces0059</i>	0.411334
17	<i>faces0012</i>	0.408574
18	<i>faces0007</i>	0.408158
19	<i>faces0044</i>	0.406146
20	<i>faces0013</i>	0.405245

B. EXPERIMENTAL RESULTS IN CALTECH-101

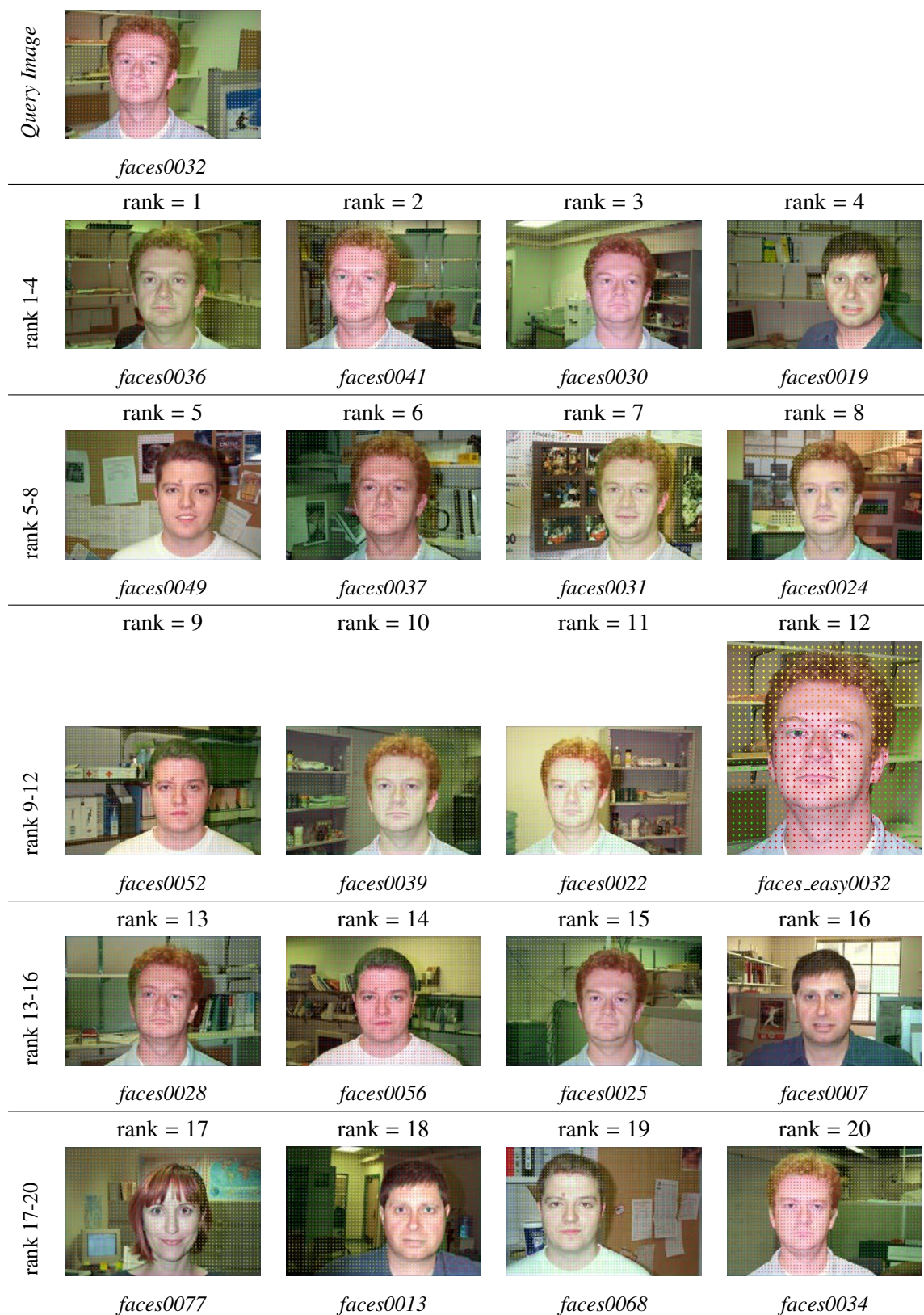


Figure B.1: Retrieval results of image “*faces0032*”. This figure is better viewed in *color*.












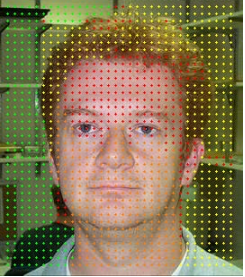






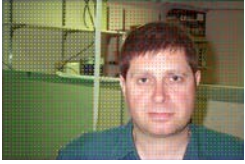


<i>Query Image</i>				
				
	<i>faces0036</i>			
rank 1-4	rank = 1	rank = 2	rank = 3	rank = 4
				
	<i>faces0028</i>	<i>faces0037</i>	<i>faces0019</i>	<i>faces0030</i>
	rank = 5	rank = 6	rank = 7	rank = 8
rank 5-8				
	<i>faces0024</i>	<i>faces0032</i>	<i>faces0039</i>	<i>faces0035</i>
	rank = 9	rank = 10	rank = 11	rank = 12
rank 9-12				
	<i>faces0041</i>	<i>faces_easy0027</i>	<i>faces_easy0036</i>	<i>faces0013</i>
	rank = 13	rank = 14	rank = 15	rank = 16
rank 13-16				
	<i>faces0060</i>	<i>faces0001</i>	<i>faces0052</i>	<i>faces0025</i>
	rank = 17	rank = 18	rank = 19	rank = 20
rank 17-20				
	<i>faces0007</i>	<i>faces0005</i>	<i>faces0049</i>	<i>faces0038</i>

Figure B.2: Retrieval results of image “*faces0036*”. This figure is better viewed in *color*.

B. EXPERIMENTAL RESULTS IN CALTECH-101

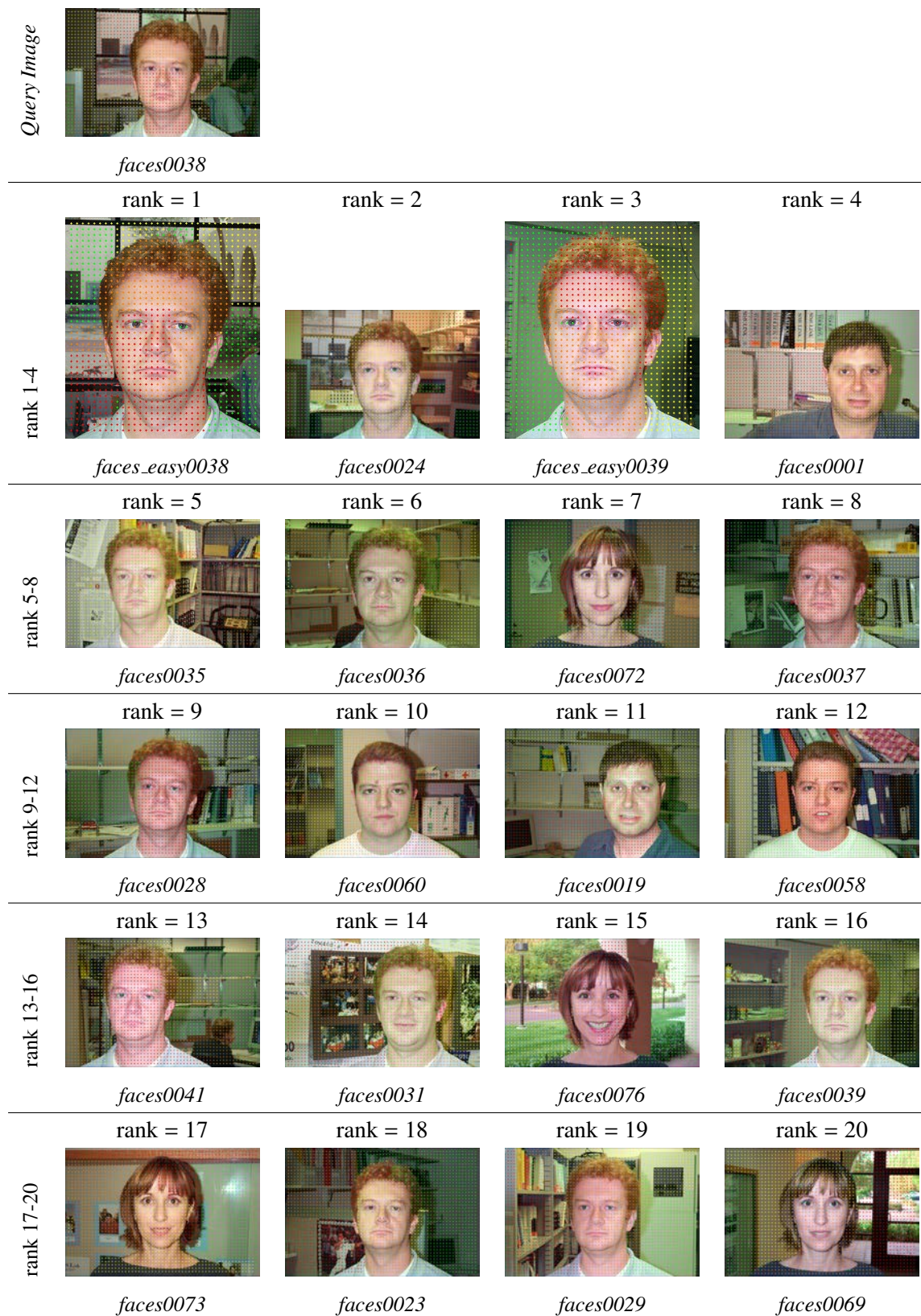


Figure B.3: Retrieval results of image “*faces0038*”. This figure is better viewed in *color*.


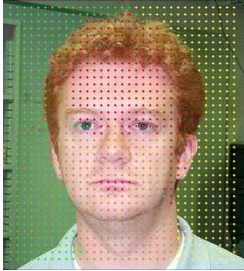



















<i>Query Image</i>				
				
	<i>faces0039</i>			
rank 1-4	rank = 1	rank = 2	rank = 3	rank = 4
				
	<i>faces_easy0039</i>	<i>faces0037</i>	<i>faces0036</i>	<i>faces0024</i>
	rank = 5	rank = 6	rank = 7	rank = 8
rank 5-8				
	<i>faces0031</i>	<i>faces0041</i>	<i>faces0025</i>	<i>faces0035</i>
	rank = 9	rank = 10	rank = 11	rank = 12
				
rank 9-12	<i>faces0001</i>	<i>faces0030</i>	<i>faces0032</i>	<i>faces0052</i>
	rank = 13	rank = 14	rank = 15	rank = 16
				
	<i>faces0028</i>	<i>faces0022</i>	<i>faces0044</i>	<i>faces0040</i>
rank 13-16	rank = 17	rank = 18	rank = 19	rank = 20
				
	<i>faces0012</i>	<i>faces0019</i>	<i>faces0006</i>	<i>faces0013</i>
rank 17-20				

Figure B.4: Retrieval results of image “*faces0039*”. This figure is better viewed in *color*.

B. EXPERIMENTAL RESULTS IN CALTECH-101

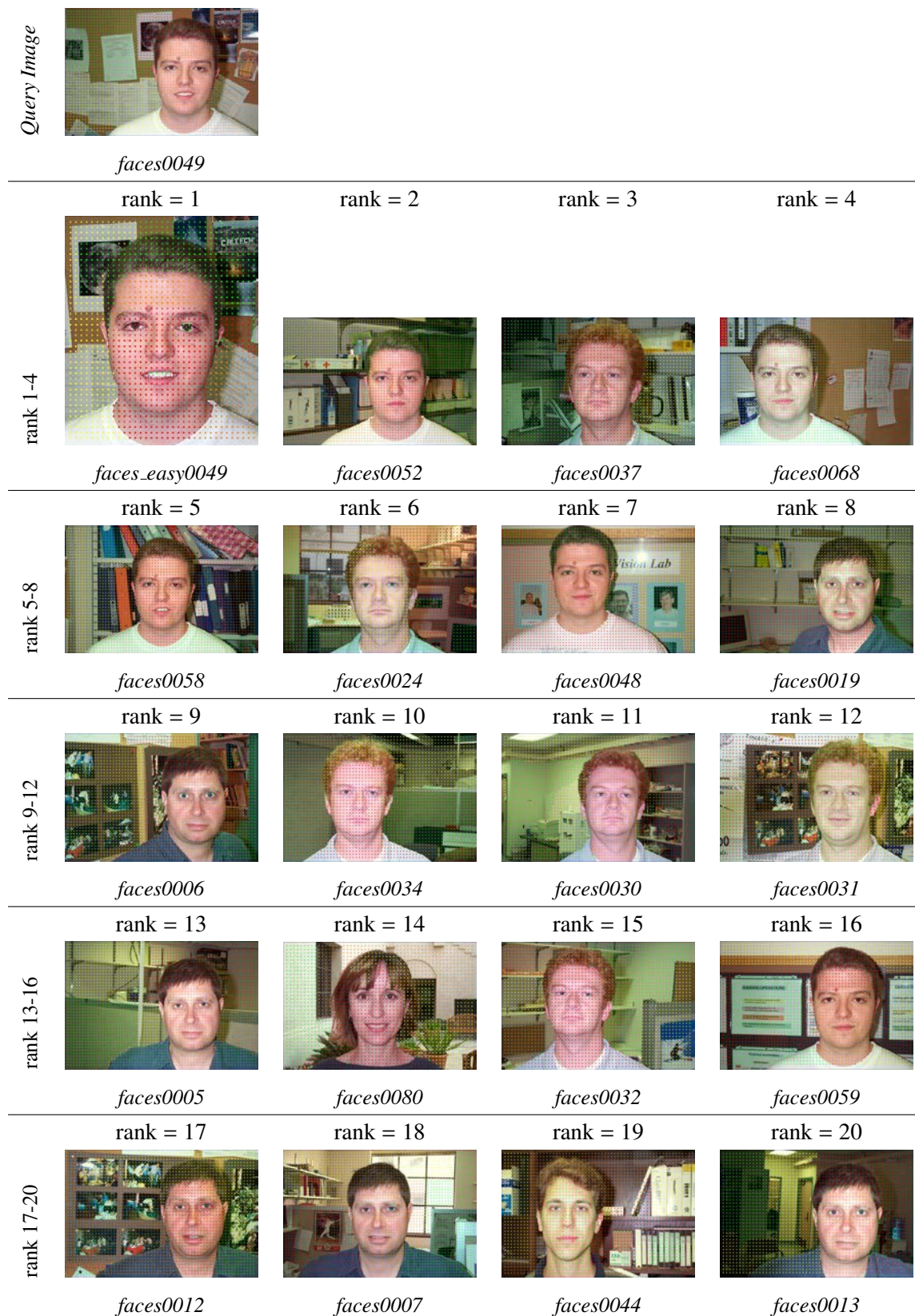
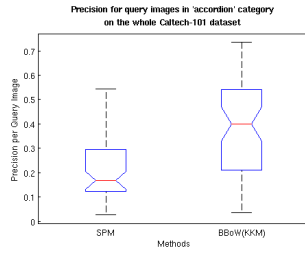
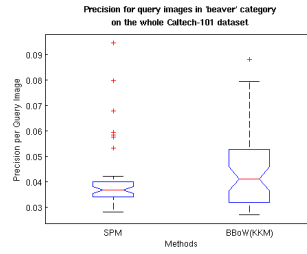


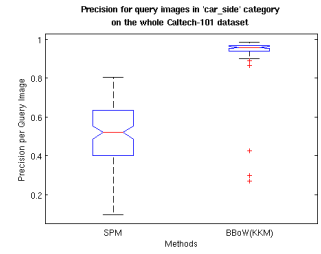
Figure B.5: Retrieval results of image “*faces0049*”. This figure is better viewed in *color*.



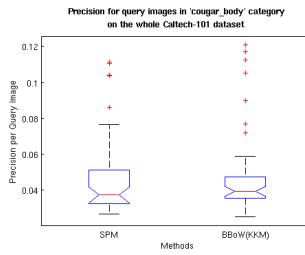
(1) “accordion”



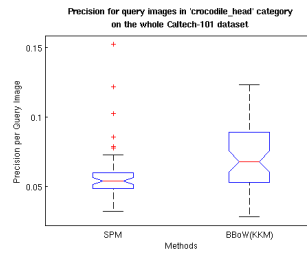
(2) “beaver”



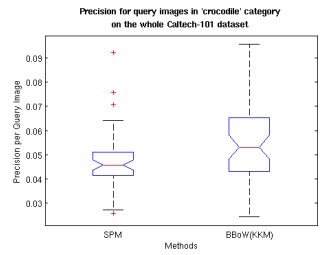
(3) “car_side”



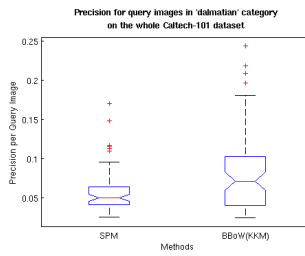
(4) “cougar_body”



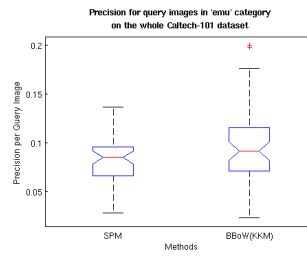
(5) “crocodile_head”



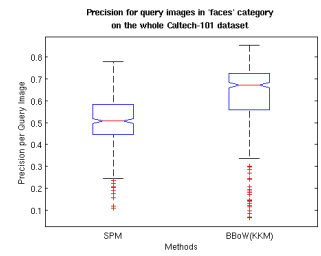
(6) “crocodile”



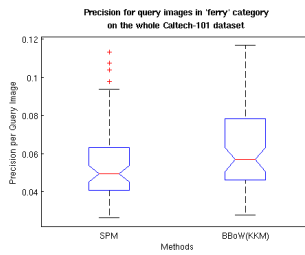
(7) “dalmatian”



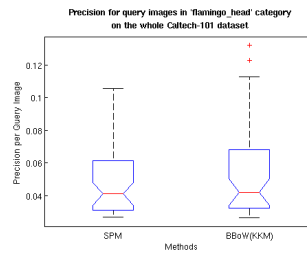
(8) “emu”



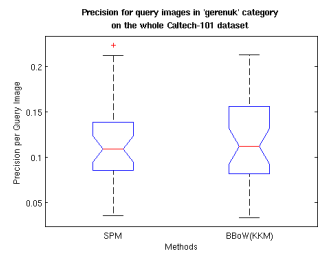
(9) “faces”



(10) “ferry”



(11) “flamingo_head”



(12) “gerenuk”

Figure is continued on next page

B. EXPERIMENTAL RESULTS IN *CALTECH-101*

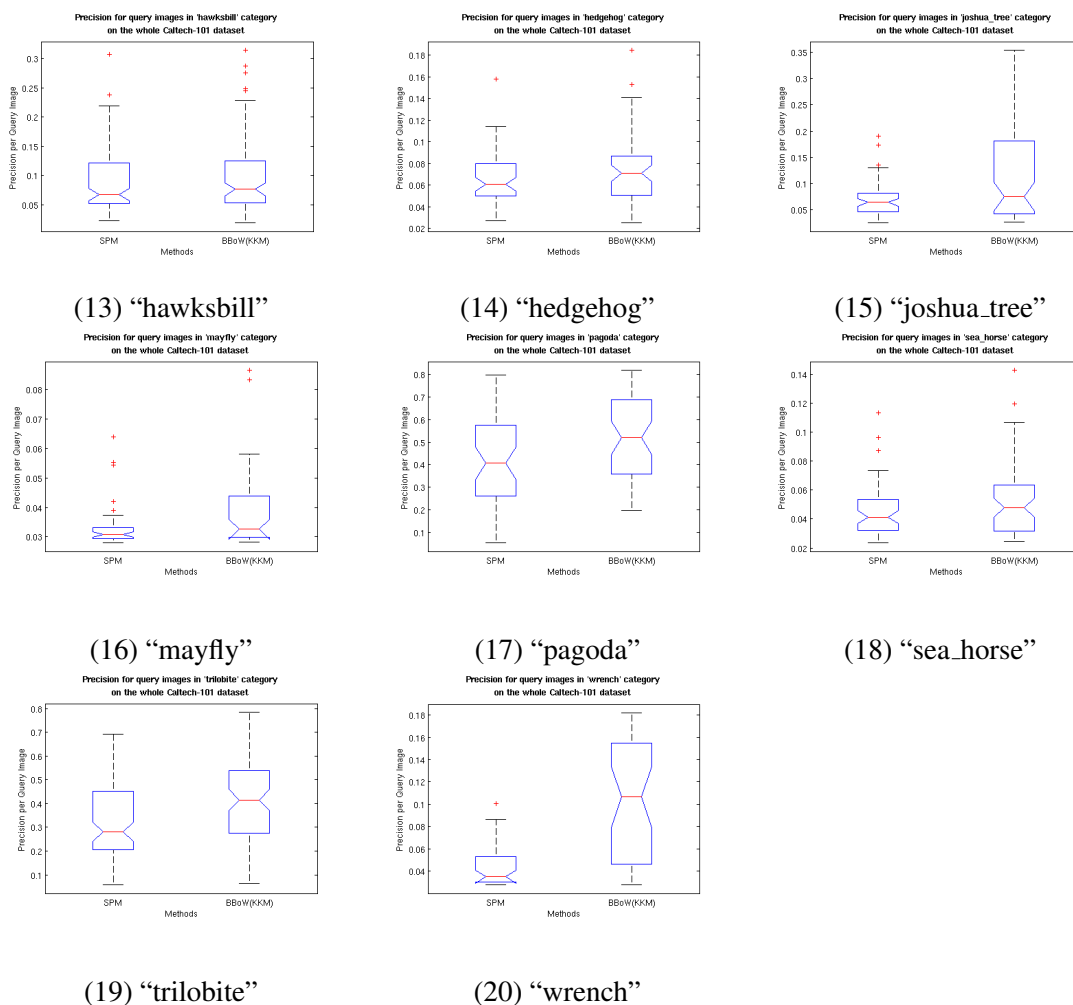


Figure B.6: The distribution of *average precision* values for query images in 19 surpassing classes + a category "car_side" that only contains grayscale images, on the whole *Caltech-101* dataset. The comparison is evaluated between SPM and BBoW (KKM) at level 1. Each image is partitioned into 4 subgraphs.

Appendix C

Experimental Results in *PPMI*

BBoVW versus SPM in 12 binary category of *PPMI*

In *PPMI* dataset [158, 159], we have used two different distance metrics: $L1$ distance or $L2$ distance, as the measure to compute the cost matrix value (see Equation (4.10)) for (sub)graphs matching via *Hungarian algorithm*.

In this Appendix, we are interested in the influence of these two metrics on image retrieval in BBoW model. We also present the performance of SPM [4] as a side-by-side comparison. The impact of $L1$ and $L2$ metrics on performance of image retrieval is investigated in Table C.1 and Table C.2.

C. EXPERIMENTAL RESULTS IN *PPMI*

Table C.1: The retrieval performance (mAP) on *PPMI* dataset, using *L1* distance as cost matrix value for graph matching via *Hungarian algorithm*.

Category	BBoW Single Level 1	BBoW Single Level 2	BBoW Pyramid Level 1	BBoW Pyramid Level 2	SPM Pyramid Level 2
bassoon	0.111035	0.113260	0.109303	0.110617	0.135067
cello	0.119489	0.112404	0.115846	0.115524	0.126036
clarinet	0.116817	0.110903	0.117761	0.116395	0.114140
erhu	0.106178	0.102879	0.107562	0.106756	0.129702
flute	0.107483	0.106279	0.109405	0.109117	0.110948
frenchhorn	0.106507	0.113634	0.107040	0.108762	0.129498
guitar	0.132001	0.123785	0.139362	0.136860	0.143438
harp	0.116316	0.121244	0.125459	0.125616	0.161372
recorder	0.124170	0.114372	0.126650	0.125308	0.116781
saxophone	0.103004	0.109306	0.099857	0.101788	0.108571
trumpet	0.114199	0.112452	0.114173	0.114380	0.109890
violin	0.104072	0.110334	0.102756	0.104535	0.105030

Table C.2: The retrieval performance (mAP) on *PPMI* dataset, using *L2* distance as cost matrix value for graph matching *Hungarian algorithm*.

Category	BBoW Single Level 1	BBoW Single Level 2	BBoW Pyramid Level 1	BBoW Pyramid Level 2	SPM Pyramid Level 2
bassoon	0.110804	0.111185	0.109103	0.110027	0.135067
cello	0.119039	0.111707	0.115819	0.115575	0.126036
clarinet	0.114322	0.109811	0.116659	0.115271	0.114140
erhu	0.105380	0.102210	0.107372	0.106662	0.129702
flute	0.107309	0.106516	0.109183	0.108834	0.110948
frenchhorn	0.106298	0.111488	0.107063	0.108518	0.129498
guitar	0.128309	0.121247	0.137139	0.134486	0.143438
harp	0.115931	0.122908	0.125046	0.125451	0.161372
recorder	0.121758	0.113676	0.125542	0.124338	0.116781
saxophone	0.102728	0.108641	0.099691	0.101784	0.108571
trumpet	0.111228	0.111266	0.112511	0.113247	0.109890
violin	0.103785	0.109715	0.102760	0.104304	0.105030

C. EXPERIMENTAL RESULTS IN *PPMI*

Appendix D

Proofs

Claim A:

Given two *L1 normalized* histograms $G = \{g_1, \dots, g_B\}$ and $H = \{h_1, \dots, h_B\}$ with B bins, *i.e.* $\sum_{b=1}^B g_b = 1$, $\sum_{b=1}^B h_b = 1$ and $\forall b \in [1, B]$, $g_b \geq 0$, $h_b \geq 0$, we have:

Histogram intersection Equation (4.2) in Chapter 4

$$K_{\cap}(G, H) = \sum_{b=1}^B \min(g_b, h_b) ,$$

is the equivalent of the Equation (4.3) in Chapter 4

$$K_{\cap}(G, H) = \frac{1}{2} \sum_{b=1}^B (g_b + h_b - |g_b - h_b|) .$$

Proof :

Case 1: if $g_b \geq h_b$, $b \in [1, B]$, then

$$\begin{aligned} \frac{1}{2} (g_b + h_b - |g_b - h_b|) &= \frac{1}{2} (g_b + h_b - g_b + h_b) \\ &= \frac{1}{2} (2h_b) \\ &= h_b \\ &= \min(g_b, h_b) . \end{aligned}$$

D. PROOFS

Case 2: if $g_b < h_b$, $b \in [1, B]$, then

$$\begin{aligned} \frac{1}{2}(g_b + h_b - |g_b - h_b|) &= \frac{1}{2}(g_b + h_b - h_b + g_b) \\ &= \frac{1}{2}(2g_b) \\ &= g_b \\ &= \min(g_b, h_b) . \end{aligned}$$

and the claim is proven. □

Claim B:

Histogram Intersection is equivalent to the use of the sum of absolute differences or city-block metric, *i.e.* L_1 distance.

Proof :

Given two $L1$ normalized histograms $G = \{g_1, \dots, g_B\}$ and $H = \{h_1, \dots, h_B\}$ with B bins, *i.e.* $\sum_{b=1}^B g_b = 1$, $\sum_{b=1}^B h_b = 1$ and $\forall b \in [1, B]$, $g_b \geq 0$, $h_b \geq 0$, as proven in Claim A, the histogram intersection between G and H :

$$\begin{aligned} K_{\cap}(G, H) &= \sum_{b=1}^B \min(g_b, h_b) \\ &= \frac{1}{2} \sum_{b=1}^B (g_b + h_b - |g_b - h_b|) . \end{aligned}$$

Hence, we have:

$$\begin{aligned} K_{\cap}(G, H) &= \frac{1}{2} \left(\sum_{b=1}^B g_b + \sum_{b=1}^B h_b - \sum_{b=1}^B |g_b - h_b| \right) \\ &= \frac{1}{2} \left(1 + 1 - \sum_{b=1}^B |g_b - h_b| \right) \\ &= 1 - \frac{1}{2} \sum_{b=1}^B |g_b - h_b| \\ &= 1 - \frac{1}{2} D_{L_1}(G, H) . \end{aligned}$$

and the claim is proven. □

Appendix E

Statistical Test

E.1 Paired samples t -interval

We trust that the samples we take are random. Instead of taking **independent** samples, we choose pair of samples, and we try to make the pair of samples as homogeneous as possible. In ideal case, test on samples themselves.

E.2 Matched Paired t -test

We have two observations on each query image. So here we have dependant samples, and methods based on independent samples would not be appropriate here. We are going to use the paired difference procedure to analyse this data. To do so we first take the differences within each pair. We would end up with these n_d differences, where n_d is the number of query image from the same category, for example, ‘faces’ class in *Caltech-101*. Then, these n_d differences represent as single sample so that we can use one sample t -test to analyse these differences.

We denote \bar{x}_d as the mean of the differences for sample, μ_d as the mean of the differences for population, the standard deviation of those differences of the samples is S_d ; the standard deviation of those differences for population is σ_d ; degree of freedom $df = n_d - 1$. We denote the Confidence Interval as CI .

Let us examine these differences (either in box plot or in histogram) to make sure they are nearly normal distribution.

We compute the mean of the differences between our observed sample from two methods (KKM vs SPM). We want to know if there is a significant difference between two methods on

E. STATISTICAL TEST

those query images.

We investigate that by carrying out a one sample t -test, and we also construct a confidence interval at confidence coefficient 95%.

E.2.1 Data preparation

Conditions to satisfy:

1. **Pair data assumption:** The sample data being tested by two methods SPM and BBoW are **not** independent. So we can not use two-sample t -test because they fail to sample *independence* conditions. We have a good reason to pair the data, as each pair of average precision values are related to the *same* query image. Hence, the data are paired by subject.
2. **Random conditions:** The subject (images) were not chosen randomly (*i.e.* images from intra-class), so we will have to assume these results are representative.
3. **Nearly normal:** The distribution (see histogram/box plots) of differences is uni-model and symmetric.

E.3 Matched Paired t -test and interval

Question: What is the magnitude of the difference for image from ‘faces’ category in performance of image retrieval between SPM and BBoW (via KKM) individuals?

Step 1: **Hypothesis**

H_0 : BBoW (KKM) does *not* improve the performance of image retrieval $\mu_d = 0$

H_1 BBoW (KKM) *does improve* the performance of image retrieval $\mu_d > 0$ (right tailed t -test)

Step 2: **Compute test statistic**

$$\begin{aligned} S_d &= \sqrt{\frac{\sum x_d^2 - \frac{(\sum x_d)^2}{n_d}}{n_d - 1}} \\ &= \sqrt{\frac{\sum x_d^2 - n_d(\bar{x}_d)^2}{n_d - 1}}. \end{aligned} \quad (E.1)$$

$$t = \frac{\bar{x}_d}{\left(S_d / \sqrt{n_d}\right)} \quad (\text{E.2})$$

Step 3: **Rejection region (R.R)**

get critical value $t_{\alpha/2}$ ($\alpha = 0.05$), compare t and $t_{\alpha/2}$.

Step 4: **Decision**

If the test statistic fall into R.R, then reject H_0 , else fail to reject H_0 .

Step 5: **Confidence Interval**

95% Confidence Interval (C.I), $\Rightarrow \alpha = 1 - 0.95 = 0.05 \Rightarrow \alpha/2 = 0.025$

compute point estimate \pm margin of error:

$$\bar{x}_d \pm t_{\frac{\alpha}{2}} \frac{S_d}{\sqrt{n_d}} \quad (\text{E.3})$$

Conclusion: We are 95% confidence that BBoW (KKM) *does improve* the performance of image retrieval between $\bar{x}_d - t_{\frac{\alpha}{2}} \frac{S_d}{\sqrt{n_d}}$ and $\bar{x}_d + t_{\frac{\alpha}{2}} \frac{S_d}{\sqrt{n_d}}$.

If p -value is small $<< \alpha$, we reject (fail to reject) the null hypothesis. There is strong (\neq) evidence that BBoW can improve the image retrieval performance than SPM in the specific category.

E.4 Measurement in theory

E.4.1 The limits of data in research

Due to time and cost, we almost always use sample data to represent the large population. But sample data is always (at best) an estimate or approximation of the large population from which it is selected.

E.4.2 Sample size

As our sample size n becomes small, we are less certain that it is representative of our entire population; there is greater risk of error. Hopefully it is intuitive that the larger our sample size, the more confident we are - that it is representative of the entire population.

In a large sample, we are likely to capture the natural variation and diversity in the population data. A small sample increases the chance that we either miss that variation or over-emphasize it. However, sample size, in most cases, does adhere to the “Law of Diminishing

E. STATISTICAL TEST

Returns”. There is a point when increasing the sample size offers no more statistical benefits, which is good because it makes research more “doable”.

E.4.3 Data preparation

Is My Data Normal? Why? Many statistical techniques assume the data fits a normal distribution. How could we tell if the data fits this shape: The normal standard curve. Does our data have “goodness of fit” relative to the normal distribution? Tools to visualize data:

1. Histograms: the frequency of values over certain intervals is called “bins”; bar width. Histogram can be misleading. The look of a histogram is largely dependent on the “bins” size; the space between the tick marks.
2. Box Plots (Box and Whisker Plots) : Box plots display variation in samples of a statistical population without making any assumptions of the underlying statistical distribution: box plots are non-parametric. The spacings between the different parts of the box indicate the degree of dispersion (spread) and skewness in the data, and show outliers.
3. Stem and Leaf Plots
4. P-P Plots
5. Q-Q Plots

Degrees of freedom Degrees of freedom is one of the most difficult things to explain in statistics. My explanation: Degrees of freedom is an adjustment to the sample size ($n - 1$) or in other areas of state ($n - 2$) or more. It is linked to the idea that we are estimating something about a larger population; often a population with variance/standard deviation is unknown. Since we do not know the population variance and standard deviation, we have to use our sample variance and standard deviation. So the degrees of freedom is a way of adjusting that estimations. What it does, in practice, is that it gives a slightly larger margin of error or “wiggle room” in our estimates. Other than that, just roll with it; it is a statistical adjustment.

E.4.4 The t distribution

When our sample size is $n \leq 30$ and/or we do *not* know the variance/standard deviation of the population, we use the t -distribution instead of the z -distribution (standard normal distribution).

The t -distribution allows us to use small samples; $n \leq 30$. But to do so we sacrifice some certainty in our calculations; margin-of-error trade-off. It is dynamic, it takes sample size into account using $n - 1$ degree of freedom; there is a different t -distribution for any given sample size. The bell curve shape is down (“squished”) in the middle and “fatter” on the end (tails); squishier and fatter the sample size.

However, as $n > 30$ and definitely by $n \geq 100$, the t -distribution and standard normal z -distribution become indistinguishable. They converge. i.e., when the sample size goes above 30, the t distribution and z distribution converges. Hence, t -distribution is more useful as sample size is below 30.

Conditions for using t -test

1. The population standard deviation is unknown
2. The sample size is less than 30

Sample size does not matter for t -Test. If the sample is less than 30, we should always do t -test and not Z -Scores. However the reverse is not true. You can still do t -Test even if the sample size is greater than 30. Main reason to do t -tests are when you do not know the population statistics like mean, standard deviation (SD) and they have to be estimated from the sample. Whereas in z -Scores, you need to know the population mean and SD.

E.4.5 p -value method

Traditional methods use something called critical values, z **score**, p -value method does not use them at all.

E.4.5.1 Basic of Hypothesis Testing

Null Hypothesis H_0 :

E. STATISTICAL TEST

$$P = \#$$

$$\mu = \#$$

$$\sigma = \#$$

Alter. Hypothesis H_1 :

$$P < \#$$

$$\mu > \#$$

$$\sigma \neq \#$$

left-tailed: $H_1 :<$

right-tailed: $H_1 :>$

two-tailed: $H_1 \neq$

The p -value is a measure of the strength of the evidence against the null hypothesis. The p -value is the probability of getting the observed value of the test statistic, or a value with even greater evidence against H_0 , if the null hypothesis is actually true. The smaller the p -value, the greater the evidence against the null hypothesis.

E.4.5.2 Level of significance

Conventionally, $\alpha = 0.01, \alpha = 0.05, \alpha = 0.10$.

1. If we have a given significance level α , then reject H_0 if $p\text{-value} \leq \alpha$ (cut-off for significance).
2. If we do not have a given significance level, then it is not as cut-and-dried. Check the distribution of p -value if H_0 is true.

E.4.5.3 A very rough guideline

1. $p\text{-value} < 0.01$, very strong evidence against H_0 .
2. $0.01 < p\text{-value} < 0.05$, strong evidence against H_0 .
3. $0.05 < p\text{-value} < 0.10$, some weak evidence against H_0 .
4. $p\text{-value} > 0.10$, little or no evidence against H_0 .

E.4.5.4 Summary

1. If the P -value is low, the null must go (reject H_0).
2. If the P -value is high, the null must fly (fail to reject H_0 , keep H_0).

E. STATISTICAL TEST

References

- [1] OTÁVIO AUGUSTO BIZETTO PENATTI, EDUARDO VALLE, AND RICARDO DA SILVA TORRES. **Comparative study of global color and texture descriptors for web image retrieval.** *Journal of Visual Communication and Image Representation*, **23**(2):359–380, 2012. iii, 7
- [2] DAVID G. LOWE. **Distinctive image features from scale-invariant keypoints.** In *International Journal of Computer Vision*, pages 91–110, 2004. iii, 6, 8, 19, 20, 31, 72, 73, 94, 95
- [3] RITENDRA DATTA, DHIRAJ JOSHI, JIA LI, AND JAMES ZE WANG. **Image retrieval: Ideas, influences, and trends of the new age.** *ACM Computing Surveys*, **40**(2), April 2008. iii, 1, 17, 18
- [4] SVETLANA LAZEBNIK, CORDELIA SCHMID, AND JEAN PONCE. **Beyond bags of features: Spatial pyramid matching for recognizing natural scene categories.** In *Computer Vision and Pattern Recognition, 2006 IEEE Computer Society Conference on*, **2**, pages 2169–2178, 2006. iv, 2, 3, 22, 32, 83, 85, 87, 88, 95, 107, 113, 147
- [5] JIANBO SHI AND JITENDRA MALIK. **Normalized Cuts and image segmentation.** *IEEE Transactions on Pattern Analysis and Machine Intelligence*, **22**(8):888–905, 2000. iv, 23, 34, 47, 48, 49, 51
- [6] GREG MORI, XIAOFENG REN, ALEXEI A. EFROS, AND JITENDRA MALIK. **Recovering human body configurations: combining segmentation and recognition.** In *IEEE Computer Society Conference on Computer Vision and Pattern Recognition*, **2**, pages 326–333, 2004. iv, 23
- [7] SVEBOR KARAMAN. *Indexation de la vidéo portée : application à l'étude épidémiologique des maladies liées à l'âge.* PhD thesis, Université Bordeaux 1, 2011. iv, 27, 28
- [8] YURI BOYKOV AND VLADIMIR KOLMOGOROV. **An experimental comparison of min-Cut/max-Flow algorithms for energy minimization in vision.** *IEEE Transactions on Pattern Analysis and Machine Intelligence*, **26**(9):1124–1137, 2004. v, 39, 40, 42, 47, 74, 94
- [9] YURI BOYKOV, OLGA VEKSLER, AND RAMIN ZABIH. **Fast approximate energy minimization via Graph Cuts.** *IEEE Transactions on Pattern Analysis and Machine Intelligence*, **23**(11):1222–1239, 2001. v, 39, 42, 43, 47, 94
- [10] ROUHOLLAH RAHMANI, SALLY A. GOLDMAN, HUI ZHANG, JOHN KRETTEK, AND JASON E. FRITTS. **Localized content based image retrieval.** In *Multimedia Information Retrieval*, pages 227–236. ACM, 2005. v, ix, 46, 91, 124

REFERENCES

- [11] INDERJIT S. DHILLON, YUQIANG GUAN, AND BRIAN KULIS. **A fast kernel-based multilevel algorithm for graph clustering.** In *International Conference on Knowledge Discovery and Data Mining*, pages 629–634. ACM, 2005. v, 55, 56
- [12] GEORGE KARYPIS AND VIPIN KUMAR. **Multilevel k-way partitioning scheme for irregular graphs.** *Journal of Parallel and Distributed Computing*, **48**(1):96129, 1998. v, 56, 74
- [13] BASTIAN LEIBE, ALES LEONARDIS, AND BERNT SCHIELE. **Combined object categorization and segmentation with an implicit shape model.** In *ECCV workshop on statistical learning in computer vision*, 2004. xviii, 2, 24
- [14] ARNOLD W. M. SMEULDERS, MARCEL WORRING, SIMONE SANTINI, AMARNATH GUPTA, AND RAMESH JAIN. **Content-based image retrieval at the end of the early years.** *IEEE Transactions on Pattern Analysis and Machine Intelligence*, **22**(12):1349–1380, 2000. 1, 17
- [15] RITENDRA DATTA, JIA LI, AND JAMES ZE WANG. **Content-based image retrieval: approaches and trends of the new age.** In *Multimedia Information Retrieval*, pages 253–262, 2005. 1, 17
- [16] J. SIVIC AND A. ZISSERMAN. **Video Google: a text retrieval approach to object matching in videos.** In *International Conference on Computer Vision*, **2**, pages 1470–1477, October 2003. 1, 19, 71, 83
- [17] XIAOFENG REN AND JITENDRA MALIK. **Learning a classification model for segmentation.** In *International Conference on Computer Vision*, **1**, pages 10–17, 2003. 1, 23, 51
- [18] STAN BIRCHFIELD AND SRIRAM RANGARAJAN. **Spatiograms versus Histograms for region-based tracking.** In *IEEE Computer Society Conference on Computer Vision and Pattern Recognition*, pages 1158–1163, 2005. 2, 24
- [19] ANKUR AGARWAL AND BILL TRIGGS. **Hyperfeatures - Multilevel local coding for visual recognition.** In *European Conference on Computer Vision*, pages 30–43, 2006. 2, 121
- [20] JOSIP KRAPAC, JAKOB J. VERBEEK, AND FRÉDÉRIC JURIE. **Modeling spatial layout with fisher vectors for image categorization.** In *International Conference on Computer Vision*, pages 1487–1494, 2011. 2, 25, 120
- [21] JORGE SÁNCHEZ, FLORENT PERRONNIN, AND TEÓFILO EMÍDIO DE CAMPOS. **Modeling the spatial layout of images beyond spatial pyramids.** *Pattern Recognition Letters*, **33**(16):2216–2223, 2012. 2, 25, 120
- [22] O. DUCHENNE, A. JOULIN, AND J. PONCE. **A graph-matching kernel for object categorization.** In *International Conference on Computer Vision*, pages 1792–1799, 2011. 2, 27
- [23] JAUME GIBERT, ERNEST VALVENY, AND HORST BUNKE. **Graph embedding in vector spaces by node attribute statistics.** *Pattern Recognition*, **45**(9):3072–3083, 2012. 2

-
- [24] HORST BUNKE AND KASPAR RIESEN. **Towards the unification of structural and statistical pattern recognition.** *Pattern Recognition Letters*, **33**(7):811–825, 2012. 2, 27
- [25] RICARDO DA SILVA TORRES AND ALEXANDRE X. FALCÃO. **Content-Based Image Retrieval: Theory and Applications.** *Revista de Informática Teórica e Aplicada*, **13**(2):161–185, 2006. 6, 17
- [26] KRYSZTIAN MIKOLAJCZYK AND CORDELIA SCHMID. **Scale & affine invariant interest point detectors.** *International Journal of Computer Vision*, **60**(1):63–86, 2004. 7
- [27] DJEMEL ZIOU AND SALVATORE TABBONE. **Edge detection techniques - An overview.** *International Journal of Pattern Recognition and Image Analysis*, **8**:537–559, 1998. 7
- [28] CHRIS HARRIS AND MIKE STEPHENS. **A combined corner and edge detector.** In *Alvey Vision Conference*, pages 1–6, 1988. 7, 24
- [29] TONY LINDBERG. **Feature detection with automatic scale selection.** *International Journal of Computer Vision*, **30**(2):79–116, 1998. 7
- [30] KRYSZTIAN MIKOLAJCZYK, TINNE TUYTELAARS, CORDELIA SCHMID, ANDREW ZISSERMAN, JIRI MATAS, FREDERIK SCHAFFALITZKY, TIMOR KADIR, AND LUC J. VAN GOOL. **A comparison of affine region detectors.** *International Journal of Computer Vision*, **65**(1-2):43–72, 2005. 7
- [31] DAVID G. LOWE. **Object recognition from local scale-invariant features.** In *International Conference on Computer Vision*, pages 1150–1157, 1999. 8, 20, 71
- [32] YAN KE AND RAHUL SUKTHANKAR. **PCA-SIFT: A more distinctive representation for local image descriptors.** In *IEEE Computer Society Conference on Computer Vision and Pattern Recognition*, pages 506–513, 2004. 9
- [33] R. ARANDJELOVIĆ AND A. ZISSERMAN. **Three things everyone should know to improve object retrieval.** In *IEEE Conference on Computer Vision and Pattern Recognition*, 2012. 9, 78, 98
- [34] JOHN M. WINN, ANTONIO CRIMINISI, AND THOMAS P. MINKA. **Object categorization by learned universal visual dictionary.** In *International Conference on Computer Vision*, pages 1800–1807, 2005. 9
- [35] HERBERT BAY, TINNE TUYTELAARS, AND LUC J. VAN GOOL. **SURF: Speeded Up Robust Features.** In *European Conference on Computer Vision*, pages 404–417, 2006. 9, 20, 27, 31, 72, 94, 95
- [36] TINNE TUYTELAARS. **Dense interest points.** In *IEEE Computer Society Conference on Computer Vision and Pattern Recognition*, pages 2281–2288, 2010. 10, 31
- [37] JIAN WU, ZHIMING CUI, VICTOR S. SHENG, PENG PENG ZHAO, DONGLIANG SU, AND SHENGRONG GONG. **A comparative study of SIFT and its variants.** *Measurement Science Review*, **13**(3):122–131, 2013. 10, 94

REFERENCES

- [38] CHARLES T. ZAHN AND RALPH Z. ROSKIES. **Fourier descriptors for plane closed curves.** *IEEE Transactions on Computers*, **21**(3):269–281, March 1972. 10
- [39] FARZIN MOKHTARIAN AND RIKU SUOMELA. **Robust image corner detection through curvature scale space.** *IEEE Transactions on Pattern Analysis and Machine Intelligence*, **20**(12):1376–1381, 1998. 10
- [40] A. KHOTANZAD AND Y. H. HONG. **Invariant image recognition by Zernike moments.** *IEEE Transactions on Pattern Analysis and Machine Intelligence*, **12**(5):489–497, May 1990. 10
- [41] JULIEN RICARD, DAVID COEURJOLLY, AND ATILLA BASKURT. **Generalizations of angular radial transform for 2D and 3D shape retrieval.** *Pattern Recognition Letters*, **26**(14):2174–2186, 2005. 10
- [42] A. AMANATIADIS, V.G. KABURLASOS, A. GASTERATOS, AND S.E. PAPADAKIS. **Evaluation of shape descriptors for shape-based image retrieval.** *Image Processing, IET*, **5**(5):493–499, August 2011. 10
- [43] DEAN S. MESSING, PETER VAN BEEK, AND JAMES H. ERRICO. **The MPEG-7 colour structure descriptor: image description using colour and local spatial information.** In *International Conference on Image Processing*, **1**, pages 670–673, 2001. 11
- [44] MICHAEL J. SWAIN AND DANA H. BALLARD. **Color indexing.** *International Journal of Computer Vision*, **7**(1):11–32, 1991. 11, 77, 82, 87
- [45] MARKUS A. STRICKER AND MARKUS ORENGO. **Similarity of color images.** In *Storage and Retrieval for Image and Video Databases (SPIE)*, pages 381–392, 1995. 11, 25
- [46] GREG PASS, RAMIN ZABIH, AND JUSTIN MILLER. **Comparing images using color coherence vectors.** In *ACM International Conference on Multimedia*, pages 65–73, 1996. 12
- [47] JING HUANG, RAVI KUMAR, MANDAR MITRA, WEI-JING ZHU, AND RAMIN ZABIH. **Image indexing using color correlograms.** In *IEEE Computer Society Conference on Computer Vision and Pattern Recognition*, pages 762–768, 1997. 12
- [48] TIMO OJALA, MATTI PIETIKÄINEN, AND TOPI MÄENPÄÄ. **Multiresolution gray-scale and rotation invariant texture classification with local binary patterns.** *IEEE Transactions on Pattern Analysis and Machine Intelligence*, **24**(7):971–987, 2002. 13, 121
- [49] ROBERT M. HARALICK, K. SAM SHANMUGAM, AND ITS’HAK DINSTEIN. **Textural features for image classification.** *IEEE Transactions on Systems, Man, and Cybernetics*, **3**(6):610–621, 1973. 13, 15, 25
- [50] JULIAN BESAG. **Spatial interaction and the statistical analysis of lattice systems.** *Journal of the Royal Statistical Society. Series B*, **36**(2):192–236, 1974. 13, 38

-
- [51] STUART GEMAN AND DONALD GEMAN. **Stochastic relaxation, gibbs distributions, and the Bayesian restoration of images.** *IEEE Transactions on Pattern Analysis and Machine Intelligence*, **6**:721–741, 1984. 13, 38
- [52] JIANCHANG MAO AND ANIL K. JAIN. **Texture classification and segmentation using multiresolution simultaneous autoregressive models.** *Pattern Recognition*, **25**(2):173–188, 1992. 13
- [53] R. SRIRAM, JOSEPH M. FRANCOIS, AND WILLIAM A. PEARLMAN. **Texture coding using a wold decomposition model.** *IEEE Transactions on Image Processing*, pages 1382–1386, 1996. 13
- [54] S.J.PARK, D.K.PARK, AND C. S. WON. **Core experiments on MPEG-7 edge histogram descriptor.** In *MPEG document, M5984, Geneva*, May 2000. 13
- [55] DONG KWON PARK, YOON SEOK JEON, AND CHEE SUN WON. **Efficient use of local edge histogram descriptor.** In *Proceedings of the ACM Multimedia Workshops*, pages 51–54. ACM Press, 2000. 13
- [56] JOHN R. SMITH AND SHIH-FU CHANG. **Transform features for texture classification and discrimination in large image databases.** In *International Conference on Image Processing*, pages 407–411. IEEE, 1994. 13
- [57] GERT VAN DE WOUWER, PAUL SCHEUNDERS, AND DIRK VAN DYCK. **Statistical texture characterization from discrete wavelet representations.** *IEEE Transactions on Image Processing*, pages 592–598, 1999. 13
- [58] CHANGREN ZHU AND RUNSHENG WANG. **Local multiple patterns based multiresolution gray-scale and rotation invariant texture classification.** *Information Sciences*, **187**:93–108, 2012. 14
- [59] ANDRÉ RICARDO BACKES, DALCIMAR CASANOVA, AND ODEMIR MARTINEZ BRUNO. **Texture analysis and classification: A complex network-based approach.** *Information Sciences*, **219**:168–180, 2013. 14
- [60] MATTI PIETIKÄINEN, ABDENOUR HADID, GUOYING ZHAO, AND TIMO AHONEN. *Computer vision using local binary patterns*. Springer, 2011. 14
- [61] HEE-JUNG BAE AND SUNG-HWAN JUNG. **Image retrieval using texture based on DCT.** In *International Conference on Information, Communications and Signal Processing*, pages 1065–1068, September 1997. 15
- [62] ISAAC NG, TELE TAN, AND JOSEF KITTLER. **On local linear transform and Gabor filter representation of texture.** In *IAPR International Conference on Pattern Recognition, Image, Speech and Signal Analysis*, pages 627–631, August 1992. 15
- [63] AUDE OLIVA AND ANTONIO TORRALBA. **Modeling the shape of the scene: A holistic representation of the spatial envelope.** *International Journal of Computer Vision*, **42**(3):145–175, 2001. 15, 16

REFERENCES

- [64] AUDE OLIVA. **Gist of the scene.** In *Neurobiology of Attention*, page 251256, 2005. 15
- [65] AUDE OLIVA AND ANTONIO TORRALBA. **Building the gist of a scene: the role of global image features in recognition.** In *Progress in Brain Research*, page 2336, 2006. 16
- [66] ANTONIO TORRALBA AND AUDE OLIVA. **Depth estimation from image structure.** *IEEE Transactions on Pattern Analysis and Machine Intelligence*, **24**(9):1226–1238, 2002. 16
- [67] JAMES HAYS AND ALEXEI A. EFROS. **Scene completion using millions of photographs.** *ACM Transactions on Graphics*, **26**(3):4, 2007. 16
- [68] ANTONIO TORRALBA, KEVIN P. MURPHY, WILLIAM T. FREEMAN, AND MARK A. RUBIN. **Context-based vision system for place and object recognition.** In *International Conference on Computer Vision*, pages 273–280, 2003. 16
- [69] ANTONIO TORRALBA. **Contextual priming for object detection.** *International Journal of Computer Vision*, **53**(2):169–191, 2003.
- [70] ANTONIO TORRALBA, ROBERT FERGUS, AND WILLIAM T. FREEMAN. **80 million tiny images: A large data set for nonparametric object and scene recognition.** *IEEE Transactions on Pattern Analysis and Machine Intelligence*, **30**(11):1958–1970, 2008. 16
- [71] MATTHIJS DOUZE, HERVE JEGOU, HARSIMRAT SANDHAWALIA, LAURENT AMSALEG, AND CORDELIA SCHMID. **Evaluation of GIST descriptors for web-scale image search.** In *ACM International Conference on Image and Video Retrieval*, 2009. 16
- [72] A. BHATTACHARYYA. **On a measure of divergence between two statistical populations defined by their probability distributions.** *Bulletin of the Calcutta Mathematical Society*, **35**:99109, 1943. 17
- [73] FRANK J. AHERNE, NEIL A. THACKER, AND PETER I ROCKETT. **The Bhattacharyya metric as an absolute similarity measure for frequency coded data.** *Kybernetika*, **34**(4):363368, 1998. 17
- [74] AMARNATH GUPTA AND RAMESH JAIN. **Visual information retrieval.** *Communications of the ACM*, **40**(5):70–79, 1997. 17
- [75] ALBERTO DEL BIMBO. *Visual information retrieval.* Morgan Kaufmann Publishers, San Francisco, CA, USA, 1999. 34
- [76] ABBY GOODRUM. **Image information retrieval: An overview of current research.** *Informing Science*, **3**:2000, 2000. 17
- [77] F.IDRIS AND S.PANCHANATHAN. **Review of image and video indexing techniques.** *Journal of Visual Communication and Image Representation*, **8**(2):146166, 1997. 18
- [78] VITTORIO FERRARI, FRÉDÉRIC JURIE, AND CORDELIA SCHMID. **From images to shape models for object detection.** *International Journal of Computer Vision*, **87**(3):284–303, 2010. 18

-
- [79] DIANE LARLUS, JAKOB J. VERBEEK, AND FRÉDÉRIC JURIE. **Category level object segmentation by combining Bag-of-Words models with Dirichlet processes and random fields.** *International Journal of Computer Vision*, **88**(2):238–253, 2010. 18
- [80] GABRIELLA CSURKA, CHRISTOPHER R. DANCE, LIXIN FAN, JUTTA WILLAMOWSKI, AND CÉDRIC BRAY. **Visual categorization with bags of keypoints.** In *In Workshop on Statistical Learning in Computer Vision, ECCV*, pages 1–22, 2004. 19, 21, 71
- [81] B. JULESZ. **Textons, the elements of texture perception, and their interactions.** *Nature*, **290**(5802):9197, March 1981. 19
- [82] THOMAS K. LEUNG AND JITENDRA MALIK. **Representing and recognizing the visual appearance of materials using three-dimensional textons.** *International Journal of Computer Vision*, **43**(1):29–44, 2001. 19
- [83] GERARD SALTON AND MICHAEL J. MCGILL. *Introduction to modern information retrieval*. McGraw-Hill computer science series. McGraw-Hill, 1983. 19
- [84] J. B. MACQUEEN. **Some methods for classification and analysis of multiVariate observations.** In *Proceedings of 5-th Berkeley Symposium on Mathematical Statistics and Probability*, **1**, pages 281–297. Berkeley, University of California Press, 1967. 20, 52
- [85] JAN VAN GEMERT, COR J. VEENMAN, ARNOLD W. M. SMEULDERS, AND JAN-MARK GEUSEBROEK. **Visual word ambiguity.** *IEEE Transactions on Pattern Analysis and Machine Intelligence*, **32**(7):1271–1283, 2010. 20, 94
- [86] PIOTR KONIUSZ AND KRYSZTIAN MIKOLAJCZYK. **Soft assignment of visual words as linear coordinate coding and optimisation of its reconstruction error.** In *International Conference on Image Processing*, pages 2413–2416, 2011.
- [87] VINAY GARG, SREEKANTH VEMPATI, AND C.V. JAWAHAR. **Bag of visual words: A soft clustering based exposition.** In *National Conference on Computer Vision, Pattern Recognition, Image Processing and Graphics*, pages 37–40, December 2011.
- [88] YUBIN KUANG, KALLE ÅSTRÖM, LARS KOPP, MAGNUS OSKARSSON, AND MARTIN BYRÖD. **Optimizing visual vocabularies using soft assignment entropies.** In *Asian Conference on Computer Vision*, pages 255–268, 2010. 20, 94
- [89] ALEX LEVINSHTAIN, ADRIAN STERE, KIRIAKOS N. KUTULAKOS, DAVID J. FLEET, SVEN J. DICKINSON, AND KALEEM SIDDIQI. **TurboPixels: Fast superpixels using geometric flows.** *IEEE Transactions on Pattern Analysis and Machine Intelligence*, **31**(12):2290–2297, 2009. 23
- [90] R. ACHANTA, A. SHAJI, K. SMITH, A. LUCCHI, P. FUA, AND S. SÜSTRUNK. **SLIC superpixels compared to state-of-the-art superpixel methods.** *IEEE Transactions on Pattern Analysis and Machine Intelligence*, **34**(11):2274–2282, November 2012. 23

REFERENCES

- [91] MICHAEL VAN DEN BERGH, XAVIER BOIX, GEMMA ROIG, BENJAMIN DE CAPITANI, AND LUC J. VAN GOOL. **SEEDS: Superpixels extracted via energy-driven sampling.** In *European Conference on Computer Vision*, pages 13–26, 2012. 23
- [92] ALEXANDER SCHICK, MIKA FISCHER, AND RAINER STIEFELHAGEN. **Measuring and evaluating the compactness of superpixels.** In *International Conference on Pattern Recognition*, pages 930–934, 2012. 23
- [93] CIARÁN O CONAIRE, NOEL E. O’CONNOR, AND ALAN F. SMEATON. **An improved spatiogram similarity measure for robust object localisation.** In *International Conference on Acoustics, Speech, and Signal Processing*, pages 1069–1072, 2007. 24
- [94] DORIN COMANICIU, VISVANATHAN RAMESH, AND PETER MEER. **Real-time tracking of non-rigid objects using Mean Shift.** In *IEEE Computer Society Conference on Computer Vision and Pattern Recognition*, 2000. 24
- [95] RAHAT KHAN, CÉCILE BARAT, DAMIEN MUSELET, AND CHRISTOPHE DUCOTTET. **Spatial orientations of visual word pairs to improve Bag-of-Visual-Words model.** In *British Machine Vision Conference*, pages 1–11, 2012. 25
- [96] FLORENT PERRONNIN AND CHRISTOPHER R. DANCE. **Fisher kernels on visual vocabularies for image categorization.** In *IEEE Computer Society Conference on Computer Vision and Pattern Recognition*, 2007. 25
- [97] FLORENT PERRONNIN, JORGE SÁNCHEZ, AND THOMAS MENSINK. **Improving the fisher kernel for large-scale image classification.** In *European Conference on Computer Vision*, pages 143–156, 2010.
- [98] FLORENT PERRONNIN, YAN LIU, JORGE SÁNCHEZ, AND HERVE POIRIER. **Large-scale image retrieval with compressed Fisher vectors.** In *IEEE Computer Society Conference on Computer Vision and Pattern Recognition*, pages 3384–3391, 2010.
- [99] K. SIMONYAN, O. PARKHI, A. VEDALDI, AND A. ZISSERMAN. **Fisher vector faces in the wild.** In *British Machine Vision Conference*, 2013. 25, 120
- [100] JIANCHAO YANG, KAI YU, YIHONG GONG, AND T. HUANG. **Linear spatial pyramid matching using sparse coding for image classification.** In *IEEE Computer Society Conference on Computer Vision and Pattern Recognition*, pages 1794–1801, June 2009. 25
- [101] JINJUN WANG, JIANCHAO YANG, KAI YU, FENGJUN LV, THOMAS S. HUANG, AND YIHONG GONG. **Locality-constrained linear coding for image classification.** In *IEEE Computer Society Conference on Computer Vision and Pattern Recognition*, pages 3360–3367, 2010. 25
- [102] SANCHO McCANN AND DAVID G. LOWE. **Spatially local coding for object recognition.** In *Asian Conference on Computer Vision*, pages 204–217, 2012. 25, 120

-
- [103] WEI HUANG, YAN GAO, AND KAP LUK CHAN. **A review of region-based image retrieval.** *Journal of Signal Processing Systems*, **59**(2):143161, 2010. 25
- [104] NARENDRA AHUJA AND SINISA TODOROVIC. **From region based image representation to object discovery and recognition.** In *Structural, Syntactic, and Statistical Pattern Recognition, Joint IAPR International Workshop*, **6218** of *Lecture Notes in Computer Science*, pages 1–19. Springer, 2010. 25
- [105] FENG JING, MINGJING LI, HONGJIANG ZHANG, AND BO ZHANG. **An effective region-based image retrieval framework.** In *ACM International Conference on Multimedia*, pages 456–465, 2002. 26
- [106] FENG JING, MINGJING LI, LEI ZHANG, HONGJIANG ZHANG, AND BO ZHANG. **Learning in region-based image retrieval.** In *ACM International Conference on Image and Video Retrieval*, pages 206–215, 2003.
- [107] FENG JING, MINGJING LI, HONGJIANG ZHANG, AND BO ZHANG. **An efficient and effective region-based image retrieval framework.** *IEEE Transactions on Image Processing*, **13**(5):699–709, 2004. 26
- [108] JEAN-FRANÇOIS OMHOVER AND MARCIN DETYNIECKI. **STRICT: An image retrieval platform for queries based on regional content.** In *ACM International Conference on Image and Video Retrieval*, pages 473–482, 2004. 26
- [109] JEAN-FRANÇOIS OMHOVER AND MARCIN DETYNIECKI. **Fast gradual matching measure for image retrieval based on visual similarity and spatial relations.** *International Journal of Intelligent Systems*, **21**(7):711–723, 2006. 26
- [110] PHILIPPE HENRI GOSSELIN, MATTHIEU CORD, AND SYLVIE PHILIPP-FOLIGUET. **Kernels on bags of fuzzy regions for fast object retrieval.** In *ICIP*, pages 177–180, 2007. 26
- [111] RÉMI VIEUX, JENNY BENOIS-PINEAU, AND JEAN-PHILIPPE DOMENGER. **Content based image retrieval using Bag-Of-Regions.** In *International Conference on Advances in Multimedia Modeling*, pages 507–517, 2012. 26, 78
- [112] JUSTINE LEBRUN, SYLVIE PHILIPP-FOLIGUET, AND PHILIPPE HENRI GOSSELIN. **Image retrieval with graph kernel on regions.** In *International Conference on Pattern Recognition*, pages 1–4, 2008. 27
- [113] JUSTINE LEBRUN, PHILIPPE HENRI GOSSELIN, AND SYLVIE PHILIPP-FOLIGUET. **Inexact graph matching based on kernels for object retrieval in image databases.** *Image and Vision Computing*, **29**(11):716–729, 2011. 27
- [114] HICHEM SAHBI, JEAN-YVES AUDIBERT, JAONARY RABARISOA, AND RENAUD KERIVEN. **Object recognition and retrieval by context dependent similarity kernels.** In *CBMI*, pages 216–223, 2008. 27

REFERENCES

- [115] EDWIN R. HANCOCK, ANDREA TORSELLO, FRANCISCO ESCOLANO, AND LUC BRUN. **Special issue on graph-based representations in computer vision.** *Computer Vision and Image Understanding*, **115**(7):903–904, 2011. 29
- [116] JONATHAN RICHARD SHEWCHUK. **Triangle: Engineering a 2D quality mesh generator and delaunay triangulator.** In *Workshop on Applied Computational Geometry*, pages 203–222, 1996. 33
- [117] Y. BOYKOV, O. VEKSLER, AND R. ZABIH. **Markov random fields with efficient approximations.** In *Computer Vision and Pattern Recognition, 1998. Proceedings. 1998 IEEE Computer Society Conference on*, pages 648–655, June 1998. 34
- [118] CHARLESS FOWLKES, SERGE BELONGIE, FAN R. K. CHUNG, AND JITENDRA MALIK. **Spectral grouping using the nystrom method.** *IEEE Transactions on Pattern Analysis and Machine Intelligence*, **26**(2):214–225, 2004. 51
- [119] INDERJIT S. DHILLON, YUQIANG GUAN, AND BRIAN KULIS. **Weighted graph cuts without eigenvectors a multilevel approach.** *IEEE Transactions on Pattern Analysis and Machine Intelligence*, **29**(11):1944–1957, November 2007. 34, 51, 52
- [120] SHENGJIU WANG. **A robust CBIR approach using local color histograms.** Technical report, University of Alberta, 2001. 34
- [121] PRATHEEP ANANTHARATNASAMY, KAAVYA SRISKANDARAJA, VAHISSAN NANDAKUMAR, AND SAMPATH DEEGALLA. **Fusion of colour, shape and texture features for content based image retrieval.** In *International Conference on Computer Science Education*, pages 422–427, April 2013. 34
- [122] CARSTEN ROTHER, VLADIMIR KOLMOGOROV, AND ANDREW BLAKE. **GrabCut - Interactive foreground extraction using iterated Graph Cuts.** *ACM Transactions on Graphics (SIGGRAPH)*, August 2004. 35, 47
- [123] INDERJIT S. DHILLON, YUQIANG GUAN, AND BRIAN KULIS. **Kernel k-means: spectral clustering and Normalized Cuts.** In *Proceedings of the Tenth ACM SIGKDD International Conference on Knowledge Discovery and Data Mining*, pages 551–556, 2004. 37, 50, 51, 54, 58
- [124] PEDRO F. FELZENSZWALB AND DANIEL P. HUTTENLOCHER. **Efficient graph-based image segmentation.** *International Journal of Computer Vision*, **59**(2):167–181, 2004. 38, 74
- [125] YURI BOYKOV AND MARIE-PIERRE JOLLY. **Interactive graph cuts for optimal boundary & region segmentation of objects in N-D images.** In *International Conference on Computer Vision*, pages 105–112, 2001. 39, 47
- [126] VLADIMIR KOLMOGOROV AND RAMIN ZABIH. **What energy functions can be minimized via graph cuts.** *IEEE Transactions on Pattern Analysis and Machine Intelligence*, **26**:65–81, 2004. 39, 94

-
- [127] L. R. FORD AND D. R. FULKERSON. **Maximal flow through a network.** *Canadian Journal of Mathematics*, **8**:399404, 1956. 39
- [128] L. R. FORD JR. AND D. R. FULKERSON. *Flows in networks*. Princeton University Press, 1962. 40
- [129] ZHENYU WU AND RICHARD M. LEAHY. **An optimal graph theoretic approach to data clustering: Theory and its application to image segmentation.** *IEEE Transactions on Pattern Analysis and Machine Intelligence*, **15**(11):1101–1113, 1993. 47
- [130] NIKOS KOMODAKIS AND GEORGIOS TZIRITAS. **Approximate labeling via Graph Cuts based on linear programming.** *IEEE Transactions on Pattern Analysis and Machine Intelligence*, **29**(8):1436–1453, 2007. 47
- [131] ANDREW DELONG, ANTON OSOKIN, HOSSAM N. ISACK, AND YURI BOYKOV. **Fast approximate energy minimization with label costs.** *International Journal of Computer Vision*, **96**(1):1–27, 2012. 47
- [132] DONG YAN AND MA YONGZHUANG. **Image restoration using Graph Cuts with adaptive smoothing.** In *International Conference on Information Acquisition*, pages 152–156, July 2007. 47
- [133] TOMMY W. H. TANG AND ALBERT C. S. CHUNG. **Non-rigid image registration using Graph-cuts.** In *International Conference on Medical Image Computing and Computer-Assisted Intervention*, pages 916–924, 2007. 47
- [134] RONALD W. K. SO, TOMMY W. H. TANG, AND ALBERT C. S. CHUNG. **Non-rigid image registration of brain magnetic resonance images using graph-cuts.** *Pattern Recognition*, **44**(10-11):2450–2467, 2011. 47
- [135] NICOLAS PAPADAKIS AND AURÉLIE BUGEAU. **Tracking with occlusions via Graph Cuts.** *IEEE Transactions on Pattern Analysis and Machine Intelligence*, **33**(1):144–157, 2011. 47
- [136] GENE H. GOLUB AND CHARLES F. VAN LOAN. *Matrix computations*. Johns Hopkins Press, 2nd edition, 1989. 49
- [137] ALEX POTHEN, HORST D. SIMON, AND KAN-PU LIOU. **Partitioning sparse matrices with eigenvectors of graphs.** *SIAM Journal on Matrix Analysis and Applications*, **11**(3):430–452, May 1990. 49
- [138] B. W. KERNIGHAN AND S. LIN. **An efficient heuristic procedure for partitioning graphs.** *The Bell system technical journal*, **49**(1):291–307, 1970. 51
- [139] PAK K. CHAN, MARTINE D. F. SCHLAG, AND JASON Y. ZIEN. **Spectral k-way ratio-cut partitioning and clustering.** *IEEE Transactions on Computer-Aided Design of Integrated Circuits and Systems*, **13**(9):1088–1096, 1994. 51, 52
- [140] STELLA X.YU AND JIANBO SHI. **Multiclass spectral clustering.** In *International Conference on Computer Vision*, **1**, pages 313–319, 2003. 51

REFERENCES

- [141] INDERJIT DHILLON, YUQIANG GUAN, AND BRIAN KULIS. **A unified view of kernel k-means, spectral clustering and graph partitioning**. Technical Report TR-04-25, University of Texas Dept. of Computer Science, 2005. 52, 57
- [142] BERNHARD SCHÖLKOPF, ALEX J. SMOLA, AND KLAUS-ROBERT MÜLLER. **Nonlinear component analysis as a kernel eigenvalue problem**. *Neural Computation*, **10**(5):1299–1319, 1998. 53
- [143] NELLO CRISTIANINI AND JOHN SHAWE-TAYLOR. *An introduction to support Vector Machines: and other kernel-based learning methods*. Cambridge University Press, 2000. 53
- [144] FEI-FEI LI, ROBERT FERGUS, AND PIETRO PERONA. **Learning generative visual models from few training examples: An incremental Bayesian approach tested on 101 object categories**. *Computer Vision and Image Understanding*, **106**(1):59–70, 2007. 58, 91, 129
- [145] LEO GRADY AND ERIC L. SCHWARTZ. **Isoperimetric graph partitioning for image segmentation**. *IEEE Trans. Pattern Anal. Mach. Intell.*, **28**(3):469–475, 2006. 74
- [146] DAVID TOLLIVER AND GARY L. MILLER. **Graph partitioning by spectral rounding: Applications in image segmentation and clustering**. In *IEEE Computer Society Conference on Computer Vision and Pattern Recognition*, pages 1053–1060, 2006. 74
- [147] G.J. McLACHLAN. **Mahalanobis distance**. *Resonance*, **4**(6):2026, 1999. 76
- [148] YOSSI RUBNER, CARLO TOMASI, AND LEONIDAS J. GUIBAS. **A metric for distributions with applications to image databases**. In *International Conference on Computer Vision*, pages 59–66, 1998. 76
- [149] JAMES L. HAFNER, HARPREET S. SAWHNEY, WILLIAM EQUITZ, MYRON FLICKNER, AND WAYNE NIBLACK. **Efficient Color Histogram Indexing for Quadratic Form Distance Functions**. *IEEE Transactions on Pattern Analysis and Machine Intelligence*, **17**(7):729–736, 1995. 76
- [150] OFIR PELE AND MICHAEL WERMAN. **The Quadratic-Chi histogram distance family**. In *European Conference on Computer Vision*, pages 749–762, 2010. 76
- [151] YOSSI RUBNER, CARLO TOMASI, AND LEONIDAS J. GUIBAS. **The Earth Mover’s distance as a metric for image retrieval**. *International Journal of Computer Vision*, **40**(2):99–121, 2000. 77
- [152] FAN-DI JOU, KUO-CHIN FAN, AND YANG-LANG CHANG. **Efficient matching of large-size histograms**. *Pattern Recognition Letters*, **25**(3):277–286, February 2004. 77, 82, 87
- [153] HAROLD W. KUHN. **The Hungarian method for the assignment problem**. *Naval Research Logistics Quarterly*, **2**:83–97, March 1955. 80
- [154] ANNICK MONTANVERT, P. MEER, AND A ROSENFIELD. **Hierarchical image analysis using irregular tessellations**. *IEEE Transactions on Pattern Analysis and Machine Intelligence*, **13**(4):307–316, April 1991. 84

-
- [155] PETER J. BURT. **Fast filter transform for image processing.** *Computer Graphics and Image Processing*, **16**(1):2051, 1981. 88
- [156] PETER J. BURT. **Fast algorithms for estimating local image properties.** *Computer Vision, Graphics, and Image Processing*, **21**(3):368382, 1983.
- [157] PETER J. BURT AND EDWARD H. ADELSON. **The laplacian pyramid as a compact image code.** *IEEE Transactions on Communications*, **31**(4):532–540, 1983. 88
- [158] BANGPENG YAO AND LI FEI-FEI. *People Playing Musical Instrument (PPMI) dataset.* Available at <http://ai.stanford.edu/~bangpeng/ppmi.html>. 91, 147
- [159] BANGPENG YAO AND LI FEI-FEI. **Grouplet: A structured image representation for recognizing human and object interactions.** In *IEEE Computer Society Conference on Computer Vision and Pattern Recognition*, June 2010. 91, 147
- [160] ROUHOLLAH RAHMANI, SALLY A. GOLDMAN, HUI ZHANG, SHARATH R. CHOLLETI, AND JASON E. FRITTS. **Localized content-based image retrieval.** *IEEE Transactions on Pattern Analysis and Machine Intelligence*, **30**(11):1902–1912, 2008. 92
- [161] KEN CHATFIELD, VICTOR LEMPITSKY, ANDREA VEDALDI, AND ANDREW ZISSERMAN. **The devil is in the details: an evaluation of recent feature encoding methods.** In *British Machine Vision Conference*, pages 1–12, 2011. 94
- [162] ALEX KRIZHEVSKY, ILYA SUTSKEVER, AND GEOFFREY E. HINTON. **ImageNet classification with deep convolutional neural networks.** In *Advances in Neural Information Processing Systems 25*, pages 1106–1114, 2012. 121
- [163] PHILIPPE HENRI GOSSELIN AND DAVID PICARD. **Machine learning and content-based multimedia retrieval.** In *21st European Symposium on Artificial Neural Networks*, April 2013. 121
- [164] YONG XU, SI-BIN HUANG, HUI JI, AND CORNELIA FERMÜLLER. **Scale-space texture description on SIFT-like textons.** *Computer Vision and Image Understanding*, **116**(9):999–1013, 2012. 121
- [165] YUHUI QUAN, YONG XU, AND YUPING SUN. **A distinct and compact texture descriptor.** *Image and Vision Computing*, **32**(4):250–259, 2014. 121
- [166] SEMA CANDEMIR AND YUSUF SINAN AKGUL. **Adaptive regularization parameter for Graph Cut segmentation.** In *International Conference on Image Analysis and Recognition*, pages 117–126, 2010. 121

Activities

Publications

The following publications were made as results of this present thesis work that was carried out in LaBRI, University of Bordeaux, France:

- Yi Ren, Jenny Benois-Pineau and Aurélie Bugeau. A Comparative Study of Irregular Pyramid Matching in Bag-of-Bags of Words Model for Image Retrieval, in International Conference on Image and Signal Processing, June 2014. Springer, Lecture Notes in Computer Science (LNCS) 8509 Proceedings, 8509, pages 539 - 548. (Oral presentation, selected as one of best papers. The extended paper is selected to submit to the journal “Signal, Image and Video Processing” on Advances in Low-Level Image representations for processing and analysis.)
- Yi Ren, Aurélie Bugeau and Jenny Benois-Pineau. Bag-of-Bags of Words - Irregular Graph Pyramids vs Spatial Pyramid Matching for Image Retrieval, in 4th International Conference on Image Processing Theory, Tools and Applications, Oct 2014. (Oral presentation, the best paper award.)

Research report - Extractions from HAL

- Yi Ren, Aurélie Bugeau and Jenny Benois-Pineau. Bag-of-Bags of Words : Irregular graph pyramids vs spatial pyramid matching for image retrieval, 2014.
- Yi Ren, Aurélie Bugeau and Jenny Benois-Pineau. Bag-of-Bags of Words model over irregular graph partitions for image retrieval, 2013
- Yi Ren, Aurélie Bugeau, Jenny Benois-Pineau. Visual object retrieval by graph features, 2013

Talk

- *October 31, 2013* Topic: Image Retrieval with non-regular pyramid partitioning via Graph-Cuts. Séminaire des Doctorants (Semi-Doc).
- *January 10, 2014* Topic: Bag-of-bags of words model - BBoW on irregular partitions via graph cuts for image retrieval. Meeting of AIV (Analyse et Indexation Vidéo) Working Group with professor Vincent Oria.
- *April 1, 2014* Topic: Bag-of-Bags of Words: Irregular graph pyramids vs spatial pyramid matching for image retrieval. École Jeunes Chercheurs en Informatique Mathématique 2014.
- *July 2, 2014* Topic: Bag-of-Bags of Words: A Comparative Study of Irregular Pyramid Matching in Bag-of-Bags of Words Model for Image Retrieval. Oral presentation@ICISP Conference
- *October 14, 2014* Topic: Bag-of-Bags of Words - Irregular Graph Pyramids vs Spatial Pyramid Matching for Image Retrieval. Oral presentation@4th International Conference on Image Processing Theory, Tools and Applications

Poster

The poster of PhD thesis

Declaration

I herewith declare that I have produced this thesis without the prohibited assistance of third parties and without making use of aids other than those specified; notions taken over directly or indirectly from other sources have been identified as such.

The thesis work was conducted from 2011/10/01 to 2014/09/30 under the supervision of Professor Jenny Benois-Pineau and Associate Professor Aurélie Bugeau at Laboratory LaBRI, University of Bordeaux, France.

Yi REN